Computational modelling of thrombotic processes and complex haemodynamics in cerebral aneurysms



Malebogo N Ngoepe

Wadham College

Department of Engineering Science

University of Oxford

Thesis submitted for the degree of

Doctor of Philosophy

Trinity Term, 2013

Abstract

A clot in a cerebral aneurysm can either accelerate the road to rupture, through inflammatory processes and furthering vascular wall degradation, or stabilise the situation by occluding the aneurysm, and thus prevent rupture. A three-dimensional computational model of clotting in patient-derived cerebral aneurysm geometries is presented. The model accounts for the biochemical reactions that make up the clotting process, for realistic three-dimensional haemodynamics in image-derived vasculature representations and for the growing clot's interaction with and impact on the flow field. The flow is accounted for by the Navier Stokes equations and the transport equation describes the changes in biochemical species concentrations. Level Set methods are used to track the surface of the growing clot in the three-dimensional geometries studied. The influence of the thrombosed region on the haemodynamics is accounted for by modifying the local porosity and permeability, to reflect the fibrous and permeable nature of the clot. The model is first developed, examined and parameterised for a physiological model of clotting in two dimensions and is then extended and demonstrated for the pathological case in three dimensions.

The framework developed is used to examine various aspects of clotting. The two-dimensional model is used to investigate the effects of critical thrombin concentration, tissue factor and the underlying biochemical cascade. The critical

thrombin concentration at which coagulation transitions from the initiation to the propagation phase was found to be [TH] = 1 – 10nM. The inclusion of blood-borne tissue factor was found to reflect a more realistic thrombin production curve and an increase in initial tissue factor concentration led to a decrease in thrombin production lag time. The different underlying biochemical cascades produce similar results.

The model is then extended to three dimensions and is used to investigate clot propagation and initiation in patient-derived aneurysms. The propagation velocity is linked to mechanical factors and biochemical species concentrations. An inverse relationship between strain rate and propagation velocity showed realistic clot growth. Realistic growth was also observed for a direct relationship with thrombin concentration and this seemed to be the most suitable approximation. The ways in which tissue factor, strain rate threshold and location of endothelial damage affect initiation are also examined. A strain rate of $500s^{-1}$ was found to be the highest strain rate at which fibrin controlled clot initiation took place. Above that value, no clotting was observed. The location of endothelial damage affected clot growth as evidenced by the reproduction of the clots observed under Lawton's classification scheme.

The three-dimensional model is then applied to patient-derived geometries and is used to examine the efficacy of flow diverter treatment. For a given geometry, clot growth is predicted for the case with and without a flow diverter. In some cases, clotting is a

positive outcome while in other cases, the clot occludes the parent vessel.

The unique contribution of this thesis is the combination of computational fluid dynamics, biochemistry and Level Set methods in complex, realistic, three-dimensional aneurysm geometries for clot prediction. The impact of the clot on the flow field is modelled by altering the porosity and permeability values of the clot region.

Acknowledgements

Thank you to my supervisor, Professor Yiannis Ventikos, for your guidance, time, and support. Thank you for giving me the opportunity to study such a fascinating and challenging topic and for providing valuable insights along the way.

Thank you to the Fluidics and Biocomplexity Group for providing a wonderful working environment. It has been a joy to come to the lab every morning over the last three years. While the collective insight is impressive, the most remarkable thing about the group is the friendship, support and commitment to seeing others through. I am grateful to Emilie Dickinson who provided a lot of guidance in the early stages of my DPhil.

Thank you to the Rhodes Trust for making my DPhil studies and stay in Oxford possible. Thank you also to my college advisor at Wadham, Dr Mark Thompson. I appreciate the time that you set aside to make sure that my stay here was a good one.

Thank you to friends and family, far and near. I really appreciate your prayers, love, support, laughter, phone calls, airport goodbyes and hellos, care packages, visits, ice-cream dates, eccentricities and strange stories told with straight faces. Thank you to my wonderful housemates at No. 99 who saw me through the intense final stage

and made sure that I kept eating, sleeping and dancing. I am also grateful to my Thursday night homegroup. Your prayers, love, words of encouragement and hilarious anecdotes keep me grounded and remind me what a privilege it is to belong to His body.

Finally, to my family, Khetlepu, Phuti and Noko. *Ke leboga go menagane. Ke lena barutishi ba ka ba mathomo. Le nthutile go re bohlale ba mathomo ke go tšhaba Modimo*. *Le nthutile gape le botho. La busha la nthuta lerato la thuto. Ruri, le ntirile motho*. I am because you are. Thank you for your love.

Contents

List of Figures and Tables x

1. Motivation and Introduction 1

1.1. Motivation 1

1.2. Aneurysms 7

1.2.1. Vascular wall structure, remodelling and aneurysms 9

1.2.2. Detection, symptoms and risk factors of aneurysms 11

1.2.3. Treatment methods 12

1.3. Coagulation under physiological conditions 16

1.3.1. Coagulation models 18

1.3.2. Platelets 29

1.3.3. Tissue Factor 34

1.3.4. Vascular endothelium 37

1.4. Clotting in aneurysms 39

1.4.1. General considerations for clotting in pathological states 40

1.4.2. Nature of clots observed in aneurysms 40

1.4.3. Spontaneous clotting in cerebral aneurysms 43

1.4.4. Non-spontaneous clotting in cerebral aneurysms 45

1.4.5. Motivation for computational model developed in this thesis 49

2. Computational models of clotting 50

2.1. Coagulation network models 50

2.2. Platelet models....51
2.3. Reaction-Mass Transport models....54
2.4. Integrated models....59
2.5. Computational models of coagulation in aneurysms....62
2.6. Summary of models presented....66
3. Methods for framework construction....68
3.1. CFD....68
3.1.1. Governing equations of fluid flow....69
3.1.2. The general transport equation....71
3.1.3. Finite volume method....72
3.1.4. Solving the discretised equations....73
3.1.5. Accounting for porosity and permeability....79
3.1.6. Error and uncertainty in CFD....80
3.2. Chemical reactions....81
3.2.1. Modelling biochemical reactions....82
3.2.2. Solving the system of biochemical equations....83
3.3. Modelling clot growth....84
3.4. Level Set methods....87
3.4.1. Explicit and implicit functions....88
3.4.2. Signed distance functions....88
3.4.3. Dynamic implicit surfaces....90

3.4.4. Construction of a signed distance function....91
3.4.5. Reinitialisation and the narrow band approach....92
3.4.6. Specific features of Level Set methods used in this work....94
3.4.7. Interfacing the Level Set code with CFD-ACE....98
3.5. Contributions made....100
4. Results: Clot growth under flow in two dimensions....102
4.1. General considerations....102
4.1.1. Critical thrombin concentration....104
4.1.2. Tissue factor expression....105
4.1.3. The effect of the chosen biochemical cascade....107
4.2. Model specifications....110
4.2.1. Simulations conducted....110
4.2.2. Computational fluid dynamics settings....112
4.2.3. Biochemical reactions....115
4.3. Findings and discussion....121
4.3.1. Grid independence study....122
4.3.2. Critical thrombin concentration....123
4.3.3. Tissue factor....129
4.3.4. Effect of chosen biochemical cascade....138
4.3.5. Comparison of results with existing models....142
4.3.6. Discussion....145

5. Results: Clot propagation and initiation in three dimensions – the effect of mechanical and biochemical factors 154

5.1. General considerations 154

5.1.1. Mechanical factors 155

5.1.2. Biochemical factors 161

5.1.3. Condition of endothelium 163

5.2. Model specifications 164

5.2.1. Geometry 165

5.2.2. Simulations conducted 166

5.2.3. Computational fluid dynamics 168

5.2.4. Biochemical reactions 169

5.2.5. Level Set methods 170

5.3. Findings and discussion 171

5.3.1. Propagation 172

5.3.2. Initiation 175

5.3.3. Discussion 179

6. Results: Evaluation of flow diverter performance in patient-derived aneurysm geometries 187

6.1. General considerations 187

6.1.1. Spontaneous clotting in cerebral aneurysms 188

6.1.2. Non-spontaneous clotting of aneurysms 190

6.2. Model specifications 192
6.2.1. Geometries 192
6.2.2. Simulations conducted 195
6.2.3. Computational fluid dynamics settings 196
6.2.4. Biochemical reactions 198
6.2.5. Level Set methods 198
6.3. Findings and discussion 199
6.3.1. Case 1 200
6.3.2. Case 2 203
6.3.3. Case 3 207
6.3.4. Discussion 210
7. Conclusions and future work 214
7.1. Summary 214
7.2. Contributions 221
7.3. Future work 222
Appendix A 226
Hamilton-Jacobi ENO 226
Hamilton-Jacobi WENO 228
References 230
List of conferences and publications 249

List of Figures and Tables

Figure 1.1: A cerebral aneurysm is a balloon-like bulge that develops from the wall of a weakened blood vessel. Clipping is a surgical technique employed for cerebral aneurysm treatment. A craniotomy is performed by a neurosurgeon (A) and the aneurysm is clipped at the neck, preventing further flow into the aneurysm sac (B). Taken from Brisman et al [3]. 2

Figure 1.2: Endovascular coiling in the aneurysm sac encourages the development of a clot which occludes the sac. A catheter is inserted into the femoral artery and is navigated to the relevant cranial artery. A microcatheter then delivers the coils into the aneurysm and the process is continued until the sac has been filled with coils. Taken from Brisman [3]..3

Figure 1.3: Stent assisted coiling can be used in cases where the aneurysm neck is too wide for coiling alone. The stent provides a scaffold which supports the coils once they are placed in the aneurysm sac. Taken from Stryker Neuroform stent promotional material [6]. 3

Figure 1.4: A flow diverter is similar to a stent in design however it is far less porous. The purpose of the implant is to reduce flow into the aneurysm sac and redirect it along the parent vessel. The reduced flow in the aneurysm should encourage clot development. Taken from Larrabide et al [7]. 4

Figure 1.5: Common sites for cerebral aneurysms found on blood vessels

supplying blood to the brain. The majority of these vessels originate in the circle of Willis and cerebral aneurysms are typically found at bifurcations. Taken from Schievink [10] 7

Figure 1.6: Three main types of cerebral aneurysms. Saccular aneurysms (A), fusiform aneurysms (B) and dissecting aneurysms (C). Taken from Johns Hopkins Medicine Health Library [27].....9

Figure 1.7: The arterial wall is composed of three layers. The outermost adventitial layer is surrounded by loose connective tissue. The medial layer is made up of collagen and elastic fibres. The intima comes into contact with flowing blood. Taken from Holzapfel et al [28]. 10

Figure 1.8: The process of coagulation. (A) When there is no injury to the wall, blood flow continues along the main vessel which is lined with endothelial cells. (B) Injury of the blood vessel wall results in the removal of the endothelial layer and exposure of the subendothelial layers and tissue factor. (C) The haemostatic system stimulates a series of responses which result in the formation of a platelet plug and a fibrin mesh. 17

Figure 1.9: The traditional waterfall coagulation cascade. Initiation in the *intrinsic* pathway is initiated by the activation of factor XII by high molecular weight kininogen and prekallikrein. The *extrinsic* pathway is initiated by exposure of tissue factor, which combines with factor VIIa. The *common* pathway commences with the activation of factor X and ends with

the production of fibrin. 21

Figure 1.10: Illustrated here are the initiation and amplification phases of the cell-based model of coagulation. In the initiation phase, a small amount of thrombin is produced from a fairly inefficient process. This thrombin then activates other factors which then allow for more rapid and efficient production of more thrombin. 24

Figure 1.11: Anticoagulation mechanisms regulate the processes which result in the formation of thrombin. Activated Protein C inactivates the co-factor, Antithrombin inactivates the factors and TFPI limits tissue factor activity. 25

Figure 1.12: The process of platelet activation in coagulation. Under normal circumstances, the platelet circulates in an inactive state and has a disc-like shape (A). Upon contact with the subendothelial layers or other activated platelets, the platelet assumes a spherical shape and extends filopods (B). The platelet undergoes further shape change as it adheres to the surface (C) and spreads out once firmly adhered (D). Taken from Kuwahara [105]. 31

Figure 1.13: The glycocalyx is a dynamic structure which is attached to the endothelial cells and interacts with the flowing blood in the vessel. Taken from Pries et al [134]. 37

Figure 1.14: The different clot types observed in cerebral aneurysms. Type 1 is a concentric thrombus, type 2 is an eccentric thrombus and type 3 is an aneurysm with multiple lobes and thrombus is found in one of the lobes.

Type 4 is a thrombus which fully occludes the aneurysm sac, type 5 is a canalized thrombus and type 6 is a thrombus induced by the presence of foreign material, such as coils. Taken from Lawton et al [148].....42

Figure 1.15: Diagrams showing different thrombus patterns following aneurysm rupture. (A) shows the outside arrest pattern where the clot develops outside the aneurysm sac to arrest bleeding while (B) is the inside arrest pattern. In this case, the clot develops on the inside of the sac. Taken from Ishikawa [150].....43

Figure 2.1: Forces that act on a mesoscale particle according to the model developed by Filipovic et al [158]. The resultant force is the sum of attractive, repulsive, dissipative and random forces. 52

Figure 2.2: Platelet model presented by Purvis et al [159]. The model accounts for different reactions with platelet activation and inhibition. The model also compartmentalizes the different signals.....53

Figure 2.3: The mathematical model developed by Basmadjian [161]. The Leveque region is thin boundary layer found near the wall. For vessels with smaller diameters, the Leveque region needs to be taken into serious consideration as it cannot be considered negligible. For larger vessels, conditions in the boundary layer can be applied as boundary conditions....55

Figure 2.4: The reaction network used by Anand et al [162]. The model describes clot development from inception to lysis. Plus signs indicate activation of an

inactive protein while minus signs indicate deactivation of an active protein. 56

Figure 2.5: Clot initiation, propagation and localization as described by Pantaleev et al [17]. The important role of different cell membranes is highlighted. 57

Figure 2.6: Reaction network used by Bodnar and Sequeira in their reaction-diffusion-convection model [163]. 59

Figure 2.7: The coagulation process and the various surfaces on which it takes place. This diagram represents the Fogelson model and the different aspects of that model [167].....61

Figure 2.8: A multiscale model presented by Xu et al [168]. Flow is considered on a continuum level while cell activity is considered on a microscale level. 62

Figure 2.9: Bedekar et al consider the different roles of platelets, thrombin and antithrombin in their model of clotting [18]. The model is applied in anatomically realistic aneurysm geometries. 63

Figure 2.10: The abdominal aortic aneurysm geometry used by Biasetti et al [21]. The model accounts for both mechanical and biochemical factors. 64

Figure 2.11: Rayz et al use a virtual ink test to calculate residence time of flow in the aneurysm geometry [19]. Ink is injected at the inlet and its movement through the geometry is tracked.....65

Figure 2.12: Clot development seen in the aneurysm sac for Ouared et al's model [20]. The processes of clot growth and initiation are governed by shear rate. 66

Figure 2.13: The relationship between the different physiological clotting models presented in this chapter and the different components which they model. 67

Figure 2.14: The relationship between the different pathological (cerebral aneurysm) clotting models presented in this chapter and the different components which they model.....67

Figure 3.1: The fluid element. The different letters indicate different sides of the element and show the direction conventions used. E and W are east and west, respectively. N is north, S is south, T is top and B is bottom. P is the cell centre. Adapted from Versteeg and Malalasekera [171]. 72

Figure 3.2: The SIMPLEC algorithm. There are no direct equations for solving pressure in the momentum equations. A pressure field is guessed and used to solve for velocity. A correction is then calculated and used to update the pressure and velocity fields. The process is repeated until convergence is reached. Adapted from Versteeg and Malalasekera [171]. 78

Figure 3.3: Classification of the different regions of the implicit function. Points which have a value less than zero are on the interior while those with a value greater are on the exterior. Those that equal zero are on the interface or boundary. Adapted from Osher and Fedkiw [176]. 89

Figure 4.1: An automated calibrated thrombogram. This shows the thrombin profile for a specific patient over time, allowing for the determination of hypocoagulability and hypercoagulability states. Taken from Hemker et al [156]. 108

Figure 4.2: The idealised, two-dimensional artery which is used for all simulations in this study. Tissue factor is expressed along the injured wall. Inactive blood proteins are present at the start of simulation and also enter at the inlet. These are changed to their active form as they react with tissue factor and other proteins. 112

Figure 4.3: Network diagram of the Wagenvoord model. Tissue factor (TF) initiates the process of clotting and results in the eventual formation of thrombin (TH). Antithrombin (AT) then inhibits the activity of thrombin by forming the product INACT. 118

Figure 4.4: (A) The initiation phase of the Mann model. Tissue factor (TF) initiates the process of initiation and the end result is the formation of a small amount of thrombin (TH). Tissue factor pathway inhibitor (TFPI) inhibits the action of TF. (B) The propagation phase of the Mann model results in the amplification of thrombin. Antithrombin inhibits the action of thrombin and other active proteins. 120

Figure 4.5: Grid independence study for an idealised, two-dimensional artery. 122

Figure 4.6: Graph illustrating the thrombin concentration over a period of 1200s

for four different critical thrombin concentrations. The critical thrombin concentration signals the end of the initiation phase and the start of the amplification phase. 123

Figure 4.7: Thrombin concentration over a range of different critical thrombin concentrations. The blue block for THCrit15 at 1200s signifies divergence of the solution. Both the THCrit15 and THCrit12 clots are rather dramatic, a situation which possibly does not represent the *in vivo* behaviour of the real system. 124

Figure 4.8: Graph illustrating the intrinsic tenase concentration over a period of 1200s for four different critical thrombin concentrations. The critical thrombin concentration signals the end of the initiation phase and the start of the amplification phase. 125

Figure 4.9: Graph illustrating the velocity magnitude at the centre of the rectangular domain over time. The velocity examined over a range of critical thrombin concentrations. 126

Figure 4.10: Velocity plot for different critical thrombin concentrations. The clot has a significant impact on the flow field for both THCrit15 and THCrit12. At 1200s, THCrit15 has diverged. 127

Figure 4.11: Porosity over time for different critical thrombin concentration. The plot complements the velocity plot and illustrates how regions of reduced porosity correspond with decreased flow velocity. 128

Figure 4.12: The effect of tissue factor exposure time on thrombin concentration in the system. The exposure time has a direct influence on the amount of extrinsic tenase that can be formed and that, in turn, influences the rate at which thrombin forms. 129

Figure 4.13: Thrombin concentration for different tissue factor exposure times. The difference is less dramatic as the exposure time increases. The greatest difference can be seen for an exposure time of 5 seconds for all time steps. 130

Figure 4.14: The effect of tissue factor concentration on thrombin production in the system over 1200s. The tissue factor is expressed at the vessel wall and the concentration remains constant throughout the simulation..... 131

Figure 4.15: The variation in thrombin concentration over a range of initial tissue factor concentrations. In this case, tissue factor is surface bound. Similar maximum thrombin concentrations are reached for all the cases at 1200s. 132

Figure 4.16: The effect of varying the initial tissue factor concentration on thrombin production. The system is modelled by using blood-borne tissue factor which is introduced as a flux at the injured vessel wall. 133

Figure 4.17: Thrombin concentration over a variation of initial blood-borne tissue factor concentrations. The most dramatic difference is noted for bbTFconc9 which diverges by 600s. 134

Figure 4.18: Velocity plot for different blood-borne tissue factor concentrations. The bbTFconc9 case diverges at 600s as the clot grows to occlude the vessel as seen by the low flow velocity at 300s. 135

Figure 4.19: Porosity contour plot over a range of initial blood-borne tissue factor concentrations. The bbTFconc9 case shows the most dramatic clot growth which eventually results in occlusion at 600s. 136

Figure 4.20: The effect of blood-borne tissue factor diffusivity on thrombin production. The diffusivity indicates the rate at which a change in tissue factor concentration is propagated through the fluid. 137

Figure 4.21: The effective of blood-borne tissue factor diffusivity on thrombin concentration. The bbTFdiff7 case shows the greatest diffusion of thrombin however the peak thrombin value is lower than that of the other cases. ... 138

Figure 4.22: Thrombin concentration for the Wagenvoord and Mann models. The results here are shown for surface bound tissue factor. 139

Figure 4.23: Thrombin contour profile for the Wagenvoord and Mann models. Thrombin production is limited to the same region but concentrations differ. 140

Figure 4.24: Thrombin profile for the Mann and Wagenvoord models. The plot shows thrombin concentration for blood-borne tissue factor. 141

Figure 4.25: Thrombin contour profile for the blood-borne tissue factor. The profiles compare the Wagenvoord and Mann models. 142

Figure 4.26: Comparison between surface-bound tissue factor results presented in this work and Butenas' work [157]. 143

Figure 5.1: The geometry used by Wootton et al for investigating occlusion risk in patients with stenosis [199]. Flow moves from left to right and the centre portion at 0.0cm is the narrowest point in the vessel. This represents the stenosed region. 160

Figure 5.2: Aneurysm geometry used for all the initiation and propagation simulations. The geometry is one of an idealised aneurysm with a relatively wide neck. Flow moves from the inlet, passes through the parent artery and the aneurysm and then exits at the outlet. This geometry was adapted from a study conducted by Mulder et al [203]. 166

Figure 5.3: The different initiating surfaces used to achieve different types of clot growth. The whole aneurysm wall is initiated to achieve a concentric thrombus, half of the sac is initiated for thrombus which fully occludes the sac (complete) and a quarter of the sac is initiated for eccentric thrombus. Although counter-intuitive, the concentric clot is achieved by initiating damage on the whole wall while a fully occlusive clot is achieved through the top half being damaged. 168

Figure 5.4: A non-conforming Cartesian mesh created for the idealised aneurysm geometry (single plane shown in this figure for clarity). The near-boundary mesh is finer than the cells in the middle of the domain. 169

Figure 5.5: Clot growth in cases where the propagation velocity is proportional to mechanical factors. The direct strain rate case results in complete occlusion of the aneurysm sac but also results in divergence of the flow field. 173

Figure 5.6: Clot propagation under the influence of different biochemical species. Linking the propagation velocity to extrinsic tenase yields the same results as linking it to total tenase. A direct relationship with thrombin results in a slower growth rate.....174

Figure 5.7: A comparison of propagation velocities with different relationships to thrombin. The direct relationship with thrombin is seen for 'Direct', an accelerated direct relationship is seen for 'Direct Fast' and an inverse relationship is seen for 'Inverse'.....175

Figure 5.8: Clot propagation for different starting concentrations of tissue factor. TFconc18 shows not clot growth at 90s. 176

Figure 5.9: Clot propagation for different critical strain rate values at which tissue factor is expressed. No growth is seen for SRcrit500g and SRcrit800 while similar trends are observed for SRcrit100 and SRcrit500l. 177

Figure 5.10: The effect of different initiation locations on clot development. An eccentric, complete and concentric clot can be formed from varying the location of 'damaged' endothelium. The location of the damage is illustrated in Figure 5.3. 178

Figure 6.1: The most common sites for aneurysms. The geometries used in this chapter are aneurysms on the internal carotid artery and the middle cerebral artery. Taken from Brisman et al [3]. 194

Figure 6.2: Case 1 - The giant aneurysm on the internal carotid artery. The inlet and one of the outlets for the geometry are a part of the artery itself. The other outlet, opposite the aneurysm, is the ophthalmic artery which supplies blood to the eye. 194

Figure 6.3: Case 2 - The aneurysm on the middle cerebral artery. The inlet and outlet of the geometry are located on the MCA itself. The aneurysm developed at a bend in the artery. 195

Figure 6.4: Case 3 - An internal carotid artery with a giant, wide-necked aneurysm at a bifurcation. 195

Figure 6.5: Clot surface for the ICA Giant Aneurysm case. Clot propagation is much more prominent in the case with the flow diverter. The case without the flow diverter illustrates almost no clot growth. 201

Figure 6.6: Clot growth and flow dynamics for the Case 1 without flow diverter placement. Little thrombin is expressed for all the time steps. 202

Figure 6.7: Clot development and flow dynamics for the case with the flow diverter. Thrombin production is very noticeable at 30s and 45s. 203

Figure 6.8: Thrombus development prior to and after the placement of a flow diverter for the middle cerebral artery. The clot which develops after the

flow diverter has been put in place extends into the parent artery and is likely to result in occlusion. 204

Figure 6.9: No clot is seen in the aneurysm prior to flow diverter placement. The strain rate on the aneurysm wall exceeds the threshold hence no tissue factor is released and no thrombin is formed. 205

Figure 6.10: Thrombus development in the middle cerebral artery after flow diverter placement. The strain rate and streamlines remain fairly constant as the clot propagates. Once the clot propagates into the parent vessel after 120s, the flow field diverges as the vessel is occluded. 206

Figure 6.11: Clot growth with and without a flow diverter for Case 3. Significant clot growth is observed in both cases however the clot advances more rapidly in the case with a flow diverter. 207

Figure 6.12: Clot growth, strain rate and thrombin concentration for Case 3 without a stent. Thrombin is produced at the dome of the aneurysm and as a result, clot propagation is seen in that region. 208

Figure 6.13: Clot growth, strain rate and thrombin concentration for Case 3 with a flow diverter. Strain rate is uniformly low across the aneurysm dome. Clot propagation is initiated at the dome. 209

Table 4.1: Simulation names and parameters for all simulations carried out in this study. 111

Table 4.2: The grid and time step sizes for the different grid independence meshes. 113

Table 4.3: Properties of proteins that participate in coagulation. The Y and N in the final two columns indicate whether or not the proteins are accounted for in the respective model. Y indicates participation while N indicates the absence of that protein 115

Table 4.4: Reaction steps and rates for the Wagenvoord model. 119

Table 4.5: Reaction steps and rates for the Mann model. 121

Table 4.6: Comparison between results presented in this chapter and other papers. 145

Table 5.1: Parameters used for the propagation and initiation runs presented in this chapter. 167

Table 6.1: Input parameters for the different geometries used in this chapter. .. 196

1. Motivation and Introduction

This chapter discusses the need and envisaged usage and value for a computational model of clotting, coupled with realistic haemodynamics, in cerebral aneurysms. The Introduction gives a background of cerebral aneurysms, physiological clotting and clotting in aneurysms.

1.1. Motivation

Healthcare organisations around the world have predicted that the prevalence of cardiovascular disease and non-communicable diseases is likely to rise dramatically in the next few decades. In 2002, ischaemic heart disease and cerebrovascular disease were the leading causes of death in the world [1]. The projection for 2030 remains the same. Initially, it was believed that this trend would be observed in developed countries due to the increase in the number of individuals living to an advanced age. It is now evident that developing countries will also need to prepare their healthcare sectors to deal with this challenge, as substantial lifestyle changes have been observed alongside significant population growth.

A cerebral aneurysm is a dilation of the blood vessel caused by a weakening of the vessel wall layers. The result, seen in Figure 1.1, is a balloon-like sac which is at risk of rupture.

Cerebral aneurysms account for a significant proportion of cerebrovascular disease cases [2]. The greatest risk with aneurysms is rupture of the sac, which results in bleeding and subsequent morbidity or mortality.

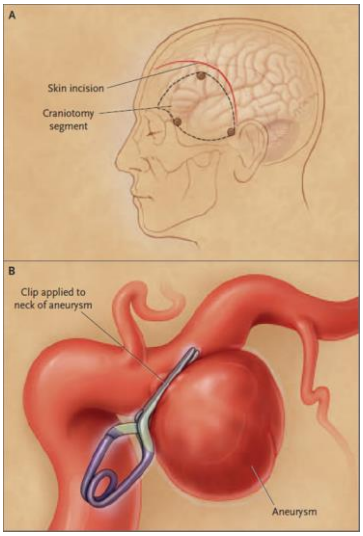


Figure 1.1: A cerebral aneurysm is a balloon-like bulge that develops from the wall of a weakened blood vessel. Clipping is a surgical technique employed for cerebral aneurysm treatment. A craniotomy is performed by a neurosurgeon (A) and the aneurysm is clipped at the neck, preventing further flow into the aneurysm sac (B). Taken from Brisman et al [3]**.**

There is consensus that ruptured cerebral aneurysms need to be dealt with promptly, in order to mitigate damage. There is less clarity on the treatment and management of unruptured cerebral aneurysms [4], [5]. Treatment methods can either be surgical or endovascular. Clipping is a surgical method which is used to treat cerebral aneurysms and can be seen in Figure 1.1. The placement of a clip isolates the aneurysm from the parent vessel, reducing the risk of rupture. Endovascular methods have become more viable and are increasingly employed for treatment. The use of coiling, stents or flow diverters has

become standard practice. Coiling is a popular endovascular treatment and is illustrated in Figure 1.2.

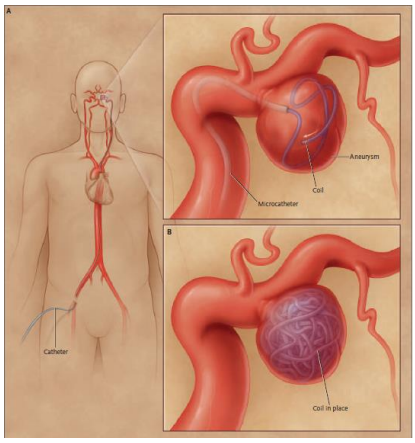


Figure 1.2: Endovascular coiling in the aneurysm sac encourages the development of a clot which occludes the sac. A catheter is inserted into the femoral artery and is navigated to the relevant cranial artery. A microcatheter then delivers the coils into the aneurysm and the process is continued until the sac has been filled with coils. Taken from Brisman [3]**.**

For wide-necked aneurysms, the coils are often supported by a stent placed in the parent artery. This technique is illustrated in Figure 1.3.

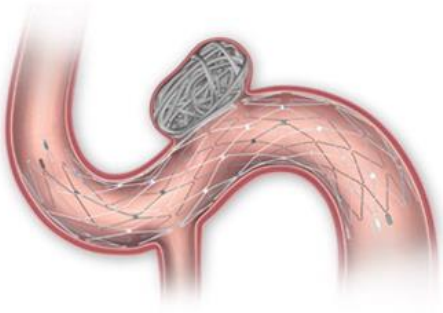


Figure 1.3: Stent assisted coiling can be used in cases where the aneurysm neck is too wide for coiling alone. The stent provides a scaffold which supports the coils once they are placed in the aneurysm sac. Taken from Stryker Neuroform stent promotional material [6]**.**

Finally, flow diverters are often employed for giant aneurysms and are seen in Figure 1.4. The porosity of flow diverters is lower than that of ordinary stents, resulting in reduced

flow into the aneurysm sac.

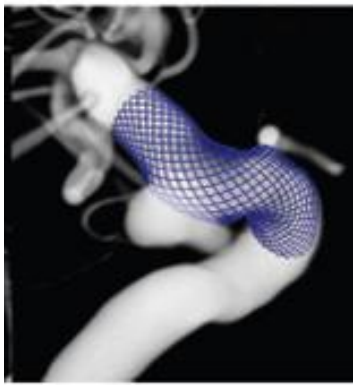


Figure 1.4: A flow diverter is similar to a stent in design however it is far less porous. The purpose of the implant is to reduce flow into the aneurysm sac and redirect it along the parent vessel. The reduced flow in the aneurysm should encourage clot development. Taken from Larrabide et al [7]**.**

A recent challenge has been the dilemma which arises when an aneurysm is accidentally sighted during routine scans. Rinkel et al noted that risk of rupture in aneurysm cases is 0.7% [8]. A clinician is likely to treat an aneurysm which would have remained asymptomatic throughout the life of the individual. With advances in imaging technology, this situation is increasingly common and is a burden on healthcare systems. Alternatively, the decision not to treat a seemingly benign aneurysm could later prove fatal should the aneurysm rupture.

The aim of endovascular treatment is the reduction of flow into the aneurysm and subsequent reduction of vorticity within the sac [9–11]. The reduced flow within the sac provides a suitable setting for the formation of a clot. The presence of a clot in the sac can

stabilise the aneurysm and further prevent complex flow. The flow is redirected back along the parent vessel, reducing the risk of rupture of the aneurysm sac. This outcome has been observed in most cases but is not guaranteed, as blood clotting is a highly patient specific process [12]. The wrong type of clot can cause further complications. In some cases, spontaneous clotting is observed in patients [13]. As with treatment-induced clotting, the effect of the clot is dependent on the patient [14]. The presence of the clot can either accelerate the road to rupture or stabilise the situation by occluding the aneurysm and preventing rupture.

Various computational models of physiological clotting are presented in the literature [15–17]. Some of these models are developed for aneurysm geometries [18–21]. The gap in the literature is a model which accounts for flow, biochemical reactions, patient-derived geometries and the clot's effect on the flow field. A computational tool which would be able to predict clot growth in cerebral aneurysms by incorporating these factors would be highly desirable, since it would serve a dual purpose. The main function of the tool would be to predict clot growth with and without endovascular intervention for specific patients. Such a tool could be used by a clinician for interventional planning prior to treatment. The secondary purpose of such a platform would be to elucidate features of clotting in aneurysms which, due to the very complex and non-linear interaction of biochemistry,

cellular mechanics and haemodynamics, remain poorly understood, if at all. The observation of clot initiation and propagation in real-time *in vivo* is difficult as clot development often takes place unannounced.

This thesis presents a computational framework which is able to predict clot growth in patient-specific cerebral aneurysm geometries. While some of the features of the model are based on assumptions, these can be altered quite easily as more experimental information becomes available. In the studies presented, various aspects of physiological clotting and clotting in aneurysms are explored using this framework. The model presented is the continuation of Timothy Bowker's work (a former DPhil student in the research group) [22]. He developed a two-dimensional model of clotting in an arteriole where clot growth was prescribed by a specified constant velocity. He also adapted the Level Set method for use in three-dimensional aneurysm geometries but excluded the role of different biochemical species. In this thesis, the two-dimensional model presented by Tim Bowker was further developed for use in an artery and clot growth is governed by biochemical species concentrations. In addition, the biochemistry code was designed to work on any grid, that is, it could be applied to two-dimensional, axisymmetric or three-dimensional geometries. The unique contribution of this thesis is the combination of computational fluid dynamics, biochemistry and Level Set methods in complex three-dimensional

aneurysm geometries, with and without interventional devices, for clot inception and growth prediction and interventional planning.

1.2. Aneurysms

G.B. Morgagni, the government death inspector in Italy, published a book in 1761 in which he suggested that most subarachnoid haemorrhage cases were the result of aneurysms which had ruptured [2]. This is one of the earliest written records of an aneurysm. The combination of complex flow conditions within the aneurysm sac and weakened vessel wall layers is thought to contribute to both the initiation and rupture of the aneurysm [23]. Aneurysms most commonly occur on arteries supplying blood to the brain (cerebral aneurysms) as seen in Figure 1.5. They are also found on the aorta (abdominal aortic aneurysms).

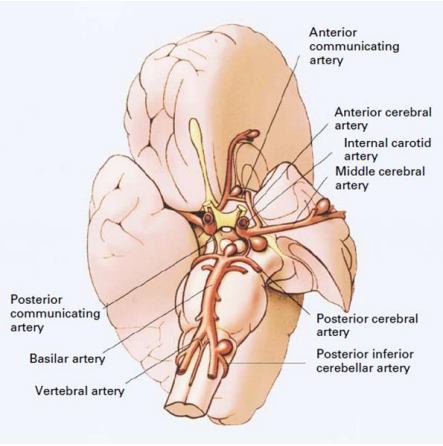


Figure 1.5: Common sites for cerebral aneurysms found on blood vessels supplying blood to the brain. The majority of these vessels originate in the circle of Willis and cerebral aneurysms are typically found at bifurcations. Taken from Schievink [10]

Aneurysms are classified according to size with those less than 10mm in size considered *small*, those between 10 – 25mm *large* and those greater than 25mm *giant* [4]. Depending on the methods employed for detection, aneurysms have been found in 2 – 6% of the population. It was also noted that the majority of these aneurysms were small and the risk of rupture was quite low (0.7%) [8]. Even though this risk is low, subarachnoid haemorrhage which takes place when aneurysms rupture results in a mortality rate of 32 – 67%. Those patients that do survive rupture are often left disabled [24].

Cerebral aneurysms are identified as saccular, fusiform or dissecting as seen in Figure 1.6. *Saccular* aneurysms occur as a result of changes that occur in the muscular layer of the vessel wall, resulting in the characteristic 'berry' shape. This is the most common type of aneurysm (90%) in the brain and is most likely to be found in bifurcation regions of arteries which originate at the circle of Willis [25]. *Saccular* aneurysms are, again, strongly linked to subarachnoid haemorrhage [26].

Fusiform aneurysms are often found on tortuous vessels within the vertebrobasilar system. They usually develop to quite a large size but are not often associated with subarachnoid haemorrhage. *Dissecting* aneurysms form when the vessel wall tears and develop as blood passes through a false lumen while the true lumen is collapsed [23].

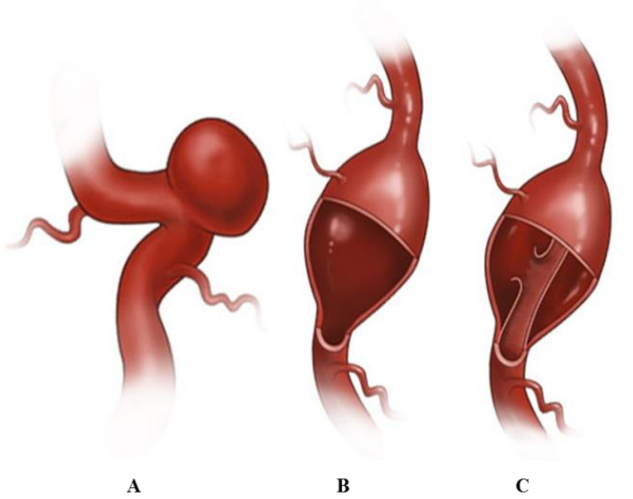


Figure 1.6: Three main types of cerebral aneurysms. Saccular aneurysms (A), fusiform aneurysms (B) and dissecting aneurysms (C). Taken from Johns Hopkins Medicine Health Library [27]**.**

1.2.1. Vascular wall structure, remodelling and aneurysms

The normal arterial wall consists of three layers as seen in Figure 1.7. The *intima* is the innermost layer which consists of endothelial cells that come into contact with flowing blood. The layer ensures that flowing blood does not come into contact with the subendothelial layers. It often undergoes changes with aging and disease. The *media* is the middle layer and consists of smooth muscle cells, collagen and elastin fibres. It is separated from the intima and adventitia by the internal elastic lamina and external elastic lamina, respectively. This layer makes the most significant contribution to the mechanical properties of the blood vessel [28]. The *adventitia* is surrounded by loose connective tissue and consists mainly of fibroblasts and collagen. The adventitial layer is usually quite stiff and its thickness is related to vessel function. Cerebral vessels have a thin adventitial layer.

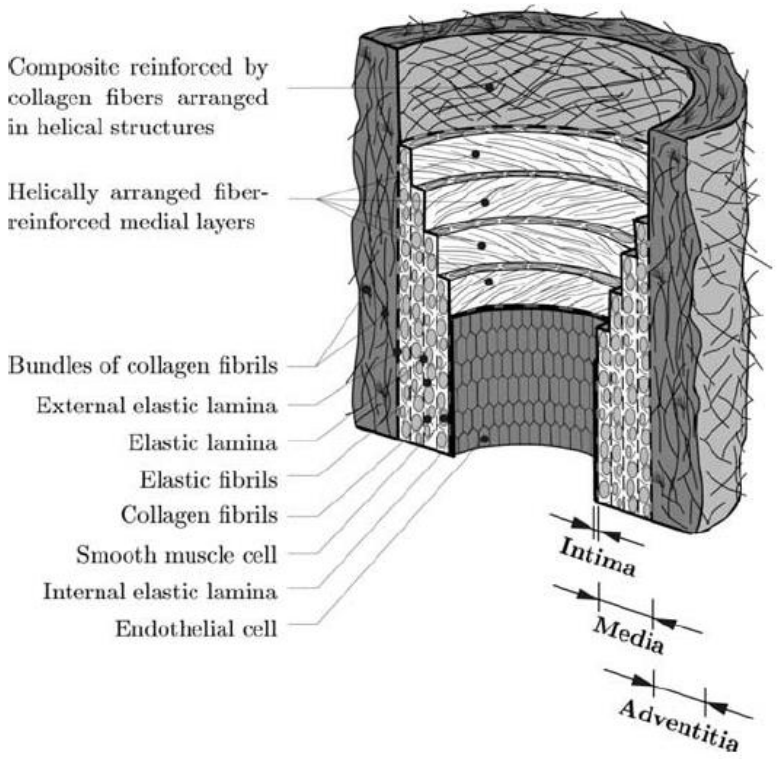


Figure 1.7: The arterial wall is composed of three layers. The outermost adventitial layer is surrounded by loose connective tissue. The medial layer is made up of collagen and elastic fibres. The intima comes into contact with flowing blood. Taken from Holzapfel et al [28]**.**

Vascular matrix remodelling is observed in most cerebral artery tissue while it is not as prevalent in normal arteries. There is consensus nowadays that such remodelling may contribute to aneurysm initiation and growth [29]. The changes in the wall are not homogeneous as more degeneration is often observed towards the aneurysm dome [30]. Degeneration of elastic fibres and disruption of the internal elastic lamina leads to weakening of the vessel wall, contributing to aneurysm formation [31]. Macrophage infiltration also contributes to vessel wall weakening [32]. Changes are observed

throughout all the layers of the aneurysm wall. The wall is generally characterized by a loss of elastin and a high concentration of collagen [33]. Significant stretching is noted in the adventitial layer [34]. This is accompanied by a loss of elastic fibrils and an accumulation of lymphocytes near the adventitia. Loss of smooth muscle cells has been noted in the medial layer [32], [35]. The endothelial layer can either be well-organised with a regular pattern of cells or it can have an irregular surface and appear quite thin along the aneurysm neck [36]. The pattern is linked to the nature of near wall flow in that region. Sufficient aneurysm remodelling often leads to rupture and various attempts have been made to identify property differences between ruptured and unruptured tissue [32], [35].

1.2.2. Detection, symptoms and risk factors of aneurysms

Most patients with cerebral aneurysms remain asymptomatic and aneurysms are often detected accidentally. The diagnosis may take place while a scan is conducted for another condition or for routine check-up. Scans may be conducted with digital subtraction angiography, magnetic resonance angiography, computed tomographic angiography or transcranial Doppler ultrasonography. The other major clinical, symptomatic presentation is subarachnoid haemorrhage. Such a patient may present with severe headache accompanied by loss of consciousness, vomiting, nausea and focal neurological deficits

[23]. Other presentations include *mass effects* (i.e., pressure of the aneurysm body on surrounding neuronal tissue) and cerebral ischaemia. The most typical symptom of mass effect is headache. Cerebral ischaemia is often a result of embolisation from the aneurysm sac and patients present with typical stroke symptoms such as headache, loss of use of limbs, nausea and vomiting [12], [37], [38].

It is understood that both genetic and environmental factors contribute to an increased risk of aneurysm development. Intracranial aneurysms were found in 9% of first degree family relatives over the age of thirty of people who had had aneurysms [39]. These findings were presented as results for a study conducted in Finland. People with autosomal dominant polycystic kidney disease are at a higher risk of developing intracranial aneurysms [40]. They are also at greater risk of developing additional intracranial aneurysms or having existing aneurysms grow in size [41]. Intracranial aneurysms are more common in women than in men, in persons over the age of fifty, in smokers and in individuals who have hypertension [25], [42].

1.2.3. Treatment methods

The main aim of aneurysm treatment is to separate the aneurysm from the rest of the vasculature in an attempt to restore normal haemodynamic conditions. The desired end

result is complete occlusion of the aneurysmal sac by a clot and restoration of normal flow in the parent vessel. An undesirable outcome would be the development of a clot which fills the sac partially. Another undesirable result would be the detachment of part of the aneurysm thrombus and the formation of emboli which may lead to ischaemic events distally.

Treatment options can be divided into three main categories. Observation involves the monitoring of an aneurysm without immediate intervention. Surgical techniques involve direct operation on the aneurysm while endovascular techniques attempt to treat in a minimally invasive manner.

Often, unruptured aneurysms are discovered accidently. Depending on the size of the aneurysm and the history of the patient, a clinician may decide that the best solution is to observe the development of the aneurysm over several check-ups and scans. If the aneurysm is seen to grow and presents risk of rupture, the clinician may decide to intervene. In other cases, the aneurysm remains stable over a long period of time and intervention may be deemed unnecessary and may, in fact, present greater risk than observation [3].

Clipping is a commonly used open surgical method that isolates the aneurysm from the parent vessel and can be seen in Figure 1.1. In 1937, Walter Dandy used this method to cut off blood supply to an aneurysm of the internal carotid artery [43]. He applied a clip across the neck of the aneurysm, preventing any further flow into the sac. Since then, major advances have been made to the technique, making the procedure safer. The use of operative microscopes and dedicated aneurysm clips has reduced the risks originally associated with the operation [5].

The idea of filling an aneurysm sac with wire in order to encourage clotting and subsequent redirection of flow along the parent vessel has been on the mind of doctors for a long time. One of the earliest records is that of Ransokoff, who filled an aortic aneurysm with silver wire fed through a tubular needle in 1886 [44]. Inspired by a successful aortic aneurysm coil intervention that they carried out in 1938, Blakemore and King, together with Werner, successfully introduced coils into an internal carotid artery [45]. Contemporary endovascular coil intervention is based on Guglielmi's detachable platinum coils which, are used for aneurysm sac occlusion [9]. The procedure involves the insertion of a catheter into the common femoral artery and its navigation to the internal carotid or vertebral artery. A microcatheter is then advanced until a view which projects the aneurysm neck and surrounding vessels is obtained. The first platinum coil, roughly the

same size as the aneurysm diameter, is deployed from the microcatheter. This coil provides a frame for subsequent coils which fill the sac. The end point is reached once the aneurysm sac is filled. This is indicated by protrusion of the final coil or microcatheter into the parent vessel or by the inability of contrast to enter the aneurysm sac. Current best practice considers the end point to be a packing of 25-35% by volume. The main challenge with coiling is that should the coils *compact* (i.e., occupy a smaller portion of the sac than they originally did), recanalization of the aneurysm sac may occur, resulting in further complications [5]. A diagram of the technique can be seen in Figure 1.2.

Stent assisted coiling allows for the use of coils in wide-necked or giant aneurysms and can be seen in Figure 1.3. Stents are made of super-elastic metals such as nitinol, which allow them to be deployed with minimal damage to the vessel wall. The stent is delivered in a microcatheter and is deployed along the parent vessel such that it covers the aneurysm neck. This provides supportive scaffolding which will hold the coils in place in a wide-necked aneurysm. The coils are then deployed through the gaps of the stent. The challenge of using a stent is that the patient will need to use long term antiplatelet medication to prevent thrombosis within the stent [5].

A *flow diverter* is quite similar to a stent in that it is a tubular structure with a mesh and is

made from highly flexible material. The diagram can be seen in Figure 1.4. Like a stent, it is deployed over the aneurysm neck. The main difference is that a flow diverter aims to reduce flow to the aneurysm sac and redirect it along the parent vessel while a stent provides structural scaffolding for coils. The effect is achieved in flow diverters by making the porosity quite low. The hope is that the significantly slowed flow in the aneurysm sac will clot, resulting in occlusion and reducing risk of rupture. The challenge with flow diverters is that they may accidentally reduce flow to other surrounding vessels. It would also prove difficult to deploy coils through the gaps in a flow diverter should secondary intervention be necessary [5].

1.3. Coagulation under physiological conditions

The haemostatic system maintains the integrity of the circulatory system. There are several biological players in the process of thrombus development and successful participation of each component ensures proper functioning of the system. When the vascular wall is intact, the endothelial cells express substances which ensure that coagulation does not occur. Damage to this wall layer results in the formation of a platelet plug and triggers the onset of coagulation. The end product of this process is a fibrin matrix which reinforces and stabilises the platelet plug, as illustrated in Figure 1.8. Once the vessel wall has been repaired, fibrinolysis occurs, ensuring that the clot is dissolved. When functioning properly,

the system sustains a fine balance between procoagulant (clot-forming) and anticoagulant (clot-dissolving) mechanisms. Disruption of this balance results in excessive bleeding or haemophilia if the anticoagulant system is favoured and thrombotic disease if the process is dominated by the procoagulant system [46–55].

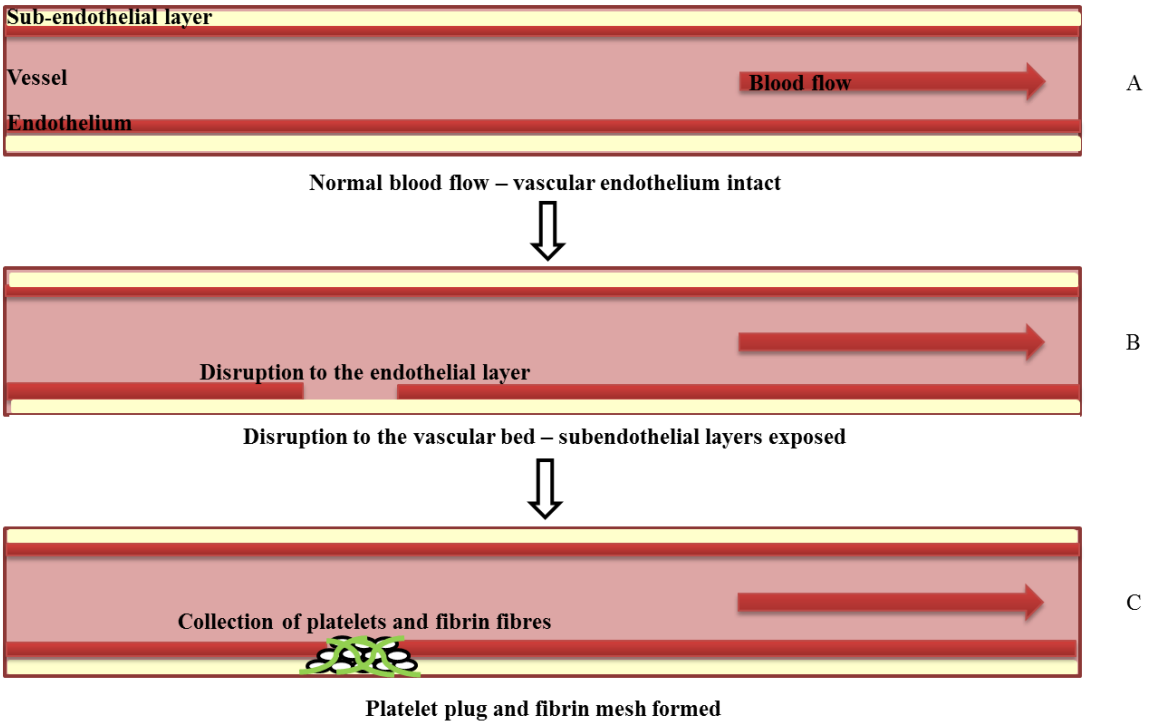


Figure 1.8: The process of coagulation. (A) When there is no injury to the wall, blood flow continues along the main vessel which is lined with endothelial cells. (B) Injury of the blood vessel wall results in the removal of the endothelial layer and exposure of the subendothelial layers and tissue factor. (C) The haemostatic system stimulates a series of responses which result in the formation of a platelet plug and a fibrin mesh.

In 1856, Virchow hypothesized that the three main contributors to clot formation are the state of the vascular endothelium, blood composition and local haemodynamics [56]. A similar hypothesis was presented a few decades later by Aschoff in 1924 [57]. He added an

additional category, by distinguishing between changes in blood plasma and blood elements. For Virchow, blood composition incorporated both of these factors. The interaction that takes place between these factors is rather complex and deeper examination of this system would improve current understanding of clot formation, treatment methods of clot-related diseases and clotting under pathological conditions.

1.3.1. Coagulation models

There are two main coagulation models presented in the literature. The traditional hypothesis, presented by two separate teams in 1964, is based on the waterfall model [58] or the cascade model [59] and is developed from observations of an *in vitro* coagulation cascade setup. Further development of this initial model led to the second hypothesis a few decades later. The cell-based coagulation model places greater emphasis on the role played by membrane surfaces in coagulation *in vivo* and proposes some variations to the traditional hypothesis [47–49], [51], [55], [60–63]. These two models are described and discussed below.

1.3.1.1. Cascade or waterfall model of coagulation

The traditional hypothesis of coagulation proposes the formation of a platelet plug followed by the development of a fibrin matrix. Upon injury to the vascular wall, von

Willebrand's factor (vWF) is expressed by the endothelial cells, causing platelets to attach to the subendothelial collagen, a layer which is not exposed unless damage has occurred [64], [65]. These platelets are then activated, further recruiting more platelets. The final result of this process is the formation of a platelet plug.

Following the aggregation and activation of platelets, a series of reactions take place, forming a fibrin[1] mesh which holds the platelets firmly in place. The coagulation cascade or waterfall model takes into account two possible starting points, the *intrinsic* pathway and the *extrinsic* pathway. After a few reaction steps, both pathways reach a common pathway which leads to the formation of fibrin. The model is described as a series of enzymatic reactions with each step representing the transformation of a protein from its inactive to active form. The activated protein then acts as an enzyme for the subsequent reaction. Fibrin, the final product, is formed from fibrinogen and is the only protein which does not act as an enzyme to any other reaction. At various stages of the pathway, calcium ions and phospholipid membranes contribute to protein activation [58], [59].

The *intrinsic* pathway is triggered by the activation of factor XII which combines with prekallikrein and high molecular weight kininogen (HMWK). In an *in vitro* setup, the

[1] Fibrin is the end product of the coagulation cascade during clot formation. It is a fibrous protein which links with other fibrin fibres to form a mesh which holds the activated platelets in place.

process can also be initiated by bringing plasma into contact with glass or other foreign substances. The factor XII-prekallikrein-HMWK complex acts as an enzyme to the reaction which forms activated factor XI (XIa). Factor XIa catalyses the activation of factor IX. Factor IXa combines with calcium and cofactor VIIIa to catalyse factor X activation. The partial thromboplastin time[2] indicates how well the *intrinsic* pathway is functioning. The *extrinsic* pathway begins with the activation of factor VII as a result of exposure to tissue factor (TF). Factor VIIa then catalyses the activation of factor X. A measure of the efficiency of the *extrinsic* pathway is obtained from the prothrombin time[3].

The common pathway takes effect from the activation of factor X. Factor Xa combines with calcium and cofactor Va to change prothrombin (factor II) into thrombin (factor IIa). Thrombin is the enzyme that participates in the reaction which results in the formation of fibrin from fibrinogen [58], [59]. Finally, a fibrin cross-linking factor ensures that a stable, insoluble fibrin clot is formed [66], [67]. Figure 1.9 illustrates the classic coagulation cascade and includes both the *intrinsic*, *extrinsic* and *common* pathways.

[2] The partial thromboplastin time test is carried out by bringing blood into contact with phospholipids, calcium and a foreign surface such as silica or kaolin. The test measures how long it takes for a clot to form. It is partial because tissue factor is missing from the blood.

[3] The prothrombin time test is initiated when tissue factor is added to plasma. The test then measures how long it takes for a clot to form.

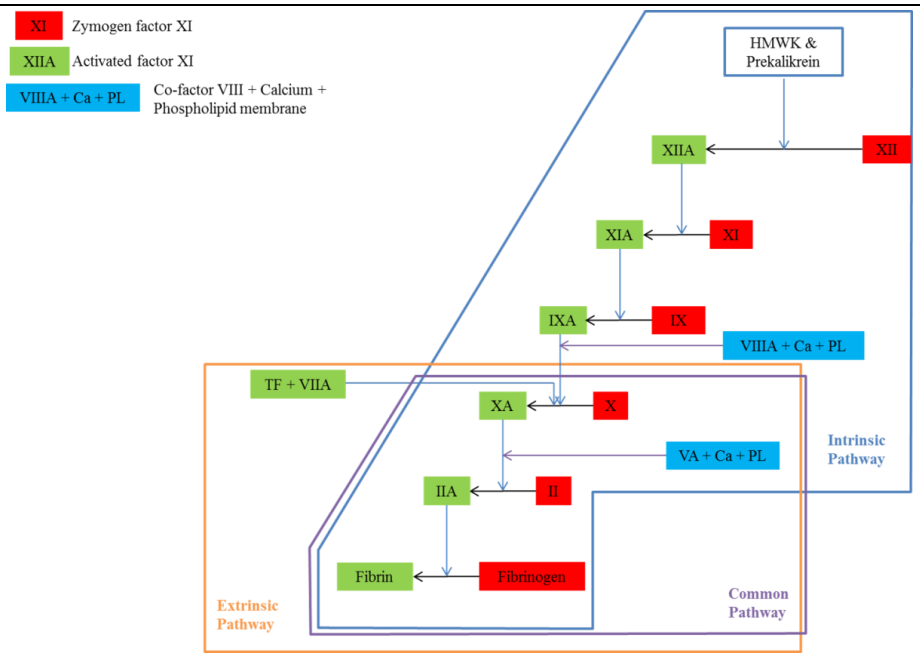


Figure 1.9: The traditional waterfall coagulation cascade. Initiation in the *intrinsic* pathway is initiated by the activation of factor XII by high molecular weight kininogen and prekallikrein. The *extrinsic* pathway is initiated by exposure of tissue factor, which combines with factor VIIa. The *common* pathway commences with the activation of factor X and ends with the production of fibrin.

1.3.1.2. Cell-based model of coagulation

The cell-based model of coagulation proposes some variation to the traditional coagulation cascade and suggests that a combination of both the *intrinsic* and *extrinsic* pathways is required for the maintenance of haemostatic balance in the body. The model places emphasis on the important role played by cell membranes in the coagulation process [47], [48], [51], [62], [63], [68]. The process is divided into the initiation, amplification and propagation phases [51], [63]. Another salient feature of this model is the spatial and temporal overlap of the formation of the platelet plug and the fibrin mesh [60], [61]. This

view is supported by data from *in vivo* observations of the microcirculation of a mouse. Such observations are made possible through the use of intravital microscopy [55].

The initiation phase is a fairly inefficient process which results in the production of a small amount of thrombin [49], [68]. In the cell based model, TF is considered the sole initiator of coagulation and is exposed on TF cell-bearing membranes at the site of injury [49], [51], [63]. It binds to factor VIIa to form TF-VIIa. A small percentage of factor VII circulates in the activated form, enabling it to form this important complex. Circulation of an activated factor prior to the expression of tissue factor is unique to factor VII [69–71]. The TF-VIIa complex then activates factors IX and X. Factor IX combines with factor VIII to form more factor X. Factor X then combines with factor V to act as a catalyst in a reaction which results in thrombin from prothrombin. The process is inefficient because factors IX and X combine with co-factors V and VIII before they are in their most active co-factor state [49]. The initiation phase as described here is the process observed *in vivo* following trauma-related injury to the vessel wall [46].

Thrombin is the key participant in the amplification phase as it activates platelets, factor XI and co-factors V and VIII [49], [62], [63], [72]. There are two existing theories of platelet activation [60]. The first theory suggests that platelet activation is thrombin

mediated and results in the formation of the platelet plug.[47], [61]. This type of platelet activation was observed in experimental mice following laser injury [60], [61]. An alternative theory of platelet activation, the collagen mediated pathway, is observed following ferric chloride injury, which is less superficial than laser injury [60]. Ferric chloride injury results in the exposure of the subendothelial collagen layer to which the platelets adhere, further activating and attracting more platelets [60], [61]. The platelets also provide the necessary membrane surface on which some of the reactions in the amplification and propagation phases occur thus limiting the coagulation process to the site of injury [48]. The relative importance of each theory is not yet well understood. The observations made, however, point to the fact that there may be interplay between different mechanisms of platelet activation and aggregation and that the relative role of each may depend on the underlying pathological condition [49], [61], [73].

The amplification phase causes a burst in the production of thrombin [63], [68]. Factor XIa activates factor IX. This activated form of factor IX then combines with co-factor VIIIa to activate factor X [62], [68]. Factor Xa forms a complex with co-factor Va and calcium to activate prothrombin. Thrombin activates fibrinogen, resulting in fibrin [49]. Factor XIII is then activated by thrombin and plays a pivotal role in fibrin cross-linking thus stabilising the clots [74], [75]. The presence of activated factor XIII is observed when a small amount

of fibrinogen (1–2%) has been converted to fibrin. This suggests that the process of cross-linking begins before a thrombus is visible [76]. Both the initiation and amplification phases are illustrated in Figure 1.10.

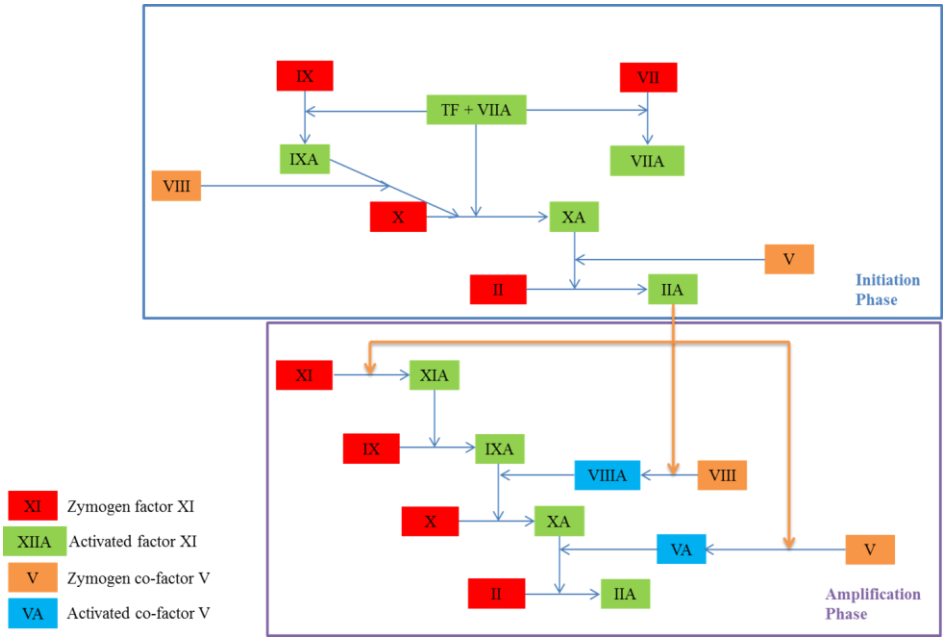


Figure 1.10: Illustrated here are the initiation and amplification phases of the cell-based model of coagulation. In the initiation phase, a small amount of thrombin is produced from a fairly inefficient process. This thrombin then activates other factors which then allow for more rapid and efficient production of more thrombin.

1.3.1.3. Anticoagulant mechanisms

Several mechanisms work together to ensure that the process of coagulation is regulated as shown in Figure 1.11. This prevents excessive procoagulant activity which is often the cause of thrombotic disease. Thrombin binds to thrombomodulin, a membrane protein. Together with the co-factor Protein S, this complex activates Protein C. Activated Protein C (APC) inactivates cofactors Va and VIIIa [77], [78]. This limits the reactions which form

factors Xa and thrombin. Antithrombin (AT) inactivates factors XIa, IXa, Xa, and thrombin [79–84]. Tissue factor pathway inhibitor (TFPI) inhibits the efficacy of the TF-VIIa complex [85]. Fibrinolysis is responsible for eventual clot dissolution once the vessel wall has been repaired. Prior to this, fibrinolysis inhibitor is activated by thrombin (thrombin activated fibrinolysis inhibitor – TAFI) to ensure that the process does not occur prematurely [86]. The fibrinolytic system consists of plasminogen, an inactive protein which is changed to plasmin by tissue plasminogen activators and urokinase. Inefficacy of this system is often the aetiology of thrombosis-related diseases [87].

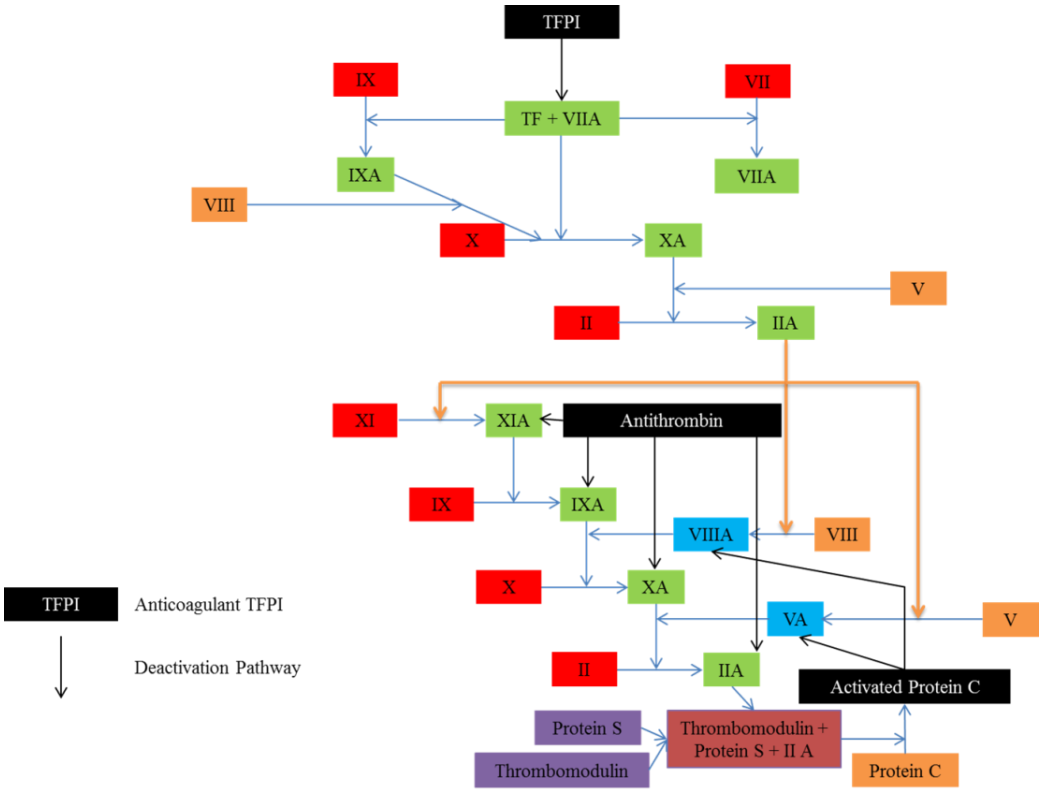


Figure 1.11: Anticoagulation mechanisms regulate the processes which result in the formation of thrombin. Activated Protein C inactivates the co-factor, Antithrombin inactivates the factors and TFPI limits tissue factor activity.

The traditional coagulation cascade or waterfall model of coagulation provided the main framework through which coagulation is understood today. The standardization of nomenclature by the International Committee on Blood Clotting Factors assisted with the partial recognition of the integrated process of coagulation. The cascade managed to incorporate the various reactions necessary for clotting into a framework which clearly illustrated the dependence of the reaction steps on proteins which had been activated earlier on in the sequence. It also pointed out the need for calcium ions and phospholipid membranes for some of the reaction steps. Finally, the model suggested that there were self-regulatory mechanisms in place to stop the process of clotting once enough fibrin had been generated, thus preventing thrombotic disease [58], [59]. This framework gave better direction for further work which would improve understanding of coagulation. An example of further investigation is the work carried out in the late 1970s and 1980s to better understand the role of von Willebrand's factor in platelet attachment at the site of injury [64], [65].

The cell-based model of coagulation evolved from the waterfall model or coagulation cascade as some crucial questions about coagulation remained unanswered. For example, there were doubts about the relative importance of the *intrinsic* pathway due to low incidence of bleeding disease in patients lacking HWMK, prekallikrein and factor XII

despite a prolonged partial thromboplastin time [47–49], [63]. The traditional models also failed to account for bleeding experienced by haemophiliacs. If indeed there are two independent pathways, an intact *extrinsic* pathway should counterbalance deficient proteins in the *intrinsic* pathway, or vice versa [63].

One of the major differences between the two models is that the waterfall or cascade model proposes two separate pathways to fibrin formation while the cell-based model postulates that both pathways work together to ensure that a stable clot is formed [48]. In addition, the cell-based model considers tissue factor as the only protein capable of initiating coagulation *in vivo*. This view is supported by the lack of bleeding disease in patients lacking protein XII, HMWK and prekallikrein. On the contrary, patients with a TF deficiency have never been identified and experimental mice lacking tissue factor do not survive beyond the embryonic stage [88–90]. The cell-based model hypothesis is also supported by the unique roles played by factor Xa activated by the TF-VIIa complex and factor Xa activated by the IXa-VIIIa complex. The former seems to play a more crucial role in platelet activation and in the generation of a small amount of thrombin for the initiation phase. This factor Xa is mostly found in the region of TF-bearing cells. The latter is instrumental in the explosion which leads to large amounts of thrombin generation in the amplification phase and more importantly, is localised to platelet membranes [62], [63],

[68]. This view provides a plausible explanation for patients presenting with haemophilia despite an intact *extrinsic* pathway.

The concentration and size of different proteins in the coagulation process is perceived as an indicator of the role played by each protein. There is a lesser concentration of smaller proteins (e.g. factor VII) which occur earlier on in the coagulation process while those occurring later on circulate in greater quantities and are physically larger (e.g. co-factor V). This supports the cell-based model's amplification phase hypothesis. In addition, platelets and proteins which are relatively large are not able to pass through the normal gaps between endothelial cells. This ensures that if some amount of thrombin is generated, a clot will not form unless injury has occurred and the gap is large enough for these to pass through it [63].

The cell-based model answers some of the questions which were not addressed by the earlier waterfall or cascade model. There are still, however, phenomena which have not as yet been fully elucidated and *in vivo* studies under physiological conditions may prove helpful [46], [51–53], [55], [61], [91], [92]. The discrepancies between the two models provide challenges when attempting to simulate the coagulation process computationally as information for the *in vitro* model may be more readily available than that of the *in vivo*

model. Examples of such challenges include the mechanism by which tissue factor operates and the relative contributions of different proteins during the stages of the coagulation process. Decisions regarding the pathways chosen and the relative weighting of the models are often made based on the availability of information.

1.3.2. Platelets

Max Schultze was the first person to record his findings on '*spherules*', a type of blood fragment which was a component of normal blood [93], [94]. He correctly observed their size to be around 2.5µm and suggested that these particles played a crucial role in coagulation. Bizzozero undertook further investigation of these fragments and published definitive work on the nature and function of '*plaquettes*' or platelets in the 1880s [94–97]. Platelets are anucleate and participate in the process of coagulation by forming a platelet plug upon injury to the blood vessel wall [98], [99]. The main features of this process are the delivery of platelets to the site of injury, deposition on and adhesion to the exposed subendothelial layer, activation and then aggregation of other platelets to the growing mass.

The delivery of platelets and their subsequent interaction with the wall is governed by convection of platelets in the bloodstream and supported by collisions between platelets and

other blood cells [100]. Blood flow or lack thereof is a major determinant of whether or not a clot with platelets and fibrin will form. The rate at which platelets attach to the subendothelial layer is much more rapid than the rate at which platelets are delivered to the site of injury [101]. Platelet-wall interactions correlate with the concentration of red blood cells (haematocrit ratio) and flow parameters such as wall shear rate and average blood flow rate [100–103]. In some cases, platelet deposition is observed where there is no visible injury to the vessel wall. Under such circumstances, deposition is observed in regions where the flow is disturbed [104].

Platelet shape changes are observed at the different thrombogenic stages [105]. Epiflourescence and scanning electron microscopy were used to observe platelet shape changes during platelet adhesion. The process is illustrated in Figure 1.12. Initially, the platelets appear as disc-shaped cells which are easily transportable in the bloodstream. Upon contact with the subendothelial layer and von Willebrand's factor specifically, platelets take on a rolling-ball shape and filopods are extruded along the surface. Once activated, the platelets then assume a hemispherical shape which allows them to form a reversible adhesive bond with the injured surface. A permanent bond is formed when the platelet starts to spread out and its diameter exceeds the initial average size of 2.5µm. It is believed that adhesion occurs most effortlessly at stagnation points. In the circulatory tree, this correlates

with regions of disturbed flow and at branching points [100].

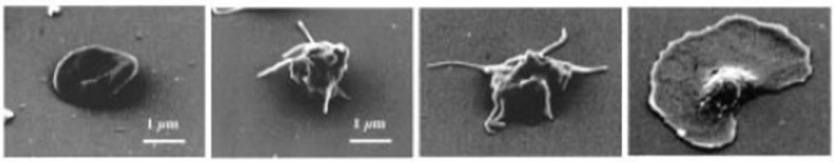


Figure 1.12: The process of platelet activation in coagulation. Under normal circumstances, the platelet circulates in an inactive state and has a disc-like shape (A). Upon contact with the subendothelial layers or other activated platelets, the platelet assumes a spherical shape and extends filopods (B). The platelet undergoes further shape change as it adheres to the surface (C) and spreads out once firmly adhered (D). Taken from Kuwahara [105]**.**

Platelet collisions with erythrocytes in the near wall region are believed to influence the rate at which platelets adhere to the collagen layer [99]. Platelet adhesion is also influenced by shear rate. Turitto et al. concluded that at shear rates less than 200 s^{-1}, platelet adhesion is dependent on physical factors while at shear rates above 800 s^{-1}, the reaction at the surface is limiting and physical factors become insignificant. These factors were determined in an *in vitro* setup [103], [106]. Savage et al. found that platelet adhesion is regulated by two mechanisms. At lower shear rates, fibrinogen and fibrin adhesion is dominant, leading to immediate irreversible attachment. The maximum value of platelet adhesion for this mechanism is seen at $50s^{-1}$. At high shear rates, vWF plays a much more prominent role with adhesion reaching a maximum at $1500s^{-1}$. In the latter case, platelets are captured by vWF on the injured surface and irreversible attachment is later observed [107].

Recent experiments have shown that calcium mobilization within platelets can be used as a marker of platelet activation [73]. Two main pathways of activation have been observed. Experiments where laser injury was inflicted on the vessel wall showed that thrombin was necessary for activation while vWF was not necessarily required. The other main pathway was mediated by collagen [61], [73], [108]. In addition to being released by platelets during activation, adenosine diphosphate (ADP) plays a crucial role in the shape changes which platelets undergo during activation [109], [110].

Accumulation of platelets into the growing thrombus happens in three stages. The first stage is characterised by the addition of platelets to the growing mass. This is followed by the loss of platelets which do not form an adhesive bond to the rest of the aggregate. The final stage is marked by a constant number of platelets which have attached to the clot and represents a stable phase. The net accumulation of platelets to the growing platelet mass is determined by platelet attachment and detachment [111]. In an *in vitro* study of platelet aggregation and adhesion on a layer of collagen, aggregates were observed to be elliptic and were aligned with the direction of flow. The same study reported that following the deposition of a few platelets on the collagen layer, platelets which arrived after that displayed a preference for areas where aggregates were already forming rather than those areas which had no platelet deposition [112]. Effective communication between calcium signals, interplatelet calcium

communication (ICC), ensures that platelets recruited to the growing aggregate form stable adhesive bonds with the rest of the platelet mass [113].

Platelets form aggregates as a result of collisions with other cells and the rate of aggregation is related to shear rate [100], [114]. The presence of red blood cells results in an increase in platelet diffusivity. In most cases, platelet aggregation is induced by adenosine diphosphate (ADP). At low shear rates, spontaneous platelet aggregation may be observed. This is likely to occur at the walls of arterioles or in larger arteries at peak systole. In healthy individuals, the aggregates are likely to be convected away a very short while after formation [115].

Platelets play a central role in the chemical reactions which take place during coagulation. The process by which prothrombin and factor Xa are activated is dependent on the presence of platelet membranes [116]. Platelet TFPI is expressed on the surface of platelets and inhibits the action of the TF-VIIa complex and factor Xa [117]. Patient specificity plays an important role in platelet populations and therefore in the coagulation reaction process. Platelets themselves are not homogeneous and two different subpopulations have been observed within one blood sample. The percentage of each subpopulation for any single patient is dependent on the potency of the various platelet agonists [98].

The embolisation of a clot presents serious complications for the patient and is strongly linked to the behaviour of both individual platelets and the entire platelet mass. It has proven rather challenging to determine the exact factors that contribute to embolisation. Basmadjian presented embolisation risk in a numerical range. Values were determined for shear rate, thrombus height, flow pulsatility and vessel dimension as these factors seem to be the largest contributors to embolisation [118].

1.3.3. Tissue Factor

Tissue factor is an integral membrane protein which plays a key role in the initiation of coagulation [119], [120]. Bovine tissue factor was first purified in 1981 and shortly thereafter, human tissue factor was purified [121], [122]. Unlike other coagulation proteins, it exists in its active state and does not require proteolysis for activation [70], [122]. Under normal circumstances, the protein does not come into contact with the bloodstream as it is confined to the medial and adventitial layers. The protein has also been identified on the plasma membranes of a variety of cells [70].

A study which aimed to determine the localization of TF in the vessel wall and in atherosclerotic plaque concluded that in normal vessels, TF was present in both the medial and adventitial layers. Unlike in atherosclerotic plaque, no TF was present in the

endothelial layer [123]. This supports the view that ordinarily, TF does not come into contact with flowing blood unless the vessel wall has experienced injury. TF was found to be more prominent in some human tissues and organs, and minimal in others. Positive TF staining was observed in the adventitial and medial layers of all blood vessels with the exception of capillaries and post-capillary venules. The brain, lungs and placenta were found to contain a significant amount of TF [124]. Epidermis, bowel and respiratory mucosa, cerebral cortex, myocardium and renal glomeruli also stained positive. No evidence of TF was found in skeletal muscle tissue [125].

In recent years, various studies have attempted to elucidate the existence and role of *blood-borne* tissue factor in coagulation. Following *in vitro* experiments, Nemerson et al found that thrombi developed on substrates which stained negative for TF (glass and TF-negative pig media) contained TF themselves. In addition, TF was isolated from freshly drawn whole blood. The experiments further showed that TF could be found on leukocytes. The researchers suggested that vascular TF could be responsible for clot initiation while blood-borne tissue factor featured in propagation, especially in atherosclerotic plaques [126]. Another set of experiments examined the transport of coagulation proteins by diffusion from the vessel wall to the clot surface. It was suggested that vessel wall TF was unlikely to be the only form of tissue factor active in thrombus

development as its reaction products, necessary for clot propagation, would not be able to diffuse across the span of the growing clot within the normal physiological time frame for clot formation [127]. Platelets and microparticles[4] are also believed to carry TF [128]. Even though the bulk of TF was observed at the experimental wall, *in vivo* observations in experimental mice showed that adhesion molecules on activated platelets played an important role in recruiting TF-bearing microparticles to the thrombus [55], [129].

On the contrary, other *in vitro* experiments carried out showed that thrombus development could not take place without the addition of tissue factor to the system. The same study stated that circulating TF values reported in other studies were unreasonably high and that this may have been a result of the type of assay used. The investigators hypothesized that if circulating TF were present, its concentration would not exceed 20fM [130]. Hoffman et al suggested that blood-borne tissue factor may play a crucial role in pathological conditions. Experimental results showed TF accumulation in a thrombotic clot but not in a haemostatic one [131].

[4] Microparticles are plasma membrane constituents which participate in the process of signaling between cells. They are derived from a range of vascular cells, including erythrocytes, leukocytes and platelets.

1.3.4. Vascular endothelium

The idea of there being separation between flowing blood and the surrounding vessel was first proposed by Malpighi while he was studying the circulatory network in the 1600s [132]. About two centuries later, von Reckinghausen suggested that there is an actual barrier composed of cells which is responsible for this separation. Technological advances in the 1950s allowed Palade and later, Gowan to confirm these views through the use of the electron microscope and physiological studies, respectively. These studies also confirmed Heidenhahn's description of the endothelium as a group of active, secretory cells in 1859, a controversial suggestion at the time. The endothelium is made up of a single layer of endothelial cells which are lined with a glycocalyx cover, seen in Figure 1.13 [133], [134].

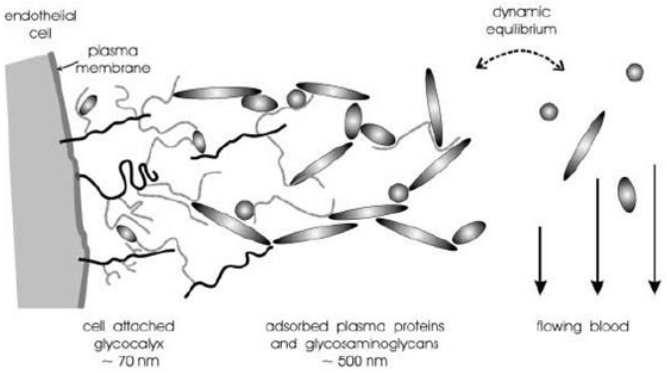


Figure 1.13: The glycocalyx is a dynamic structure which is attached to the endothelial cells and interacts with the flowing blood in the vessel. Taken from Pries et al [134]**.**

The endothelium plays a crucial role in coagulation. In their resting state, endothelial cells

inhibit coagulation, ensuring that the process takes place solely when repair to the endothelial layer is necessary. They achieve this by secreting nitric oxide (NO) and prostacyclin (PGI_2) which regulate vasodilatation [132], [135], [136]. These regulate blood pressure and blood flow, a vital element in clotting. In addition, NO, PGI_2 and ectonucleotidase CD 39 (ADPase) inhibit platelet activity [137–139].

When the layer is damaged, the process of coagulation is initiated, resulting in the eventual repair of the gap [47]. The endothelium plays a key role in both procoagulant and anticoagulant mechanisms. Subendothelium bound vWF mediates platelet adhesion, ensuring that a platelet plug develops [64], [65]. Tissue factor, responsible for coagulation initiation, is exposed on the subendothelial layers and has been found between endothelial cells in *in vitro* experiments [140]. The endothelial cell layer is also able to support the activation of factor X, thus contributing to the formation of the prothrombinase complex [141]. Once clotting is underway, the anticoagulant system becomes active, ensuring that the process is regulated. TFPI antigen and mRNA have been found on microvascular endothelial and luminal cells [142]. *In vitro* experiments have also shown that AT is expressed in vascular tissue in close proximity to endothelial cells [143]. Finally, protein S, a co-factor in protein C production, is synthesized and secreted by endothelial cells [144].

1.4. Clotting in aneurysms

The previous sections have focused on clotting under physiological conditions. Special focus needs to be placed on clotting under pathological conditions, with particular emphasis on aneurysms. It cannot be assumed that the mechanisms for clotting in disease are identical to those for normal haemostasis. It proves much more of a challenge to find information relating to clotting in aneurysms than it does to locate physiological clotting data. This is mainly because aneurysms are often identified by chance or following stroke-like symptoms, and clotting in aneurysms proves an even more elusive phenomenon to study. Data which would prove useful for clotting in cerebral aneurysms would include the mechanisms leading to clot initiation within the aneurysm sac. Determining the extent of damage to the endothelial layer during aneurysm formation and subsequent exposure of subendothelial layers would also prove useful. This data would elucidate the extent to which clot formation is governed by subendothelial layer tissue factor as opposed to blood-borne tissue factor. In addition, determining the key biochemical players in clot propagation would be valuable. Documenting the temporal evolution of spontaneous and non-spontaneous clots in cerebral aneurysms would be of great benefit. Finally, keeping a database of patients' thrombin evolution curves and coagulation protein concentrations alongside imaging scans of their aneurysms would assist with validation of models presented.

1.4.1. General considerations for clotting in pathological states

Under physiological conditions, it is generally assumed that platelet activation is the end result of the exposure of the subendothelial layers to which platelets attach. Platelets are also activated when they attach to other platelets in the growing clot. It is also possible, however, for platelets to become activated when exposed to abnormal flow patterns and high shear stresses characteristic of disease states. In addition, recirculation zones encourage procoagulant factor mixing, resulting in the formation of fibrin [145] . The activated platelets would then provide a procoagulant surface able to support coagulation reactions. It is also important to consider the contribution of microparticles in disease states. It is believed that microparticles may contribute to coagulation and that their composition, source and numbers may vary depending on the pathology [146].

1.4.2. Nature of clots observed in aneurysms

A porcine model was developed to better understand the mechanisms of thrombus formation in aneurysms [147]. The model examined the changes in the thrombus over time in an idealised aneurysm created with a venoarterial anastomosis. Complete aneurysm occlusion was observed in angiograms following surgery. Three days following the procedure, no differences were noted when the aneurysms were compared with aneurysms at time zero. After seven days, some fibrous tissue was seen to cover the aneurysm dome.

Further increase of this tissue was noted after fourteen days and the aneurysms had decreased in size. The aneurysms had thickened and shrunk at day thirty and a small, fibrous scar was left by the ninetieth day. The healing process was described in three stages. The first stage consisted of leukocyte and macrophage replacement of the thrombus and peaked between days three and seven. The second stage was characterized by fibrous tissue growth and peaked at day fourteen. The final stage consisted of collagen deposition and aneurysm shrinkage. The model deviated from the *in vivo* situation in a number of ways. Aneurysms *in vivo* tended to remain patent and spontaneous occlusion by a thrombus is not a guaranteed event. In addition, venous tissue with all three wall layers was used for the aneurysm sac. This differs from the compromised arterial wall often seen in aneurysms.

A classification scheme for types of aneurysm thrombosis was developed from a study which examined sixty-eight patients presenting with thrombotic aneurysms [148]. The different thrombus types are classified according to six categories seen in Figure 1.14. All the thrombi have different layers. This suggests an evolution of the thrombus over time with different layers being deposited at different stages. Thrombus development in aneurysms is sometimes seen to occur over a number of months with some layers being older than others. Type 1 is an aneurysm with a concentric thrombus. A spherical lumen is

found at the centre of the aneurysm and is surrounded on all sides with thrombus. Type 2 is an aneurysm with an eccentric thrombus. The aneurysm has an elliptical lumen and is capped by a clot on one or some of the sides. Type 3 is an aneurysm with multiple lobes and the thrombus is located in one of these lobes. Type 4 is an aneurysm where the entire sac is occluded by thrombus. Type 5 is an aneurysm which has a canalized thrombus through which blood can flow. In this type, the inflow and outflow arteries are connected. Finally, type 6 is an aneurysm with a thrombus which has developed due to the presence of foreign material resulting from endovascular treatment. There was an even distribution of concentric, eccentric, canalized and foreign-material thrombi in aneurysms. Complete and lobular aneurysms are rarely sighted.

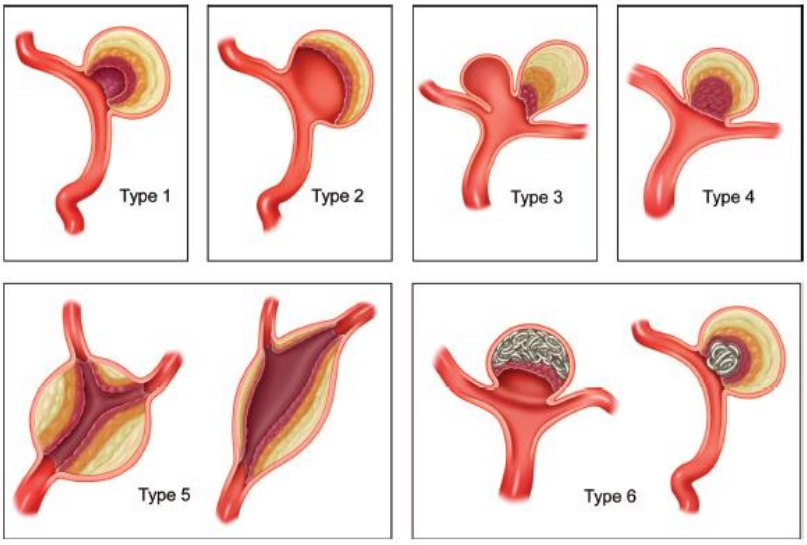
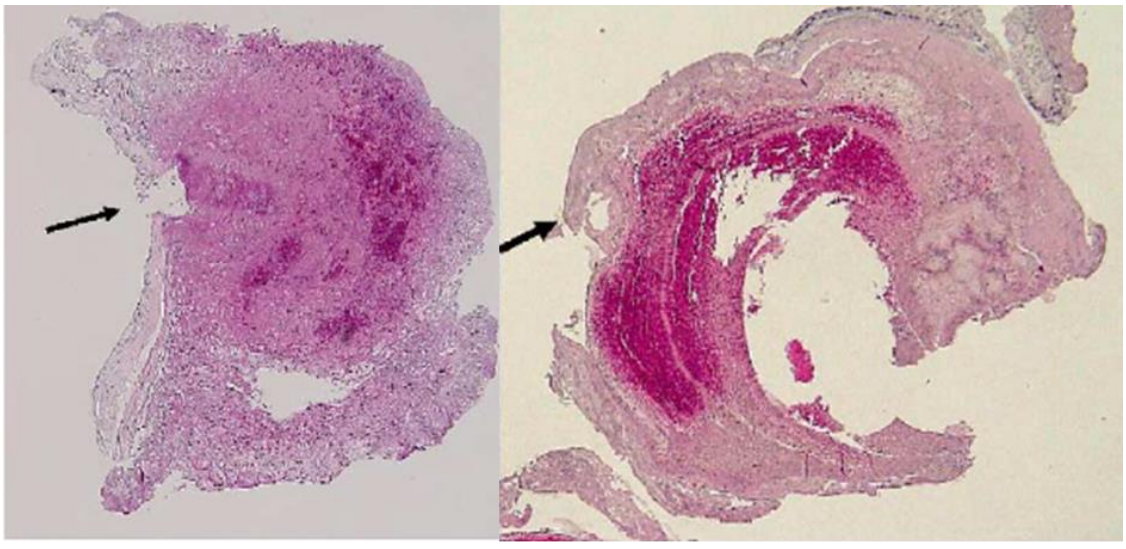


Figure 1.14: The different clot types observed in cerebral aneurysms. Type 1 is a concentric thrombus, type 2 is an eccentric thrombus and type 3 is an aneurysm with multiple lobes and thrombus is found in one of the lobes. Type 4 is a thrombus which fully occludes the aneurysm sac, type 5 is a canalized thrombus and type 6 is a thrombus induced by the presence of foreign material, such as coils. Taken from Lawton et al [148]**.**

1.4.3. Spontaneous clotting in cerebral aneurysms

Spontaneous clotting has been observed in both ruptured and unruptured cerebral aneurysms [12], [149], [150]. In ruptured aneurysms, clotting takes place in order to arrest subarachnoid haemorrhage. Different clot modes of arrest have been observed and attempts to categorise these have been made [150]. The outside-arrest-pattern is the most commonly observed arrest mode and involves the formation of a clot on the exterior of the aneurysm sac. The clot seals the point at which rupture occurred. The inside-arrest-pattern is so named as the clot forms on the interior of the aneurysm sac. In a bursting-pattern, the aneurysm wall is almost entirely lost and a thrombus covers the gap and only has a small remnant of aneurysm wall to attach to. The different patterns are illustrated in Figure 1.15.



A B

Figure 1.15: Diagrams showing different thrombus patterns following aneurysm rupture. (A) shows the outside arrest pattern where the clot develops outside the aneurysm sac to arrest bleeding while (B) is the inside arrest pattern. In this case, the clot develops on the inside of the sac. Taken from Ishikawa [150]**.**

Spontaneous clotting in giant, unruptured, cerebral aneurysms has been observed in 50% of cases [13]. They also suggested that intra-aneurysmal clotting would only prevent subarachnoid haemorrhage if the aneurysm was completely thrombosed. Thrombus deposition was observed to be non-uniform and this was attributed to variation in endothelial layer damage and flow dynamics within the aneurysm sac. The probability of parent artery occlusion from thrombus growth within the aneurysm sac is quite low while the risk of clot embolisation is quite high.

A study examining non-giant, unruptured, intracranial aneurysms and cerebral ischaemia found that two-thirds of patients presented with aneurysm thrombosis [12]. Some of the aneurysms were fully occluded while others only had partial occlusion. The investigators noted that in the early stages, the thrombus tended to be quite unstable and then regressed over time. It was suggested that blood flow within the aneurysm played a significant role in thrombus evolution and that thrombus initiation was linked to endothelial damage. In smaller aneurysms, higher flow velocities were likely to cause embolisation or thrombolysis while in larger aneurysms, slower flow velocities could prevent embolisation and impede thrombolysis.

Cohen et al also examined patients with non-giant, cerebral aneurysms presenting with

symptoms of ischaemia [38]. Two out of the three patients had fully occluded aneurysms and this was still the case after a one-year follow-up. In one of the two patients, the aneurysm was stably occluded and had, in fact, decreased in size. In contrast to this, a patient presented with two aneurysms which were mirror images of each other on the left and right internal carotid arteries [151]. The left hand side aneurysm thrombosed, grew to giant proportions, recanalized and eventually ruptured while the right hand side aneurysm remained unchanged.

1.4.4. Non-spontaneous clotting in cerebral aneurysms

Endovascular treatment of cerebral aneurysms results in an alteration of flow conditions within the aneurysm sac. Clot development has been observed in aneurysms which have been treated with coils, stents and a combination of the two.

The successful design of Guglielmi detachable coils (GDC) in 1991 meant that there was a controlled manner in which coils could be inserted into aneurysms while inflicting minimal damage to the vessels through which the guidewire was passed [9]. The presence of platinum coils encouraged the development of a clot within the aneurysm sac. A study was carried out in swine and coils were inserted three to fifteen days following creation of the aneurysm. In all these cases, complete aneurysm occlusion was observed two to six

months following the procedure. Byrne et al. also carried out experiments in swine to determine the influence of coil material on the type and stability of clot formed [152]. It was found that in the initial stages, tungsten coils were more successful at achieving occlusion than GDC. The effect of electrically induced thrombosis was not examined. In the longer term, there was little difference between uncoiled, tungsten- and GDC-coiled aneurysms. The formation of fibrous tissue which replaced the clot was most likely the major determinant of stability for all three methods. This fibrous tissue excludes the aneurysm from the parent vessel.

A study of small neck aneurysms conducted in humans found endothelial covering at the neck of the aneurysm and across individual coils in the same region two weeks after treatment [153]. This supported the view that the development of an endothelial layer which excludes the aneurysm from the parent vessel following coil insertion was likely to lead to clot stability. Vallée et al examined aneurysmal occlusion for small and large, but not giant, aneurysms which had been treated with coils [154]. Two parameters were used as measures of occlusion. Angiographic occlusion occurred when no more contrast agent was seen to be entering the aneurysm sac due to the presence of coils in the sac and at the neck. Volumetric occlusion was the percentage of coil occupying the aneurysm volume. Angiographic occlusion was 71% for all aneurysms with a 4% difference between smaller

and larger necked aneurysms (72% and 68% respectively). Volumetric occlusion was 30.4% with a 1.4% difference between the two groups. Angiographic occlusion at initial treatment was a better predictor of clot stability in the long term.

Jou and Mawad presented results for the change in haemodynamic conditions following the placement of a Neuroform stent [11]. The study also attempted to correlate thrombus formation and intimal hyperplasia with flow conditions in a patient specific geometry. Albeit inconclusive, it was suggested that intimal hyperplasia and thrombus grew at similar rates and that they were likely to develop in high oscillatory shear environments which were promoted by the placement of the stent. A different study presented cases where thrombosis had been observed following stent deployment [10]. One of the patients had a fully occluded aneurysm following intervention. Follow-up imaging two years later showed that the aneurysm had been obliterated and that the parent vessel was patent. Another patient had an aneurysm which fully thrombosed and was still fully occluded three months later.

In their work, Kulcsár et al aimed to examine delayed aneurysm rupture as a result of intra-aneurysmal thrombosis developed post flow diverter placement [14]. It was observed that post treatment, contrast material became stagnant in the aneurysm sac. All the patients

presented with high rupture risk and rupture was delayed following flow diverter deployment. The paper suggested that changes in local flow conditions caused by flow diverter treatment were patient specific and that in some cases, intervention could be undesirable. Sudden changes in flow pattern could increase stress, cause partial or no thrombosis and speed up the process of rupture. A similar study of a different type of flow diverter reported that 70% of aneurysms were fully occluded following intervention and on average, this persisted nine months following intervention [155].

It is clear from the above descriptions and discussion that the benefit of thrombosis in cerebral aneurysms is highly patient specific. In some cases, thrombosis begins the healing process which results in endothelialization, vascular wall remodelling and aneurysm stabilization. In other cases, the presence of a clot speeds up the time to aneurysm rupture. Provided the processes of embolisation or parent artery occlusion do not take place, it seems full occlusion of the aneurysm sac and development of a neointimal layer which excludes the aneurysm from the parent artery is more likely to result in a more stable situation. The presence of a partial clot, on the other hand, still allows for intra-aneurysmal flow and continual thrombus renewal. This lack of stability may result in aneurysm rupture.

1.4.5. Motivation for computational model developed in this thesis

The literature survey illustrates that clotting in cerebral aneurysms remains quite elusive. The development of a computational model may prove useful for framing some of the questions which need to be answered when considering aneurysm thrombosis. Such a model would need to incorporate both haemodynamics and coagulation reactions. While the formation of a platelet plug is an important process in coagulation, more important would be examining clots which are held securely in place by a fibrin mesh. These are more critical as their presence is more guaranteed than platelet clots which can be carried downstream quite easily. The underlying clotting cascade chosen to describe the coagulation reactions would need to be simple enough to collect a specific patient's data in a clinical setting.

The clotting model would also need to provide a framework capable of linking clot initiation and growth to both mechanical and biochemical factors. This would allow for the examination of factors believed to be major contributors to clotting. Finally, the model would need to be implementable in realistic, three-dimensional geometries. These geometries may or may not contain endovascular devices.

2. Computational models of clotting

There are many existing models of coagulation in literature. Some of them focus on platelet processes while others focus on the coagulation cascade. The motivation behind the development of a model directs its focus. Before a pathological model can be developed, it is important that the physiological model be properly established as a lot of the details of clotting in diseases, with emphasis on aneurysms, are still somewhat unclear. Computational models can be used to elucidate some of these features.

2.1. Coagulation network models

The main focus of coagulation network models is the use of mathematical formulae to describe the reactions that occur during coagulation and the subsequent changes in species concentration. Some of the models presented are more comprehensive than others, describing the process from clot initiation to lysis. The Wagenvoord and Mann models described here are explored in greater depth in Chapter 4 where they are implemented.

Wagenvoord et al present a six reaction model linked to a thrombogram[5] [156], a graph

[5] A thrombogram is a graph obtained from a clinical test known as a Calibrated Automated Thrombogram (CAT). The test is able to measure hypocoagulability and hypercoagulability. This is achieved by using a slow fluorogenic thrombin substrate and comparing it continuously to a calibrator.

depicting the change in thrombin concentration over time for a specific patient. The set of reactions used to describe coagulation are fitted to the graph and are not necessarily unique in describing it. What differentiates one set of equations from the next is the use of initial conditions. The reactions account for the initiation and regulation of clot growth via the tissue factor pathway and anticoagulant regulation of thrombin generation [15]. Mann et al present a twenty-seven reaction model that describes the process of coagulation as per the cell-based model [16], [157]. The model is derived from individual reactions for which rate constants have been obtained experimentally. Both the initiation and lysis of the clot are described by several equations and the amplification of thrombin generation is also described by a complex set of equations.

2.2. Platelet models

The defining feature of platelet models is that the processes governing adhesion, activation, accumulation and aggregation of platelets are central to the functioning of the model. It is now widely accepted that platelets play a crucial role in coagulation as they provide some of the membranes on which coagulation reactions occur. As a result, models of this nature are important as they give insight into the complex interaction between platelets and the coagulation proteins.

Filipovic et al. use dissipative particle dynamics to model thrombus development [158]. Plasma and platelets (components of the colloidal mixture in consideration) are modelled as mesoscale particles and the interaction between them is described by attractive, dissipative, repulsive and random forces as seen in Figure 2.1. The movement of the particles is accounted for by Newton's second law. Unlike continuum methods, this approach places a lot of emphasis on the contribution of individual particles. The particles are small enough to track the movement of plasma and platelets but are larger than atoms. Molecular dynamics is therefore not required to resolve changes in the colloidal system. Thrombus growth is accounted for by platelet accumulation and adhesion. Activated platelets which attach to the wall assume a different spring constant. The value is not known but is determined by fitting simulation results to *in vitro* data. The model is able to account for both inactive and active platelets and is therefore very applicable to platelet-mediated thrombosis.

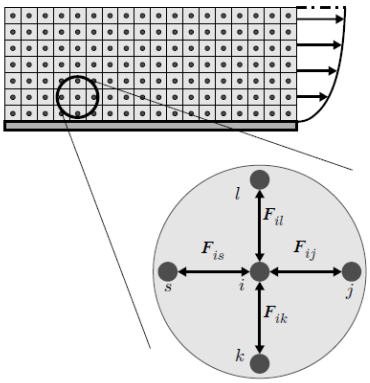


Figure 2.1: Forces that act on a mesoscale particle according to the model developed by Filipovic et al [158]**. The resultant force is the sum of attractive, repulsive, dissipative and random forces.**

Diamond et al developed a comprehensive platelet model which consists of seventy-seven reactions and is able to accurately predict the events that occur during platelet signalling [159], [160]. The model combines different species with electrochemistry, platelet ultrastructure readings and new and existing experimental data. Figure 2.2 illustrates the different regions of the model and the reactions. An *in vitro* model where platelet activation is initiated by the addition of ADP was set up. The changes in intracellular calcium concentration following this addition were monitored using high resolution electron micrographs. The *in vitro* model provided the experimental data necessary for the computational model. The *in silico* model comprises modules which describe the various stages in platelet activation and is able to mimic behaviour observed in both resting and activated platelets. The reactions are modelled using ordinary differential equations and are solved in MATLAB.

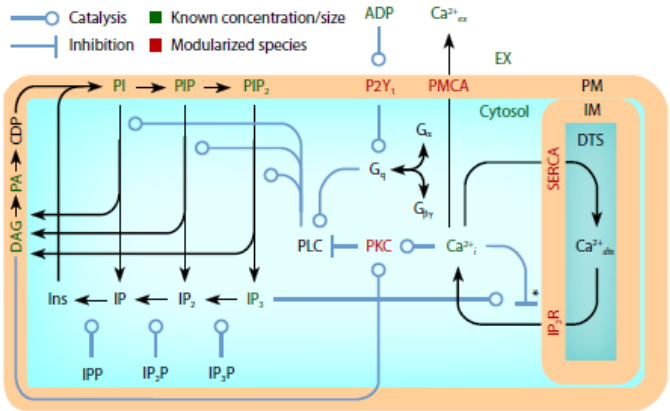


Figure 2.2: Platelet model presented by Purvis et al [159]**. The model accounts for different reactions with platelet activation and inhibition. The model also compartmentalizes the different signals.**

2.3. Reaction-Mass Transport models

The logical starting point for the development of a coagulation model is to begin by focusing on the coagulation reactions or on the activity of platelets. It soon becomes evident that neither approach can be fully developed without the inclusion of blood flow. Reaction-mass transport systems aim to couple the reactions with blood flow and examine the effect that the two systems have on each other. While the geometry of the model influences the flow field, the link between the geometry and clot development cannot be easily predicted as the biochemical reactions play a rather major role in patient specific clot development.

Basmadjian presented a model which connected flow and transport of chemical species in 1990 [161]. The model is illustrated in Figure 2.3. The model aimed to express *in vitro* coagulation models in mathematical terms without oversimplifying the biological events or compromising on mathematical rigour. The model presents a single reaction at the blood vessel wall and examines the link between flow and transport in a relatively simple framework. The eventual aim of the model was to then incorporate all the reactions that take place during coagulation. The work shows that at the vessel wall, reactions can be modelled as algebraic equations under steady state conditions and as ordinary differential equations under transient conditions. Several simplifications could be made depending on

the size of the vessel in question. For vessels with diameter greater than d = 0.1mm, radial changes in transport coefficient and protein concentration are confined to the boundary layer. This allows for the use of boundary conditions for the description of some of these changes. For vessels with diameter less than d = 0.1mm, the same assumption cannot be made as the boundary layer is not thin relative to the rest of the fluid domain. In such vessels, however, flow is not pulsatile hence certain coefficients remain constant with transience. The model was used to examine the effect of flow, vessel geometry and reaction kinetics on a protein's transport coefficient and mural concentration. An earlier paper by the same author examined embolisation of clots [118]. The study found that changes in shear rate and vessel diameter were good indicators for embolisation risk.

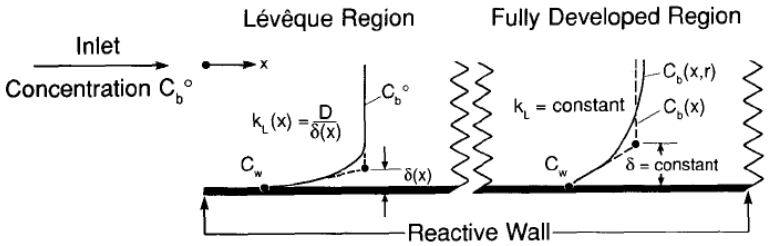


Figure 2.3: The mathematical model developed by Basmadjian [161]**. The Leveque region is thin boundary layer found near the wall. For vessels with smaller diameters, the Leveque region needs to be taken into serious consideration as it cannot be considered negligible. For larger vessels, conditions in the boundary layer can be applied as boundary conditions.**

Anand et al developed a mathematical model which looked at the progression of a clot from inception to lysis [162]. This is achieved by modelling twenty-three

reaction-diffusion equations which describe the process of coagulation. Figure 2.4 shows the biochemical cascade used in this model where blood is considered to be stagnant. The model does not account for the activity of antithrombin or protein C. The validation for the model is therefore achieved by considering clinical cases with similar conditions. Clot formation and growth occurs in regions where the fibrin concentration exceeds a given value (C_{crit}) and fibrinolysis occurs in regions where the fibrin concentration drops below C_{crit} after having previously equalled or exceeded that value. The concentrations of the different biochemical species are taken from a paper by Butenas et al [157]. The concentrations for activated proteins are 0.1% at the start of simulation. The main limitation of the model is that it does not account for platelet activity.

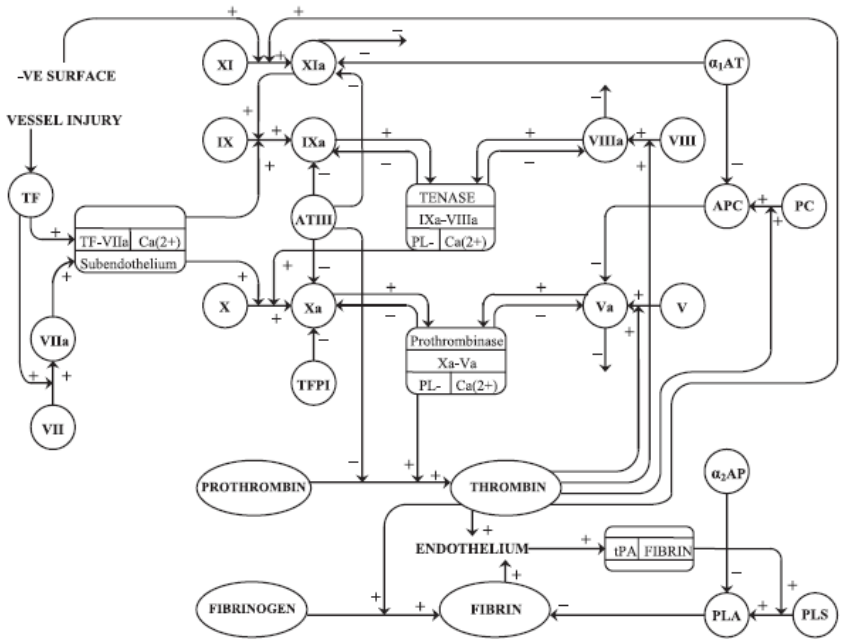


Figure 2.4: The reaction network used by Anand et al [162]**. The model describes clot development from inception to lysis. Plus signs indicate activation of an inactive protein while minus signs indicate deactivation of an active protein.**

A computational model was developed by Ataullakhanov et al [17] as seen in Figure 2.5. This is complemented by *in vitro* studies carried out by the same group. The computational model consists of mathematical formulae which describe surface and volume reactions in a reaction-diffusion system. Diffusion operators are applied to the protein concentrations to account for species transport. The model consists of twenty-seven reactions and fifty rate constants and is implemented in a biphasic manner. Surface densities are used to account for proteins and reactions which take place on the surface of tissue factor bearing cells. Reactions which take place on platelet membranes are accounted for by altering volume concentrations.

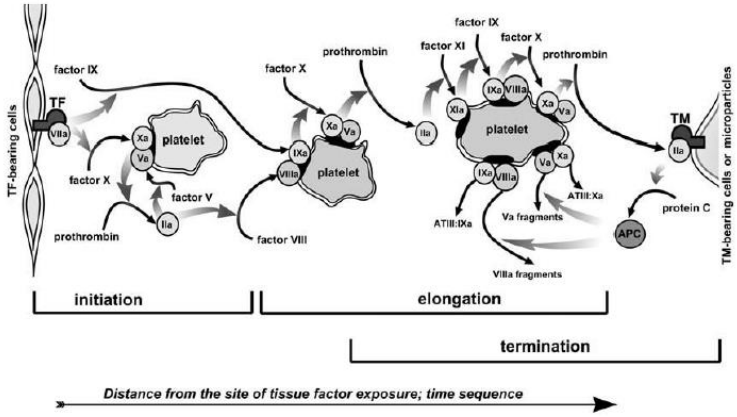


Figure 2.5: Clot initiation, propagation and localization as described by Pantaleev et al [17]**. The important role of different cell membranes is highlighted.**

A few assumptions were made in the development of this model. It was assumed that platelet membranes provide the surface on which procoagulant proteins are activated. While the investigators acknowledge that microparticles may play a similar role, no distinction is made between platelets and microparticles. It was also assumed that the

diffusivity of coagulation proteins is the same in liquid plasma and in a fibrin clot. This model was then used to examine the relative contributions of different coagulation proteins. From the studies carried out, they conclude the extrinsic tenase[6] plays a key role in clot initiation while intrinsic tenase regulated propagation. It was also observed that thrombomodulin played an important role in localizing and terminating clot development.

Bodnar and Sequeira generated a model which incorporates biochemical reactions, flow and the effect of the growing clot on the fluid field [163]. They make use of the biochemical network developed by Anand et al [162]. The changes in the concentrations of different protein species are described by twenty-three convection-diffusion-reaction equations. The equations account for the initiation, propagation and dissolution of clots. The flow is described using the Navier-Stokes equations and the viscosity is considered to be shear-thinning. The Cross model is used to describe the changes in viscosity. A finite-volume formulation is used to account for spatial discretisation while the Runge-Kutta scheme is used for temporal integration. At the start of simulation, no clots are present in the domain. As clotting is initiated and propagated, clotting is observed. The clot and normal plasma regions are differentiated by assigning different viscosities to these

[6] Factor X can be activated in one of two ways and the compound responsible for its activation is known as tenase. Intrinsic tenase is the complex which consists of factor IXa, co-factor VIIIa and calcium. Extrinsic tenase consists of tissue factor, factor VIIa and calcium.

regions. The viscosity increases linearly with fibrin concentration. Above a certain fibrin concentration, the viscosity reaches an upper limit. At this value, the viscosity is one hundred times the viscosity of blood. The model was implemented in a three-dimensional cylinder and tissue factor was expressed along a portion of the vessel wall. Figure 2.6 describes the reaction network employed in this study.

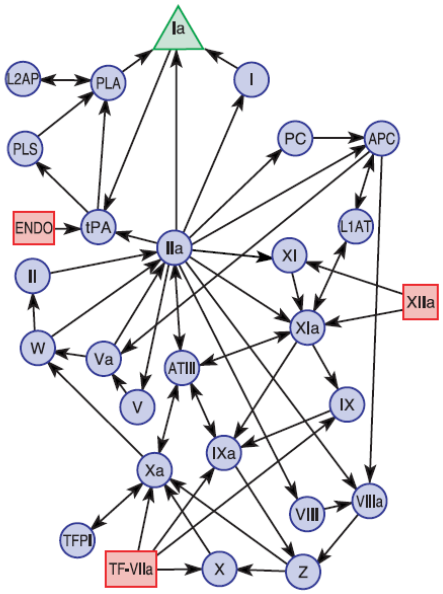


Figure 2.6: Reaction network used by Bodnar and Sequeira in their reaction-diffusion-convection model [163]**.**

2.4. Integrated models

Integrated models of coagulation could be regarded as the most developed of all the models as they account for coagulation reactions, platelets and haemodynamics. These can be used to examine some of the more complex aspects of coagulation as systems can be studied together or in isolation.

Fogelson et al have developed a model which integrates most of the complex processes which occur in thrombus development [164–167]. The model accounts for both platelet activity and biochemical reactions. These systems are examined within a two-dimensional flow regime. The platelet model incorporates mobile, subendothelium-bound and platelet-bound platelets. Once activated by thrombin and/or ADP, the platelets are able to support certain reactions which require platelet membranes. These activated platelets are able to attract and bind to other active platelets, forming a growing platelet mass. Non-activated platelets move with the flow. The central role played by thrombin is highlighted in the model. The platelets are not modelled as individual particles but are rather accounted for by number density. Partial differential equations are used to describe the changes in concentration of the different platelet groups. Similarly, the biochemical species which participate in coagulation are described using partial differential equations. Distinction is made between subendothelium-bound, platelet-dependent and fluid-phase proteins. The flow is described using Navier-Stokes equations. The growing clot region has a different porosity to the rest of the flow region thus registering the effect of the clot on the flow field and vice versa. Spatial discretisation is achieved using a finite-volume solver while a Runge-Kutta formulation is used for temporal integration. Limitations of this model include certainty of the cohesion rate and maximum resistance to flow within the thrombus (inverse of permeability), effect of APC on the system and the activation

state of platelets activated in different ways. The model has also been developed in a two-dimensional framework and Figure 2.7 illustrates the system.

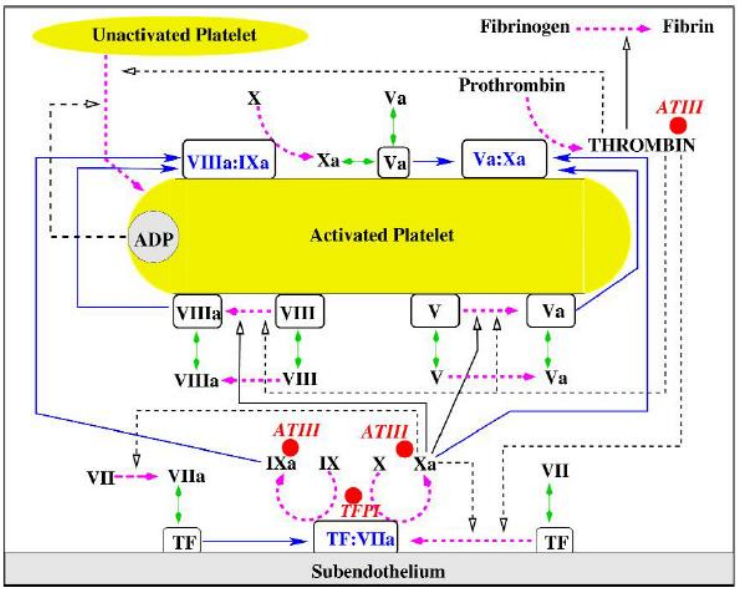


Figure 2.7: The coagulation process and the various surfaces on which it takes place. This diagram represents the Fogelson model and the different aspects of that model [167]**.**

A multiscale model which takes into account the different spatial scales involved in thrombus growth was developed by Xu et al [168], [169]. It consists of a number of submodules which account for different aspects of coagulation. The microscale cell submodule is described by the Cellular Potts Model and accounts for platelet aggregation, adhesion and activation. Platelet activation takes place above a chosen threshold thrombin concentration. It also accounts for platelet-wall and platelet-platelet interactions. The macroscopic continuum fluid submodule is implemented by applying the Navier-Stokes

equations. The biochemical reactions are described by the Mann model and are described using partial differential equations [157]. The interface submodule ensures communication between the micro- and macroscale models which are spatially superimposed. Figure 2.8 shows the different cells which participate in the system.

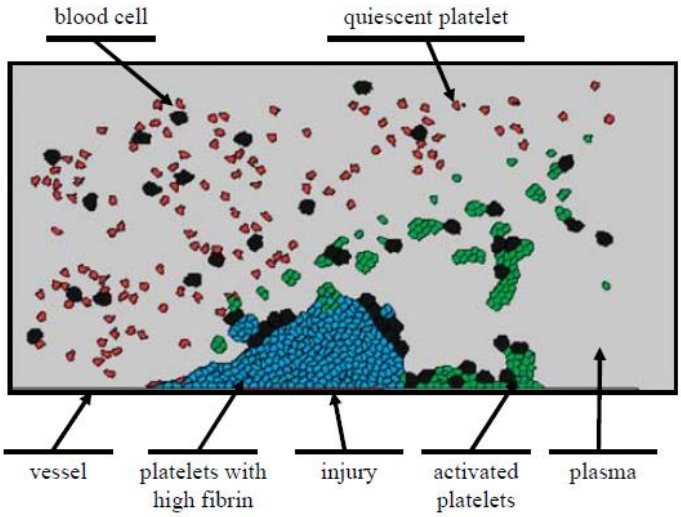


Figure 2.8: A multiscale model presented by Xu et al [168]**. Flow is considered on a continuum level while cell activity is considered on a microscale level.**

2.5. Computational models of coagulation in aneurysms

All the previous sections focused on coagulation models under physiological conditions. A few models which focus on coagulation in aneurysms are described below.

Bedekar et al developed a model, illustrated in Figure 2.9, which described clot growth in an anatomically accurate geometry of a cerebral aneurysm [18]. The realistic patient

geometry was obtained from computed tomography scans. Transport is accounted for using the Navier Stokes equations which are discretized using the finite volume method. A convective-diffusive transport equation is used to account for changes in the concentration of platelets and different protein species. Coagulation reactions taken into account were platelet adhesion, platelet activation, thrombin generation and thrombin inhibition. At the start of simulation, the concentration of thrombin and surface bound platelets is zero. Some activated platelets are present at the start (5% of the resting platelet concentration). The model does not account for the clot's influence on the flow field.

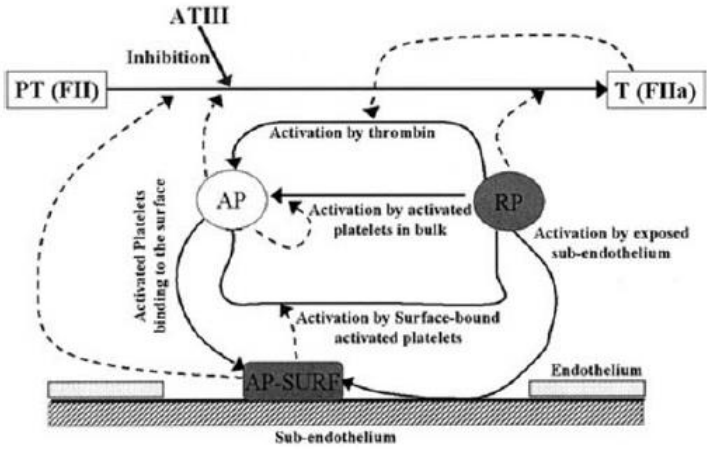


Figure 2.9: Bedekar et al consider the different roles of platelets, thrombin and antithrombin in their model of clotting [18]**. The model is applied in anatomically realistic aneurysm geometries.**

A similar model is presented by Biasetti et al but focusses on abdominal aortic aneurysms [21]. While geometry and aetiology are quite different in cerebral and abdominal aortic aneurysms, the clotting concentrations would remain constant for a single patient. Even

though the mechanisms of clot initiation and propagation would need to be examined carefully, a model which accounts for haemodynamics and biochemical reactions could be used for either pathology. In their study, an idealised two-dimensional axisymmetric model of an abdominal aortic aneurysm is utilised for simulation of clot growth. The model accounts for mechanical and biochemical factors. The fluid field is described by the Navier-Stokes equations and is discretized using a finite element formulation. A shear-thinning model is used to describe blood viscosity. The model applies the Mann model of coagulation [157] and consists of sixteen reactions. Like the Bedekar model, the framework does not account for the clot's effect on the flow field. Figure 2.10 shows the geometry used in the study.

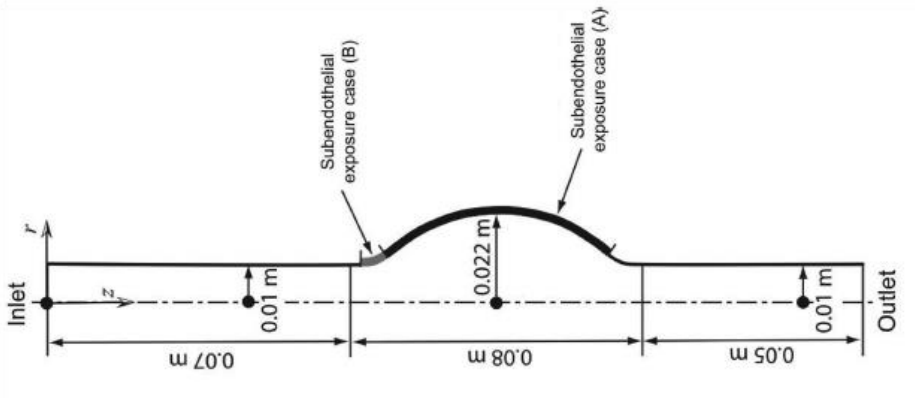


Figure 2.10: The abdominal aortic aneurysm geometry used by Biasetti et al [21]**. The model accounts for both mechanical and biochemical factors.**

Rayz et al also examined thrombus development in patient specific in aneurysm geometries which were reconstructed from MRI scans [19], [170]. The flow is accounted

for by use of the Navier Stokes equations and solved using a finite volume method. Flow residence time and wall shear stress were correlated with regions of clot development. The residence time was estimated by injecting a scalar called 'ink' at the inlet at the start of simulation as seen in Figure 2.11. The transport equation was then used to calculate the change in concentration of 'ink'. For this study, the diffusion coefficient of ink was set to zero. The model does not directly account for the biochemical reactions involved in coagulation.

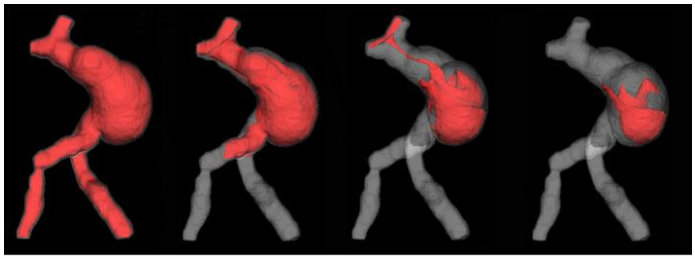


Figure 2.11: Rayz et al use a virtual ink test to calculate residence time of flow in the aneurysm geometry [19]**. Ink is injected at the inlet and its movement through the geometry is tracked.**

Ouared et al present a shear rate regulated model of thrombosis in cerebral aneurysms as seen in Figure 2.12 [20]. Lattice Boltzmann methods are used to describe the movement of fluid particles in this model. Thrombosis is initiated and develops in regions which fall below a specific shear rate threshold. This approach gives an explanation for the different types of thrombosis observed *in vivo* (spontaneous, complete, and partial). Regions which are clotted become solid. Even though the biochemical reactions are not explicitly defined, the model accounts for clot initiation and cessation of thrombus growth.

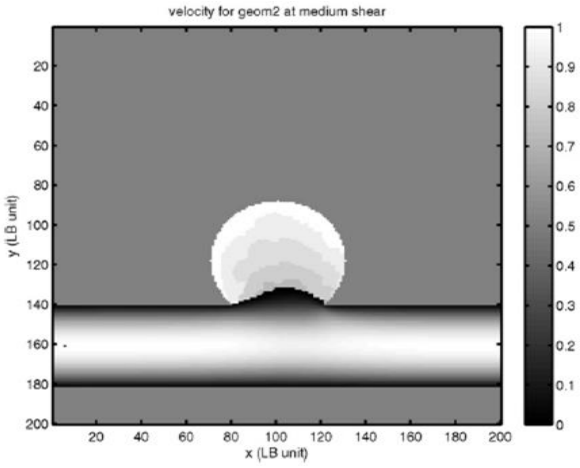


Figure 2.12: Clot development seen in the aneurysm sac for Ouared et al's model [20]**. The processes of clot growth and initiation are governed by shear rate.**

2.6. Summary of models presented

Figure 2.13 illustrates the different physiological models discussed in this chapter while Figure 2.14 illustrates the aneurysm models. It shows how the models incorporate different aspects of Virchow's triad depending on the intended purpose of the model. Some models are more advanced than others because they are used for the elucidating the physiological process of clotting. Others are geared for disease treatment. While all the models presented are extremely useful within their various contexts, the Wagenvoord model provides the most practical framework for the purposes of this thesis. The simplicity of the model would allow a clinician to determine constants for a patient within a realistic timeframe. The calibrated automated thrombogram would be used to determine the patient's thrombin profile. This information would prove useful when determining a patient specific model of

clot development in an aneurysm.

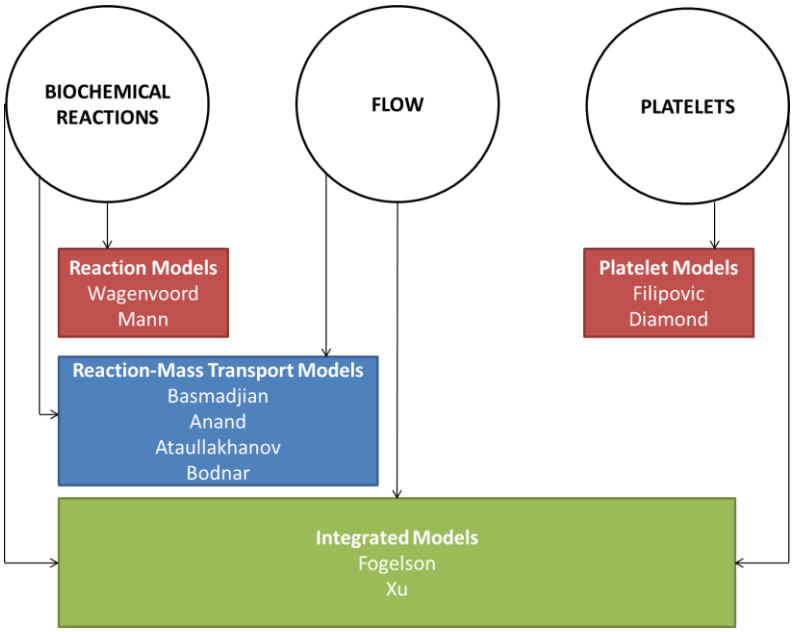


Figure 2.13: The relationship between the different physiological clotting models presented in this chapter and the different components which they model.

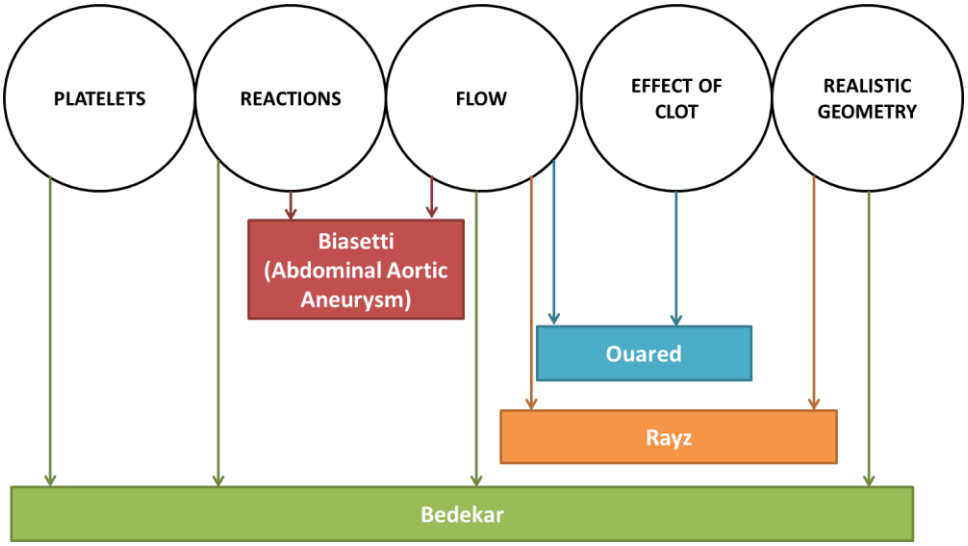


Figure 2.14: The relationship between the different pathological (cerebral aneurysm) clotting models presented in this chapter and the different components which they model.

3. Methods for framework construction

A combination of computational methods is used to construct a framework which will enable the modelling of coagulation in cerebral aneurysms. The flow of blood through the vessel geometry is accounted for by computational fluid dynamics. This blood contains biochemical species which are transported by the blood. The chemical reactions are solved using a stiff equation solver. Finally, the surface of the growing clot is tracked using Level Set methods. All of these methods are detailed in this chapter. This chapter presents the range of methods used. The actual values employed and methods chosen for specific cases are detailed in Chapters 4, 5 and 6.

3.1. CFD

Computational fluid dynamics (CFD) is a branch of fluid mechanics that aims to solve fluid flow problems through the use of computational methods. Recent advances in computing technology have allowed for more widespread use of the method, which can be more cost effective than traditional experimental methods. Even though this is the case, experimental work remains an indispensable part of the problem-solving chain as it provides data which is then used to validate CFD codes and solutions.

In most cases, CFD solvers are divided into three key stages. During pre-processing, the geometry of interest is processed to ensure that it can be discretized in a meaningful manner. In many cases, this implies the generation of a *mesh* or a *grid.* The mesh needs to be refined enough to capture critical features of the flow and to solve the equations within a desired accuracy. Once the mesh is complete, the simulation stage allows for the solution of the discretised equations on the mesh. Depending on the code used, the user may be required to define a number of variables. These may include boundary conditions, initial conditions, fluid properties, relaxation parameters, solver settings and any other required parameters. The solver then carries out all the relevant calculations over a specified number of iterations. A number of different methods may be employed to obtain the solution, which is considered to converge when the difference between the values for two consecutive iterations is deemed sufficiently small. Once the solution has been calculated, post-processing allows for the display and manipulation of results. At this stage, results can also be verified against experimental data. The discussion presented in this section is guided predominantly by Versteeg and Malalasekera [171] and the CFD-ACE+ User Manual [172]; other sources are cited as necessary.

3.1.1. Governing equations of fluid flow

The motion of fluid is described by the Navier-Stokes equation. For unsteady fluid flow

problems in three dimensions, the description is given by four equations. The first equation is the continuity equation. The other three result from the casting of the Navier-Stokes equation in the three spatial dimensions and correspond to the conservation of momentum in each direction.

The continuity equation states that the rate of increase of mass in a fluid element is equal to the net rate of flow of mass into that element. The equation is given by Eq. 3.1.

$$\frac{\partial \rho}{\partial t} + \nabla(\rho \boldsymbol{u}) = 0 \qquad \textbf{Eq. 3.1}$$

where ρ is density, t is time and $\boldsymbol{u}$ is the velocity vector. For an incompressible fluid, the density remains constant therefore Eq. 3.1 reduces to Eq. 3.2.

$$\nabla \boldsymbol{u} = 0 \qquad \textbf{Eq. 3.2}$$

The momentum equations are based on Newton's second law and state that the rate of change of momentum of a fluid element is equal to the sum of the forces acting on that element and is seen in Equations below. Eq. 3.3 describes momentum in the x-direction, Eq. 3.4 gives a description for the y-direction and Eq. 3.5 describes momentum in the z-direction.

$$\frac{\partial(\rho u)}{\partial t} + \nabla(\rho u \boldsymbol{u}) = -\frac{\partial p}{\partial x} + \nabla(\mu \nabla u) + S_{Mx} \qquad \textbf{Eq. 3.3}$$

$$\frac{\partial(\rho v)}{\partial t} + \nabla(\rho v \boldsymbol{u}) = -\frac{\partial p}{\partial y} + \nabla(\mu \nabla v) + S_{My} \qquad \textbf{Eq. 3.4}$$

$$\frac{\partial(\rho w)}{\partial t} + \nabla(\rho w \boldsymbol{u}) = -\frac{\partial p}{\partial z} + \nabla(\mu \nabla w) + S_{Mz} \qquad \textbf{Eq. 3.5}$$

where u is the x-direction velocity, v is the y-direction velocity, w is the z-direction velocity, p is pressure, μ dynamic viscosity and S is the momentum source term for each dimension. The Navier-Stokes equations do not have a closed form solution and need to be approximated and discretised over a defined, finite region. This then makes it possible to approximate a solution for the equations.

3.1.2. The general transport equation

A general transport equation can be used to describe conservation equations for fluid flow and for other scalar quantities such as chemical species concentrations. If a general quantity ϕ is defined, the general transport equation can be described in words below:

$$\begin{pmatrix} Rate\ of\ increase \\ of\ \phi\ of\ a\ fluid \\ element \end{pmatrix} + \begin{pmatrix} Net\ rate\ of \\ flow\ of\ \phi \\ out\ of\ fluid \\ element \end{pmatrix}$$
$$= \begin{pmatrix} Rate\ of\ increase \\ of\ \phi\ due\ to \\ diffusion \end{pmatrix} + \begin{pmatrix} Rate\ of\ increase \\ of\ \phi\ due\ to \\ sources \end{pmatrix}$$

The mathematical description of this statement is given by Eq. 3.6.

$$\frac{\partial(\rho\phi)}{\partial t} + \nabla(\rho\phi\boldsymbol{u}) = \nabla(\Gamma\nabla\phi) + S_\phi \qquad \textbf{Eq. 3.6}$$

where Γ is the diffusion coefficient. Eq. 3.6 expresses the main features of the transport of quantity ϕ. The first term on the left hand side accounts for rate of change (time) while the second term accounts for convective transport. The first term on the right hand side accounts for diffusive transport while the second term describes the source term.

3.1.3. Finite volume method

The finite volume method is one of the major subcategories of numerical techniques for the solution of partial differential equations of the nature described above. Others include the finite element method, the finite difference method, particle methods but to mention a few. In the finite volume method, the geometry of interest is subdivided into finite volumes, known as control volumes, over which Eq. 3.6 is integrated. The control volume is seen in Figure 3.1.

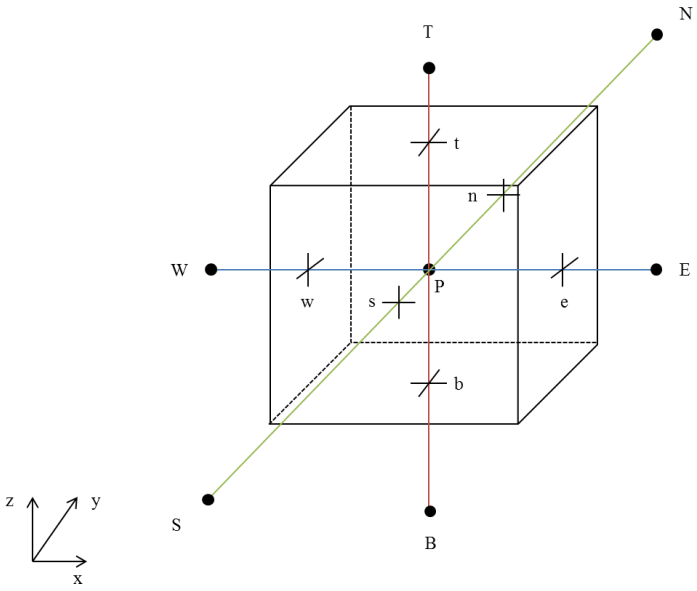


Figure 3.1: The fluid element. The different letters indicate different sides of the element and show the direction conventions used. E and W are east and west, respectively. N is north, S is south, T is top and B is bottom. P is the cell centre. Adapted from Versteeg and Malalasekera [171]**.**

The grid developed during the pre-processing stage subdivides the geometry into smaller control volumes over which the transport equations can be integrated as seen in Eq. 3.7.

$$\int_{CV} \frac{\partial(\rho\phi)}{\partial t} dV + \int_{CV} \nabla(\rho\phi \boldsymbol{u}) dV = \int_{CV} \nabla(\Gamma \nabla\phi) dV + \int_{CV} S_\phi dV \qquad \textbf{Eq. 3.7}$$

where CV is the control volume. The Gauss theorem can be used for the convective and diffusive terms yielding Eq. 3.8.

$$\int_{CV} \frac{\partial(\rho\phi)}{\partial t} + \int_{A} \boldsymbol{n}.(\rho\phi \boldsymbol{u}) dA = \int_{A} \boldsymbol{n}.(\Gamma \nabla\phi) dA + \int_{CV} S_\phi dV \qquad \textbf{Eq. 3.8}$$

where A is the area of the control volume face and $\boldsymbol{n}$ is the normal vector of that face. For time dependent problems, the description is given by Eq. 3.9.

$$\int_{\Delta t} \int_{CV} \left(\frac{\partial(\rho\phi)}{\partial t} dV \right) dt + \int_{\Delta t} \int_{A} \boldsymbol{n}.(\rho\phi \boldsymbol{u}) dA\, dt = \int_{\Delta t} \int_{A} \boldsymbol{n}.(\Gamma \nabla\phi) dA\, dt + \int_{\Delta t} \int_{CV} S_\phi dV dt \qquad \textbf{Eq. 3.9}$$

The integration produces a discretised equation at the control volume centre. The terms which are integrated over area are accounted for by the area of the control volume faces.

3.1.4. Solving the discretised equations

Several methods are utilised to solve the discretised equations. It is necessary to discretise each of the terms in the transport equation. Pressure velocity coupling then needs to be applied and iterative methods employed to solve the system of equations.

3.1.4.1. Temporal term

In the framework we discuss, the temporal term is discretised using either the Euler method or the Crank-Nicholson method. The Euler method results in a first order fully implicit scheme. The Crank Nicholson scheme can be adjusted to give an implicit or explicit scheme. When used in conjunction with the central differencing scheme for spatial discretisation, the expression can be seen in Eq. 3.10 for a function φ.

$$\frac{\varphi_i^{n+1} - \varphi_i^n}{\Delta t} = \beta\left(\frac{\varphi_{i+1}^{n+1} - 2\varphi_i^{n+1} + \varphi_{i-1}^{n+1}}{2\Delta x^2}\right) + (1-\beta)\left(\frac{\varphi_{i+1}^{n} - 2\varphi_i^{n} + \varphi_{i-1}^{n}}{2\Delta x^2}\right) \quad \textbf{Eq. 3.10}$$

where I is the spatial node and β is the relative weight of the time step n. $\beta = 0$ gives an explicit scheme while $\beta = 1$ gives a fully implicit scheme.

3.1.4.2. Diffusive term

There are a variety of schemes which can be used to determine values for the diffusion and convection terms in Eq. 3.6. When approximating the gradient at the control volume face, $\nabla\phi$, in the diffusion term, the central differencing scheme assigns proportional-to-distance weighting to the values of ϕ for each of the neighbouring cells. Using Figure 3.1 for the nomenclature, the integrated form of the diffusion term in three dimensions is seen in Eq. 3.11.

$$\int_A n.(\Gamma\nabla\phi)dA = [\Gamma_e A_e(\phi_x)_e - \Gamma_w A_w(\phi_x)_w] + \left[\Gamma_n A_n(\phi_y)_n - \Gamma_s A_s(\phi_y)_s\right] + [\Gamma_t A_t(\phi_z)_t - \Gamma_b A_b(\phi_z)_b] \quad \textbf{Eq. 3.11}$$

The discretised form of the equation is then seen in Eq. 3.12.

$$\int_A \boldsymbol{n}.(\Gamma\nabla\phi)dA = \left[\Gamma_e A_e \frac{(\phi_E - \phi_P)}{\delta x_{PE}} - \Gamma_w A_w \frac{(\phi_P - \phi_W)}{\delta x_{WP}}\right] + \left[\Gamma_n A_n \frac{(\phi_N - \phi_P)}{\delta y_{PN}} - \Gamma_s A_s \frac{(\phi_P - \phi_S)}{\delta y_{SP}}\right] + \left[\Gamma_t A_t \frac{(\phi_T - \phi_P)}{\delta z_{PT}} - \Gamma_b A_b \frac{(\phi_P - \phi_B)}{\delta z_{BP}}\right] \quad \textbf{Eq. 3.12}$$

3.1.4.3. Convective term

The value of ϕ in the convective term can be approximated by using the central difference scheme (second order) or upwind differencing scheme (first order). At times, a combination of the two schemes is used. The discretised form of the convection term is given by Eq. 3.13.

$$\int_A \boldsymbol{n}.(\rho\phi\boldsymbol{u})dA = \sum_{i=1}^{N}(\rho_i\phi_i u_i^n)A_i = \sum_{i=1}^{N} C_i\phi_i \quad \textbf{Eq. 3.13}$$

where N is the number of cell faces for a control volume and i is the cell face under examination. u_i^n is the velocity component in the direction normal to the cell face and C_i is the mass flux.

The central differencing scheme for cell face, i, which borders control volumes with cell centres P and I is given by Eq. 3.14.

$$\phi_i = \gamma_i \phi_P + (1 - \gamma_i)\phi_I \qquad \textbf{Eq. 3.14}$$

where γ_i is the geometric weighting function at face i. Eq. 3.14 assumes that there a linear variation in ϕ between the two cell centres.

When determining the value of ϕ at a cell face, the upwind differencing scheme assigns different weightings to the contributions of neighbouring control volumes depending on the direction in which the flow is moving. ϕ_i assumes the value of the upstream cell centre and is seen in Eq. 3.15.

$$\phi_i = \begin{cases} \phi_P \; if \; u_i^n > 0 \\ \phi_I \; if \; u_i^n < 0 \end{cases} \qquad \textbf{Eq. 3.15}$$

At times, it is necessary to use a blend of the central differencing and upwind differencing schemes. This is often done to increase stability. The expression for such a blend is given by Eq. 3.16.

$$\phi_i = \alpha \phi_i^{Upwind} + (1 - \alpha)\phi_i^{Central} \qquad \textbf{Eq. 3.16}$$

where α is the relative fraction of each scheme. $\alpha = 1$ yields a pure upwind scheme while $\alpha = 0$ is the pure central differencing scheme. Values very close to 0 are always used in this study.

3.1.4.4. Pressure-velocity coupling

Once all the discretised terms have been accounted for, it becomes apparent that there is no equation which solves for pressure in the momentum equations. Pressure is solved for through pressure-velocity coupling – what is known as a pressure correction methodology. At the start of computation, a pressure field is guessed and this is used to solve for velocity. The velocity field obtained needs to satisfy both the momentum and continuity equations; however at the end of this first stage of the computation it satisfies momentum conservation but not continuity. This velocity field is then used to calculate a pressure correction term from the linearised continuity equation. This term is used to update the velocity and pressure fields and the process is repeated until convergence is reached. The SIMPLEC algorithm for pressure velocity coupling is illustrated in Figure 3.2.

3.1.4.5.Iterative methods

The algebraic equations derived via the process described above resemble systems of linear equations. In reality, the coefficients depend on the variables and are thus non-linear. In an iterative approach, these coefficients need to be treated as linear and are solved up to a desirable level of approximation for each iteration. Since the coefficients are bound to change in the next iteration, they are not solved to full convergence as this would be superfluous and unnecessarily time-consuming. For the cases examined in this work, the

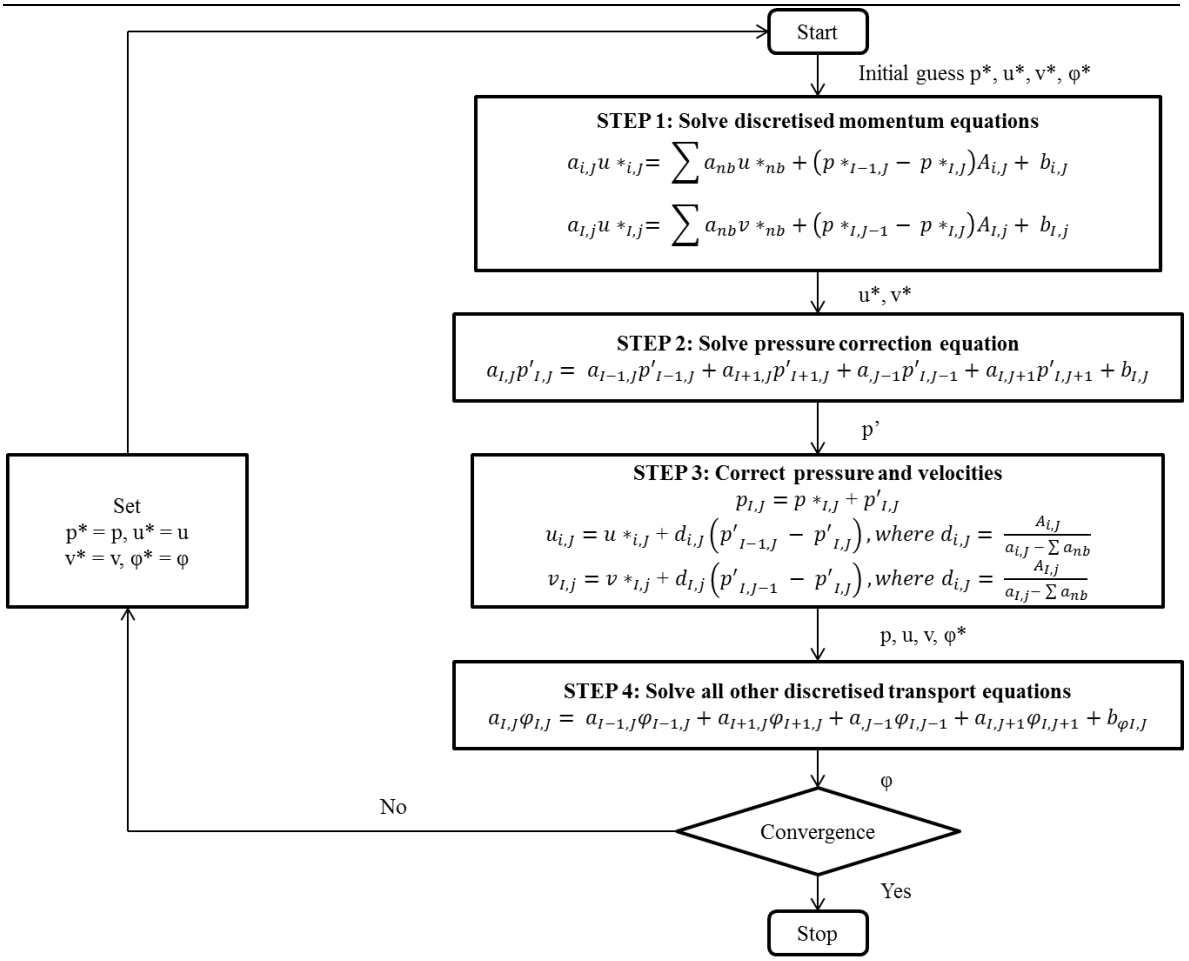


Figure 3.2: The SIMPLEC algorithm. There are no direct equations for solving pressure in the momentum equations. A pressure field is guessed and used to solve for velocity. A correction is then calculated and used to update the pressure and velocity fields. The process is repeated until convergence is reached. Adapted from Versteeg and Malalasekera [171]**.**

Algebraic Multigrid method is used. The basic rationale behind the technique is that convergence can be sped up by interpolating among a sequence of meshes of variable fineness. The cycle starts by solving iterations on a fine mesh. After a few iterations on the fine mesh, the residuals are moved to the next coarse level. This is repeated until the coarsest mesh is reached and information is then passed back on to the finest grid. During

the cycle, the residual is smoothed from the fine mesh to the coarse mesh and the correction is interpolated from the coarse mesh to the fine mesh. This is repeated until convergence is reached. The method is called algebraic as the coarser mesh is not defined by the problem geometry. Rather, it is calculated from the system matrix [173]. The technique allows for the simultaneous reduction of multiple wavelengths of error and thus speeding up convergence significantly.

3.1.5. Accounting for porosity and permeability

Several approaches can be used to model the effect of the growing clot on the flow field. Bodnar and Sequeira model the clot region by assigning a different viscosity value (a value one hundred times that of normal blood) [163]. Fogelson assigns a different porosity to the clot region [167]. Diamond carried out experimental studies which showed that a clot has different permeability and porosity values when compared with plasma [174]. On the basis of this data, the model presented in this thesis follows the porosity and permeability approach. Porosity (ε) is the measure of void spaces in a material and is expressed as the ratio of void volume to total volume. Permeability (κ) is the inverse of the linear resistance of a material to movement of fluid through it. The two variables are included in the conservation and momentum equations and can be seen in Eq. 3.17, Eq. 3.18, Eq. 3.19 and Eq. 3.20.

$$\frac{\partial(\varepsilon\rho)}{\partial t} + \nabla(\varepsilon\rho\boldsymbol{u}) = 0 \qquad \textbf{Eq. 3.17}$$

$$\frac{\partial(\varepsilon\rho u)}{\partial t} + \nabla(\varepsilon\rho u\boldsymbol{u}) = -\varepsilon\frac{\partial p}{\partial x} + \nabla(\varepsilon\mu\nabla u) - \frac{\varepsilon^2\mu}{\kappa}u + S_{Mx} \qquad \textbf{Eq. 3.18}$$

$$\frac{\partial(\varepsilon\rho v)}{\partial t} + \nabla(\varepsilon\rho v\boldsymbol{u}) = -\varepsilon\frac{\partial p}{\partial y} + \nabla(\varepsilon\mu\nabla v) - \frac{\varepsilon^2\mu}{\kappa}v + S_{My} \qquad \textbf{Eq. 3.19}$$

$$\frac{\partial(\varepsilon\rho w)}{\partial t} + \nabla(\varepsilon\rho w\boldsymbol{u}) = -\varepsilon\frac{\partial p}{\partial z} + \nabla(\varepsilon\mu\nabla w) - \frac{\varepsilon^2\mu}{\kappa}w + S_{Mz} \qquad \textbf{Eq. 3.20}$$

3.1.6. Error and uncertainty in CFD

It is important to acknowledge that the results produced by a CFD code will have some deviation from the physical reality. There is a distinction between error and uncertainty. In this work, uncertainty is defined as the deficiency in a CFD model which is the result of a lack of knowledge. Error is considered to be a discrepancy from the exact solution due to well-documented discretization parameters.

The main sources of error are numerical error and user error. Numerical error exists because a mathematical model is used to describe a physical phenomenon and that model is then solved using a computer, which has its limitations. Some of the errors introduced in such a system include roundoff error, iterative convergence error and discretisation error. User error includes errors and bugs which exist in the code.

Uncertainty exists because information for CFD models is often incomplete and various

assumptions have to be introduced along the way. The domain geometry, boundary conditions and physical properties of the fluid may not be known and these values are sometimes approximated. The physical model being simulated may not be fully understood thus limiting the accuracy which can be achieved.

Techniques for quantifying error and uncertainty have been and are being developed. It is important to routinely verify the CFD model by examining it and ensuring that the CFD results are within a reasonable range for a given problem. If experimental data is available, it is important that the CFD results be compared to this data in order to validate the model.

3.2. Chemical reactions

Clotting in aneurysms is modelled as a convection-diffusion-reaction system in this work. The reaction part of the system comprises the delivery of biochemical species to the site of clot initiation and growth. In addition, these proteins interact with each other and the growing clot, resulting in the production and depletion of the species. Two biochemical models are used to model the change in concentration of each species and then the calculations are carried out using a stiff equation solver. The code implemented in this section functions regardless of the dimension of the grid (two-dimensions, axisymmetric, three-dimensions).

3.2.1. Modelling biochemical reactions

The transport equation discussed in Section 3.1.2. is used to describe the change in concentration for each protein and is illustrated in Eq. 3.21.

$$\frac{\partial C_j}{\partial t} + \nabla(C_j \boldsymbol{u}) = \nabla(\Gamma \nabla C_j) + S_j \qquad \textbf{Eq. 3.21}$$

where C is the concentration for protein j.

The reaction rates are calculated using first order stoichiometric kinetics or Michaelis-Menten kinetics. For first order reaction kinetics, the relationship between reactant and product is shown in Eq. 3.22 while the Eq. 3.23 shows how the change in concentration for the product is calculated.

$$A + B \xrightarrow{k} C \qquad \textbf{Eq. 3.22}$$

$$\frac{d[C]}{dt} = k[A][B] \qquad \textbf{Eq. 3.23}$$

where k is the reaction rate, A and B are reactants and C is the reaction product.

Michaelis-Menten kinetics describes the behaviour of enzymatic action. At low substrate concentration, the amount of substrate limits the reaction. At high substrate concentration, the number of available enzyme sites limits the rate at which the reaction takes place. For a given enzyme concentration, the rate eventually reaches a constant value and further addition of substrate cannot alter this rate. This relationship between enzyme, E, substrate,

S, and product, P, is described by Eq. 3.24 and the rate at which product is formed is given by Eq. 3.25.

$$E + S \leftrightarrow ES \rightarrow E + P \qquad \textbf{Eq. 3.24}$$

$$\frac{d[P]}{dt} = \frac{k_{cat}[E][S]}{K_m + [S]} \qquad \textbf{Eq. 3.25}$$

where K_m is the substrate concentration for which the rate is at half maximal value and k_{cat} is the number of substrate molecules converted to product by each enzymatic site per unit time.

3.2.2. Solving the system of biochemical equations

The Rosenbrock method is used to solve the differential equations which describe the chemical reactions in the system. The method was developed for the solution of stiff equations and belongs to the family of implicit Runge-Kutta methods. A stiff system of equations in one where there is great variation in reaction rates between different reactions in the system. The method replaces non-linear systems with a system of linear equations.

The method starts off with an ordinary differential equation seen in Eq. 3.26. Implicit differencing results in Eq. 3.27. Eq. 3.28 gives the gradient which can then be arranged to make $f(y_{n+1})$ the subject of the equation. This is substituted into Eq. 3.27 to yield Eq. 3.29. Finally, rearranging yields Eq. 3.30.

$$y' = f(y) \qquad \textbf{Eq. 3.26}$$

$$\frac{y_{n+1} - y_n}{h} = f(y_{n+1}) \qquad \textbf{Eq. 3.27}$$

$$\frac{\partial f}{\partial y_n} = \frac{f(y_{n+1}) - f(y_n)}{y_{n+1} - y_n} \qquad \textbf{Eq. 3.28}$$

$$y_{n+1} = y_n + h\left[f(y_n) + \frac{\partial f}{\partial y_n}(y_{n+1} - y_n)\right] \qquad \textbf{Eq. 3.29}$$

$$y_{n+1} = y_n + \frac{h.f(y_n)}{\left[1 - h\frac{\partial f}{\partial y_n}\right]} \qquad \textbf{Eq. 3.30}$$

The method seeks a solution of the form seen in Eq. 3.31. The corrections, k_i, with coefficients, c_i, are calculated by solving s linear equations that generalise Eq. 3.29.

$$y(x_0 + h) = y_0 + \sum_{i=1}^{s} c_i k_i \qquad \textbf{Eq. 3.31}$$

The method is fourth-order and is fairly easy to programme. A code, which is used in this study, is provided alongside a description of the model in Hairer and Wanner [175].

3.3.Modelling clot growth

In the two-dimensional models presented in this thesis, clot growth is modelled by coupling growth to thrombin concentration. In work done by Tim Bowker, the growth of the clot was prescribed by a constant velocity. It was decided that a more realistic method

of determining clot growth would be to link it to a protein present in the coagulation cascade. Given the central role of thrombin discussed in Chapter 1, it was thought that this would be an appropriate choice. The idea of coupling clot growth with protein concentration is not an altogether absurd one. The models presented by Anand [162] and Bodnar [163] both depend on fibrin concentration to differentiate the clot region from the rest of the fluid region.

Decisions about whether or not cells lie within this clot region are made on the basis of thrombin concentration and location on the grid. A cell needs to meet one of two criteria: the cell should either exceed the threshold thrombin concentration and fall along the initiating wall or it should exceed the threshold concentration and have a neighbour cell which is already in the clot region. This simulates the *in vivo* process where platelets can only really become a part of the growing clot mass if they attach to the injured surface or to other activated platelets. In addition, a high enough thrombin concentration around the platelets ensures the formation of a fibrin mesh which stabilises the mass. The adherence of platelets to the membrane surface is observed from the start of clot development, prior to thrombin formation. Based on observations made by Falati et al [55] and Hoffman et al [68], the model presented in this chapter has a predetermined layer which represents the clot region. This layer is located along the zone of injury, representing the initial layer of

adhered platelets. It is present from 10s and not from the beginning because the flow simulation first needs to stabilise.

In complex, three-dimensional geometries, it becomes very difficult to keep track of connectivity of different cells. In addition, it is plausible that the clot may be initiated along different portions of the aneurysm wall as the case under examination is a pathological one. These clots may continue to grow independently or may merge to form a single clot which then propagates towards the centre of the aneurysm sac. It becomes necessary to employ a method which is able to handle clot growth with the added complexity of the three-dimensional geometries under consideration. While the scenarios encountered may not always be extremely complex, the method should be able to account for all situations. The method should also be able to propagate clot growth for a number of different variables acting at the same time. This condition needs to be fulfilled as the model needs to be used for further elucidating clot growth in aneurysms. The next section explores Level Set methods which are used to track the surface of the growing clot. These methods are considered appropriate in this case as they do not require explicit representation of the clot front, thus making it easy to deal with surfaces of varying complexity.

Chapter 5 presents a detailed account of modelling clot initiation and propagation in three-dimensions. Various factors which may be thought to contribute to clotting in aneurysms are explored. In the end, a strain rate threshold is used for clot initiation in realistic three-dimensional geometries. Clot propagation velocity is linked directly to thrombin concentration, thus the velocity at which the clot advances resembles a thrombin production curve during clot formation.

3.4. Level Set methods

There are many applications in CFD where it may be necessary to track the interface between two fluids. The complexity of such problems is varied and both Lagrangian and Eulerian approaches are employed to solve the problems. Lagrangian methods track the movement of specific points and particles and incorporate advanced methods of monitoring the connectivity between these points. Eulerian approaches embed an interface on a fixed, external grid and track –or solve for – the movement of a surface relative to that grid. An example of the latter approach would be the Volume of Fluid method which is widely used in CFD codes. Another technique which is implemented in CFD is Level Set methods. These can be used for both the location of an interface and for its propagation. The Level Set method used in this work was taken from Osher and Fedkiw [176] and adapted for use in coagulation in aneurysms by Bowker [22]. The description of implicit

functions and Level Set methods given below is based on Osher and Fedkiw. The components of the methodology are discussed in the sections that follow.

3.4.1. Explicit and implicit functions

An explicit function is one where the mathematical description of the function defines points found on the function. An implicit function is one where the points belonging to the function are not explicitly stated but rather the function is implied by the values of a different function. An example of this would be a surface which has points with different values. An implicit function could be the curve joining all the points with value 10.

An explicit interface representation would therefore be an explicit description of all the points on that interface. An implicit interface representation would then be an interface described as the isocontour of another function. An implicit function is defined in all of R^n and the isocontour has dimension n-1.

3.4.2. Signed distance functions

The signed distance function, a type of implicit function, is a Euclidean distance function with a sign (positive or negative). For points which fall outside the interface, Ω^+, the signed distance function, ϕ, assumes a positive sign, a negative sign for points on the

inside of the interface, Ω^-, and zero for points on the interface, $\partial\Omega$. This description is illustrated in Figure 3.3 and given by Eq. 3.32.

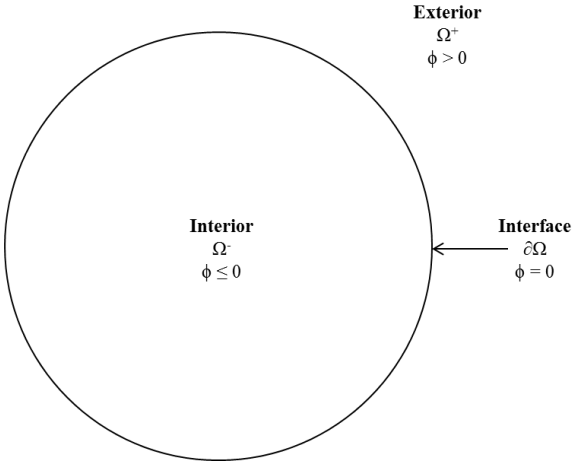


Figure 3.3: Classification of the different regions of the implicit function. Points which have a value less than zero are on the interior while those with a value greater are on the exterior. Those that equal zero are on the interface or boundary. Adapted from Osher and Fedkiw [176]**.**

$$\phi(\vec{x}) \leq 0 \; for \; all \; (\vec{x}) \; \in \Omega^-$$

$$\phi(\vec{x}) > 0 \; for \; all \; (\vec{x}) \; \in \Omega^+ \qquad \textbf{Eq. 3.32}$$

$$\phi(\vec{x}) = 0 \; for \; all \; (\vec{x}) \; \in \partial\Omega$$

The signed distance function is used often as it is fairly smooth and can be resolved with a reasonable number of grid points. The distance function, d, is given by Eq. 3.33.

$$d(\vec{x}) = \min(|\vec{x} - \overrightarrow{x_I}| \; for \; all \; \overrightarrow{x_I} \in \partial\Omega \qquad \textbf{Eq. 3.33}$$

This implies that $d(\vec{x}) = 0$ if $\vec{x}$ is a point on the interface. For points which do not fall on the interface, $d(\vec{x})$ is the distance from $\vec{x}$ to the nearest interface point $\overrightarrow{x_I}$.

3.4.3. Dynamic implicit surfaces

Level Set methods apply a dynamic element to implicit functions. The interface movement can be governed by an externally generated velocity field or by an internally generated velocity field.

The evolution of ϕ is defined using the convection equation given by Eq. 3.34, Eq. 3.35 and Eq. 3.36 where *t* represents time. Eq. 3.34 is the main Level Set equation. The partial differential equation defines the motion of the interface where $\phi(\vec{x}) = 0$.

$$\phi_t + \vec{V}.\nabla\phi = 0 \qquad \textbf{Eq. 3.34}$$

$$\vec{V}.\nabla\phi = u\phi_x + v\phi_y + w\phi_z \qquad \textbf{Eq. 3.35}$$

$$\phi_t + u\phi_x + v\phi_y + w\phi_z = 0 \qquad \textbf{Eq. 3.36}$$

Careful consideration needs to be given to the velocity field, $\vec{V}$. In most cases, this field is not only defined at the interface but over the entire computational domain, Ω. While this information is useful to have, the main area of interest is the interface region so focus is placed on the interface and on a bandwidth of the velocity field surrounding it. The bandwidth chosen is dependent on the numerical scheme used.

There are many applications where the velocity field is dependent on the Level Set function

itself. An example of this could be a velocity field which is dependent on mean curvature as seen in Eq. 3.37 where b is constant.

$$\vec{V} = -b\kappa\vec{N} \qquad \textbf{Eq. 3.37}$$

3.4.4. Construction of a signed distance function

In this work, the initial interface surface is the aneurysm surface obtained from the geometry file. The surface is represented as triangular and quadrilateral elements. Each of the quadrilateral elements is subdivided into two triangles. This is done because the operations for determining the signed distance field are dependent on surface elements being triangular, and thus, since any surface element can be reduced to a series of triangles, this operation allows for maximum generality and simplicity.

The algorithm used to determine the signed distance field is as follows:

1. All grid points are marked as being exterior to the surface.
2. All the Level Set points which are used as interpolation data points for transferring information from the flow grid to the Level Set grid are marked as interior to the surface.
3. The code loops over the triangular surfaces which form the initial aneurysm surface:

a. The Level Set grid point closest to each triangle node is determined.

b. A list of points neighbouring those determined in a. is created. The neighbours are selected by looking at $i \pm n_{NBRS}, j \pm n_{NBRS}, k \pm n_{NBRS}$. For each neighbour, the Euclidean distance is determined. In addition, the neighbour point has the interior/exterior test applied to it.

4. The reinitialisation routine is carried out to obtain a signed distance function. This routine is explained in the next two sections.

3.4.5. Reinitialisation and the narrow band approach

When the signed distance function is used, the field is reinitialised periodically during the course of the calculation. This is necessary because the function tends to deviate from a signed distance function as it is propagated. The frequency of reinitialisation is dependent on numerical techniques employed in a specific case. With implicit functions, the zero isocontour is of main interest and it is crucial that the methods chosen behave well in that region. All other points in the domain may be reinitialised to a signed distance function at any point during the calculation. Often, a small band around the interface is given attention for reinitialisation. As the interface evolves, some points no longer fall within the band while others will need to be added. Peng described reinitialisation as replacing ϕ with a better behaved function $\tilde{\phi}$ while keeping the interface the same [177]. When

reinitialisation is applied again, $\tilde{\phi}$ acts as the new initial condition.

Sussman et al proposed a reinitialisation equation which is given by Eq. 3.38 [178].

$$\tilde{\phi}_t + S(\tilde{\phi}_0)(|\nabla\tilde{\phi}| - 1) = 0 \qquad \textbf{Eq. 3.38}$$

$S(\tilde{\phi}_0)$ is a sign function and takes on value 0 on the interface, 1 outside the interface (Ω^+) and -1 inside the interface (Ω^-). $\tilde{\phi}_0$ is the initial value of the function. The sign function can be spatially discretised using the Godunov method and propagated forward in time using Runge-Kutta methods.

There exist some cases where the velocity or any other relevant quantity, for example chemical species concentration, is correct over the entire domain. In many cases, however, this quantity, q, is only correct at the interface, thus introducing error. To deal with this, reinitialisation could be applied at every time step. Alternatively, the quantity could be extended from the interface to relevant portions of the domain. This is achieved using Eq. 3.39.

$$q_t + S(\phi)\frac{\nabla\phi}{|\nabla\phi|}.\nabla q = 0 \qquad \textbf{Eq. 3.39}$$

In their paper, Kurenkov and Oberlack [179] indicate that reinitialisation is implemented until one of three conditions is met:

a. The number of iterations in the routine reaches the maximum number (n = 10000)

b. The local errors drop below the set limit $max_{\tilde{\phi}^{i,j,k}} \left| |\nabla\tilde{\phi}| - 1 \right| < 10^{-6}$

c. Changes observed in the $\tilde{\phi}$ field are sufficiently small:

$$max\left(\left| \frac{max_{\tilde{\phi}^{i,j,k}} \left| |\nabla\tilde{\phi}^{n}| - 1 \right|}{max_{\tilde{\phi}^{i,j,k}} \left| |\nabla\tilde{\phi}^{n+1}| - 1 \right|} - 1 \right| ; \left| \frac{\Sigma_{\tilde{\phi}^{i,j,k}} \left| |\nabla\tilde{\phi}^{n}| - 1 \right|}{\Sigma_{\tilde{\phi}^{i,j,k}} \left| |\nabla\tilde{\phi}^{n+1}| - 1 \right|} - 1 \right| ; \left| \frac{\Sigma_{\tilde{\phi}^{i,j,k}} (|\nabla\tilde{\phi}^{n}| - 1)^2}{\Sigma_{\tilde{\phi}^{i,j,k}} (|\nabla\tilde{\phi}^{n+1}| - 1)^2} - 1 \right| \right) < 10^{-4}$$

3.4.6. Specific features of Level Set methods used in this work

The implementation of the Level Set code in this work is based on the implementation of Peng et al [177] and was adapted by Timothy Bowker [22] for use in clotting in aneurysms. The focus of the paper was to develop the Level Set method for tracking dynamic interfaces rather than capturing them. An important feature of the implementation is the importance placed on localization of the method. In many ways, this simplifies the method and cuts down computational cost by concentrating calculations on the region around the interface rather than the entire domain. The method is then coupled to flow and chemistry calculations carried out in the CFD-ACE suite. This gives provision for linking clot propagation to both flow and chemistry variables.

In this work, we consider motion of the interface due to an internally generated "velocity" field. This "velocity" is dependent on the direction of the normal. This method is chosen as it best described clot growth observed in aneurysms. The clot is initiated at the aneurysm wall

and propagates inwards (normal to the wall) depending on various factors. The magnitude of the velocity field is calculated using different factors, depending on the specific case. In some studies, the velocity is proportional to strain rate while in others, it is related to thrombin concentration. Although these are the main variables explored in this work, the velocity can be related to any other variables which are calculated during simulation. The mathematical description for this motion is given by Eq. 3.40.

$$\phi_t + \overrightarrow{V_n}.|\nabla\phi| = 0 \qquad \textbf{Eq. 3.40}$$

Various factors need to be taken into account when discretizing the equation spatially. Several schemes exist to approximate the value of the derivative at the grid point of interest. The three schemes described in this paragraph are based on the method of characteristics. This method is used to determine the direction from which information should be taken to approximate ϕ_x. If $V_n > 0$, there will be no information available to the right of the grid point hence a backward difference should be used to approximate ϕ_x. Similarly, if $V_n < 0$, there will be no information available to the left of the grid point hence a forward difference should be used. The other two methods are built around a similar idea but use more sampling points or assign weights to those sampling points in order to determine the value of ϕ_x^- or ϕ_x^+. The Hamilton-Jacobi essential non-oscillatory (HJ ENO) scheme is third order accurate and uses polynomial interpolation to find ϕ which is then differentiated to

approximate values for ϕ_x, ϕ_y, ϕ_z [180]. Using HJ ENO, there are three approximations for ϕ_x. The Hamilton-Jacobi weighted essential non-oscillatory (HJ WENO) scheme assigns a weight to each of the three approximations in order to determine an appropriate upwind value [181]. Features such as discontinuities change the weight of each contribution. This scheme is fifth-order accurate. The HJ ENO and HJ WENO schemes are described in detail in Appendix A.

Two temporal discretisation schemes are used in this work. The forward Euler method is a first order scheme and is seen in Eq. 3.41. For improved accuracy, the Total Variation Diminishing Runge-Kutta (TVD RK) scheme is used [182]. This is second order accurate and this is sufficient as temporal errors have far less of an impact on the solution than spatial errors. The TVD-RK is given by Eq. 3.41, Eq. 3.42 and Eq. 3.43. Eq. 3.41 is a normal forward Euler step which advances the solution to t+Δt. The second Euler step, given by Eq. 3.42, then advances the solution to time t+2Δt. An averaging step is then required as illustrated by Eq. 3.43.

$$\frac{\phi^{n+1} - \phi^n}{\Delta t} + V_n . |\nabla \phi^n| = 0 \qquad \textbf{Eq. 3.41}$$

$$\frac{\phi^{n+2} - \phi^{n+1}}{\Delta t} + V_n . |\nabla \phi^{n+1}| = 0 \qquad \textbf{Eq. 3.42}$$

$$\phi^{n+1} = \frac{\phi^n + \phi^{n+2}}{2} \qquad \textbf{Eq. 3.43}$$

In order to ensure that calculations are stable, it is advisable that the velocity at which information travels across the Cartesian grid be at least as fast as the actual physical velocity of flow. This can be enforced using the Courant-Friedreichs-Lewy (CFL) condition. This is given by Eq. 3.44 in one dimension and is often calculated as Eq. 3.45 for multiple dimensions.

$$CFL = \Delta t \left(\frac{\max(|U_n|)}{\Delta x} \right) \leq 1 \qquad \textbf{Eq. 3.44}$$

$$CFL = \Delta t \left(\frac{\max(|\overrightarrow{U_n}|)}{\min(\Delta x, \Delta y, \Delta z)} \right) \leq 1 \qquad \textbf{Eq. 3.45}$$

The narrow band constructed needs to be appropriate for the scheme chosen to calculate derivatives. An inner band, I, bounded by $|\phi| \leq \beta(\Delta x)$, and an outer band, O $\beta(\Delta x) \leq |\phi| \leq \gamma(\Delta x)$ where $\gamma > \beta$, are defined. The inner band represents the interface region and the immediate neighbouring points. The outer band provides a zone where values can transition to the exterior region, avoiding gradient errors.

The Level Set code is implemented using the narrow band approach previously described and follows the following steps:

1. ***Initialisation.*** The interface is known hence a band of cells is built around it where calculations will take place. The reinitialisation equation is applied to ensure that a signed distance function is returned.

2. ***Interface velocity calculation.*** The interface velocity is calculated from ϕ itself or from an external velocity field.
3. ***Extension of interface velocity.*** The interface is the only place where the velocity is correctly known hence the velocity is extended to the remainder of the grid points in the band.
4. ***Advancing of the Level Set.*** The computed normal velocity is then used to propagate the Level Set appropriately.
5. ***Inspection.*** The field is examined and corrected if necessary. This can take place in several ways
    a. The gradient is calculated. If it falls outside of the accepted bounds, then ϕ is reinitialised and then step 2 is executed.
    b. If the interface moves too close to the edge of the band, the band needs to be rebuilt by going back to step 1 and including or excluding appropriate points. From there, step 2 is carried out again.

3.4.7. Interfacing the Level Set code with CFD-ACE

It is necessary that information travel between the Level Set Cartesian grid and the flow and chemistry solver grid in order to create a coupled, interdependent system.

For a given variable, information is transferred from the Level Set domain (M) to the flow domain (m) using trilinear interpolation. For a unit cube, Eq. 3.46 gives the calculation which transfers this information. If the cube is arbitrary, it is scaled and translated back to a unit cube.

$$\begin{aligned} m(\boldsymbol{p}) = {} & M_{000}.(1-p_x).\left(1-p_y\right).(1-p_z) + M_{100}.p_x.\left(1-p_y\right).(1-p_z) \\ & + M_{010}.(1-p_x).p_y.(1-p_z) \\ & + M_{001}.(1-p_x).\left(1-p_y\right).p_z + M_{101}.p_x.\left(1-p_y\right).p_z \\ & + M_{011}.(1-p_x).p_y.p_z + M_{110}.p_x.p_y.(1-p_z) \\ & + M_{111}.p_x.p_y.p_z \end{aligned} \qquad \textbf{Eq. 3.46}$$

where p is the point where information is being transferred to on the flow grid.

Interpolation from the flow grid (m) to the Level Set grid (M) is achieved by using inverse-weighted distance interpolation from the nearest N neighbours. The code determines a Level Set point's nearest flow neighbours. These neighbours are then assigned a weight depending on their distance from the Level Set point. The value of the variable on the Level Set grid is then given by Eq. 3.47.

$$M = \frac{\sum_{n=1}^{N} w'_n m_n}{\sum_{n=1}^{N} w'_n} \qquad \textbf{Eq. 3.47}$$

where w'_n is the weighting for the specific flow grid point and is given by Eq. 3.48.

$$w'_n = d_n^{-E} \qquad \textbf{Eq. 3.48}$$

where E is a positive integer which ensures that flow grid points closer to the Level Set grid point of interest have greater weighting.

3.5.Contributions made

The methods presented in this chapter are all existing methods. The level set methods were adapted for use in three-dimensional, realistic geometries by Tim Bowker.

The unique contributions made in this thesis are found in three main areas. The first is in the two-dimensional model presented in Chapter 4. Rather than prescribing the growth of the clot by assigning a steady velocity for propagation of the clot, clot growth was linked to a threshold thrombin concentration. This exhibits much more realistic clot growth (when compared with videos of intravital microscopy). Like Anand and Bodnar's models, once concentration exceeds a threshold value, the cell falls within the clot region and assumes properties of the clot zone rather than the plasma zone.

The second main contribution is the adaptation of the biochemistry code to ensure that it functions regardless of the dimension of the geometry being examined. This is achieved by assigning dependencies to cell centres and boundary conditions rather than to regions specified by dimensions.

Finally, in three dimensions, the biochemistry, level set and flow codes were linked. Previously, the level set code was only linked to the flow code. The addition of the biochemistry code made it possible to examine the effect of biochemical proteins on clot propagation and initiation. In addition, it makes it possible to examine the effects of mechanical and biochemical effects simultaneously.

4. Results: Clot growth under flow in two dimensions

In this chapter, the process of blood clot development in a two-dimensional flow domain is examined. The flow delivers proteins and cells to the site of blood clot development. The growing clot, in turn, influences the flow field by assuming different porosity and permeability values to the rest of the fluid region. The clot thus "obstructs" the flow mechanically [47], [48]. *The models presented here form the basis of all other results presented in this thesis. The initial use of a simple two-dimensional idealized template allows for the verification of model specifics without the added complexity of a realistic, pathological, three-dimensional geometry. The chapters which follow on then present the exploration of factors thought to contribute to clotting in aneurysms. The advantage of in silico models in this case is that they allow for the investigation of phenomena which may prove difficult to observe in vitro or in vivo.*

4.1. General considerations

Blood clot formation is the result of the confluence of many intricate processes. Central to this system is the transport of relevant cells and proteins to the site of clot initiation. The

cardiovascular system provides an efficient mechanism of transporting nutrients to cells and organs around the body and is no less important in haemostasis.

A large portion of the solid mass of a thrombus is formed by platelets which are held in place by the fibrin mesh [99]. The centrality of platelets to the process of healing a vascular wall injury cannot be overstated [55]. The stability of the clot, however, is guaranteed by the effective formation of the fibrin mesh. Modellers often select one of these two aspects of the clot to focus on. For example, Filipovic [158] and Diamond [159], [160] place emphasis on the role of platelets. Others, such as Basmadjian [161] and Mann [16] place emphasis on the transport of chemical species which contribute to the formation of a fibrin mesh. The focus is guided by the intended purpose of the model and the ability to represent the less focal feature without going into too much detail.

In this work, greater focus is placed on the chemical reactions which eventually lead to clot formation. The platelets are represented by assigning a different porosity to the clot region, an effect which is observed *in vivo* [174]. This region is also able to support reactions which would only take place on platelet membranes [51], [60]. In the models presented in this work, intrinsic tenase production is only supported on cells which are deemed to be in the clot region.

In developing a two-dimensional model of clotting in an artery, it becomes evident that there are details which are presented in a rather vague and not adequately quantitative manner in the literature. There are a few sources which report the value of the critical thrombin concentration at which coagulation transitions from the initiation to the propagation phase. The effect of tissue factor is also not fully understood. Finally, the sensitivity of the model to the biochemical network chosen is unknown. The work presented in this chapter attempts to answer some of these questions.

4.1.1. Critical thrombin concentration

The central role played by thrombin in the process of coagulation has already been thoroughly discussed in the Chapter 1. Many coagulation proteins are required for the formation of thrombin and it, in turn, activates other proteins and blood cells. In one way or another, all haemostatic pathways encounter thrombin [156]. It has been shown that a small amount of thrombin is formed in the initiation stage. This same thrombin is then central to the activation of co-factors and amplification of thrombin production [49], [63]. What remains vague in the literature is the actual quantity of thrombin produced in the initiation stage; a wide range of values is presented: Furie [49] and Hoffman [63] state that a small amount of thrombin is formed. Mann et al give a more specific value and estimate the value to be in the nanomolar order of magnitude [183]. Once this threshold

concentration of thrombin is reached, platelet activation takes place and co-factors are activated, leading to the accelerated formation of thrombin and then fibrin. It is hypothesized that the value of this critical thrombin concentration has a significant impact on the nature of the clot formed. A value which is too low will overestimate clot growth. It is therefore important to determine this threshold value as it affects the development of the clot in the computational model.

In the two-dimensional model, computational cells which have reached the critical thrombin concentration assume different porosity and permeability values to the rest of the fluid domain. This change in parameters simulates the *in vivo* process where platelets aggregate and are activated, changing the fluid properties of the clot. Once fibrin is formed a stable clot is formed. The appearance of fibrin coincides with the end of the initiation phase [184]. Examination of the critical thrombin concentration allows for the estimation of a figure of what this critical value may be and for verifying whether or not this value has a significant impact on clot development.

4.1.2. Tissue factor expression

It is important to determine the computational clotting model's sensitivity to tissue factor. *In vivo*, the inactive proteins circulating in the blood would come into contact with a

limited concentration of surface bound tissue factor. The number of available binding sites would eventually limit the rate at which the reaction could occur [185]. This system is modelled by limiting the exposure time of tissue factor in the computational model. The amount of thrombin produced is examined over a range of exposure times. Different tissue factor concentrations are used to initiate clotting in literature [15], [16]. An examination of the initial tissue factor concentration and the effect that this has on thrombin production is observed. Finally, in the blood-borne tissue factor cases, the model's sensitivity to tissue factor diffusivity is examined.

It is now widely accepted that tissue factor is the initiator of clotting *in vivo* [49], [63]. The relative roles of membrane bound tissue factor and blood-borne tissue factor are not yet well understood. Work carried out by Nemerson and various collaborators over the years supports the view that tissue factor circulates on microparticles and contributes to clot development [126], [128], [186]. It is thought that this especially true in pathological states where the mechanisms of clotting may be slightly altered to those observed under physiological conditions [131]. A microscopic study in mice by Falati et al showed that although tissue factor was present throughout the growing thrombus, the bulk of the protein was located along the vessel wall [55]. A different study by Butenas et al argued that quantities of circulating tissue factor in plasma were too low to produce quantities of

thrombin observed in other studies thus questioning the role of blood-borne tissue factor in growing clots [130]. In this work, a comparison is made between simulations run with blood-borne tissue factor and those computed with surface-bound tissue factor only. We hypothesise that blood-borne tissue factor may give a more realistic physiological thrombin curve.

4.1.3. The effect of the chosen biochemical cascade

A wide variety of models have been developed in an attempt to describe the process of coagulation. Different investigators approach clotting from different starting points and the intended purpose of the model determines the emphasis placed on different aspects of the process of coagulation. Of particular interest to this study are existing biochemical models which focus on the clotting cascade. These can be coupled with flow to observe the influence of flowing blood on the growing clot and vice-versa. Even within this subset of coagulation models, diversity in approach is evident. While considerable variation exists, the outcome of these different models should be somewhat constant provided that they describe the same physiological process. This hypothesis is examined by coupling two very different biochemical networks with blood flow.

The Wagenvoord model employs a ‘top-down’ approach to describe the coagulation

process [187]. The laboratory developed the calibrated automated thrombogram (CAT), a technique which can be used to determine hypercoagulability and hypocoagulability [156]. The end product is a graph which shows thrombin concentration for a specific patient over time as seen in Figure 4.1.

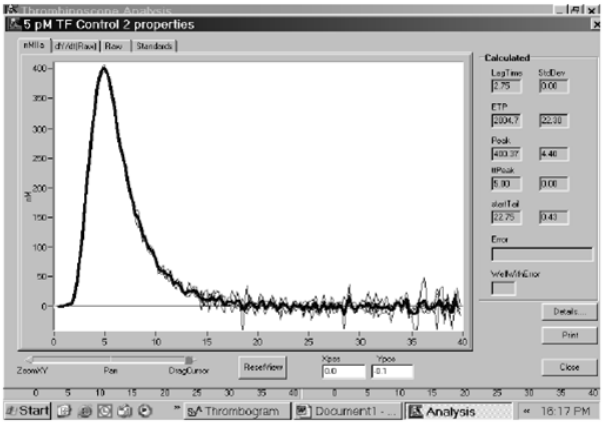


Figure 4.1: An automated calibrated thrombogram. This shows the thrombin profile for a specific patient over time, allowing for the determination of hypocoagulability and hypercoagulability states. Taken from Hemker et al [156]**.**

The chemical equations for this model are obtained by fitting six reactions to the thrombin curve. The limitation of this model is that the set of equations fitted to a curve is not unique. Much emphasis is placed on validating the computational results with experimental work. A graph which does not match the experimental data is confirmation that the chosen equations are incorrect. A graph which does match the data, however, does not necessarily confirm that the chosen equations are correct as many different combinations can be used to achieve the reproduce the thrombin graph [187]. Even though

this is the case, in a fast-paced, clinical setting where intervention is patient-specific, the Wagenvoord model allows for the development of the most expedient and user-friendly solution, as it allows for practical measurement of parameters on a per patient basis.

Other models employ a 'bottom-up' approach where individual reactions describing the process of coagulation are built up into a system. One such example is the Mann model which consists of twenty-seven reactions and forty-two reaction constants [16]. The equations and constants are determined experimentally and implemented *in silico*. This model was the first comprehensive model to be able to take in a set of inputs and predict empirical outcomes for clotting and has become a gold standard. The challenge with using this model in a clinical setting is the amount of effort required to determine all the reaction constants for a patient-specific solution.

The Wagenvoord model and Mann model approach the challenge of finding equations and constants for coagulation reactions from dramatically different perspectives. Coupling each of the aforementioned models to flow would allow for examining the effect of the chosen biochemical model on clot development. It would also confirm whether or not the hypothesis that the chosen model does not have that significant an impact on clot formation is true.

4.2.Model specifications

Two main computational methods are used in this chapter. Computational fluid dynamics is used to account for the transport of chemical species to and from the site of injury. It is also within this framework that porosity and permeability are accounted for. A stiff equation solver is used to calculate the change in concentration for the different biochemical species. Details of each approach are given in subsequent sections.

4.2.1. Simulations conducted

The simulations conducted in this study can be subdivided into three main groups. The first group focused on the effect of critical thrombin concentration. The second set of simulations focused on tissue factor studies. They are further subdivided into four groups. The first two groups are limited to surface bound tissue factor. The effect of tissue factor exposure time is examined and then the model's sensitivity to initial tissue factor concentration is investigated. These two groups are followed by blood-borne tissue factor studies. The first investigation examines the model's sensitivity to initial blood-borne tissue factor concentration while the second focuses on blood-borne tissue factor diffusivity. The third set of simulations examines the effect of the underlying biochemical cascade. A table with all the simulation identifications and input parameters can be seen in Table 4.1.

Name	Critical [TH] (M)	TF Exposure Time (s)	TF Type	Initial [TF] (M)	TF diffusivity (m^2s^{-1})	Model
Critical thrombin concentration						
THCrit15	1.00E-15	1200	Surface	1.25E-10	1.00E-11	Wagenvoord
THCrit12	1.00E-12	1200	Surface	1.25E-10	1.00E-11	Wagenvoord
THCrit9	1.00E-09	1200	Surface	1.25E-10	1.00E-11	Wagenvoord
THCrit8	1.00E-08	1200	Surface	1.25E-10	1.00E-11	Wagenvoord
Tissue factor exposure time						
TFexp5	1.00E-08	5	Surface	1.25E-10	1.00E-11	Wagenvoord
TFexp10	1.00E-08	10	Surface	1.25E-10	1.00E-11	Wagenvoord
TFexp30	1.00E-08	30	Surface	1.25E-10	1.00E-11	Wagenvoord
TFexp60	1.00E-08	60	Surface	1.25E-10	1.00E-11	Wagenvoord
TFexp1200	1.00E-08	1200	Surface	1.25E-10	1.00E-11	Wagenvoord
Initial tissue factor concentration						
TFconc13	1.00E-08	1200	Surface	1.25E-13	1.00E-11	Wagenvoord
TFconc12	1.00E-08	1200	Surface	1.25E-12	1.00E-11	Wagenvoord
TFconc11	1.00E-08	1200	Surface	1.25E-11	1.00E-11	Wagenvoord
TFconc10	1.00E-08	1200	Surface	1.25E-10	1.00E-11	Wagenvoord
Initial blood-borne tissue factor concentration						
bbTFconc18	1.00E-08	1200	Blood-borne	1.25E-18	1.00E-11	Wagenvoord
bbTFconc15	1.00E-08	1200	Blood-borne	1.25E-15	1.00E-11	Wagenvoord
bbTFconc12	1.00E-08	1200	Blood-borne	1.25E-12	1.00E-11	Wagenvoord
bbTFconc9	1.00E-08	1200	Blood-borne	1.25E-09	1.00E-11	Wagenvoord
Blood-borne tissue factor diffusivity						
bbTFdiff11	1.00E-08	1200	Blood-borne	1.25E-12	1.00E-11	Wagenvoord
bbTFdiff10	1.00E-08	1200	Blood-borne	1.25E-12	1.00E-10	Wagenvoord
bbTFdiff9	1.00E-08	1200	Blood-borne	1.25E-12	1.00E-09	Wagenvoord
bbTFdiff8	1.00E-08	1200	Blood-borne	1.25E-12	1.00E-08	Wagenvoord
bbTFdiff7	1.00E-08	1200	Blood-borne	1.25E-12	1.00E-07	Wagenvoord
Model effect						
Mann	1.00E-08	1200	Surface	1.25E-10	1.00E-11	Mann
MannBB	1.00E-08	1200	Blood-borne	1.25E-12	1.00E-11	Mann
Wvoord	1.00E-08	1200	Surface	1.25E-10	1.00E-11	Wagenvoord
WvoordBB	1.00E-08	1200	Blood-borne	1.25E-12	1.00E-11	Wagenvoord

Table 4.1: Simulation names and parameters for all simulations carried out in this study.

4.2.2. Computational fluid dynamics settings

The computational fluid dynamics studies are carried out using the CFD-ACE Suite (ESI Group, Paris, France). This code uses a finite volume method solver and details of this method are given in Chapter 3. An idealised, two-dimensional artery is selected as the region of interest for the solution of the flow equations. A rectangle of length 100mm and width 10mm is defined. The width is comparable with the diameter of human arteries of interest *in vivo* [188]. This is important as the model is applied in realistic geometries in subsequent chapters and needs to fall within the appropriate scale range. Inlet, outlet and wall boundaries are applied. Both the geometry and the grid are created in CFD-GEOM and Figure 4.2 shows the geometry and the relevant labels.

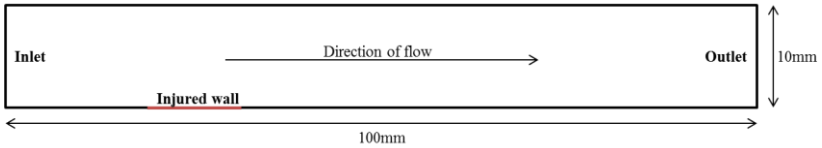


Figure 4.2: The idealised, two-dimensional artery which is used for all simulations in this study. Tissue factor is expressed along the injured wall. Inactive blood proteins are present at the start of simulation and also enter at the inlet. These are changed to their active form as they react with tissue factor and other proteins.

The geometry is discretised into a regular, Cartesian grid. Initially, results were examined over a range of grid sizes, to ensure that they are not dependent on mesh resolution. The results presented in this section are computed on a grid consisting of 32205 nodes and 31584 quadrilateral cells, shown to be sufficient for this study. The parameters for the different grid independence meshes are shown in Table 4.2.

Name	Number of cells in grid	Time step size (s)
Art4_5	15483	0.5
Art4_1	15483	0.1
Art4_05	15483	0.05
Art5_5	31584	0.5
Art5_1	31584	0.1
Art5_05	31584	0.05
Art8_5	62963	0.5
Art8_1	62963	0.1
Art8_05	62963	0.05
Art10_5	98703	0.5
Art10_1	98703	0.1
Art10_05	98703	0.05

Table 4.2: The grid and time step sizes for the different grid independence meshes.

The Crank-Nicholson scheme is used to account for the transient nature of the simulations. A time step of $\Delta t = 0.5s$ is used and the calculations are set to run for 2400 time steps. This simulates a real thrombosis time of 20 minutes. The blending factor for the Crank-Nicholson scheme is set at $\beta = 0.5$ thus making the method second order accurate. The central differencing method is used for spatial differencing. The method is blended with upwind differencing. The relative contribution from upwind differencing is set at $\alpha = 0.1$ while that from the central differencing scheme is set at $(1 - \alpha) = 0.9$. An algebraic multigrid solver is used.

The density of blood is constant and is set at $\rho = 1000 kg.m^{-3}$. The dynamic viscosity is also constant and has value $\mu = 0.004 kg.m^{-1}.s^{-1}$. Blood is assumed to be an incompressible,

Newtonian fluid in this case as the vessels under examination are considered sufficiently large for such an assumption to be made [100], [188]. Both the inlet and outlet boundary conditions are set at constant pressure. This imitates the *in vivo* condition where a pressure gradient drives the flow through the different vessels [189]. The pressure gradient, ΔP, between the two boundaries is set such that the velocity of flow is equal to that observed in physiological arteries. The velocity of flow in medium-sized, physiological arteries is often observed to be $v_{artery} = 0.07 m.s^{-1}$ [190] a value that is used in this parametric analysis, without any loss of generality. A no-slip condition is applied at the walls. A 10mm portion of the bottom wall is the initiating surface on which tissue factor is expressed. This replicates initiation of *in vivo* clotting where tissue factor expression is the trigger which instigates the formation of fibrin via a series of chemical reactions.

The CFD-ACE solver makes provision for adjusting porosity and permeability values. Through the use of user subroutines written in FORTRAN, it is possible to specify user variations and attach them at available handles in the solver code. Using porosity and permeability values specified in Diamond [174], computational cells which are within the clot region assume different values to those that are not. In the clot region, the porosity value is $\varepsilon = 0.75$ and the permeability value is $\kappa = 1.0 \times 10^{-12} m^2$.

4.2.3. Biochemical reactions

The biochemical reaction networks for the different *in silico* models are presented and described in the paragraphs below. A table of the different reaction species and their properties is seen in Table 4.3.

Protein	Inlet/Initial Concentration (nM)	Diffusion coefficient (m^2s^{-1})	Wagenvoord	Mann
TF	Variable	Unknown	Y	Y
AT	3400.00	5.50E-11	Y	Y
PT	1400.00	5.00E-11	Y	Y
X	160.00	5.50E-11	Y	Y
IX	90.00	5.50E-11	N	Y
V	20.00	2.70E-11	Y	Y
VII	10.00	5.80E-11	N	Y
TFPI	2.50	6.50E-11	N	Y
VIII (+vWF)	0.70	4.40E-12	N	Y
VIIA	0.10	5.80E-11	N	Y
IXA	0.00	6.20E-11	N	Y
XA	0.00	6.20E-11	N	Y
TH	0.00	6.70E-11	Y	Y
VIIIA	0.00	3.50E-11	N	Y
VA	0.00	3.70E-11	N	Y
XA-TFPI	0.00	4.50E-11	N	Y
IXA-VIIIA	0.00	3.20E-11	N	Y
IXA-VIIIA-X	0.00	2.90E-11	N	Y
XA-VA	0.00	3.30E-11	Y	Y
XA-VA-PT	0.00	2.90E-11	N	Y
INACT	0.00	4.50E-11	Y	Y

Table 4.3: Properties of proteins that participate in coagulation. The Y and N in the final two columns indicate whether or not the proteins are accounted for in the respective model. Y indicates participation while N indicates the absence of that protein

The proteins are transported in the flow. Temporal discretisation is achieved using the

Crank-Nicholson method as discussed in the previous section. Similarly, spatial discretisation is achieved using a blended central differencing scheme. A CFD-ACE user subroutine is used to calculate the changes in species concentration. A stiff equation solver, coded by Hairer and Wanner [175] is incorporated into the subroutine. This solver calculates the concentration updates and these are then introduced into the CFD-ACE species transport solver through the use of source terms.

Diffusivity of solutes within a porous medium is somewhat different to diffusivity in a pure fluid region. In a porous clot, the solutes would not be able to follow a direct path as they would be obstructed by platelets and fibrin strands. It is therefore necessary to define the effective diffusivity, which is the macroscopically observable diffusion through a porous medium. The concept is analogous to electrical conductivity in a dilute suspension of non-conducting spheres. Maxwell's formula is used to describe the conductivity and is applied to effective diffusivity in the case of the coagulation proteins. Eq. 4.1 describes Maxwell's equation.

$$\frac{D_e}{D_o} = \frac{\varepsilon}{[1 + 0.5(1 - \varepsilon)]} \qquad \textbf{Eq. 4.1}$$

Where D_e is the effective diffusivity and D_o is the observable diffusivity.

It is also important to note that within the clot, there are several binding sites on which

some of the reactions occur. These also affect the rate at which substances are able to diffuse through the clot. Hathcock and Nemerson observed that the diffusivity for factor Xa moving through a clot was different from that moving in plasma by a factor of 10^{-3} whereas Maxwell's formula only predicts a factor of 2/3 [127]. Bowker examined the effect of diffusivity in his computational thrombosis model. He noted that Maxwell's formula resulted in much lower thrombin concentration. The Maxwell model is implemented in this study.

Tissue factor is expressed along a portion of the bottom wall by specifying a flux value or a fixed concentration value. The flux value would represent blood-borne tissue factor while the fixed value represents membrane bound tissue factor. Inactive species concentrations are specified at the inlet of the domain. Activated species are not present as they form from the interaction between tissue factor, inactive species and other products which form during the series of reactions. The same inactive species which have a concentration greater than zero at the inlet have the same concentration throughout the fluid domain at the start of the simulation.

Figure 4.3 depicts the chemical reactions used for the Wagenvoord model in this study [15]. As seen in the diagram, thrombin (TH) is the most important product in the coagulation

process. It is also responsible for amplifying its own production. Tissue factor (TF) is the initiator of the process and results in the formation of the tenase (Xa-Va) complex. This acts as an enzyme which catalyses the formation of thrombin from prothrombin (PT). These two steps represent the initiation phase of coagulation. Thrombin then acts as an enzyme for producing more tenase, thus amplifying its own production. This step represents the propagation phase. The model also includes anticoagulant mechanisms which limit the amount of thrombin formed. Thrombin combines with antithrombin (AT) to form inactivated thrombin (INACT, in this case). This final step accounts for the anticoagulant mechanism present in coagulation. Table 4.4 lists the reactions and the constants used for each equation.

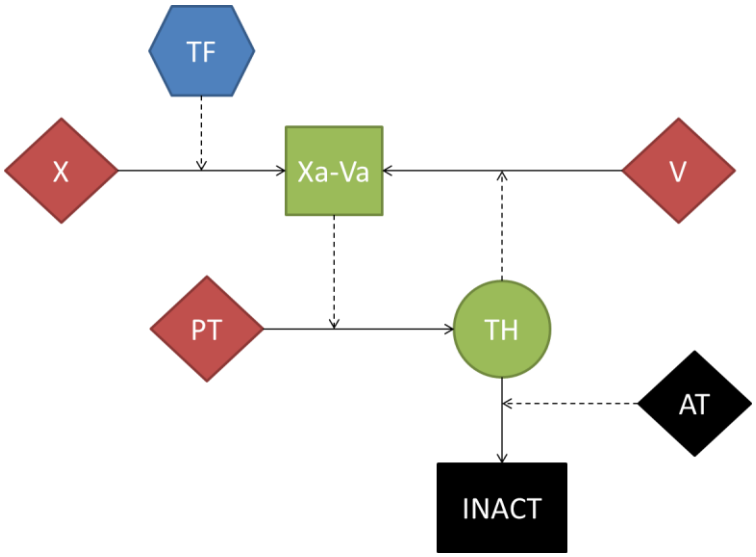


Figure 4.3: Network diagram of the Wagenvoord model. Tissue factor (TF) initiates the process of clotting and results in the eventual formation of thrombin (TH). Antithrombin (AT) then inhibits the activity of thrombin by forming the product INACT.

Step	Reaction Pathway	Forward Reaction Rate ($nM^{-1}s^{-1}$)	kcat (s^{-1})	kM (nM)
1	X + TF → XA-VA + TF		5.00E-02	1.00E+02
2	PT + XA-VA → TH + XA-VA		8.00E-02	1.00E+03
3	V + TH → XA-VA + TH		2.50E+01	5.50E+04
4	TH + AT → INACT	5.00E-06		

Table 4.4: Reaction steps and rates for the Wagenvoord model.

Figure 4.4 depicts the reaction networks for the Mann model. Figure 4.4 (A) is an illustration of the initiation stage of the coagulation cascade while Figure 4.4(B) depicts the amplification stage. The initiation stage is instigated by the exposure of tissue factor (TF). Tissue factor combines with factor VIIA to form TF-VIIA. This complex acts as an enzyme for reactions which result in the formation of factor VIIA from factor VII and factor IXA from factor IX. The complex is also an enzyme for the reaction which results in the formation of factor XA from factor X. Factor XA is crucial as it is the enzyme which catalyses the reaction which results in the formation of thrombin (TH) from prothrombin (PT). Thrombin then amplifies its own production by acting as a catalyst for the formation of factor VIIA from factor VII. Anticoagulant mechanisms can be seen clearly in both the initiation and amplification stages. In the initiation stage, tissue factor pathway inhibitor (TFPI) plays an important role in inactivating all tissue factor related complexes to prevent the formation of more thrombin than is necessary. Once a small amount of thrombin has been generated, thrombin rather than tissue factor takes the leading role in amplifying the

amount of thrombin in the system. This is clearly seen when comparing the initiation and amplification stages. Co-factors V and VIII are activated to VA and VIIIA respectively by thrombin. This results in the generation of greater quantities of thrombin by assisting the catalytic processes for factors IX and X. Also present in the amplification stage is meizothrombin (mTH), an intermediate form between prothrombin and thrombin. It has some of the characteristics of thrombin but is not as efficient in generating vast quantities of thrombin. Finally, antithrombin (AT), a component of the anticoagulant system ensures that active factors are inactivated once they have completed their task. Table 4.5 lists the equations and reaction constants for the Mann model.

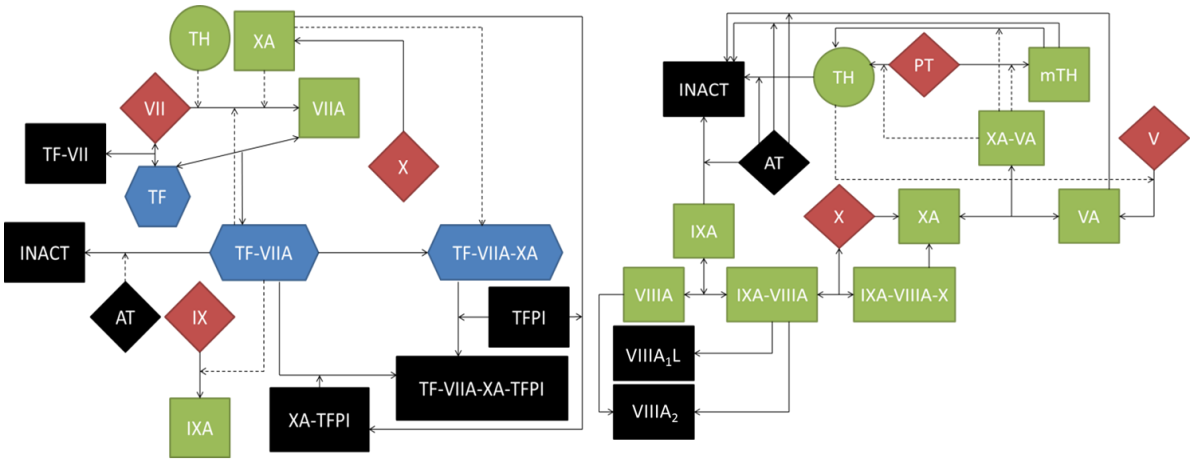


Figure 4.4: (A) The initiation phase of the Mann model. Tissue factor (TF) initiates the process of initiation and the end result is the formation of a small amount of thrombin (TH). Tissue factor pathway inhibitor (TFPI) inhibits the action of TF. (B) The propagation phase of the Mann model results in the amplification of thrombin. Antithrombin inhibits the action of thrombin and other active proteins.

Step	Reaction Pathway	Backward Rate (s^{-1})	Forward Rate 1 ($nM^{-1}s^{-1}$)	Forward Rate 2 (s^{-1})
1	TF + VII ↔ TF-VII	3.10E-03	3.20E-03	
2	TF + VIIA ↔ TF-VIIA	3.10E-03	2.30E-02	
3	TF-VIIA + VII → TF-VIIA + VIIA		4.40E-04	
4	XA + VII → XA + VIIA		1.30E-02	
5	TH + VII → TH + VIIA		2.30E-05	
6	TF-VIIA + X ↔ TF-VIIA-X → TF-VIIA-XA	1.05E+00	2.50E-02	6.00E+00
7	TF-VIIA + XA ↔ TF-VIIA-XA	1.90E+01	2.20E-02	
8	TF-VIIA + IX ↔ TF-VIIA-IX → TF-VIIA + IXA	2.40E+00	1.00E-02	1.80E+00
9	XA + PT → XA + TH		7.50E-06	
10	TH + VIII → TH + VIIIA		2.00E-02	
11	VIIIA + IXA ↔ IXA-VIIIA	5.00E-03	1.00E-02	
12	IXA-VIIIA + X ↔ IXA-VIIIA-X → IXA-VIIIA + XA	1.00E-03	1.00E-01	8.20E+00
13	VIIIA ↔ VIIIA1L + VIIIA2	2.20E-05	6.00E-03	
14	IXA-VIIIA-X → VIIIA1L + VIIIA2 + X + IXA		1.00E-03	
15	IXA-VIIIA → VIIIA1L + VIIIA2 + IXA		1.00E-03	
16	TH + V → TH + VA		2.00E-02	
17	XA + VA ↔ XA-VA	2.00E-01	4.00E-01	
18	XA-VA + PT ↔ XA-VA-PT → XA-VA + mTH	1.03E+02	1.00E-01	6.35E+01
19	mTH + XA-VA → TH + XA-VA		1.50E-02	
20	XA + TFPI ↔ XA-TFPI	3.60E-04	9.00E-04	
21	TF-VIIA-XA + TFPI ↔ TF-VIIA-XA-TFPI	1.10E-04	3.20E-01	
22	TF-VIIA + XA-TFPI ↔ TF-VIIA-XA-TFPI		5.00E-02	
23	XA + AT → INACT		1.50E-06	
24	mTH + AT → INACT		7.10E-06	
25	IXA + AT → INACT		4.90E-07	
26	TH + AT → INACT		7.10E-06	
27	TF-VIIA + AT → INACT		2.30E-07	

Table 4.5: Reaction steps and rates for the Mann model.

4.3.Findings and discussion

Three main topics are examined in this chapter. The results illustrating the computational model's sensitivity to the background biochemical model are presented and discussed. The

effect of the critical thrombin concentration which signals the start of the amplification phase is examined. An exploration of various aspects of tissue factor is also presented.

4.3.1. Grid independence study

A grid independence study was carried out to see what level of grid refinement was required to accurately capture results. Grids ranging from 15483 cells to 98703 cells were examined. For each spatial refinement level, three time steps were implemented. The solution was found to be grid independent at 31584 cells for a time step of $\Delta t = 0.5s$. Figure 4.5 shows the grid independence study results.

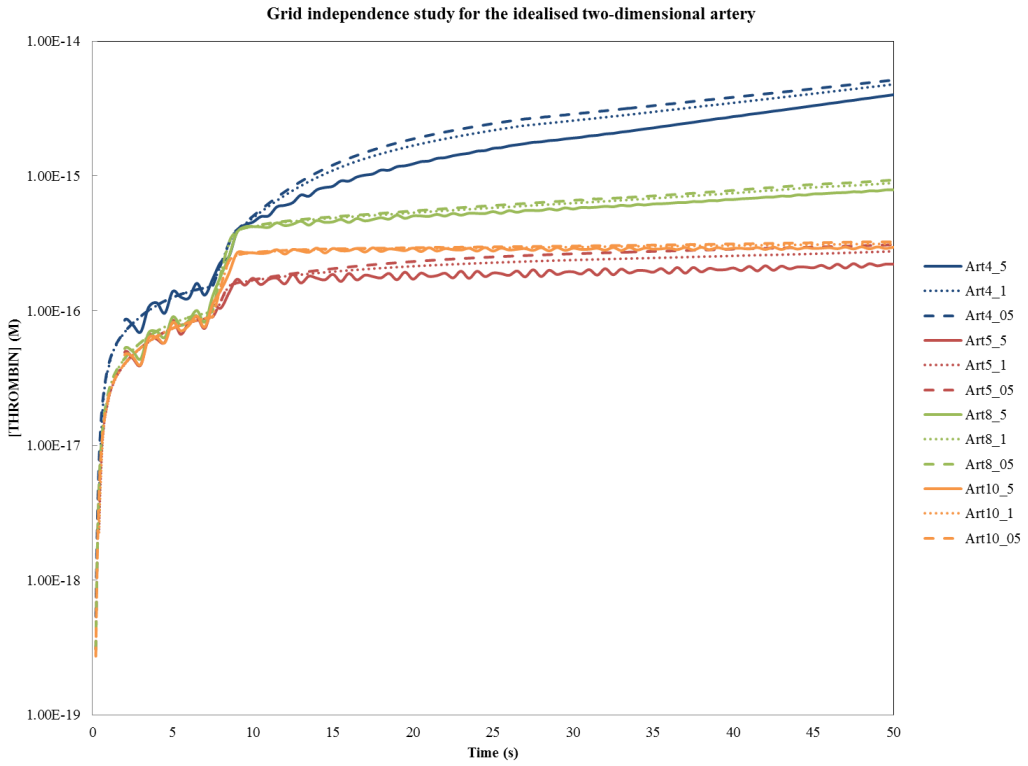


Figure 4.5: Grid independence study for an idealised, two-dimensional artery.

4.3.2. Critical thrombin concentration

A plot illustrating the effect of critical thrombin concentration on thrombin production is seen in Figure 4.6. The measurement is taken at the wall in the centre of the injured zone. THCrit15 stops at t = 1000s as divergence occurs at that point[7]. Up until that point, the curve is comparable to that of THCrit12, reaching a maximum value of [TH] = 5.3×10^{-8}M. Both THCrit15 and THCrit12 predict greater thrombin production than THCrit9 and THCrit8. The latter two models predict a maximum value of [TH] = 4.5×10^{-8}M.

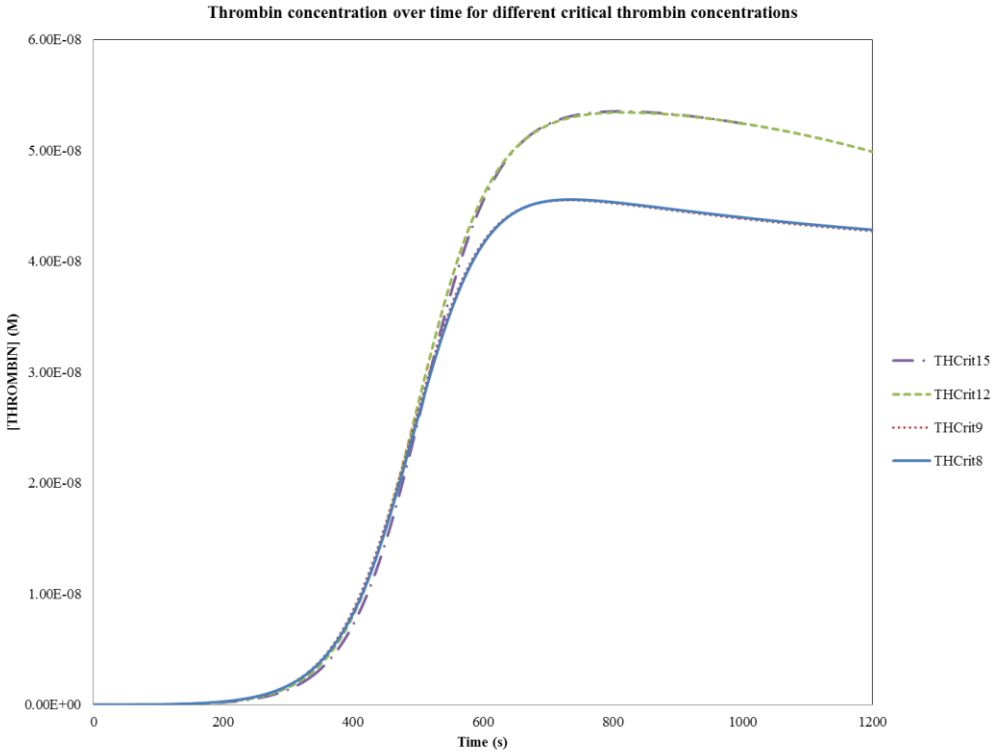


Figure 4.6: Graph illustrating the thrombin concentration over a period of 1200s for four different critical thrombin concentrations. The critical thrombin concentration signals the end of the initiation phase and the start of the amplification phase.

[7] In this case, divergence occurs because the threshold value is too low thus it overpredicts clot growth. The presence of a fully occlusive clot in the vessel disrupts the flow field, eventually resulting in divergence.

A contour plot illustrating the effect of critical thrombin concentration on thrombin production is seen in Figure 4.7. From t = 150s, it is evident that THCrit15 and THCrit12 have greater thrombin production than THCrit9 and THCrit8. This trend remains constant until t = 600s. At t = 1200s, THCrit15 has diverged while THCrit12 still has greater thrombin production in the entire domain when compared with THCrit9 and THCrit8.

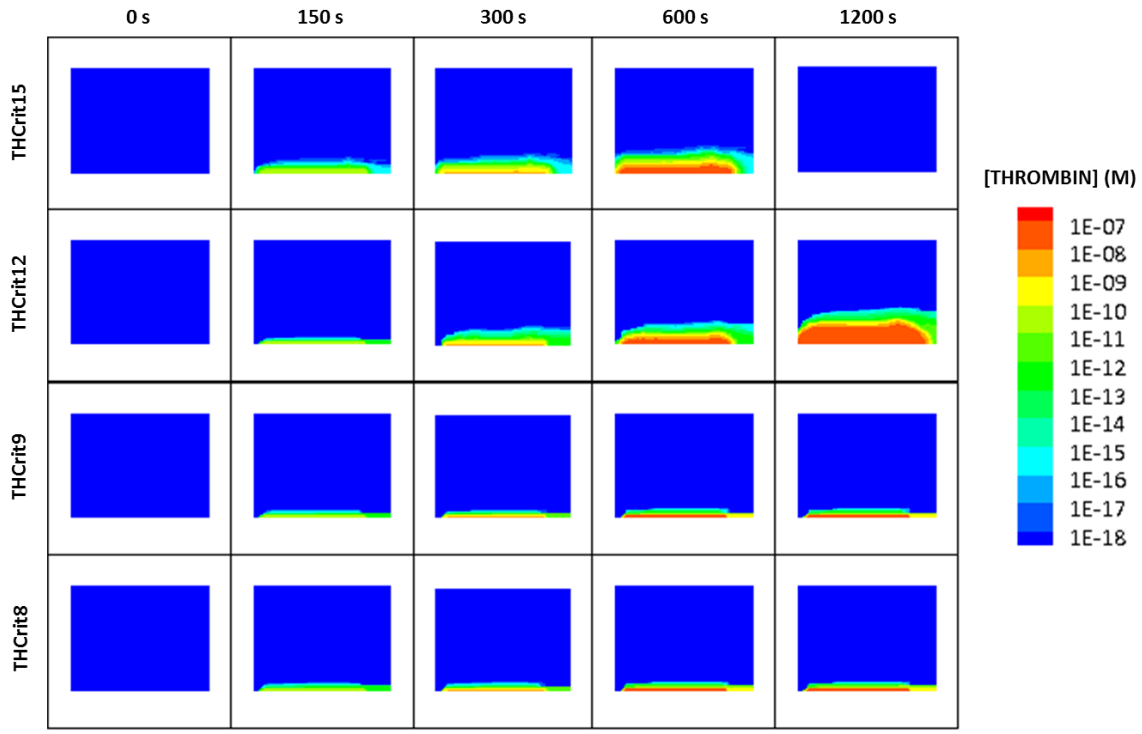


Figure 4.7: Thrombin concentration over a range of different critical thrombin concentrations. The blue block for THCrit15 at 1200s signifies divergence of the solution. Both the THCrit15 and THCrit12 clots are rather dramatic, a situation which possibly does not represent the *in vivo* behaviour of the real system.

The monitor point is placed at the centre of the zone of injury at the wall. Figure 4.8 shows that THCrit15 and THCrit12 have similar intrinsic tenase profiles. THCrit15 diverged at t = 1000s as the clot had occluded the flow domain. Unlike thrombin which reaches a

maximum concentration at [TH] = 2.0×10^{-8}M and then declines for THCrit15 and THCrit12, intrinsic tenase production levels off and reaches a constant value. THCrit9 and THCrit8 have similar profiles and these profiles are similar to those for thrombin production, seen in Figure 4.6.

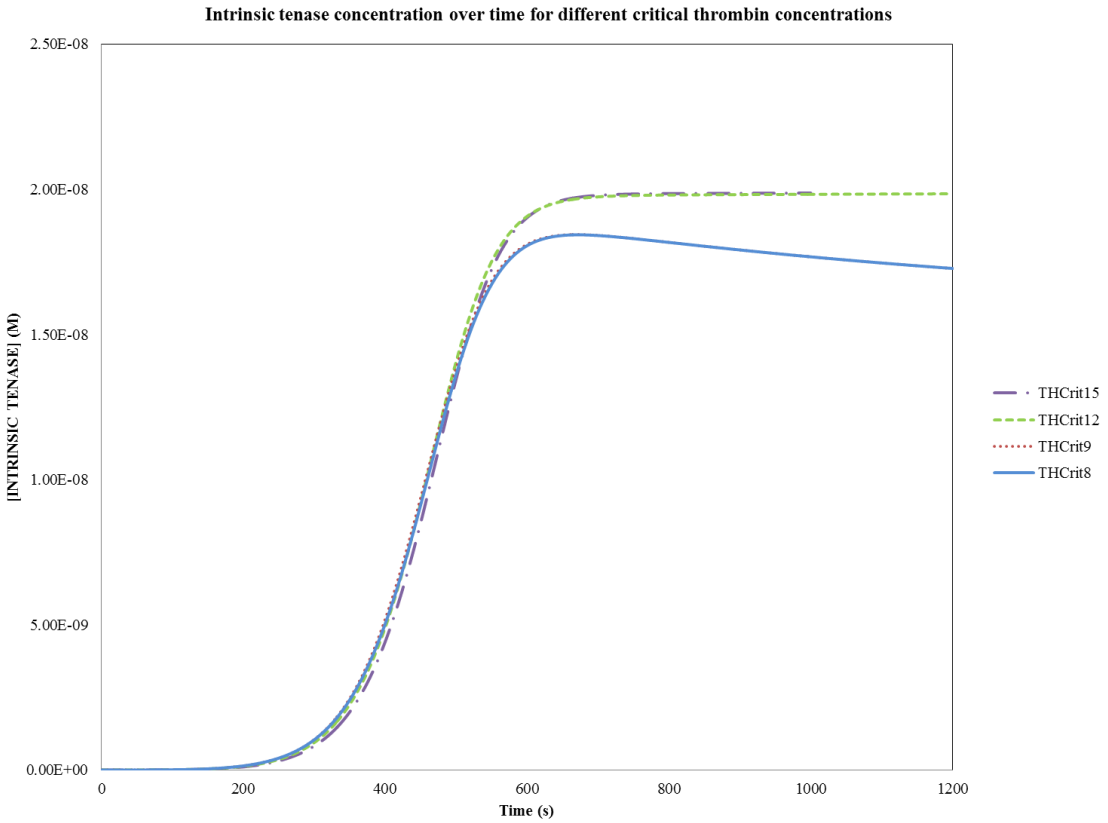


Figure 4.8: Graph illustrating the intrinsic tenase concentration over a period of 1200s for four different critical thrombin concentrations. The critical thrombin concentration signals the end of the initiation phase and the start of the amplification phase.

The monitor point for the velocity profile is placed at the centre of the rectangular domain and the result can be seen in Figure 4.9. THCrit15 shows the greatest change in velocity

magnitude over time. The velocity decreases as the clot grows towards the centre of the geometry. After t = 1000s, divergence occurs. THCrit12 has a similar decreasing trend as the clot grows but the effect is much less pronounced than it is in THCrit15. THCrit9 and THCrit8 exhibit identical trends. Following the initial stabilization of the flow field, the velocity remains constant as the clot does not grow very much.

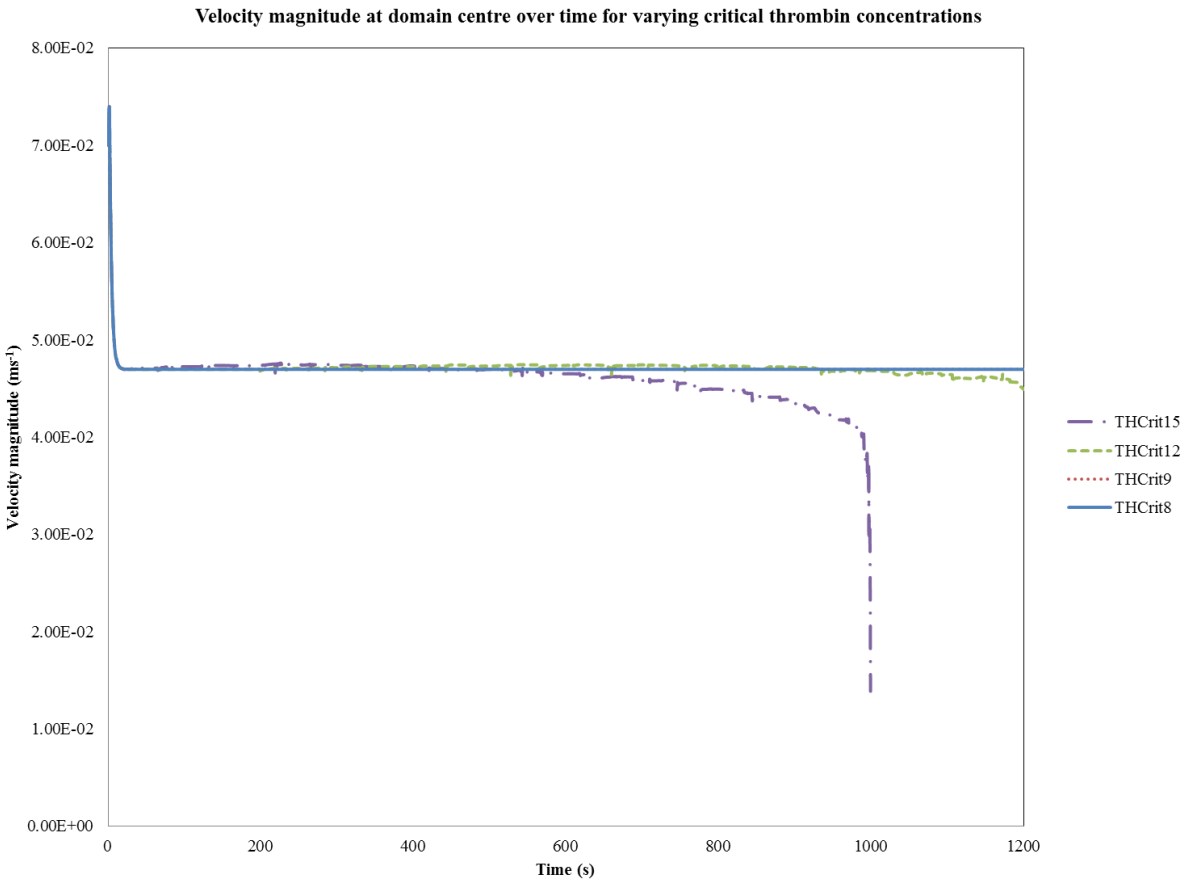


Figure 4.9: Graph illustrating the velocity magnitude at the centre of the rectangular domain over time. The velocity examined over a range of critical thrombin concentrations.

The velocity magnitude contour plot for critical thrombin concentration echoes the results

in Figure 4.9 and can be seen in Figure 4.10. The clot has the most significant impact on the flow field for the THCrit15 and THCrit12 cases. Divergence is observed at t = 1200s for the THCrit15 case. The clot region is less permeable to blood flow; hence the flow velocity is reduced in this region when compared to the rest of the fluid domain. The clot has less significant impact on the flow field for the THCrit9 and THCrit8 cases.

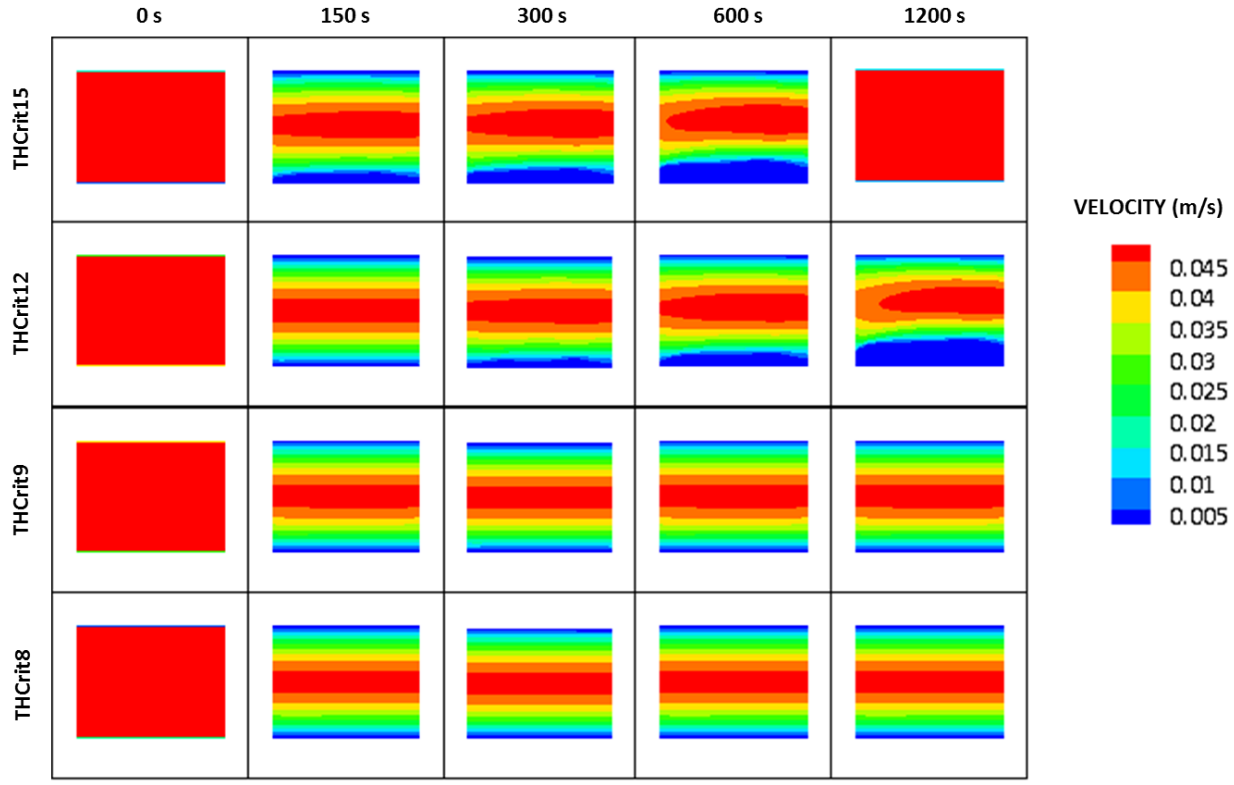


Figure 4.10: Velocity plot for different critical thrombin concentrations. The clot has a significant impact on the flow field for both THCrit15 and THCrit12. At 1200s, THCrit15 has diverged.

Figure 4.11 shows the porosity plot for a range of critical thrombin concentrations. As with

the velocity magnitude plot seen in Figure 4.9, divergence is observed at t = 1200s for the THCrit15 case. The change in porosity in the clot region is reflected in the reduced flow velocity seen in the velocity plot. THCrit15 and THCrit12 exhibit the largest clots while the clots for THCrit9 and THCrit8 are similar. The latter two cases show clot development which does not cause much disruption to the flow in the vessel. The former cases show clot development which tends towards occlusion of the blood vessel. In the THCrit15 case, occlusion does occur, resulting in the divergence of the flow field in general.

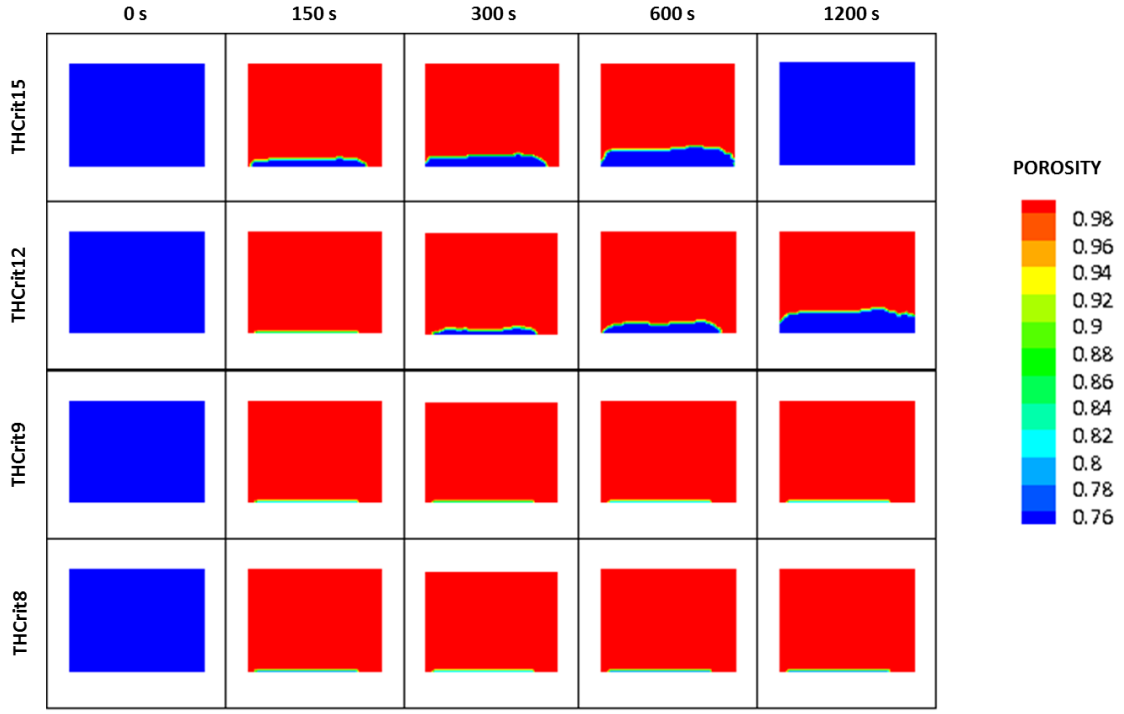


Figure 4.11: Porosity over time for different critical thrombin concentration. The plot complements the velocity plot and illustrates how regions of reduced porosity correspond with decreased flow velocity.

4.3.3. Tissue factor

The effect of tissue factor exposure time for surface bound tissue factor is examined in Figure 4.12. The exposure time is the amount of time where a concentration of surface tissue factor is exposed in the system, hence making allowance for the interaction of tissue factor and other proteins present in the system. At the lowest end of the scale, an exposure time of t = 5s results in no thrombin formation as seen for TFexp5. A rather interesting result is that lag time is similar for the TFexp10 and TFexp1200 cases while a similar trend is observed for the TFexp30 and TFexp60 cases.

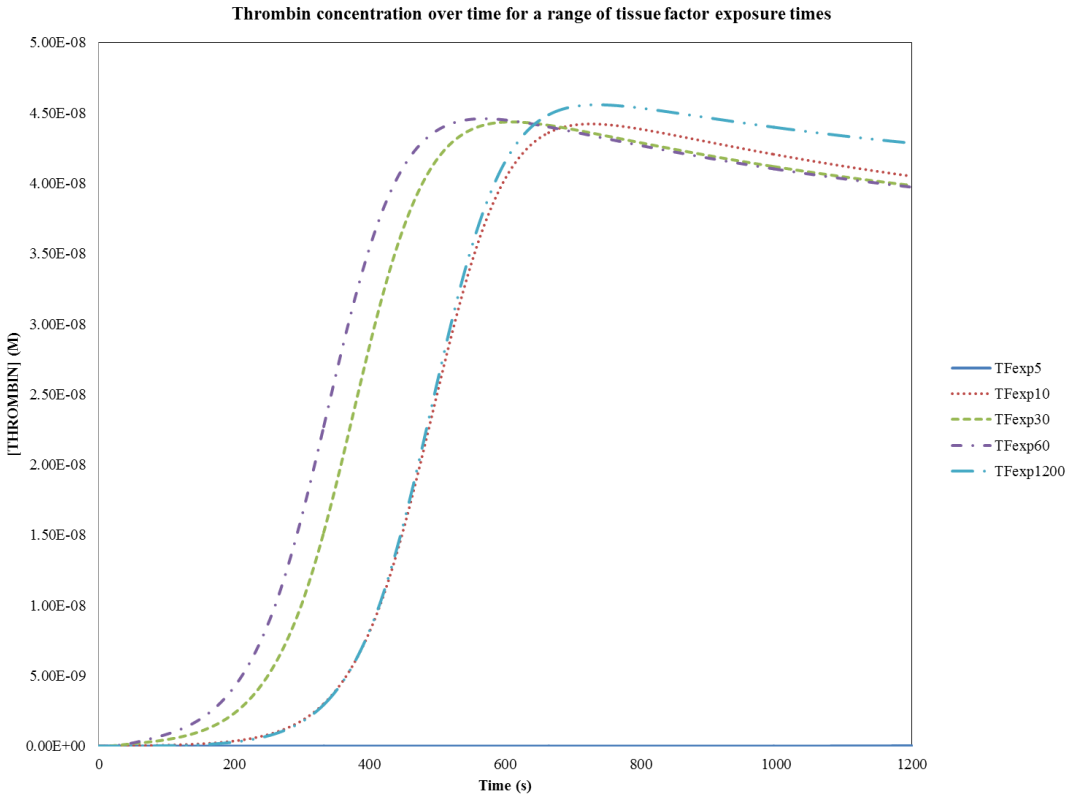


Figure 4.12: The effect of tissue factor exposure time on thrombin concentration in the system. The exposure time has a direct influence on the amount of extrinsic tenase that can be formed and that, in turn, influences the rate at which thrombin forms.

Figure 4.13 illustrates contour plots of thrombin concentration over time for different tissue factor exposure times. The greatest difference is visible for TFexp5 case. While similar maximum values of thrombin are reached for all the plots, less thrombin forms over the injury zone for the TFexp5 case. This is in agreement with the graph in Figure 4.12 where TFexp5 is plotted as a flat line at zero. The point for which the data in the graph is plotted is at the centre of the injury zone where, according to the thrombin contour plot, no thrombin forms for TFexp5.

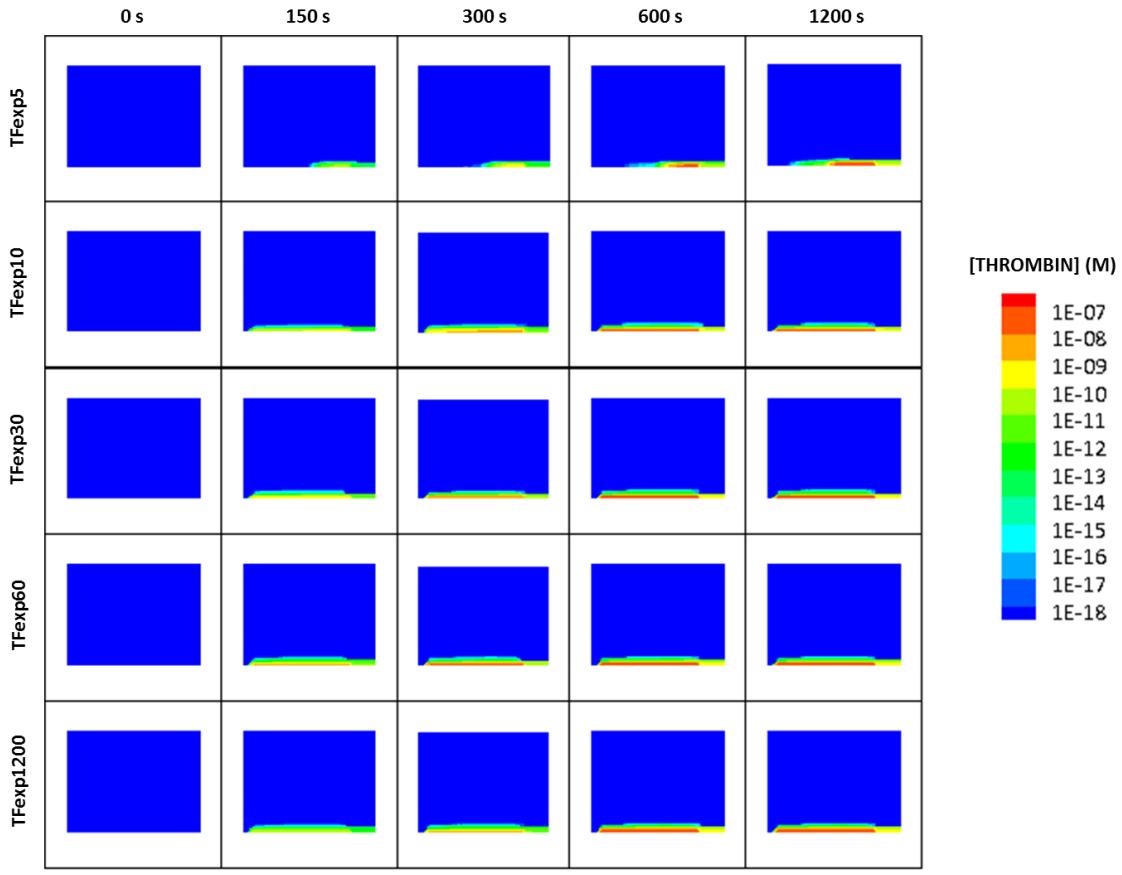


Figure 4.13: Thrombin concentration for different tissue factor exposure times. The difference is less dramatic as the exposure time increases. The greatest difference can be seen for an exposure time of 5 seconds for all time steps.

Figure 4.14 illustrates the effect of tissue factor concentration on thrombin production in the system. These results are reported for surface bound tissue factor. As the amount of tissue factor is increased, the system's lag time decreases. For TFconc11, TFconc12 and TFconc13, similar maximal thrombin concentration values at [TH] = 4.4×10^{-8}M are observed. These maximum values are reached at different points in time. TFconc11 has a lag time of approximately t = 300s while TFconc13 has a lag time of about 600s. TFconc10 has the shortest lag time and the highest thrombin value, reaching a maximum of about [TH] = 4.5×10^{-8}M.

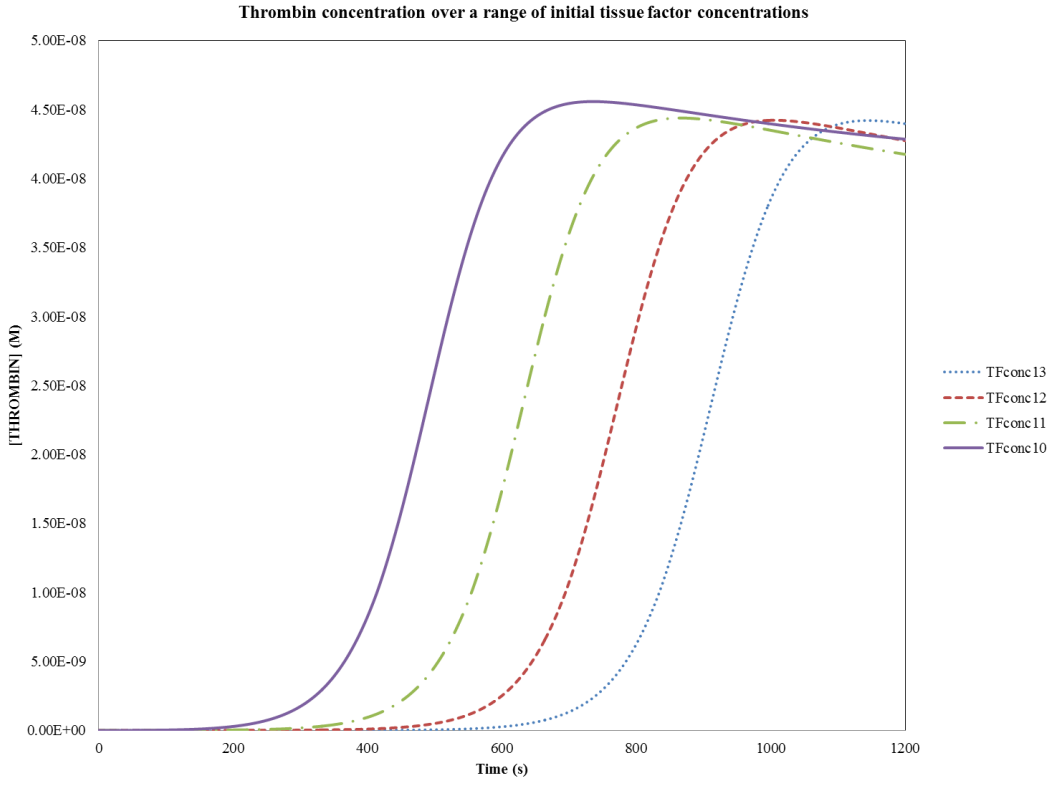


Figure 4.14: The effect of tissue factor concentration on thrombin production in the system over 1200s. The tissue factor is expressed at the vessel wall and the concentration remains constant throughout the simulation.

The illustration of thrombin concentration over a range of initial tissue factor concentrations can be seen in Figure 4.15. By t = 1200s, the maximal thrombin concentration seems fairly similar for all the cases. The greatest difference is noticeable at t = 600s where maximum thrombin concentration in the field increases with increasing initial thrombin concentration. A similar trend can also be seen at t = 300s. Prior to that point, thrombin concentration seems to fall within the same range for all the values. These observations agree with the graph in Figure 4.14.

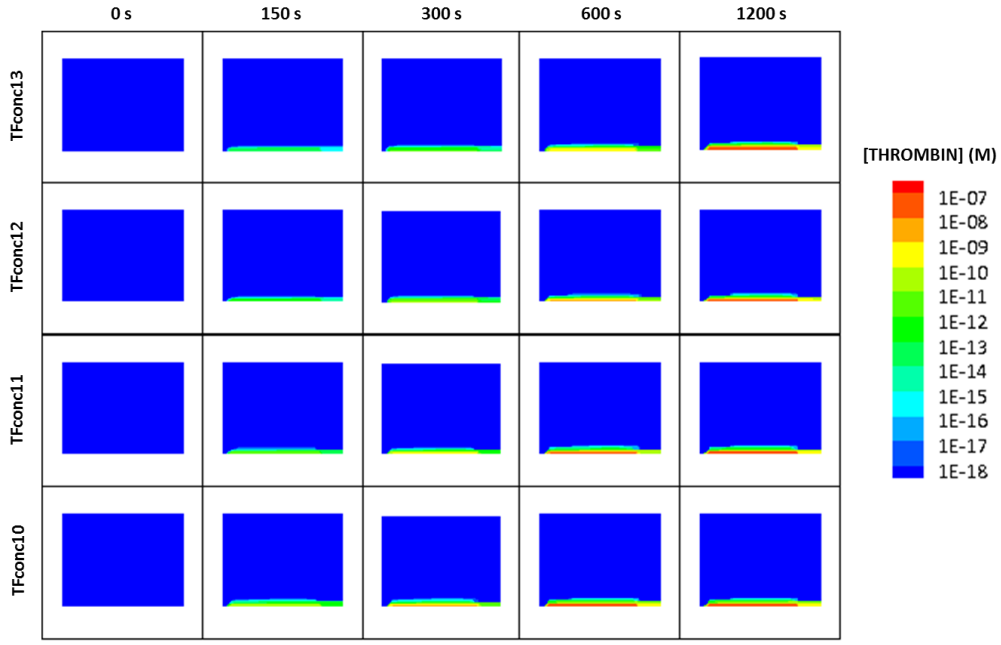


Figure 4.15: The variation in thrombin concentration over a range of initial tissue factor concentrations. In this case, tissue factor is surface bound. Similar maximum thrombin concentrations are reached for all the cases at 1200s.

The effect of the initial concentration of blood-borne tissue factor on thrombin production is seen in Figure 4.16. The highest concentration shown by bbTFconc9 reaches the highest

thrombin concentration at [TH] = 4.0×10^{-7}M. The production then ends abruptly just before t = 400s as the clot occludes the vessel and divergence of the flow field is observed. A similar trend is observed for bbTFconc12 which reaches a peak at [TH] = 3.4×10^{-7}M. Unlike bbTFconc9, thrombin production decreases and then eventually reaches a constant value. Unlike the higher TF values, the lower values do not exhibit increase-peak-decrease trends. A small peak is observed for bbTFconc15 while bbTFconc18 evens out at the peak value of [TH] = 4.0×10^{-8}M.

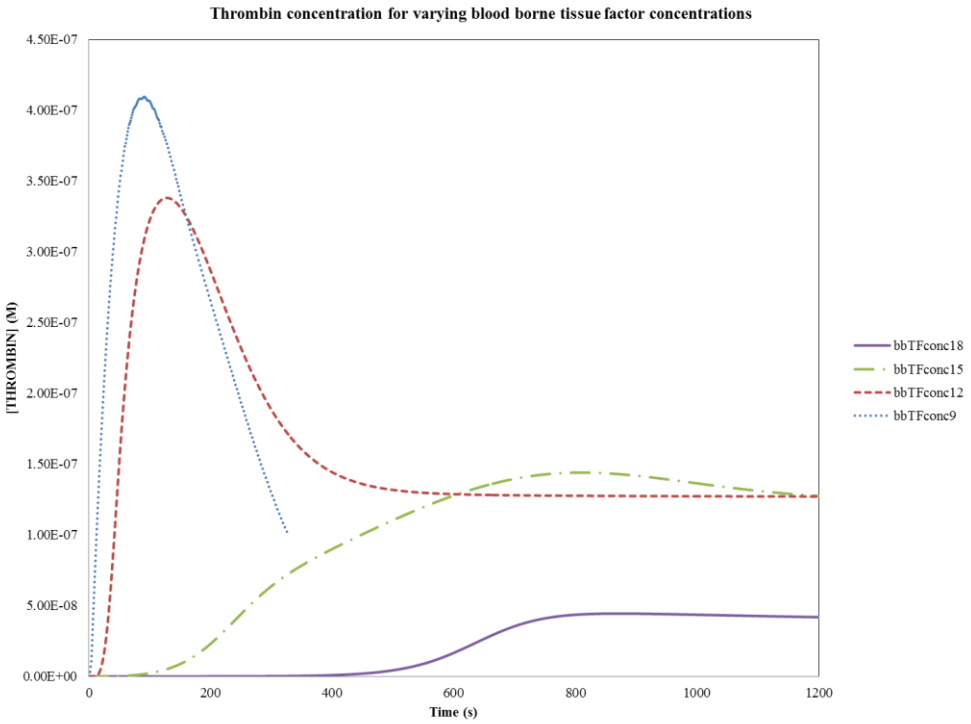


Figure 4.16: The effect of varying the initial tissue factor concentration on thrombin production. The system is modelled by using blood-borne tissue factor which is introduced as a flux at the injured vessel wall.

Figure 4.17 is a contour plot illustrating the effect of initial blood-borne tissue factor on

thrombin concentration. The greatest maximal concentration is achieved by bbTFconc9 at t = 300s. After that point, divergence occurs for that specific case. While the results for the other three cases seem similar at t = 1200s, the contour plot shows that bbTFconc12 reaches its peak thrombin concentration at t = 150s while bbTFconc15 and bbTFconc18 reach their peaks at a later stage. As can be expected, an initial blood-borne tissue factor concentration of [TF] = 1×10^{-18}M produces the least amount of thrombin as seen for bbTFconc18 and in the graph Figure 4.16.

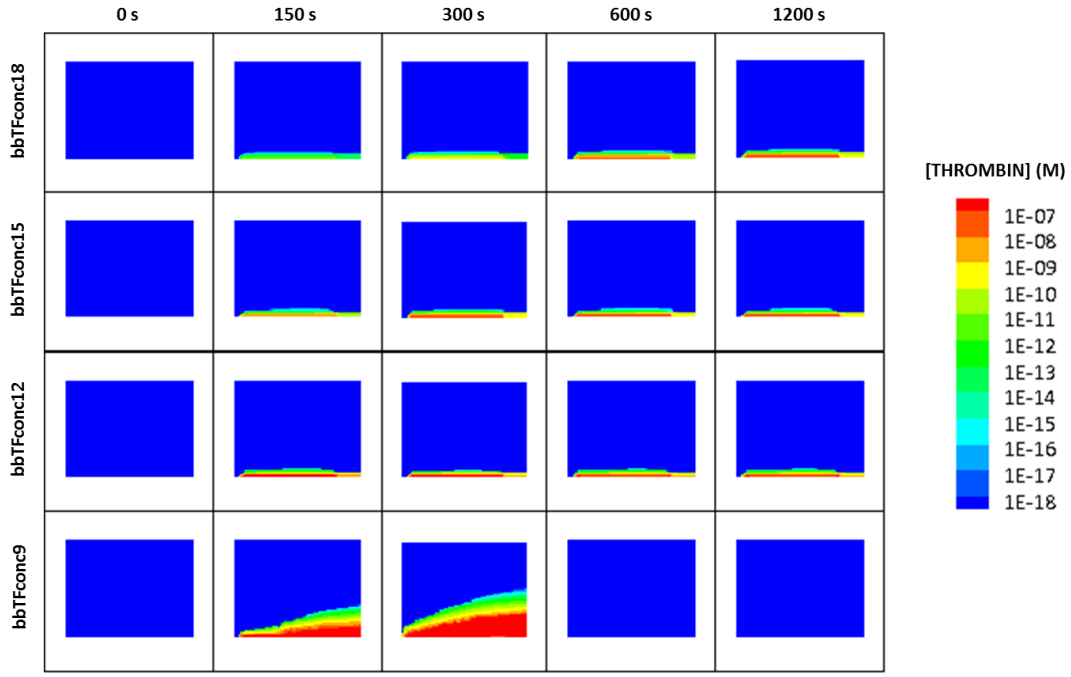


Figure 4.17: Thrombin concentration over a variation of initial blood-borne tissue factor concentrations. The most dramatic difference is noted for bbTFconc9 which diverges by 600s[8].

[8] Divergence is observed as the clot occludes the artery. The clot disrupts the flow field, resulting in complex flow in the artery. While the transitional flow phenomena could be observed on a more refined grid, this falls beyond the scope of this work. In a simple two-dimensional physiological case such as this one, occlusive clots are seen as misrepresenting the *in vivo* situation.

The velocity magnitude contour plot for different blood-borne tissue factor concentrations can be seen in Figure 4.18. The first three cases (bbTFconc18, bbTFconc15 and bbTFconc12) have similar results. The growing clot causes little disruption to the flow field in the rest of the vessel. In a similar fashion to the thrombin concentration plot in Figure 4.17, it is evident that the growing clot for bbTFconc9 disrupts the velocity field. At t = 300s, the flow velocity for this case is relatively slow and divergence occurs shortly thereafter. This agrees with the thrombin concentration graph in Figure 4.16.

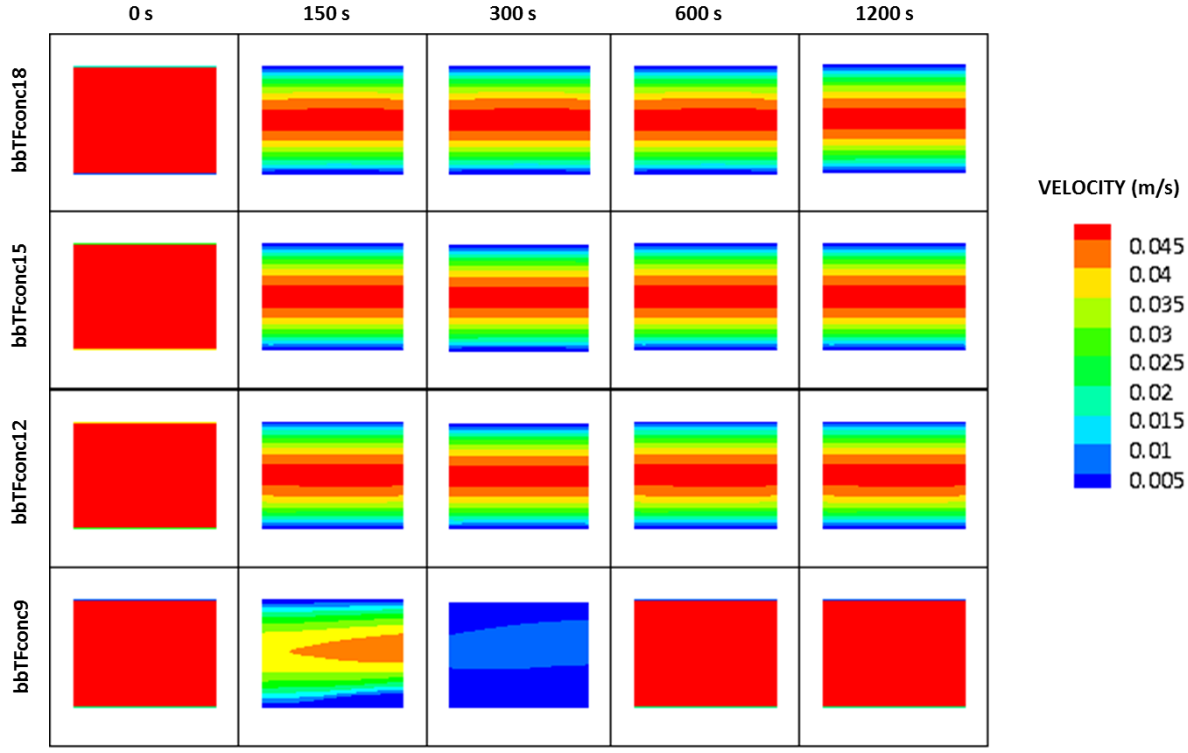


Figure 4.18: Velocity plot for different blood-borne tissue factor concentrations. The bbTFconc9 case diverges at 600s as the clot grows to occlude the vessel as seen by the low flow velocity at 300s.

Figure 4.19 is an illustration of porosity for different initial blood-borne tissue factor

concentrations. As observed in the velocity contour plot in Figure 4.18, bbTFconc18, bbTFconc15 and bbTFconc12 produce similar results. The clot which develops for bbTFconc9 develops at a rapid rate and eventually occludes the domain of interest as seen at t = 1200s. The decreased porosity in the clot region seen in the bbTFconc9 case corresponds to the reduced flow velocity in this region as seen in the velocity contour plot.

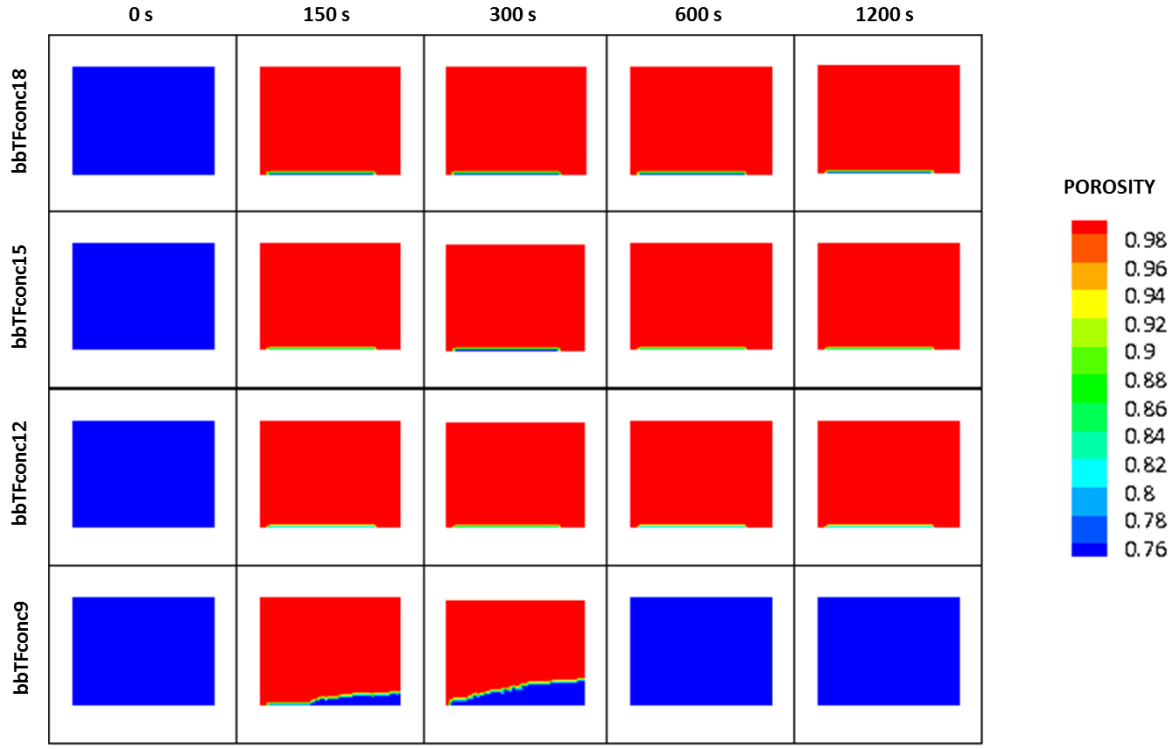


Figure 4.19: Porosity contour plot over a range of initial blood-borne tissue factor concentrations. The bbTFconc9 case shows the most dramatic clot growth which eventually results in occlusion at 600s.

Figure 4.20 shows the effect of blood-borne tissue factor diffusivity on thrombin concentration in the system. The diffusivity produces very similar results for models bbTFdiff11, bbTFdiff10 and bbTF9. Once the diffusivity is increased beyond

$1.00\times10^{-9}m^2s^{-1}$, the lag time for the systems increases and the peak thrombin concentration decreases. The minimum peak thrombin concentration observed is [TH] = 1.70×10^{-7}M for bbTFdiff7 while the maximum concentration is [TH] = 3.40×10^{-7}M for bbTFdiff11, bbTFdiff10 and bbTF9.

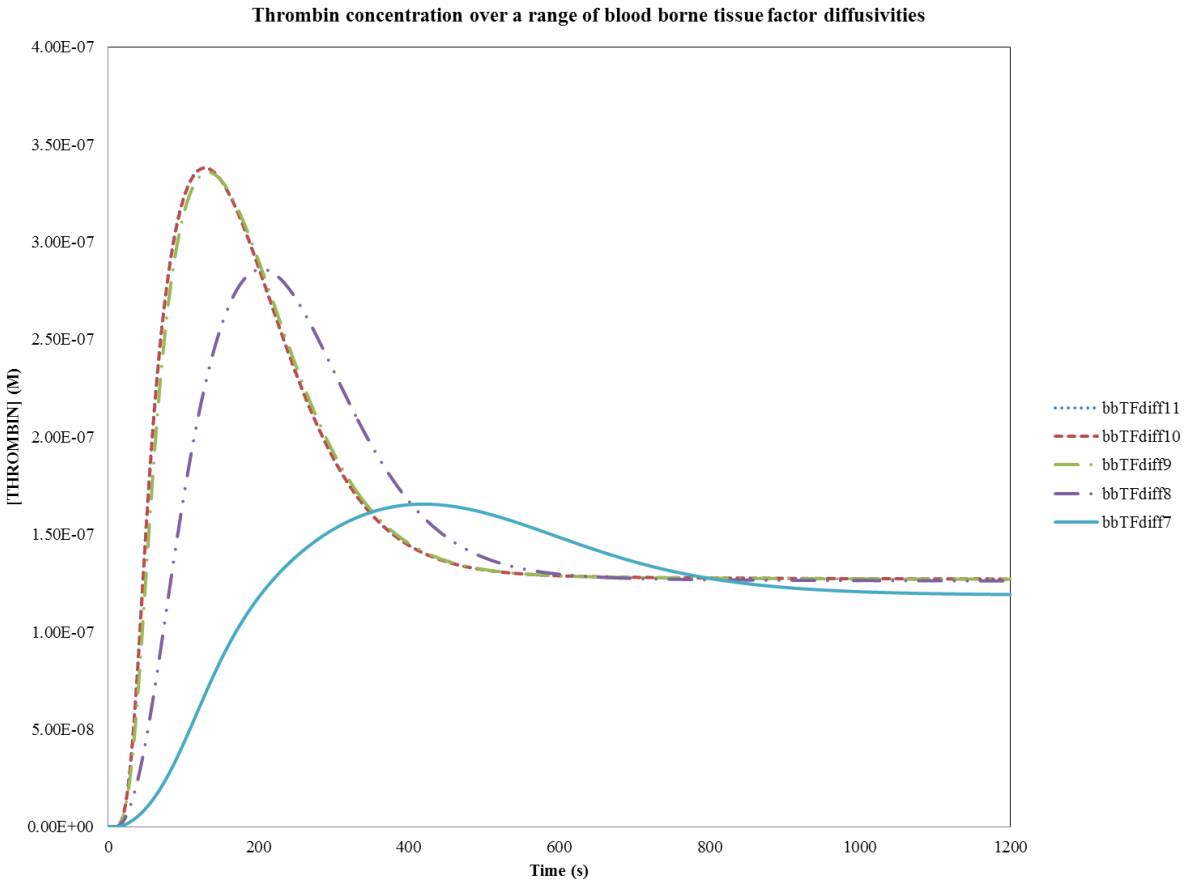


Figure 4.20: The effect of blood-borne tissue factor diffusivity on thrombin production. The diffusivity indicates the rate at which a change in tissue factor concentration is propagated through the fluid.

Figure 4.21 illustrates the effect of blood-borne tissue diffusivity on thrombin production. The results are similar for bbTFdiff11, bbTFdiff10 and bbTF9. Thrombin production is

slower and reaches a smaller peak for bbTFdiff8. The most interesting result is observed for bbTFdiff7 where the blood-borne tissue factor diffuses further in the domain than for the other cases. Even though the tissue factor diffusion is more widespread, this case still has the smallest thrombin peak. The production of thrombin is, however, similar to the other cases at t = 1200s.

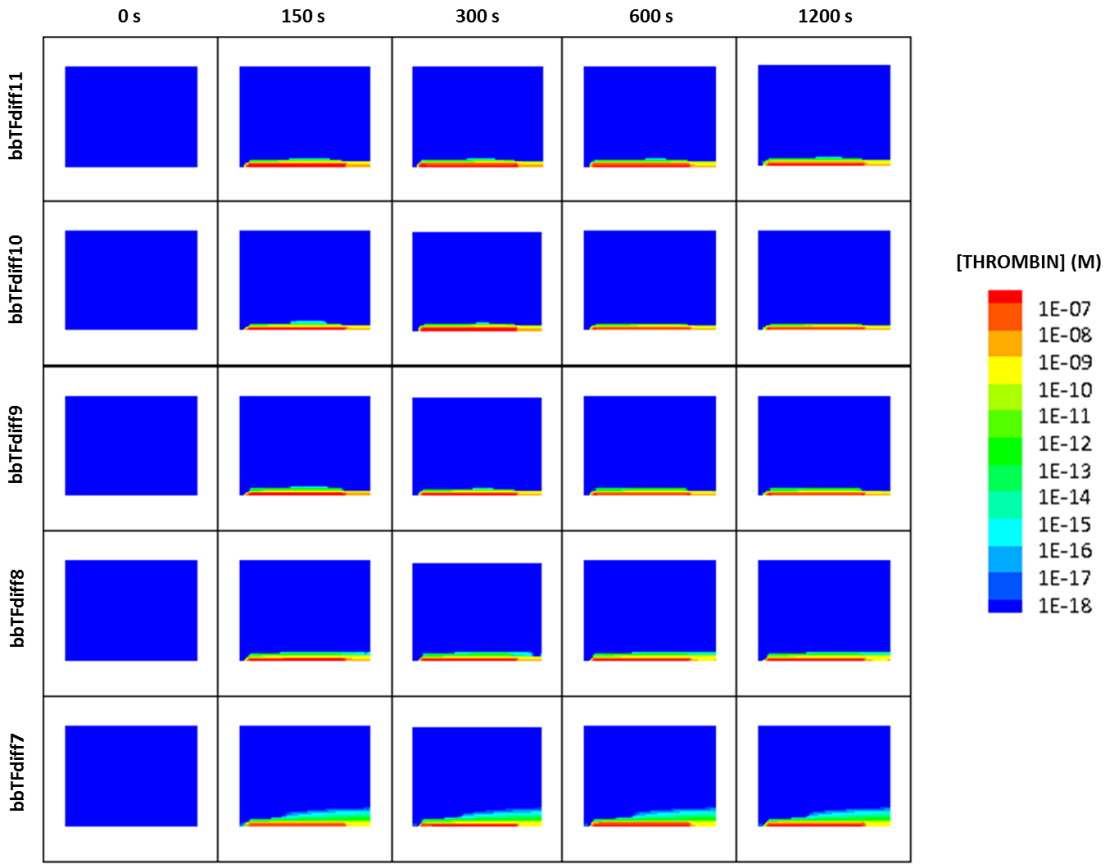


Figure 4.21: The effective of blood-borne tissue factor diffusivity on thrombin concentration. The bbTFdiff7 case shows the greatest diffusion of thrombin however the peak thrombin value is lower than that of the other cases.

4.3.4. Effect of chosen biochemical cascade

The effect of the chosen biochemical cascade is explored by comparing the thrombin

production profiles for the Mann and Wagenvoord models. Simulations with surface-bound and blood-borne tissue factor are run for both models. Figure 4.22 is an illustration of the surface-bound tissue factor case. The Mann model illustrates the characteristic lag, increase, peak and decrease of thrombin production. The Wagenvoord model depicts a much longer lag phase, slight increase and reaches a much lower peak.

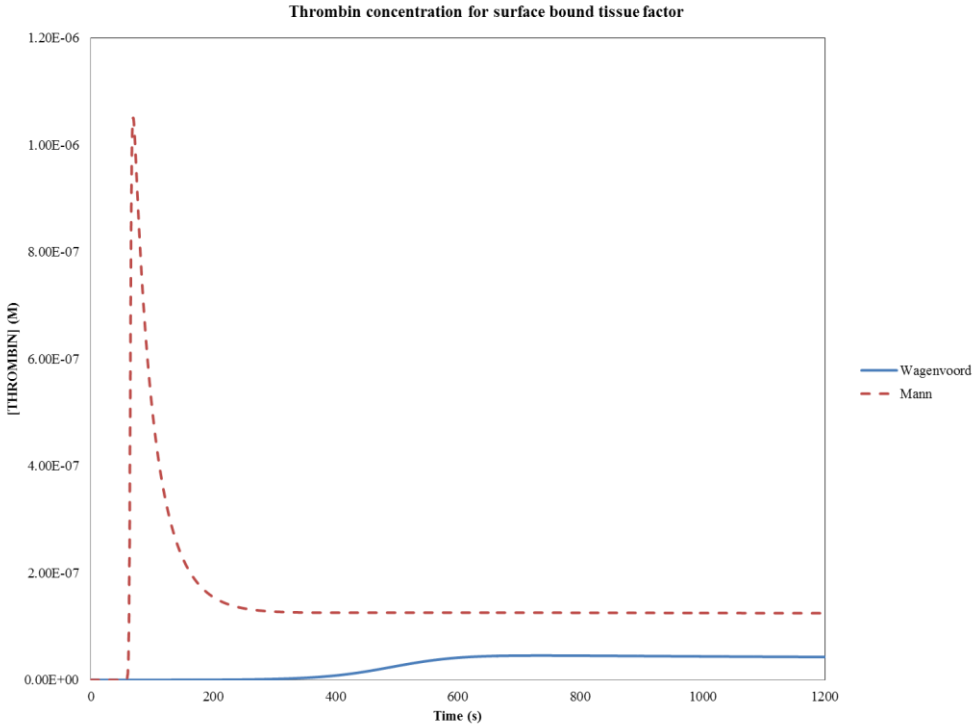


Figure 4.22: Thrombin concentration for the Wagenvoord and Mann models. The results here are shown for surface bound tissue factor.

Figure 4.23 illustrates the thrombin contour profiles for the Wagenvoord and Mann models. The Mann model reaches a peak concentration of around [TH] = 1.05×10^{-6}M while the Wagenvoord model reaches a lower peak of around [TH] = 1.00×10^{-7}M. Both models

depict thrombin production in the region of injury and the clot does not occlude the blood vessel.

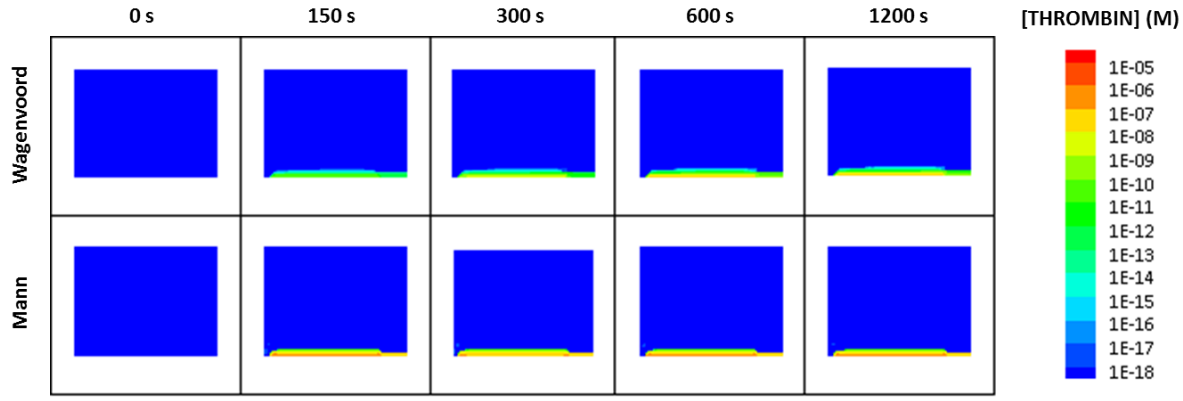


Figure 4.23: Thrombin contour profile for the Wagenvoord and Mann models. Thrombin production is limited to the same region but concentrations differ.

The thrombin concentration profile comparing the Mann and Wagenvoord models for blood-borne tissue factor can be seen in Figure 4.24. Both the Mann and Wagenvoord models depict a lag, increase, peak, and subsequent decrease in thrombin production. In addition, both models reach the same value at t = 600s. The lag times are comparable but the Mann model has a much higher peak than the Wagenvoord model. The Mann model reaches a peak of just under [TH] = 1.20×10^{-6}M while the Wagenvoord model peaks at [TH] = 3.50×10^{-7}M. The peak for the Mann model also occurs at an earlier time than that for the Wagenvoord model. The Mann model then experiences a much sharper drop in thrombin concentration. Following that, both models stabilise to a comparable thrombin concentration. Interestingly, the thrombin curve for the Mann model is similar to its

counterpart for surface-bound tissue factor as seen in Figure 4.22. A similar comparison shows that for the Wagenvoord model, the addition of blood-borne tissue factor makes a significant difference to the thrombin profile.

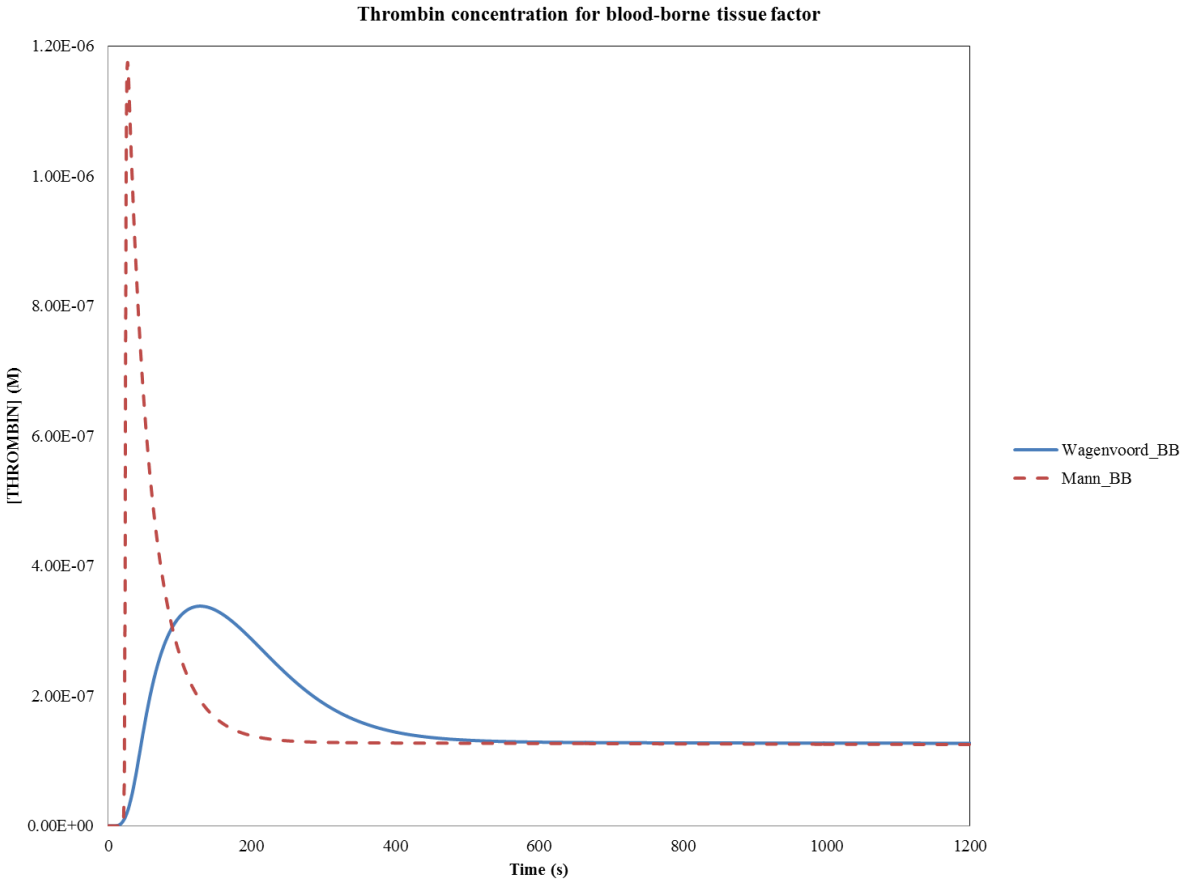


Figure 4.24: Thrombin profile for the Mann and Wagenvoord models. The plot shows thrombin concentration for blood-borne tissue factor.

Figure 4.25 illustrates the thrombin contour plot for the Mann and Wagenvoord models. This plot includes the effect of blood-borne tissue factor. Maximal values are comparable for both models; however the thrombin concentration is seen to decrease earlier in the Mann model. When comparing the t = 600s frames, it is clear that the maximum thrombin

concentration is lower in the Mann model. The same observation is true for the t = 1200s frame.

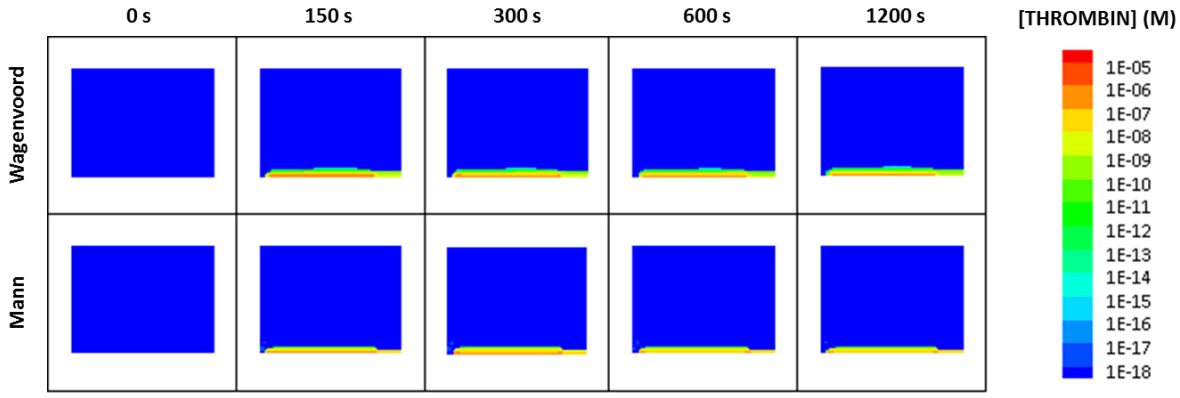


Figure 4.25: Thrombin contour profile for the blood-borne tissue factor. The profiles compare the Wagenvoord and Mann models.

4.3.5. Comparison of results with existing models

In order to ascertain the validity of the results presented in this chapter, comparisons are drawn with models found in the literature.

The results for the critical thrombin concentration and surface-bound tissue factor curves are comparable with those seen in a paper presented by Butenas et al as seen in Figure 4.26 [157]. The results for that paper were derived from experimental data. The peak thrombin concentration value observed in this study is 0.1 times less than that observed by Butenas et al. This is related to the starting concentration of prothrombin which was higher in the Butenas case. In addition, the Butenas case reaches its peak later. Even though a few

differences are observed, the most striking similarity is the very slow drop in thrombin concentration following the peak value. At t = 1200s, both cases have not dropped very much from the peak thrombin concentration value. An earlier paper presented by Jones and Mann shows a similar trend where the rate of decrease of thrombin is quite slow [191]. They observe thrombin generation over a much shorter time scale than the one used in this study.

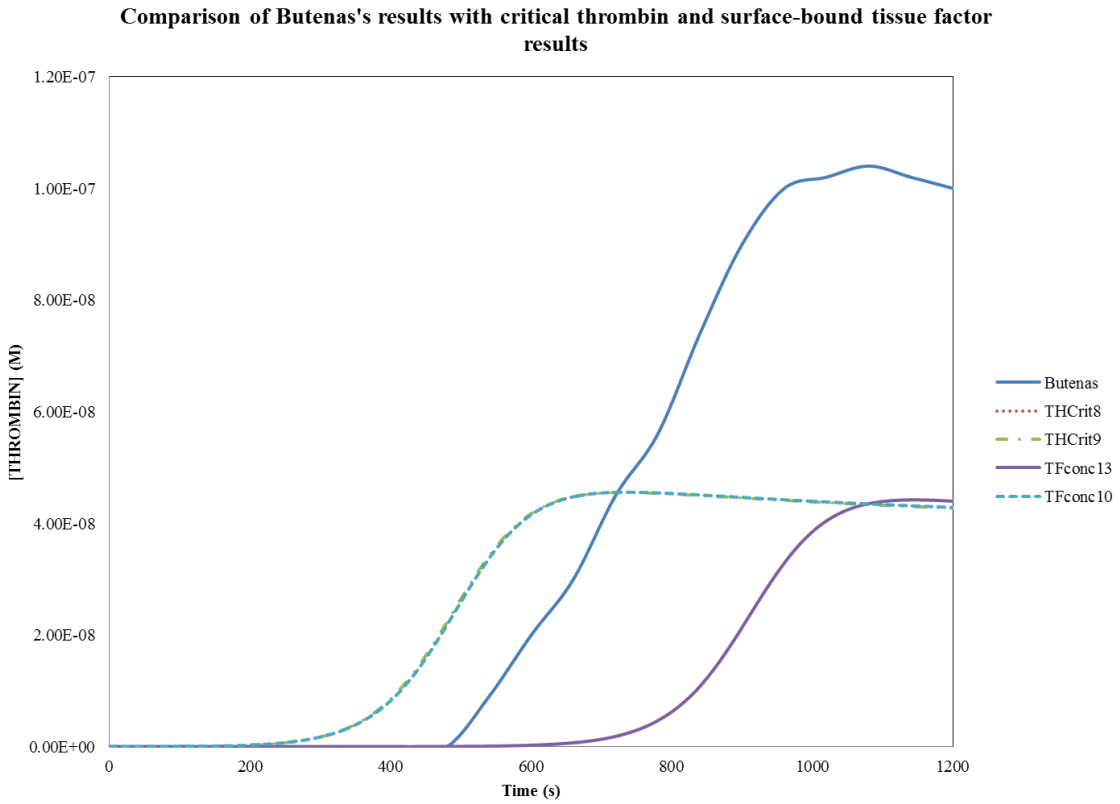


Figure 4.26: Comparison between surface-bound tissue factor results presented in this work and Butenas' work [157]**.**

The results for the study which compares initial blood-borne tissue factor concentrations

are similar to those presented by Hockin et al [16]. In both cases, an increase in initial tissue factor concentration results in a decreased time lag and shorter time to peak thrombin concentration. In both cases, the peak values are also related to initial tissue factor concentration. A higher initial tissue factor concentration results in a higher peak thrombin concentration value. Finally, the values lie within the same order of magnitude with peaks of around [TH] = 500nM in both cases. Hockin et al present a computational study backed by experimental data collected by the same team at an earlier stage.

The result for the Mann model simulated in this study is similar to that observed in a computational paper by Bodnar and Sequeira [163]. Both models experience a sharp rise in thrombin production following a very short time lag. The time lag in this study is approximately t = 50s while that in Bodnar and Sequeira's study is t = 40s. Both models then experience a dramatic decrease in thrombin production which then levels off before t = 200s. The peak value presented in this model is higher than that recorded by Bodnar and Sequeira, who account for the activity of protein C, an anticoagulant. Computational work by Anand et al shows a similar trend with a sharp rise and drop in thrombin production following a short time lag [162]. They show that varying antithrombin concentrations affects the time lag and rate of thrombin production. The Wagenvoord model produces a fairly standard curve, although it reaches a lower peak and has a slower decline. The

overall trend is comparable to that seen in a model by Hockin et al [16]. The main difference observed between the Wagenvoord and Mann models and other models in literature is the effect of missing anticoagulation proteins. Comparisons with other model values can be seen in Table 4.6.

Model	Maximum Thrombin Concentration (nM)	Minimum Thrombin Concentration (nM)	Lag time (s)
Work presented in this thesis			
Wagenvoord	350	125	50
Mann	1180	125	50
Papers			
Wagenvoord [15]	320	10	180
Hockin (Mann) [16]	550	10	100
Bodnar [163]	45	10	40

Table 4.6: Comparison between results presented in this chapter and other papers.

4.3.6. Discussion

This study presents a physiological model of clot development which incorporates the flow field and the biochemical reactions which result in fibrin formation. The model has been used to examine the critical thrombin concentration which marks the transition from the initiation phase to the propagation phase. It has also been used to examine the effect of tissue factor with some focus placed on blood-borne tissue factor. Finally, the effect of the underlying biochemical network was examined. The thrombin curves included in the results section are comparable to range of thrombin curves available in literature. They are similar both in temporal evolution and in the range of values obtained from simulations

conducted in this study. The curves can be compared to work by Mann et al, Wagenvoord et al and Fogelson et al [15], [16], [157], [167].

The results for the critical thrombin concentration illustrated the importance of this value for modelling a growing clot. While it is now widely accepted that the initiation phase of coagulation is characterized by the inefficient production of a small amount of thrombin and that this is followed by a large burst in thrombin formation, little focus has been placed on the quantity of thrombin which marks the transition from one phase to the next [49], [51]. The absence of an exact concentration of thrombin which marks the end of the initiation phase and the start of the amplification phase may indicate that this value is of little significance when trying to improve current understanding of physiological coagulation *in vivo*. For the purposes of the *in silico* model developed in this study, this value has proven fairly significant as it is used to make a distinction between the clot and the rest of the fluid domain.

It is clear from the results presented in this chapter that this value has a significant effect on clot development. Models with a critical thrombin concentration below [TH] = 1nM tended to predict an exaggerated clot which disrupted the flow in the rest of the blood vessel. While there is a tendency for thrombosis to occur under pathological conditions,

one would not expect such an outcome for a physiological model in an idealised, two-dimensional flow field [145], [192] . Under physiological conditions, the clot formed would need to be sufficiently large to cover the zone of injury but would then need to cease growing once the injury had been bridged by platelets secured by a fibrin mesh [49], [51], [58], [59].

A critical thrombin value of around [TH] = 1nM – 10nM seemed to best reflect the most likely physiological conditions. At this value, a clot was formed but did not grow to exaggerated proportions which are likely to result in vessel occlusion. Mann et al found that the transition from the initiation phase to the propagation phase occurred at a thrombin concentration of around [TH] = 5nM – 10nM [184]. They found that fibrin was visible from around 10nM. This is in strong agreement with the results which are observed in this study.

Vessel wall tissue factor is membrane-bound protein [119], [123], [124]. This implies that there is a limited amount of tissue factor in the subendothelial vessel layers. This tissue factor interacts with other coagulation proteins to form thrombin and then, fibrin. Owing to some of the constraints of the modelling techniques used in this study, it was not possible to model tissue factor as a receptor which participates in a surface reaction. It was

therefore necessary to find other means of modelling the finite supply of tissue factor within the model. This is distinct from other inactive coagulation proteins which are ever present and circulate within the bloodstream. A study by Bach et al showed that the availability of tissue factor sites had significant impact on the formation of the TF-VIIa complex [185]. In order to model the limited tissue factor availability, tissue factor was available for different amounts of time. This mimicked the limited availability of tissue factor, especially at saturation level.

The results show that a tissue factor exposure time of t_{exp} = 5s was far too short to accurately capture the process of thrombin formation. For this time duration, an insignificant amount of tenase is formed. This, in turn, affects the system's ability to produce sufficient thrombin for a stable clot to be formed. The trend for the remainder of the exposure times was not altogether intuitive. Below an exposure time of t_{exp} = 60s, it seemed that an increase in exposure time resulted in a decrease in the lag time. This could be explained by the fact that a longer exposure time allowed for the formation of greater quantities of the TF-VIIa complex, thus speeding up the rate at which thrombin could be formed. The result for the t_{exp} = 1200s, however, went against this trend and illustrated a similar lag time to that of the t_{exp} = 10s case. The main difference between these two cases was that the t_{exp} = 1200s reached a higher peak thrombin concentration than the t_{exp} = 10s

case.

Leiderman and Fogelson examined the effect of initial tissue factor exposure on thrombin production [167]. They defined tissue factor exposure by the density of tissue factor exposed on the injury zone. They found that after 10 minutes, there was a threshold below which thrombin production was dependent on tissue factor exposure. Above this threshold, however, it is evident that thrombin production is independent of initial tissue factor exposure. Once tissue factor density was sufficiently high, in their case $TF_{density}$ = 10fmol/cm^2, thrombin production remained constant. In this study, it seemed that thrombin production is governed by exposure time for short exposure time periods. Past 10 minutes, it was difficult to predict the thrombin production trend.

A wide range of values of initial tissue factor concentrations are suggested in literature [15], [16], [157], [163], [167]. The reason for this variation is that different researchers attempt to answer specific questions with each of their models. Most models employ a value in the picomole range but others are initiated by nanomolar concentrations of tissue factor. A range of values was examined in this study. The lowest value was 0.125pM and the highest value was 0.125nM. As the initial tissue factor concentration increased, the lag time for thrombin formation decreased. Past 900s, however, the thrombin concentration

profiles were comparable across the models. A similar time lag pattern was observed by Hockin et al [16]. In their model, they examined thrombin production over a range of initial tissue factor concentrations (1pM – 25pM). As the initial tissue factor concentration was increased, the time lag decreased.

Blood-borne tissue factor was modelled as a flux value while surface bound tissue factor was modelled as fixed concentration at the boundary. The effect of the flux value versus boundary condition can be seen when comparing the surface bound tissue factor graphs with those of blood-borne tissue factor. The blood-borne tissue factor curves have a closer resemblance to normal thrombin profiles. The surface bound tissue factor graphs resemble those seen in Hockin's models where the effect of tissue factor pathway inhibitor is not present, as in this study. This observation provides some support for the existence of blood-borne tissue factor in clot development [126], [193]. It is, however, still difficult to draw conclusions on the issue of blood-borne tissue factor as the modelling assumptions clearly contribute to the results.

The effect of the initial concentration of blood-borne tissue factor on thrombin production was examined. In a similar fashion to the surface bound tissue factor results, an increase in initial concentration lead to a decrease in lag time. In the blood-borne tissue factor case,

however, the initial tissue factor concentration affected the peak thrombin concentration and results did not seem to reach a stage where they were uniform. An initial tissue factor flux of $[TF]_{flux}$ = 1nM/m^2 has the highest thrombin peak but the simulation diverged just before 400s. The graphs observed for blood-borne tissue factor are similar to the thrombin profiles seen in Pantaleev et al and Butenas et al [17], [157].

Blood-borne tissue factor has been found on various blood cells and their fragments [194], [195]. Suggestions about the location of blood-borne tissue factor have included leukocytes, microparticles and platelets [196]. While the transport properties of most of these cells are known, information about the diffusivity of blood-borne tissue factor is scarce. An additional complication of determining such a value is that the tissue factor may be found on cells which are somewhat deviant from regular cells. A parametric study was conducted to determine the effect of blood-borne tissue factor diffusivity on thrombin production. For values below a blood-borne tissue factor diffusivity of $1\times10^{-9}m^2.s^{-1}$, the thrombin profiles are very similar. As the diffusivity increases, lag time increases and peak thrombin concentration decreases. All the models exhibit similar behaviour after 800s. Turitto and Baumgartner reported platelet diffusivities in the range of $1\times10^{-11}m^2.s^{-1}$ [101]. Platelet diffusivity is the most commonly reported blood cell property in coagulation literature. An assumption that blood-borne tissue factor may be found on platelets makes

the diffusivity results acceptable.

The effect of the underlying biochemical model is seen in the results comparing the Wagenvoord and Mann models. The Wagenvoord model is a simple, four reaction, top-down model. The Mann model is a comprehensive, twenty-seven reaction, bottom-up model. While these differences exist, both models attempt to model the same physiological process of coagulation. The most striking difference between the two models is the effect of blood-borne tissue factor. In the Wagenvoord model, the effect of antithrombin is not visible for the surface-bound tissue factor case. Once blood-borne tissue factor is added, the effect of antithrombin is more defined. Antithrombin limits thrombin production, thus resulting in the peak and subsequent decrease of thrombin concentration in the system. The anticoagulant pathways are well defined for both the surface-bound and blood-borne tissue factor cases for the Mann model. An interesting observation is that the Mann model produces similar results for the surface-bound and blood-borne tissue factor cases. For both the Mann and Wagenvoord models, the thrombin concentration never fully returns to zero. This may be a result of the incomplete anticoagulant systems in both models. The Mann model goes an additional step by including the effect of tissue factor pathway inhibitor but both models do not account for Protein C action. This protein would limit co-factor activity and thus return thrombin concentration to zero.

Hockin et al observe similar results [16]. The addition of different anticoagulant proteins affects the decline of thrombin production in different ways. A full anticoagulant system would return thrombin production back to zero once the clot is formed. While the Mann model describes the process of coagulation more comprehensively by including both antithrombin and tissue factor pathway inhibitor, it is more computationally expensive to run as it consists of twenty-seven reactions and forty-two reaction constants. The Wagenvoord model, in comparison, has four reactions. In addition, it would prove challenging to determine the Mann parameters for a specific patient.

Further development of this model would include a more accurate description of platelet activity. While the effect of platelets is considered, the modelling of platelet reactions may reveal subtle details which would otherwise not be apparent. Most of the parametric studies carried out were conducted sequentially. Once one unknown variable was determined, the most appropriate value of that variable would be used for subsequent simulations. A more thorough method would be to examine the unknown parameter over a range of previously determined variables. It would also be helpful to examine more biochemical models.

5. Results: Clot propagation and initiation in three dimensions – the effect of mechanical and biochemical factors

The initiation and propagation of clots in aneurysms is a process which has proven difficult to observe. It is known that both mechanical and biochemical factors contribute to the process. This chapter presents the application of the model developed in the previous chapter to an idealised three dimensional aneurysm geometry. The model is then used to explore clot initiation and propagation in aneurysms.

5.1. General considerations

The earliest models of coagulation recognised the central role that thrombin plays in clotting [58], [59]. Later models based on the cell-based model of coagulation further elucidated the ability of thrombin to amplify its own production [51], [61]. A small amount of thrombin is formed during the initiation stage. This thrombin then activates the co-factors and results in an increased rate of thrombin formation during the propagation stage. There are, however, details which remain unclear about the initiation and propagation of clots. This is especially true for clot development in cerebral aneurysms.

In 1856, Virchow hypothesized that the three main contributors to clot development are flow conditions, blood composition and state of the vascular endothelium [56]. The review

of *in silico* models of coagulation in Chapter 2 illustrates that current models use different combinations of Virchow's conditions to develop context appropriate models. The models developed in this chapter aim to better understand the propagation and initiation of clots or thrombi in an idealised three-dimensional geometry of a cerebral aneurysm. This section commences with a short review of mechanical, biochemical and wall factors. This review expands on what is presented in Chapter 1. Propagation is examined by linking the velocity of clot propagation to mechanical (flow conditions) or biochemical (blood composition) factors. Clot initiation is modelled by examining mechanical factors or by varying the area where vascular endothelium has been injured. Level Set methods are employed to track the surface of the growing clot.

5.1.1. Mechanical factors

Blood flow plays a fundamental role in clot development. The most obvious role played by flowing blood is the transport of the required proteins to the site of injury. In addition, mechanical factors which are a result of the movement of blood are thought to contribute to platelet activation, intra-platelet interactions and platelet-wall interactions.

Shear rate contributes to both initiation and propagation of clots. The main influence of shear stress is exerted on platelets. During initiation, platelets are more likely to gather in

and adhere to regions of lower shear stress because the flow is slow enough for significant bonds to form. Propagation of the clot is related to recruitment of platelets to the growing mass. Once again, shear stress plays a role in activating platelets which are then able to recruit other platelets. As with initiation, stable platelet-platelet bonds are more likely to form in regions where flow is sufficiently slow.

Chesnutt and Han examined the effect of curvature on shear-induced platelet activation in tortuous vessels [192]. The study showed that platelet activation is observed in curved regions, with the highest concentration of activated platelets at the inner wall. It was then suggested that this may be a result of altered strain rates and increased platelet collisions in these regions. The activated platelets were observed to aggregate and adhere to the wall and to each other. Thrombus development could easily be initiated under the conditions described in this study.

A study by Turitto and Baumgartner in 1975 showed that platelet deposition on the subendothelium was dependent on flow conditions [101]. It was shown that in the region of injury, the ability of platelets to diffuse in the blood was more limiting than the rate of attachment at the subendothelium. The rate of diffusion was directly related to strain rate. A study conducted by the same researchers at a later time revealed that platelet diffusivity

increased with increasing wall shear rate while the surface reaction rate had an inverse relationship with wall shear rate. It was shown that below $350s^{-1}$, the diffusion-controlled rate is dominant while above $800s^{-1}$, the surface reaction controlled rate becomes more important. A transition zone was observed between the two values [106].

Platelet aggregation and adhesion are strongly linked to shear rate. At shear rates below $1000s^{-1}$, platelet aggregation and adhesion is governed by collagen and fibrinogen. This is observed in veins and larger arteries. In smaller vessels, where shear rates exceed $1000s^{-1}$, von Willebrand's factor plays a greater role in platelet adhesion [197], [198]. It is thought that the fibrinogen pathway plays a more dominant role than the von Willebrand's factor pathway at lower shear rates because the bond rate between fibrinogen and platelets is much slower than that between von Willebrand's factor and platelets [107].

Studies conducted by Goldsmith show the effect of strain rate on platelet aggregation [114]. The studies also focused on the effect of red blood cells on platelet behaviour. Platelets activated by ADP in a flow chamber showed a decreasing aggregation rate with a decreasing strain rate. After a certain critical time, platelet aggregation is more dependent on collision frequency with other platelets rather than shear rate. A later study revealed that far away from the zone of injury, platelets are transported and heavily affected by

convective transport [100], [115]. They also found that thrombus formation is more likely to be observed in stenosed vessels, near aortic and venous valves and at bifurcations. Closer to the injured wall, shear-induced collisions between red blood cells and platelets contributed to cell-wall interactions and subsequent adhesion. A similar observation was noted by Ataullakhanov et al [99].

Embolisation of a clot is dependent on the height of the clot, the maximum shear rate to which it is exposed and the pulsatility of the flow. Basmadjian showed that shear rate and thrombus height had the most significant effect on embolisation risk [118]. These two factors played a more significant role on risk of embolisation than convective pulsatile flow.

Rayz et al examined the effect of wall shear stress and flow residence time on platelet deposition and thrombus initiation in cerebral aneurysms [19]. Their computational fluid dynamics study showed that increased flow residence time and low wall shear stress were good indicators of regions where thrombus was likely to develop. They noted, however, that these two factors were not the only ones responsible for thrombus initiation and that biochemical effects would also need to be taken into consideration.

Wootton et al developed a computational thrombosis model for use as a predictive tool in a clinical setting [199]. This work was complemented by *ex vivo* experiments in a baboon. Measurements of platelet accumulation were made in a region of acute arterial thrombosis. The model focuses on stenosis and can be used to determine the occlusion risk of patients presenting with stenosis. The geometry used for the investigation can be seen in Figure 5.1. The computational model is based on existing biochemical reaction networks and accounts for flow using computational fluid dynamics. It accounts for shear-enhanced diffusivity and the rate of platelet activation using a kinetic parameter. For this study, 50%, 75% and 90% stenosis was examined. The peak shear rate observed for each respective percentage is $1300s^{-1}$, $4700s^{-1}$ and $22000s^{-1}$. This peak value was observed just upstream of the stenosis throat. The maximum platelet accumulation velocity, equivalent to propagation velocity in our case, was observed in the stenosis throat section. The minimum platelet accumulation velocity was observed in the 50% stenosis case in the region upstream of the stenosis. The value is $0.6\times10^{-5}ms^{-1}$ and was observed in the experimental case. The maximum velocity was recorded for the 90% stenosis case and was observed in the stenosis neck region. The value is $3.0\times10^{-5}ms^{-1}$.

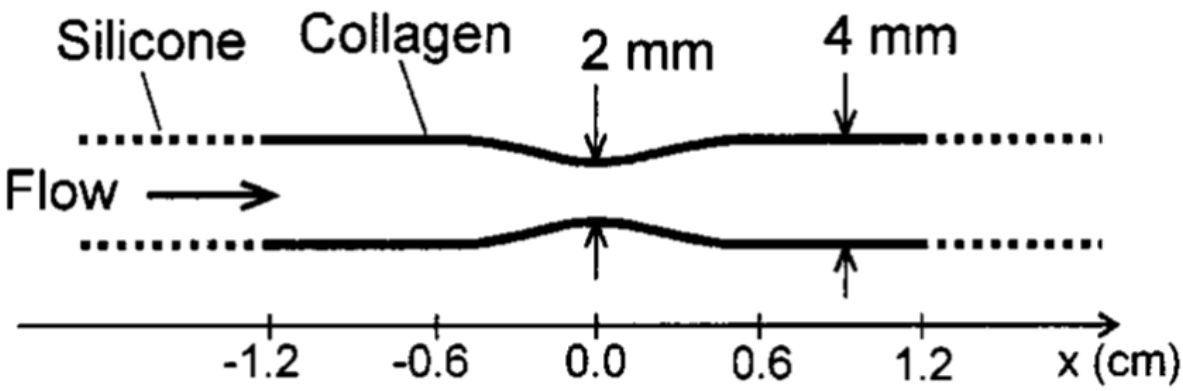


Figure 5.1: The geometry used by Wootton et al for investigating occlusion risk in patients with stenosis [199]**. Flow moves from left to right and the centre portion at 0.0cm is the narrowest point in the vessel. This represents the stenosed region.**

A different computational model was presented by Goodman et al [200]. The model predicts thrombus initiation, growth and where appropriate, embolisation. The main area of application for this model is cardiovascular devices such as hemodialyzers and oxygenators. The model accounts for platelet transport, shear-enhanced diffusivity, the action of platelet agonists such as thrombin and antithrombin and embolisation forces. The fluid flow is accounted for by computational fluid dynamics and thrombus regions assume a different viscosity to the rest of the fluid domain. The model was validated by an *in vitro* experimental setup where blood passed through an experimental flow cell. The growth of the clot was monitored using video microscopy embolism was assessed visually. Wall shear rates in this model range from $653s^{-1}$ to $5800s^{-1}$. The propagation velocity of the clot was $5.0\times10^{-6}ms^{-1}$.

Ouared et al presented a model of thrombus development in intracranial aneurysms [20]. Although they do not explicitly model the coagulation reactions, they assume that the processes of platelet activation and fibrin formation are likely to occur below a threshold shear rate. In their model, this threshold value is $100s^{-1}$. Clot growth is therefore initiated and supported in regions where the strain rate falls below this value. Using Lattice Boltzmann methods, they account for fluid flow. The model presented also accounts for the movement of platelet particles. Using their method, they observe the different types of thrombus development often observed *in vivo*. These include fully occluded, partially occluded and thrombus free aneurysms.

It is evident from the survey presented in this section that shear stress plays a key role both in the initiation and propagation of clots. It is therefore necessary to examine the relationship between shear rate and the initiation and growth of clots.

5.1.2. Biochemical factors

Fibrin formed by the biochemical cascade ensures that platelets are held securely in place thus stabilising the clot. Without this mesh, activated platelets may become deactivated and drift away from the clot mass. While this is the primary role of the biochemical cascade, there are other functions which it serves. Central to the amplification and

propagation of the growing clot mass is the activation and production of various chemical species.

As discussed previously, thrombin plays a key role both in the production of fibrin and in the activation of platelets. A small amount of thrombin is formed during the initiation phase. Following that, thrombin activates co-factors V and VIII, resulting in an increased rate of production for thrombin itself. There are two pathways to platelet activation. The collagen-mediated pathway relies on platelets attaching to the subendothelial collagen layer. The thrombin-mediated pathway is observed in the propagation phase where thrombin activates platelets which are attached to the growing platelet mass [49], [63].

Panteleev et al examined the role of tissue factor bearing cells and the effect of different chemical species on clot propagation [17], [201]. Extrinsic tenase formed on tissue factor bearing cells is abundant during the initiation phase of clotting but is inhibited before it can travel through the rest of the clot. Intrinsic tenase is more instrumental during the propagation phase as its formation occurs mostly on activated platelet membranes. Factor IXa is produced by extrinsic tenase and is able to diffuse to cell membranes where it contributes to the formation of intrinsic tenase. The study also found that thrombomodulin is able to terminate clot growth. The addition of plasma tissue factor did not make a

significant contribution to clot propagation. A reason for this may have been that the system did not account for flow.

Hathcock and Nemerson postulated that in *in vitro* clots, blood borne tissue factor plays an important function in clot propagation [186]. They observed that the time that it takes for factors IXa and Xa to diffuse from the tissue factor bearing cells to the outer surface of the growing clot is disproportionate to the rate at which clots develop. These two proteins need to travel to the outer surface where they contribute to the formation of thrombin.

5.1.3. Condition of endothelium

The vascular endothelium separates the subendothelial layers from the flowing blood. One of its numerous functions is to prevent spontaneous clots from forming. In cases where the vascular endothelium is compromised, tissue factor can come into contact with flowing blood, initiating clot growth. Sutherland et al hypothesized that altered haemodynamics within the aneurysm sac may result in damage to the vascular endothelium [202]. This would result in the exposure of the subendothelial matrix and its subsequent interaction with other components involved in the process of coagulation. The state of the vascular endothelium is therefore an important factor when considering clot initiation and growth [118].

Lawton devised a classification scheme for different types of cerebral aneurysm thrombus [148]. He categorised the clots into concentric, eccentric, complete, lobular, canalized and foreign-material induced. In this study, it is hypothesized that the different types of thrombus are a result of the initial region of initiation of the clot. This initial region is considered injured and is therefore capable of exposing tissue factor, thus having the ability to initiate a clot.

5.2. Model specifications

The general considerations highlight the effect of mechanical and biochemical factors on platelets. While this study does not model platelet activity directly, it takes into account the conditions which are likely to result in realistic platelet responses. Emphasis is placed on the chemical reactions which make up the coagulation cascade. Without the presence of a fibrin mesh, a collection of platelets is not really considered to be a stable clot. Focusing on the formation of a fibrin mesh and a haemodynamic environment which would support realistic platelet activity is therefore a justifiable simplification.

In order to develop a robust clotting model which is applicable in patient-specific geometries, it is necessary to first determine certain details pertaining to the initiation and propagation of the clot in a three-dimensional space. While it is possible to do so in a

realistic geometry, it would be risky to tailor everything to a specific geometry and later discover that it is not easily transferrable to other geometries. In this chapter, an idealised three-dimensional aneurysm geometry is used to determine initiation and propagation variables and this information is later transferred to patient-specific geometries.

The modelling of clot growth in three dimensions is similar to the modelling approach used for the two dimensional work discussed in the previous chapter. The fundamental difference between the two is that in three dimensions, the complexity of the geometries needs to be taken into serious consideration. In the previous chapter, it was possible to decide whether or not a computational cell fell within the clot region by looking at that specific cell's thrombin concentration. In complex three dimensional geometries, it becomes more difficult to locate the exact surface of the growing clot. In this chapter, Level Set methods are employed to solve this problem and details are given in the subsections that follow.

5.2.1. Geometry

A three dimensional idealised geometry of a cerebral aneurysm is used for the studies in this chapter. The neck of the aneurysm is fairly wide and the aneurysm has a spherical shape. The geometry is adapted from Mulder et al and the shape of the geometry affects

the results from the fluid computations [203]. The geometry provides a standard, generic model which can be used for determining propagation and initiation parameters. These values are then used for patient-specific geometries which are presented later in the study. An image of the geometry is seen in Figure 5.2. Flow enters at the inlet of the geometry, passes through the parent vessel and the aneurysm and exits at the outlet.

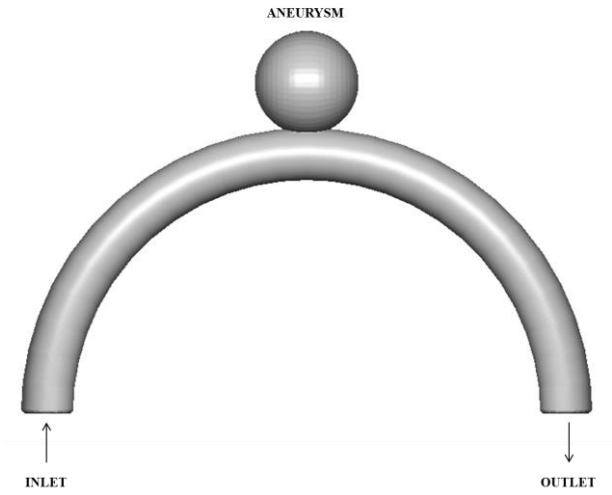


Figure 5.2: Aneurysm geometry used for all the initiation and propagation simulations. The geometry is one of an idealised aneurysm with a relatively wide neck. Flow moves from the inlet, passes through the parent artery and the aneurysm and then exits at the outlet. This geometry was adapted from a study conducted by Mulder et al [203]**.**

5.2.2. Simulations conducted

The simulations conducted in this study focus on the propagation and initiation of clotting in an idealised cerebral aneurysm geometry. The simulation names and specific parameters can be seen in Table 5.1.

Name	Propagation Velocity	Initial [TF] (M)	Critical strain rate (s^{-1})	Initiating wall (initial surface/tissue factor expression)
Mechanical propagation				
Mech_Const	Constant	N/A	N/A	Entire wall
Mech_SRDir	Strain rate direct	N/A	N/A	Entire wall
Mech_SRInv	Strain rate inverse	N/A	N/A	Entire wall
Biochemical propagation				
Bio_ThromDir	Thrombin direct	1.00E-12	N/A	Entire wall
Bio_ThromInv	Thrombin inverse	1.00E-12	N/A	Entire wall
Bio_ExtTenase	Extrinsic tenase direct	1.00E-12	N/A	Entire wall
Bio_TotTenase	Total tenase direct	1.00E-12	N/A	Entire wall
Tissue factor concentration initiation				
TFconc18	Thrombin direct	1.00E-18	N/A	Entire wall
TFconc17	Thrombin direct	1.00E-17	N/A	Entire wall
TFconc15	Thrombin direct	1.00E-15	N/A	Entire wall
TFconc12	Thrombin direct	1.00E-12	N/A	Entire wall
Strain rate threshold initiation				
SR100	Thrombin direct	1.00E-17	100	Strain rate less than $100s^{-1}$
SR500L	Thrombin direct	1.00E-17	500	Strain rate less than $500s^{-1}$
SR500G	Thrombin direct	1.00E-17	500	Strain rate greater than $500s^{-1}$
SR800	Thrombin direct	1.00E-17	800	Strain rate greater than $800s^{-1}$
Lawton (Different portion of initiating wall)				
Complete	Thrombin direct	1.00E-12	N/A	See diagram
Concentric	Thrombin direct	1.00E-12	N/A	See diagram
Eccentric	Thrombin direct	1.00E-12	N/A	See diagram

Table 5.1: Parameters used for the propagation and initiation runs presented in this chapter.

Table 5.1 states that the initiating wall where tissue factor is expressed can be seen in a diagram. Figure 5.3 shows which areas of the aneurysm sac are considered ‘damaged’ and are therefore able to express tissue factor for different thrombus types. While the selected initiating surfaces may be counterintuitive in some cases, normal propagation by the clot

surface achieves the different results.

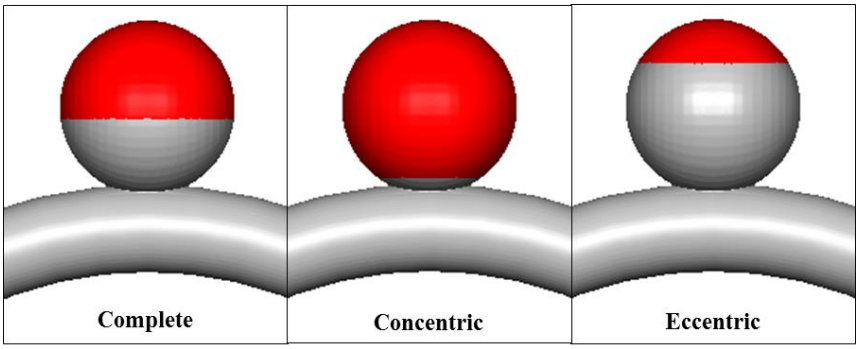


Figure 5.3: The different initiating surfaces used to achieve different types of clot growth. The whole aneurysm wall is initiated to achieve a concentric thrombus, half of the sac is initiated for thrombus which fully occludes the sac (complete) and a quarter of the sac is initiated for eccentric thrombus. Although counter-intuitive, the concentric clot is achieved by initiating damage on the whole wall while a fully occlusive clot is achieved through the top half being damaged.

5.2.3. Computational fluid dynamics

The CFD-ACE Suite (ESI Group, Paris, France) was used to create the relevant geometries and carry out computations. The geometry described in the previous subsection was created using CFD-GEOM and then converted to a discrete surface and saved as a stereo-lithography file. This allowed the file to be imported into CFD-VisCART where a non-conforming, Cartesian mesh was created as illustrated in Figure 5.4. The mesh consists of 487660 nodes and 392293 cells. Inlet, outlet and wall boundaries were created. The wall is divided into two regions: the aneurysm sac and the parent vessel wall.

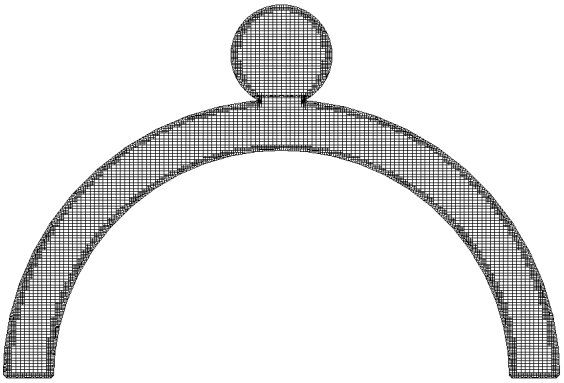


Figure 5.4: A non-conforming Cartesian mesh created for the idealised aneurysm geometry (single plane shown in this figure for clarity). The near-boundary mesh is finer than the cells in the middle of the domain.

The flow is considered transient but is not pulsatile. A time step size of $\Delta t = 0.5s$ is used. The Crank-Nicholson time scheme is used and a blending factor of $\beta = 0.5$ is used. This makes the method second order accurate. The central differencing method is used for spatial differencing. The relative contribution of the upwind differencing scheme is set at $\alpha = 0.1$. An algebraic multigrid solver is used. Blood is modelled as a Newtonian fluid with density $\rho = 1000kg/m^3$ and viscosity $\mu = 0.004kg/ms$. Blood is considered laminar and incompressible. The inlet boundary condition is set as a constant normal velocity with $V_{normal} = 0.25m/s$. The outlet is fixed as a constant pressure condition.

5.2.4. Biochemical reactions

As discussed in Chapter 4, the Mann model is comprehensive but it is computationally expensive to run. It would also prove challenging to obtain the required constants for a

specific patient in a clinical setting. The Wagenvoord model is used in all the cases presented in this chapter. The concentrations of the proteins for the inlet and initial conditions can be seen in Table 4.4.

Tissue factor is expressed as a flux value, thus it is assumed that blood-borne tissue factor contributes to thrombus development. This is a valid assumption to make because in this chapter, clot development is examined under pathological conditions [131]. For the propagation simulations, tissue factor is expressed along the entire aneurysm wall. For the initiation runs, tissue factor is expressed along the surface of the entire wall for the tissue factor concentration simulation, along portions of the wall which are below a certain strain rate for the strain rate simulations and along specific designated regions for the Lawton simulations. The solver settings and diffusivity parameters used in this chapter are identical to the ones used in Chapter 4.

5.2.5. Level Set methods

Level Set methods are used track the surface of the growing clot. Greater detail of the specifications of the method is given in Chapter 3. Nearly all the simulations assume that the entire aneurysm sac is the initiation surface. An extra condition is applied to initiation studies as described in the previous section. The signed distance function is therefore

calculated for the entire aneurysm dome. The exception is the Lawton simulations where the initiation surface is seen in Figure 5.3. The clot grows from the aneurysm surface and propagates inwards, normal to the initial surface. The propagation velocity is variable for the propagation studies and is directly proportional to thrombin concentration for the initiation studies. Cells that fall within the interface form part of the clot and assume a porosity value of $\varepsilon = 0.75$ and a permeability value of $\kappa = 1.0\times10^{-12}m^2$. This allows for differentiation between the clot and fluid region. A narrow band Level Set solver is used.

The forward Euler method of order 1 is used for temporal discretisation of the Level Set grid. The HJ-WENO method is employed for spatial discretisation. Reinitialisation is applied when the interface approaches the edge of the narrow band. The accuracy for interpolation between the Level Set and flow grids is order one. Information is transferred from the Level Set domain to the flow solver using trilinear interpolation. Nearest-neighbour inverse-weighted interpolation is used to transfer information from the flow solver to the Level Set domain.

5.3. Findings and discussion

The results presented in this chapter illustrate clot growth in an idealised three-dimensional aneurysm geometry. The propagation results presented explore the effect of both

mechanical and biochemical factors on clot development. The initiation results consider the effect of tissue factor concentration, threshold strain rate value and location of damaged endothelial tissue. The time scales used in this chapter are exaggerated. This allows for faster visualization of eventual results. Applying a more realistic time scale could be achieved by altering the coefficient used for the propagation velocity. The results are somewhat more qualitative than quantitative as the effect of the different factors is judged by the nature of the clot which is observed in the aneurysm sac. For all the results, the clot surface seen is the isosurface where porosity equals one.

5.3.1. Propagation

Figure 5.5 illustrates propagation of the clot under mechanical factors. For these cases, the propagation velocity is correlated to strain rate or is kept constant. In the constant velocity model, the clot is initiated on one side of the aneurysm wall. As time progresses, uniform growth is observed and by t = 50s, the clot is concentric with equal growth on all sides of the wall. This pattern is also observed at t = 75s. The eventual result is that clot growth progresses into the parent vessel. The direct strain rate case shows very little growth up until the t = 75s frame. The clot is initially sighted at t = 12.5s near the neck of the aneurysm. The clot quickly progresses into the parent vessel as observed in both the t = 25s and t = 50s frames. By t = 75s, the clot has fully occluded the aneurysm sac however

this is accompanied by full occlusion of the parent vessel. The inverse strain rate case shows early clot development at t = 5s. The clot grows eccentrically and eventually pulls away from all the walls as observed at the t = 75s frame.

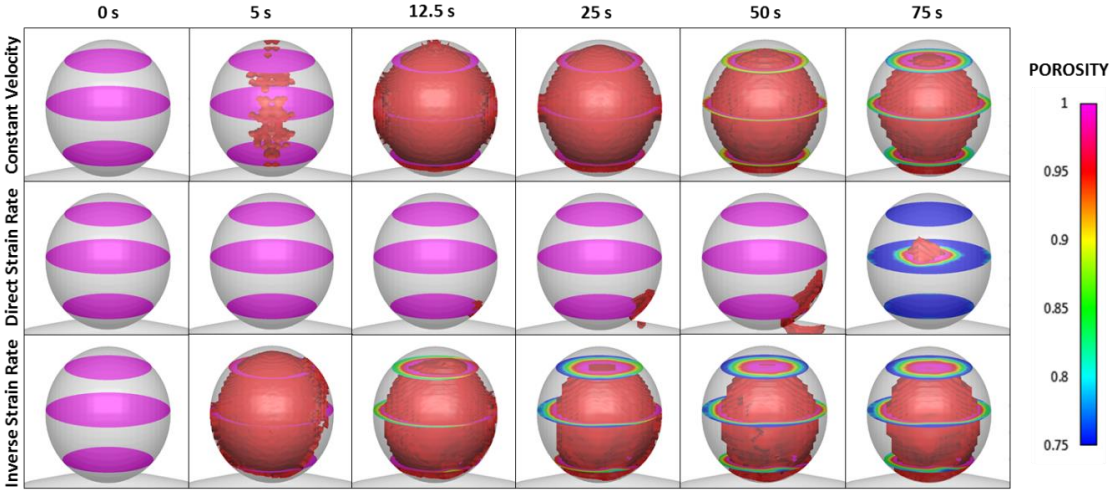


Figure 5.5: Clot growth in cases where the propagation velocity is proportional to mechanical factors. The direct strain rate case results in complete occlusion of the aneurysm sac but also results in divergence of the flow field[9].

The effect of different biochemical species on clot propagation is illustrated in Figure 5.6. The results for extrinsic tenase and total tenase are identical. In this study, extrinsic tenase is tenase which forms from factor X activation by the TF-VIIa complex. Total tenase is the sum of intrinsic tenase and extrinsic tenase. For the tenase complexes, clot growth is first evident at t = 30s. Half of the aneurysm sac is covered by a clot at t = 60s. Not much difference is observed between the t = 120s and t = 180s frames. Both frames exhibit the

[9] The constant velocity clot is initiated on a portion of the aneurysm wall because of the solver's porosity settings. After a while, the clot is seen to spread to the rest of the sac as would be expected.

spread of the clot from the left-hand half of the aneurysm sac to the rest of the wall. At t = 300s, the clot is concentric in nature and its shape imitates that of the aneurysm sac. The thrombin case is slower than the tenase cases with the clot first appearing at t = 60s. It follows a similar course to the tenase cases but the changes are observed at a later stage. The clot is nearly concentric at t = 300s. The minimum porosity observed in the tenase cases is ε = 0.85 at t = 300s while the minimum observed in the thrombin case is ε = 0.90.

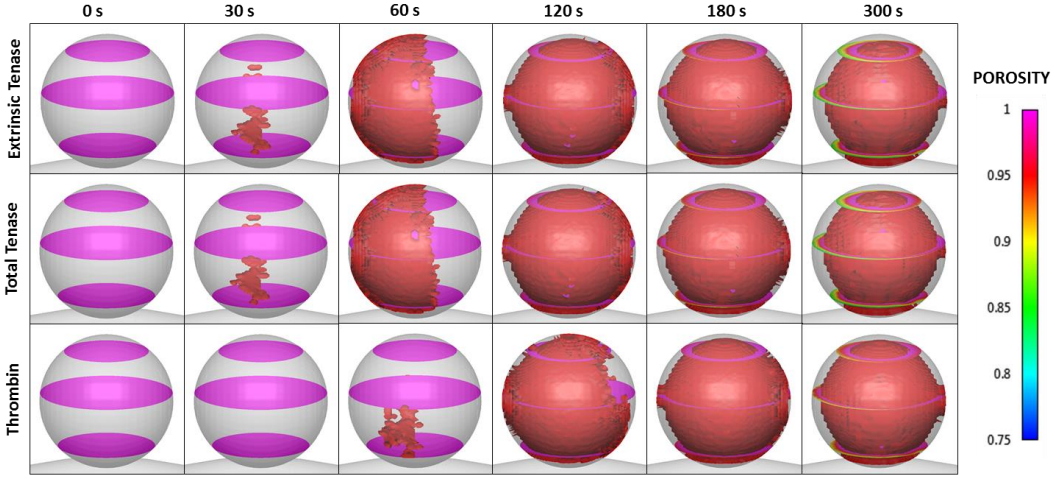


Figure 5.6: Clot propagation under the influence of different biochemical species. Linking the propagation velocity to extrinsic tenase yields the same results as linking it to total tenase. A direct relationship with thrombin results in a slower growth rate[10].

The different relationships between thrombin and propagation velocity can be seen in Figure 5.7. A direct relationship reflective of the changes in the thrombin production curve is displayed by Direct. Clot growth first appears at t = 60s and a concentric clot is seen at

[10] The asymmetry observed is a result of the flow within the sac. Tissue factor is expressed along the entire vessel wall but the transport of the other reacting proteins to the wall is dependent on the flow. The flow is influenced by the location of the inlet.

the last time step where t = 450s. An accelerated direct relationship is illustrated by Direct Fast. The clot first appears at t = 30s and a fully concentric clot is observed at t = 110s. This is less reflective of the changes that occur in a thrombin production profile. Finally, the inverse relationship can be seen in Inverse. The clot first appears at t = 15s but very little change is observed through all the time steps. A similar clot is still evident at the last time step which is taken at t = 164s.

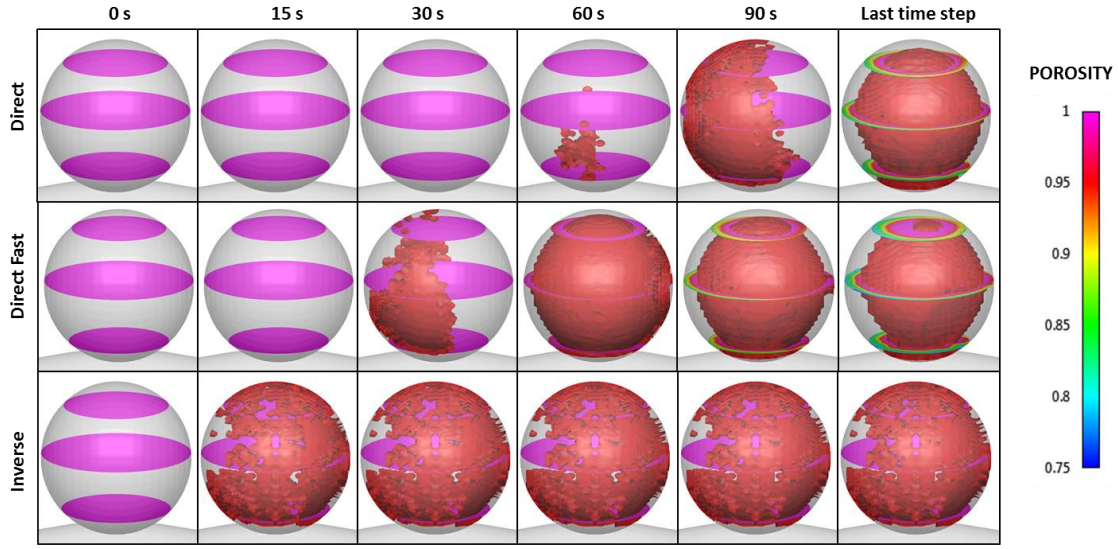


Figure 5.7: A comparison of propagation velocities with different relationships to thrombin. The direct relationship with thrombin is seen for 'Direct', an accelerated direct relationship is seen for 'Direct Fast' and an inverse relationship is seen for 'Inverse'.

5.3.2. Initiation

Figure 5.8 illustrates the effect of different tissue factor concentrations on clot propagation. In this chapter, tissue factor is expressed as blood-borne tissue factor. No clot growth is

observed for the TFconc18 case. This is true for all time frames. TFconc17 first produces a clot at t = 60s. Progression of the clot to the rest of the aneurysm wall can be seen at t = 90s. The TFconc15 case shows the first signs of clot growth at t = 15s. The clot has progressed rather rapidly at t = 30s. The clot continues to grow and covers the entire surface of the aneurysm sac. By t = 90s, the clot has propagated away from the aneurysm wall and takes on a concentric shape. The TFconc12 presents a similar trend to the TFconc15 case. The values for the TFconc12 case are, however, higher. The clot first appears at t = 15s and covers a significant portion of the aneurysm sac. The first signs of the concentric nature of the clot can be seen at t = 45s and this is confirmed by the t = 60s and t = 90s frames. A porosity of $\varepsilon = 0.75$ can be observed at the wall of the aneurysm at t = 90s. The TFconc15 case reaches a minimum porosity of $\varepsilon = 0.775$.

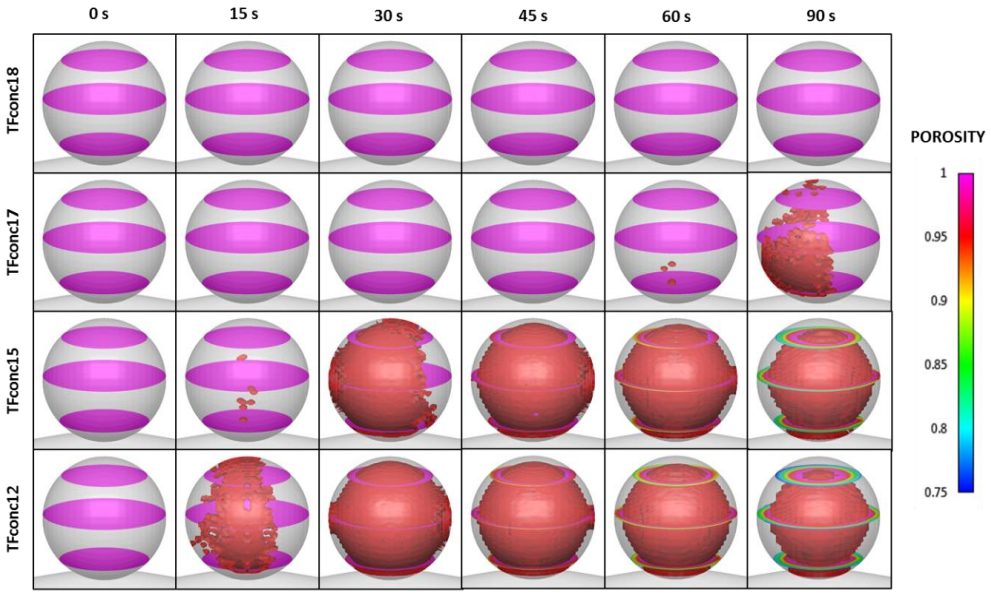


Figure 5.8: Clot propagation for different starting concentrations of tissue factor. TFconc18 shows not clot growth at 90s.

In order to link initiation to strain rate, it was necessary to test clot growth for different critical strain rate thresholds as seen in Figure 5.9. The results for SRcrit100 and SRcrit500l are identical. For both these cases, tissue factor is expressed for strain rates below $100s^{-1}$ and $500s^{-1}$, respectively. The first signs of clotting are observed at t = 60s. At t = 180s, the clot has spread to the rest of the aneurysm wall. Propagation of this clot continues for both the t = 300s and t = 360s frames. The clot at t = 300s seems to take on a concentric form and this is seen to develop at t = 360s. No clot growth is observed for the SRcrit500g and SRcrit800 cases. Tissue factor is expressed for strain rates above $500s^{-1}$ and $800s^{-1}$, respectively. From the figure, it can be said that these shear rate levels do not exist within this particular aneurysm dome.

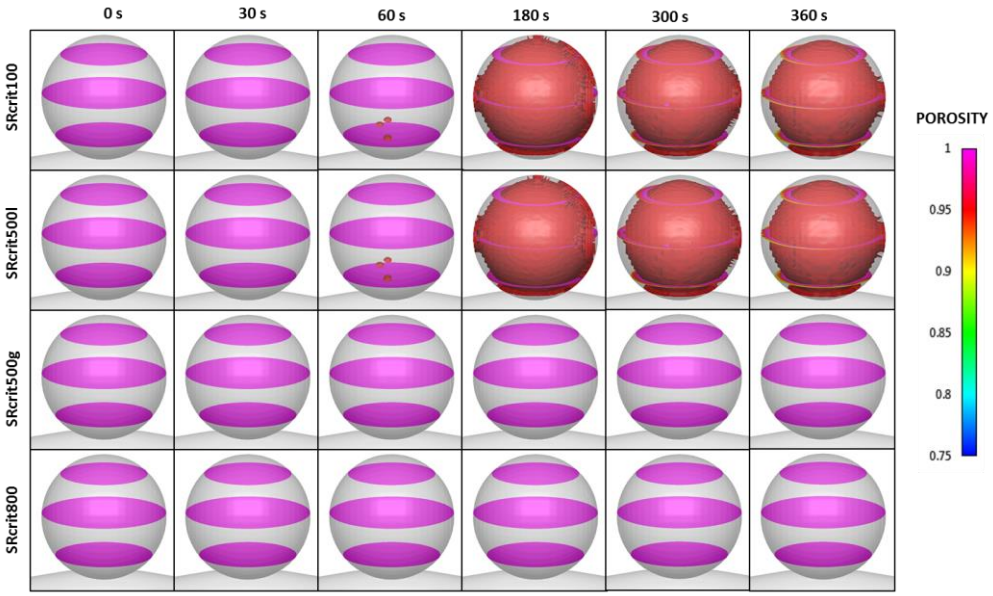


Figure 5.9: Clot propagation for different critical strain rate values at which tissue factor is expressed. No growth is seen for SRcrit500g and SRcrit800 while similar trends are observed for SRcrit100 and SRcrit500l.

Figure 5.10 illustrates the effect of the location of damaged tissue on the type of clot observed. Figure 5.3 shows the exact parts of the aneurysm sac which are able to express tissue factor. By using the top quarter of the aneurysm sac, an eccentric clot is observed. The clot is first sighted at t = 30s and has spread out at t = 60s. By t = 120s, the clot has taken an eccentric shape. The complete clot also first appears at t = 30s however the clot covers a greater surface area of the clot at this point. The clot spreads evenly to the top half of the aneurysm sac as depicted at t = 60s. The clot begins to propagate towards the neck of the aneurysm t = 120s and this trend continues for the last time step frame. The concentric clot first appears at t = 60s. By t = 120s, the clot has covered most of the aneurysm sac and a concentric clot which has propagated normal to the aneurysm wall is observed at the last time step.

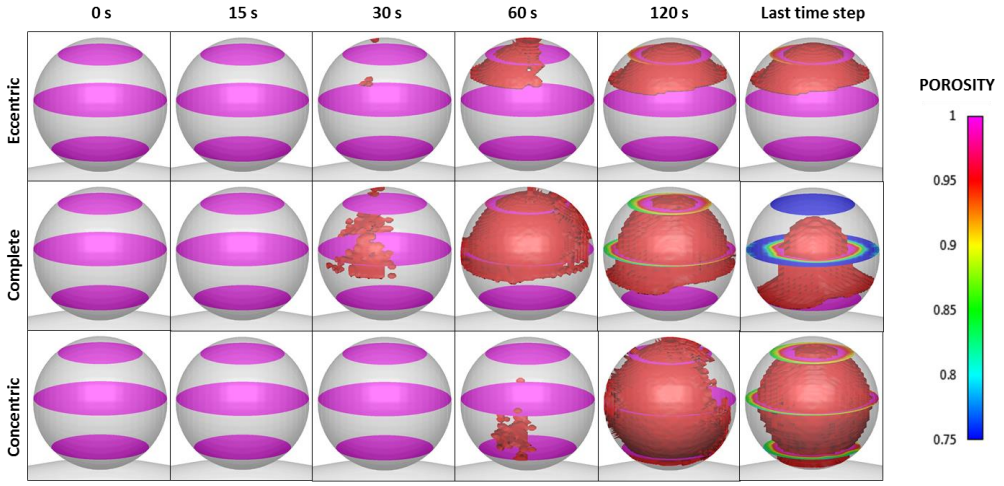


Figure 5.10: The effect of different initiation locations on clot development. An eccentric, complete and concentric clot can be formed from varying the location of 'damaged' endothelium. The location of the damage is illustrated in Figure 5.3.

5.3.3. Discussion

In this chapter, a three-dimensional model of thrombus development in an idealised aneurysm geometry is presented. The model accounts for the biochemical cascade which results in the formation of fibrin and for the propagation of the clot in a complex geometry. This is achieved by coupling computational fluid dynamics, biochemical models and Level Set methods. The model presents a powerful tool for understanding clotting in aneurysms and for predicting clot growth under a variety of circumstances. The results presented in this chapter provide a qualitative picture of the different factors which affect clot propagation and initiation. The effect of mechanical factors, biochemical factors and location of endothelial damage are examined to some extent. This provides a basic exploration of Virchow's coagulation triad [56].

The mechanical environment has a significant effect on clot propagation and initiation [99], [105], [161]. This was thoroughly explored in the introduction of this chapter. The initial set of results explored the effect of mechanical factors on clot propagation. The propagation velocity was set to a constant value and as expected, a concentric clot developed. Setting the propagation velocity to be directly proportional to strain rate resulted in a clot which quickly grew into the parent artery while an inverse relationship resulted in an eccentric clot which had a more stable growth rate. These results observed

here are reasonable. Areas of low shear rate and low shear stress are more supportive of platelet deposition and aggregation than areas of higher shear rate. It is more likely that a stable clot will therefore be observed in a model which reflects this observation.

For clot initiation, different threshold strain rates were explored. Below or above these values, tissue factor is expressed at various wall locations and clotting is initiated. Below a strain rate of $500s^{-1}$, clot initiation was observed on a significant portion of the aneurysm wall. Below this threshold, results were identical, regardless of the actual threshold value. Above the same value, there is no clotting. This suggests that above a certain value in the aneurysm sac, it is highly unlikely that platelets will settle and form stable bonds which will later be secured by the presence of a fibrin mesh.

Savage et al found that platelet adhesion which was regulated by fibrin, the end product of the process of coagulation, occurred at lower shear rates (shear rates lower than $600s^{-1}$ to $900s^{-1}$) [107]. The platelets circulating in the blood were seen to adhere to fibrin at lower shear rates. At higher shear rates (shear rates greater than $1500s^{-1}$), adhesion was governed by interactions with von Willebrand's factor. Their observation is confirmed by the work of Maxwell et al [198]. They considered lower shear rates to be those below a shear rate of $1000s^{-1}$ while higher shear rates were those between $1000s^{-1}$ and $10000s^{-1}$. The inverse

strain rate model presented in this chapter showed steady growth when growth was linked to lower strain rates. The direct strain model showed growth in higher strain rate regions. This presented a very small area within the aneurysm sac and growth quickly progressed into the parent artery. The models presented in this chapter do not incorporate the effect of von Willebrand's factor hence modelling its activity accurately would prove challenging.

In their computational model of clot growth in intracranial aneurysms, Rayz et al found that a model which incorporated both low wall shear stress and increased residence time predicted areas prone to thrombosis development quite well [19]. They constructed CFD images from MRI data and had information for both the pre- and post-thrombotic state. While they found that the use of either low wall shear stress or residence time was effective, it was the combination of the two variables that yielded the most accuracy in prediction. The models presented in this chapter do not take into account the residence time of individual particles as platelets are not modelled. While this is a potential gap in the model, it is encouraging to see that low strain rates, related to low wall shear stress for constant viscosity is a good predictor of clot growth. The preliminary foray into the effects of the mechanical environment in this study suggests support for this widely held view.

The effect of biochemical proteins is as important as the influence of the mechanical

environment when considering clot propagation. In this study, the effect of the tenase complexes and thrombin were considered. While it would have been desirable to show the effect of intrinsic tenase, the complex forms on the clot region only; therefore the propagation velocity would remain at zero if directly proportional to it. Linking the propagation velocity to extrinsic tenase and total tenase, the sum of extrinsic and intrinsic tenase, produced identical results. This is possibly a time dependent observation as intrinsic tenase is formed on activated platelets [63], [167]. As coagulation progressed and a significant amount of intrinsic tenase is produced, one would expect to see total tenase growth exceeding extrinsic tenase growth.

Panteleev et al carried out studies to determine which protein factors were the most significant contributors to clot propagation [17]. They suggested that despite its complexity, the different stages of coagulation were regulated by one key player: during initiation, extrinsic tenase had the most significant effect on clot growth. Once the propagation phase was underway, intrinsic tenase formed on the surface of activated platelets took the lead. In this study, the effects of extrinsic and total tenase seemed identical. This suggests that extrinsic tenase formed the bulk of the total tenase sum. It is also difficult to make any conclusive judgments as Panteleev et al produced results for a physiological model while the results presented in this chapter are working towards a pathological model.

As discussed in Chapter 4, the initial tissue factor concentration used in existing computational models varies widely depending on the intention of the researcher. Concentrations ranging from picomolar to nanomolar values have been reported in literature [16], [163], [187], [204]. It proved necessary to examine the effect of tissue factor concentration for the three-dimensional aneurysm configuration in order to ensure that clotting happened within a reasonable time period. It was also necessary to examine which tissue factor concentration resulted in reasonable thrombin production. This is especially true for cases where strain rate initiates clot growth as different patches of the aneurysm wall would experience different thrombin concentrations. Even though TFconc12, TFconc15 and TFconc17 all showed reasonable clot growth, TFconc17 produced the most likely clot growth for the given time period.

The effect of thrombin is slightly different from that of the two tenase complexes. Clot development begins at a later stage. This is partially because thrombin is the product of the extrinsic tenase complex and prothrombin hence a time lag is to be expected. Once clot growth is underway, the nature of the clot which forms is quite comparable to that formed by the tenase complex. Thrombin is expected to have a fairly significant effect on clot growth as it has the ability to activate platelets, thus encouraging platelet aggregation and it can amplify its own production [61], [63]. The results from all three biochemical factors

produced concentric, stable clots which did not progress into the parent vessel.

The effect of thrombin was further explored by relating thrombin to propagation velocity in different ways. The first set of results illustrated a direct relationship with thrombin for a constant which would allow propagation to occur at a rate such that the changes in the thrombin profile would be registered in clot growth. The second set of results was similar to the first with the exception that the constant was larger, hence speeding up the rate of growth. The clot was already fairly well developed early on. Further growth would have eventually led to parent vessel occlusion. Finally, an inverse relationship with thrombin showed early clot development but little progress after that. The clot remained fairly close to the aneurysm wall in small patches.

The classification system presented by Lawton assigns different names to clot types depending on the shape of the clot within the aneurysm sac [148]. In this study, it was hypothesised that the type of clot formed is closely linked to the exact location of the damaged endothelial surface. Damage incurred to the top quarter of the aneurysm sac would result in an eccentric clot while damage of the entire sac would result in a concentric clot. A complete clot would fall between the aforementioned two regions of damage. The results give preliminary evidence of the possibility of this proposition. The

eccentric and concentric clot cases match Lawton's description quite well. The complete clot is not entirely wrong but further normal propagation would be required to confirm the proposition for this specific case. The hypothesis is explored further in the following chapter where device-induced clotting is considered.

The models presented have their limitations. As previously expressed, the models are more qualitative than quantitative in nature. In addition, the effect of platelet activity is not directly modelled. Further work would include linking the propagation velocity to both biochemical and mechanical factors. In addition, it could be useful to link the propagation velocity to different biochemical proteins for different phases of coagulation. A more realistic wall model would prove useful in understanding clot initiation and better predicting parts of the wall where clotting is likely to begin. Finally, modelling a pathological condition in an idealised geometry is likely to introduce a further margin of error. Part of the challenge of attempting to understand a highly patient-specific disease is making decisions about what types of geometries would be most conducive to understanding basic elements of the problem.

The biggest challenge in modelling clotting in cerebral aneurysms is that many of the details and variables of the disease itself are not well understood or documented. While the

model presented here may make many assumptions, it does present a platform which can be used to further investigate a phenomenon which would be difficult to observe *in vivo*. It is relatively easy to change variables in the model and as the details of aneurysm thrombosis become clearer, details of this model can be changed to give more accurate responses. This may, in turn, elucidate further details about the realistic process.

6. Results: Evaluation of flow diverter performance in patient-derived aneurysm geometries

In this chapter, the methodologies developed and presented in the previous two chapters are implemented in realistic patient-derived aneurysm geometries. Such a tool could be used by a clinician for interventional planning.

6.1. General considerations

A 2013 review by Moiseyev and Bar-Yoseph highlighted the need for a computational model of thrombosis which would be able to evaluate vascular implants [205]. They conducted a review of existing models of coagulation which are used mostly for the understanding of physiological clotting. It is believed that some of these models could be adapted for use as research and design tools for cardiovascular implants. The paper highlighted some of the salient features that the desired tool would have. It would need to use a coagulation cascade which would be simple enough to run within a reasonable time while capturing the key features of the coagulation process. It would also need to effectively integrate the coagulation cascade and haemodynamics. The model could be used for both implant design and for the understanding of haemodynamically-induced thrombosis. The model presented in this chapter brings together the previous chapters and

presents a tool similar to the one envisioned by Moiseyev and Bar-Yoseph.

Endovascular treatment of cerebral aneurysms has gained popularity over the last decade. This mode of treatment has become more widespread as it is less invasive, hence recovery time is faster. Even though endovascular methods have advantages over traditional surgical methods, there are still complications associated with coiling and stenting. Secondary haemorrhage and compacting of coils are examples of such difficulties. The other challenge which has arisen as a result of advances in medical imaging technology is that many more asymptomatic aneurysms have been detected unintentionally while conducting routine scans for other pathologies. A dilemma arises from having to decide whether or not to treat such an aneurysm. The aneurysm could rupture at a later stage or may remain asymptomatic. In both the treatment method and accidental diagnosis cases, it would prove useful to have a tool which could predict the eventual outcome of the aneurysm and/or its treatment. A major predictor of outcome in aneurysms is clot development within the aneurysm sac. A predictor of clot development in aneurysms would therefore be beneficial.

6.1.1. Spontaneous clotting in cerebral aneurysms

Determining whether or not clotting is desirable in aneurysms continues to be quite a perplexing task. Part of the challenge arises from the limited understanding of different

clot types observed in aneurysms and from incomplete knowledge about clotting in this particular pathology. Both spontaneous and device-induced clots have been examined in literature and suggestions have been made about the effects of clotting on aneurysm evolution.

There are many cases where clotting has been observed in aneurysms which have not undergone prior intervention. In cases where the aneurysm had already ruptured, a clot develops in an effort to arrest bleeding and prevent further subarachnoid haemorrhage [150]. In such cases, clots have been observed to develop in different ways. Some clots develop on the inside of the aneurysm sac while others develop from the outside. In both cases, the aim of clot development is repair and closure of the aneurysm rupture point.

Of greater interest to this study is the spontaneous development of clots in aneurysms which have not ruptured. Such cases are less common than those where clotting occurs following rupture and the mechanisms by which such aneurysms clot are not well understood. The spontaneous clotting of unruptured cerebral aneurysms is most commonly observed in giant cerebral aneurysms. About fifty percent of giant aneurysms are partially or completely thrombosed [13]. Thrombosis observed in these cases is non-uniform as a result of complex flow conditions and non-uniform wall damage within

the aneurysm sac. Even less common are non-giant unruptured cerebral aneurysms presenting with thrombosis. In both giant and non-giant cases, it appears that fully occluded aneurysms seem to be more stable than non-thrombosed ones. Partially occluded aneurysms present the greatest risk as they tend to recanalize and rupture at a later stage [38], [151].

It is clear that the temporal and spatial evolution of spontaneous clots in cerebral aneurysms remains unclear. It would prove useful to have a research tool which could be used to elucidate some of the features which are unique to aneurysmal thrombosis.

6.1.2. Non-spontaneous clotting of aneurysms

The aim of aneurysm treatment methods is to occlude the aneurysm sac and to restore flow along the original parent vessel. Both surgical and endovascular techniques attempt to achieve this objective. Surgical clips placed at the neck of the aneurysm prevent flow from entering the aneurysm sac [43]. Guglielmi detachable coils are designed to fill and occlude the aneurysm sac [9]. This results in full separation of the clot from the parent vessel. Complications may arise from coil compaction. In wide-necked aneurysm cases, the combination of a stent and coil has produced a similar occlusive outcome.

Flow-diverters are an increasingly common solution in aneurysms which cannot be coiled easily. At first glance, flow-diverters seem similar to stents. The main difference is the porosity of the mesh is reduced in flow-diverters. This reduces the amount of fluid flowing into the aneurysm sac and redirects it along the parent vessel [5].

All forms of endovascular treatment result in the formation of a clot within the cerebral aneurysm sac. Under such circumstances, clotting in the sac is considered to be a positive outcome, provided that the clot fully occludes the sac. As with the spontaneous clots, partial occlusion is likely to result in secondary complications within the sac. An additional undesirable outcome for flow diverter treatment is the actual *absence* of a clot which, like partial occlusion, may lead to rupture at a later stage. Such an outcome is adverse because it is indicative of insufficient flow diversion. Under such conditions, flow patterns within the aneurysm are altered from the original state. Albeit suboptimal, the initial state may still be better than a partially altered state which exists as a result of insufficient flow diversion [14].

It is evident that a tool which is able to predict the outcome of endovascular treatment is desirable. Such a tool would be able to predict the growth of a clot for a specific patient before intervention. The tool would then also be able to the predict clot growth post

intervention, thus giving an idea of likely outcome prior to intervention.

6.2. Model specifications

In this chapter, realistic three-dimensional geometries are used to examine clot development. For a given geometry, two simulations are conducted. One of the simulations examines clot growth without the presence of a flow diverter while the other simulation models clot growth with a flow diverter. This demonstrates a possible application for the computational tool developed in this work – the evaluation of endovascular devices prior to intervention in specific patients. All the methods used in this chapter were used and discussed in previous chapters.

6.2.1. Geometries

The geometries used in this chapter are reconstructed from computed tomography scans. We have access to a database of reconstructed geometries which are used for different flow simulations and other computational investigations. Some of these geometries have stents which are positioned using a manual in-house method. The slices that represent the vasculature, as produced by the imaging modality used, are processed using @neufuse (developed for the European project @neurist, www.aneurist.org: Integrated Biomedical

Informatics for the Management of Cerebral Aneurysms see [206])[11]. The product of the segmentation, manipulation and surface reconstruction algorithms used (not a topic of this dissertation) is a triangulated surface which can be exported to various formats and developed for further use. Whereas these operations are extremely important in the workflow envisaged (reconstructing geometries and ensuring that key features are preserved), the focus of this work lies elsewhere, since Medical Imaging and Image Computing are well-identified disciplines on their own which would require specialized training in order to fully understand the very advanced strides being made, and very detailed (and lengthy) descriptions to present adequately. For this, we shall take those steps as covered and we shall refer the reader to several excellent textbooks and papers on the topic [207–209].

Three geometries are used in this chapter. Figure 6.1 shows a diagram of the major vessels of the brain where most aneurysms occur. The first, named Case 1, is an internal carotid artery with a giant, wide-necked aneurysm. The internal carotid artery is a major artery which branches from the common carotid artery [210]. It supplies blood to the brain. The reconstructed geometry used for this chapter can be seen in Figure 6.2. The second

[11] @neufuse is an integrated biomedical informatics platform which links aneurysm data from different modalities for specific patients. It was developed as part of the @neurist project, a European initiative which aims to provide integrated decision support for cerebral aneurysm treatment.

geometry, named Case 2, is a middle cerebral artery with a wide-necked aneurysm. The middle cerebral artery supplies blood to cerebrum and the reconstructed geometry can be seen in Figure 6.3. The third geometry, named Case 3, is another internal carotid artery aneurysm seen in Figure 6.4.

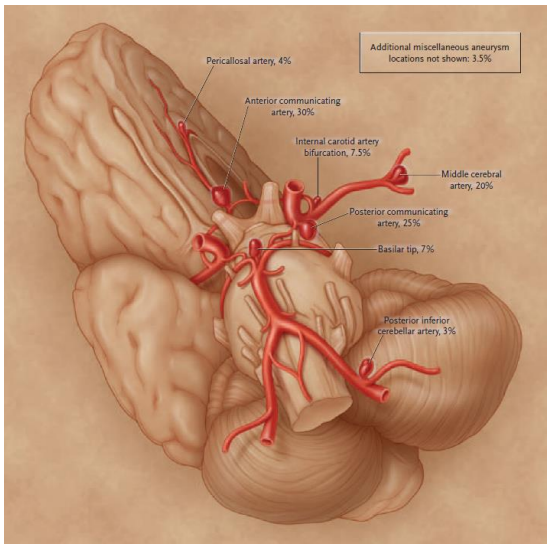


Figure 6.1: The most common sites for aneurysms. The geometries used in this chapter are aneurysms on the internal carotid artery and the middle cerebral artery. Taken from Brisman et al [3]**.**

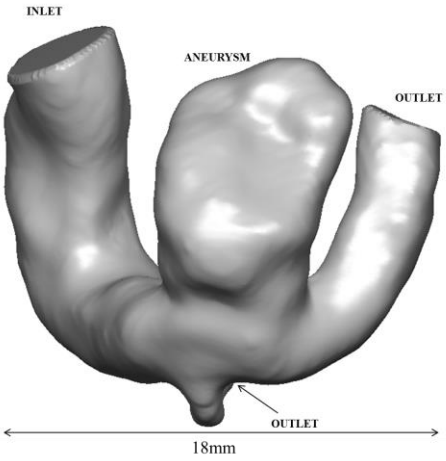


Figure 6.2: Case 1 - The giant aneurysm on the internal carotid artery. The inlet and one of the outlets for the geometry are a part of the artery itself. The other outlet, opposite the aneurysm, is the ophthalmic artery which supplies blood to the eye.

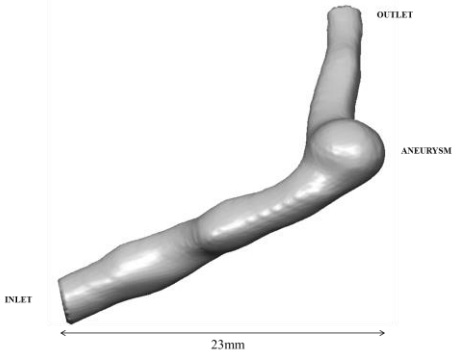


Figure 6.3: Case 2 - The aneurysm on the middle cerebral artery. The inlet and outlet of the geometry are located on the MCA itself. The aneurysm developed at a bend in the artery.

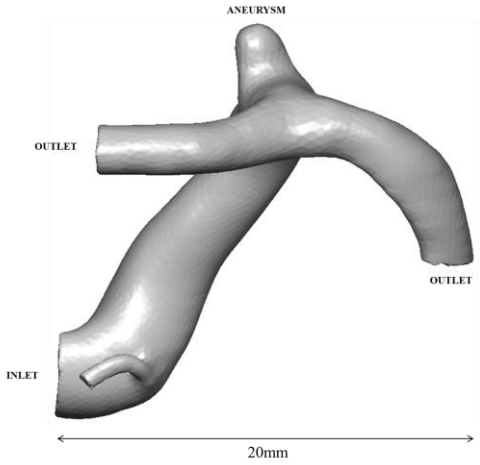


Figure 6.4: Case 3 - An internal carotid artery with a giant, wide-necked aneurysm at a bifurcation.

6.2.2. Simulations conducted

The simulations conducted in this chapter consider the effect of endovascular treatment on clot development. This is achieved by running a simulation without a flow diverter and then one with a flow diverter. The flow diverter has an impact on both the mechanical environment and on the haemodynamics. The clotting tool, therefore, needs to be able to incorporate the change in mechanical environment and still account for the biochemical

reactions. The clot is initiated using a strain rate threshold and propagation is dependent on thrombin concentration. The parameters used for runs in this chapter are seen in Table 6.1.

Name	Propagation Velocity	Initial [TF] (M)	Critical strain rate (s^{-1})	Initiating wall (initial surface/tissue factor expression)
Case1	Thrombin direct	1.00E-17	100	Strain rate less than $100s^{-1}$
Case1Stent	Thrombin direct	1.00E-17	100	Strain rate less than $100s^{-1}$
Case2	Thrombin direct	1.00E-17	100	Strain rate less than $100s^{-1}$
Case2Stent	Thrombin direct	1.00E-17	100	Strain rate less than $100s^{-1}$
Case3	Thrombin direct	1.00E-17	100	Strain rate less than $100s^{-1}$
Case3Stent	Thrombin direct	1.00E-17	100	Strain rate less than $100s^{-1}$

Table 6.1: Input parameters for the different geometries used in this chapter.

6.2.3. Computational fluid dynamics settings

The CFD-ACE suite (ESI Group, Paris, France) was used to create the computational grid on which the flow simulations are run. More detail about the specific features of the CFD-ACE solver is given in Chapter 3. The grid was created using CFD-VisCART, a mesh generator which is able to create non-conforming, adaptive grids. For the geometries used in this chapter, unstructured projected meshes are generated. A projected mesh is one where the bulk of the mesh is made up of Cartesian cells with the exception of cells close to the solid boundary. In order to ensure that the geometry is not too compromised, cells closer to the geometry are projected from the wall thus maintaining the geometry's actual shape. A combination of hexahedral and polyhedral cells is used for the mesh. Case 1 consists of 338 118 cells without the flow diverter and 426 231 cells with the flow diverter.

The mesh without a flow diverter for Case 2 consists of 124 663 cells while the flow diverter case consists of 132 106 cells. Finally, for Case 3, the mesh without a flow diverter consists of 497 564 cells while the mesh with a flow diverter consists of 598 219 cells. It should be noted that although these meshes are not of particularly high density, out aim here is to demonstrate the capabilities of the methodology and, importantly, to highlight the differences between intervened and not-intervened cases. As such, comparable resolutions that capture the main trends are sufficient and alleviate the very taxing computational requirements of very long time histories and many additional transport equations to be solved that couple haemodynamics-thrombosis modelling entails.

The flow is transient but is not pulsatile; a simplifying assumption we adopted for expedience of the computations. The inlet boundary condition is set as a normal velocity and has a value of $V_{normal} = 0.189 ms^{-1}$. This is velocity averaged over the cardiac cycle. The outlets are set at a constant pressure of P = 0Pa. Blood is modelled as a Newtonian fluid as the arteries under consideration are sufficiently large. The density of blood is set at $\rho = 1000 kgm^{-3}$ and the dynamic viscosity is set at $\mu = 0.004 kgm^{-1}s^{-1}$. The Crank-Nicholson temporal differencing scheme is used. The blending factor is $\beta = 0.5$ and the time step is $\Delta t = 0.5s$. The central differencing method is used for spatial differencing. A small contribution is made by the upwind differencing method and the blending factor is $\alpha = 0.1$.

An algebraic multigrid solver is used for solving the iterations.

6.2.4. Biochemical reactions

As with Chapter 5, the Wagenvoord model is used to describe the biochemical changes taking place in the system. All the settings used for the biochemical reactions used in this chapter are discussed in Chapter 4. A description of the solver used for these reactions is given in Chapter 3.

Tissue factor is expressed on selected portions of the aneurysm sac. Ouared et al developed a computational model of thrombus development in aneurysms which was able to account for partial, full and no occlusion of the aneurysm sac [20]. They found that this was achieved by setting a strain rate threshold below which thrombosis was able to occur. This value was $100s^{-1}$. In this study, those parts of the wall which experience a strain rate of less than $100s^{-1}$ are able to express tissue factor. This allows for the initiation of thrombosis on those parts of the aneurysm wall. As with Chapter 5, tissue factor is expressed as blood-borne because in this case, thrombosis is considered under pathological conditions.

6.2.5. Level Set methods

The exact details of the narrow band reinitialisation method used in this study are given in

Chapter 3. For this chapter, the signed distance function is calculated for the entire geometry. In order to isolate the aneurysm, a Boolean intersection is then performed between the calculated function and relevant planes. This isolation reduces computational cost by focusing calculations on the aneurysm wall. From the signed distance function, cells which fall within the interface assume porosity and permeability values of $\varepsilon = 0.75$ and $\kappa = 1.0\times10^{-12}m^2$, respectively. This creates a distinction between the clot and fluid region and enables the clot to have an effect on the fluid field and vice versa.

The forward Euler method of order 1 is used for temporal discretisation of the Level Set grid. The HJ-WENO method is employed for spatial discretisation. Reinitialisation is applied when the interface approaches the edge of the narrow band. The accuracy for interpolation between the Level Set and flow grids is order one. Information is transferred from the Level Set domain to the flow solver using trilinear interpolation. Nearest-neighbour inverse-weighted interpolation is used to transfer information from the flow solver to the Level Set domain.

6.3. Findings and discussion

The results presented in this chapter show comparisons between clots formed with and without the presence of a flow diverter, for individual aneurysm configurations. In some

cases, it is evident that clot development after the placement of a flow diverter is a positive outcome while in others, it is a more detrimental outcome than the situation prior to the placement of a flow diverter.

6.3.1. Case 1

The placement of a flow diverter for Case 1 results in much more prominent clot growth. This is illustrated in Figure 6.5 where clot growth is much slower in the case without a flow diverter. The red surface indicates the surface of the growing clot within the aneurysm sac. At t = 7.5s, clot development is fairly insignificant in both cases. Even though this is the case, the clot in the case with the flow diverter is already more noticeable than in the case without. At t = 15s, both cases seem quite similar to the previous time step. Significant changes are observed for the flow diverter case at t = 30s. The clot has extended to most of the top half of the aneurysm sac. No change is observed for the case without the flow diverter. Some change is observed for this case at t = 45s. Two spots are now seen to have clot development. The flow diverter case depicts propagation of the clot which was observed at t = 30s. The clot observed seems to be eccentric in nature as it begins to propagate inwards from the aneurysm sac. Albeit in the early stages of development, the clot observed in the flow diverter case seems to be fairly stable. At t = 75s, the clot in the flow diverter case has progressed further into the aneurysm sac. The

clot in the case without the flow diverter remains in the wall region.

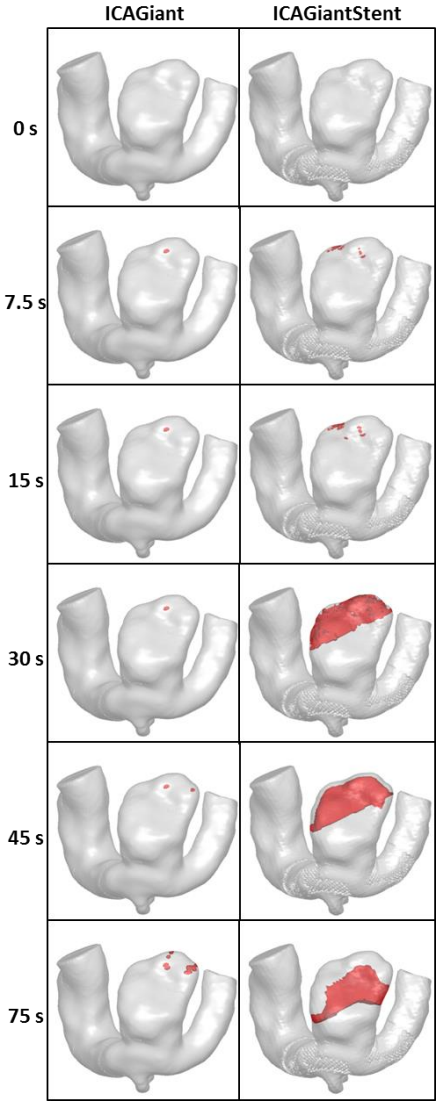


Figure 6.5: Clot surface for the ICA Giant Aneurysm case. Clot propagation is much more prominent in the case with the flow diverter. The case without the flow diverter illustrates almost no clot growth.

Clot growth, flow dynamics and thrombin development for the case without a flow diverter can be seen in Figure 6.6. Very little clot development is observed from t = 0 – 45s. While not dramatic, more clot growth is observed at t = 75s. This coincides with thrombin

production observed in the clot region. The maximum thrombin concentration observed is [TH] = 1.4×10^{-8}M. Flow within the aneurysm sac is quite complex as seen in the strain rate image. The strain rate is variable over the surface of the aneurysm sac with values ranging from $0s^{-1}$ to just under $100s^{-1}$. Thrombin production on the aneurysm sac is very low, resulting in insignificant clot development.

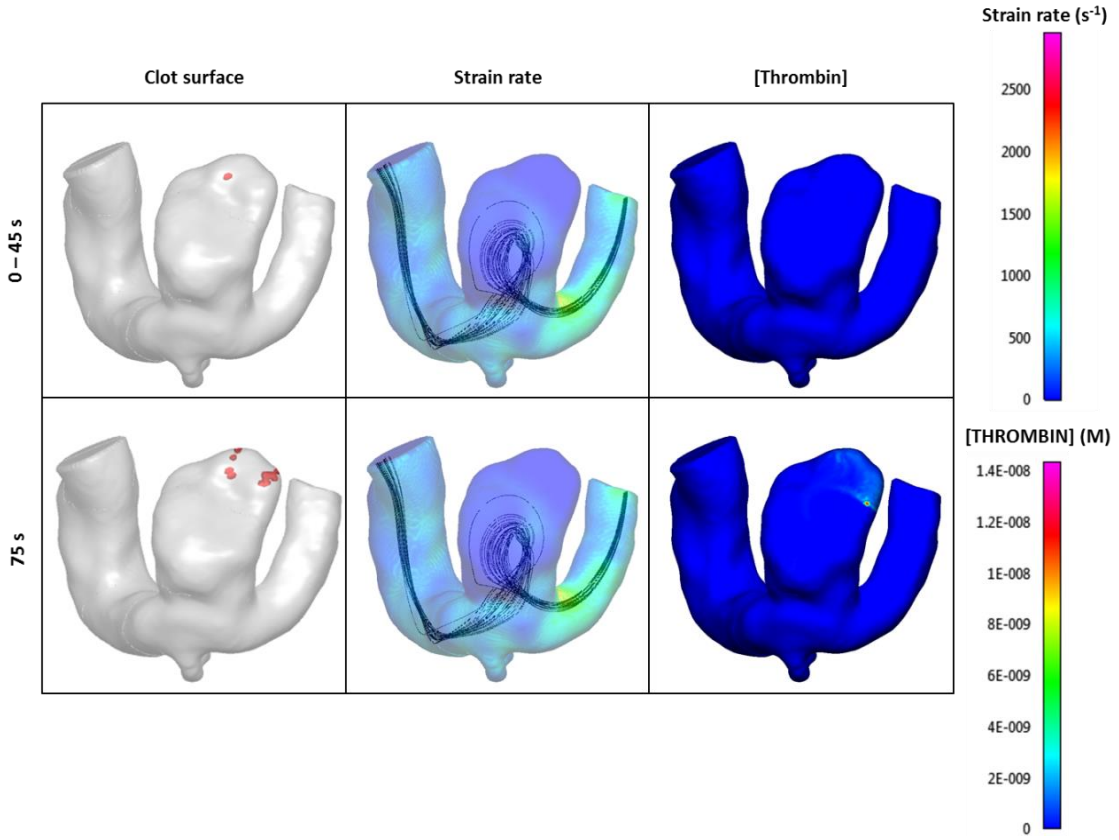


Figure 6.6: Clot growth and flow dynamics for the Case 1 without flow diverter placement. Little thrombin is expressed for all the time steps.

Significant clot growth is observed in the case with the flow diverter. Unsurprisingly, thrombin production is also fairly substantial. Both of these results can be observed in

Figure 6.7. Thrombin production is insignificant up until t = 30s where the concentration varies over the aneurysm sac. The concentration intensifies at t = 45s. At this time, the maximum thrombin concentration observed is [TH] = 1.2×10^{-7}M. Strain rate and flow in the geometry is fairly constant throughout the run. Interestingly, strain rate is mostly constant over the surface of the aneurysm sac unlike in Figure 6.6.

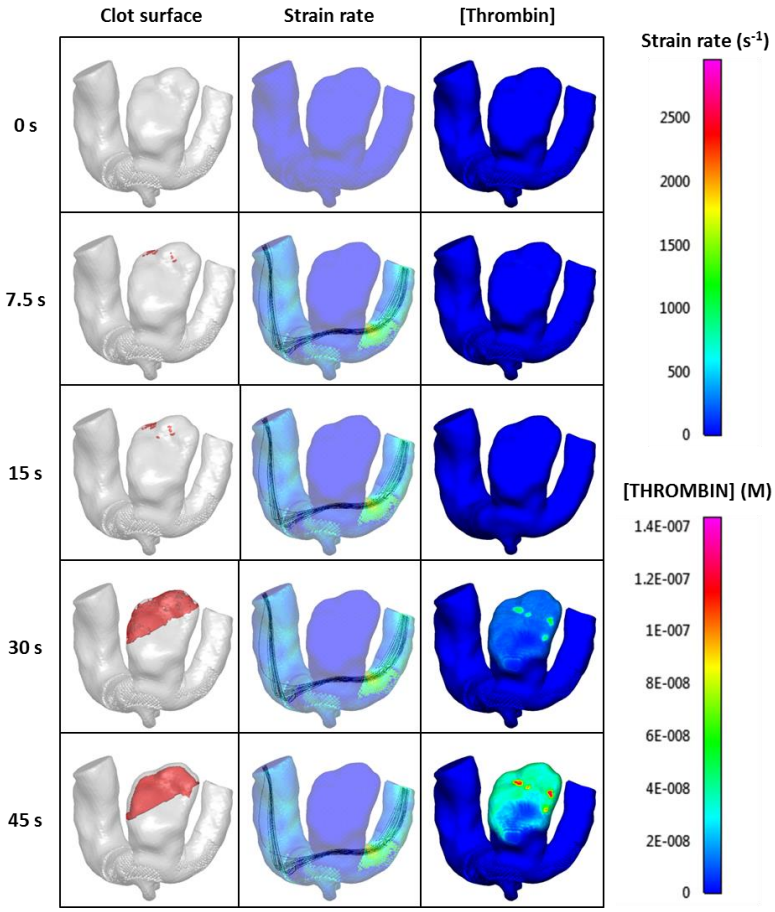


Figure 6.7: Clot development and flow dynamics for the case with the flow diverter. Thrombin production is very noticeable at 30s and 45s.

6.3.2. Case 2

Figure 6.8 illustrates thrombus development before and after flow diverter placement.

Before flow diverter placement, no clot is observed in the aneurysm for all time steps. Once a flow diverter is put in place, the first signs of clot development are observed at t = 30s. The clot propagates inwards from the aneurysm wall but quickly grows into the middle cerebral artery. The first sign of this occlusive growth is seen at t = 120s. By t = 150s, the flow field has diverged as the clot has made notable progress into the parent vessel.

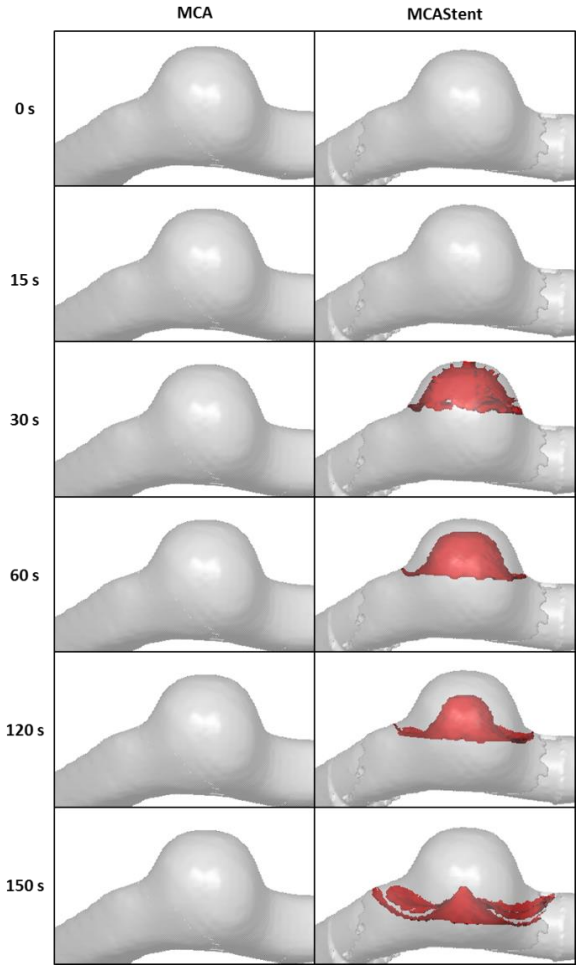


Figure 6.8: Thrombus development prior to and after the placement of a flow diverter for the middle cerebral artery. The clot which develops after the flow diverter has been put in place extends into the parent artery and is likely to result in occlusion.

Prior to flow diverter placement, the strain rate on the aneurysm wall is quite high and varied as seen in the strain rate image in Figure 6.9 . Complex flow patterns can also be seen in the aneurysm in the same image. The high strain rates result in no tissue factor release. As a result, no thrombin is formed. This is illustrated in the thrombin concentration diagram. The figure below is true for all time steps with the exception t = 0s, where strain rate and flow are also zero.

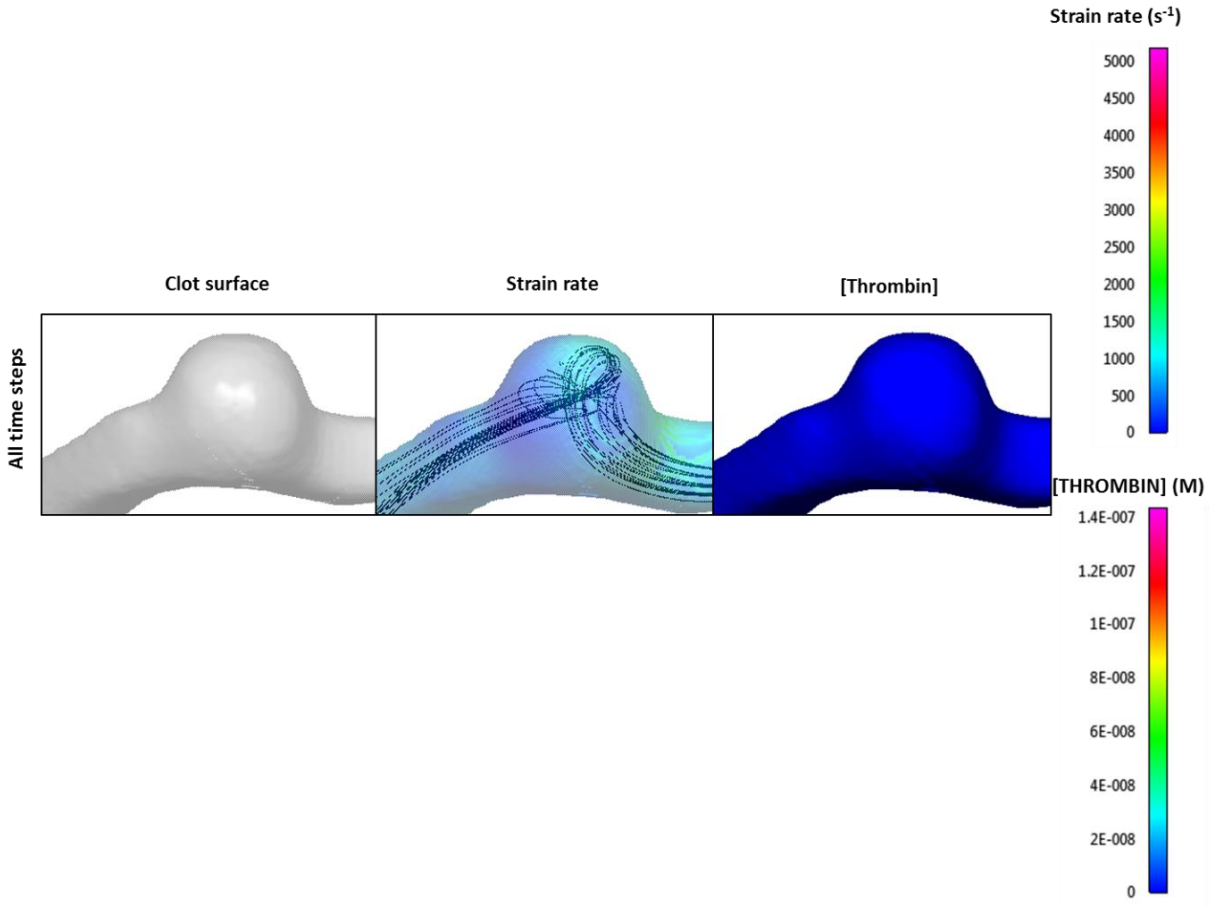


Figure 6.9: No clot is seen in the aneurysm prior to flow diverter placement. The strain rate on the aneurysm wall exceeds the threshold hence no tissue factor is released and no thrombin is formed.

Flow conditions and thrombin concentration in the aneurysm after stent placement are illustrated in Figure 6.10. The strain rate remains very low for all the times steps and the flow field in the parent vessel remains fairly stable for the duration of clot growth (prior to occlusion and divergence). The strain rate is low enough for tissue factor to be expressed on the vessel wall. The first trace of thrombin is sighted at t = 30s when concentrations below [TH] = 1.0×10^{-8}M are detected. The concentration steadily increases and intensifies as the clot progresses in the aneurysm sac.

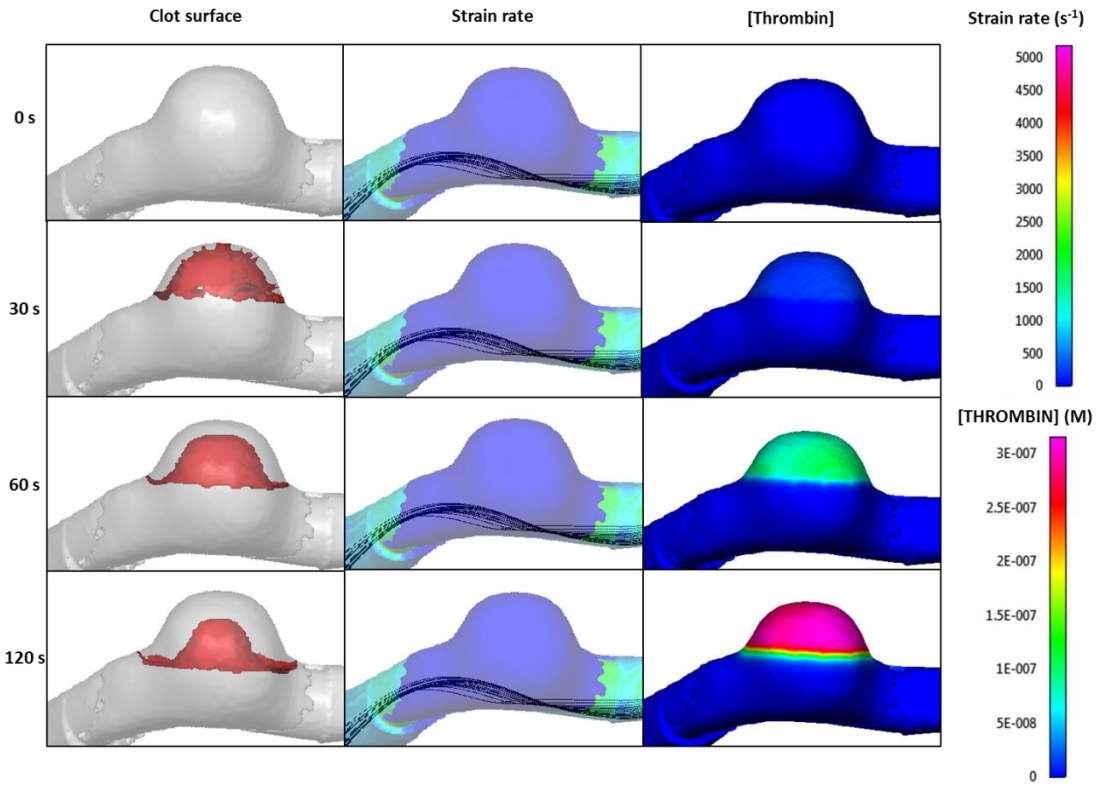


Figure 6.10: Thrombus development in the middle cerebral artery after flow diverter placement. The strain rate and streamlines remain fairly constant as the clot propagates. Once the clot propagates into the parent vessel after 120s, the flow field diverges as the vessel is occluded.

6.3.3. Case 3

A comparison of scenarios with and without a flow diverter for Case 3 is seen in Figure 6.11. Initially, more clotting is observed in the case without a flow diverter as seen at t = 7.5s. The same observation holds for t = 15s. At t = 30s, however, the clot for the case with the flow diverter has propagated further from the wall than the case without. This trend remains true for the remainder of the time steps. While the case without the stent does not exhibit rapid propagation of the clot surface, the clot spreads out more over the aneurysm wall.

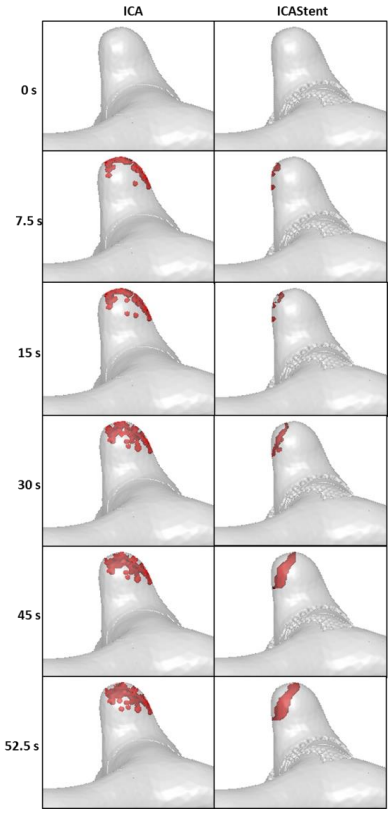


Figure 6.11: Clot growth with and without a flow diverter for Case 3. Significant clot growth is observed in both cases however the clot advances more rapidly in the case with a flow diverter.

Figure 6.12 illustrates clot growth, strain rate and thrombin production for Case 3 without a flow diverter. Unlike Cases 1 and 2, a fair amount of thrombin is produced for the case without a flow diverter. This is related to the shape of the aneurysm sac where limited flow in the dome allows for thrombin accumulation. The maximum thrombin concentration observed is [TH] = 2.0×10^{-9}M at t = 52.5s. The clot is close to the dome and is seen to spread over the surface of the aneurysm sac. Little propagation away from the aneurysm wall is observed. Strain rate is fairly low over the aneurysm sac but the neck region experiences strain rate values of around 1000s^{-1}. Flow within the sac is quite complex.

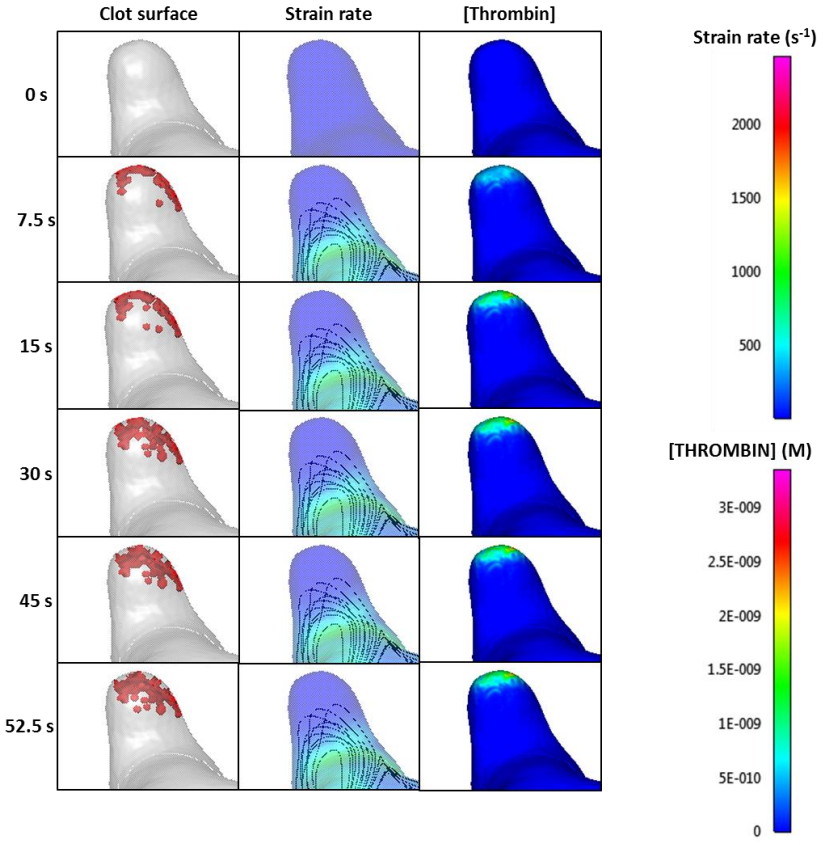


Figure 6.12: Clot growth, strain rate and thrombin concentration for Case 3 without a stent. Thrombin is produced at the dome of the aneurysm and as a result, clot propagation is seen in that region.

Clot growth, strain rate and thrombin concentration for Case 3's flow diverter case is illustrated in Figure 6.13. It is clear from the figure that flow patterns within the aneurysm sac are less complicated than those observed in Figure 6.12. Clot growth is initiated on a small portion of the aneurysm sac close to the dome. As time passes, the clot propagates away from the aneurysm wall. Relatively high thrombin concentrations are observed for this case. The maximum thrombin concentration is [TH] = 9.0×10^{-8}M. This is higher than the maximum without the flow diverter. The value observed in Figure 6.12 is [TH] = 2.0×10^{-9}M.

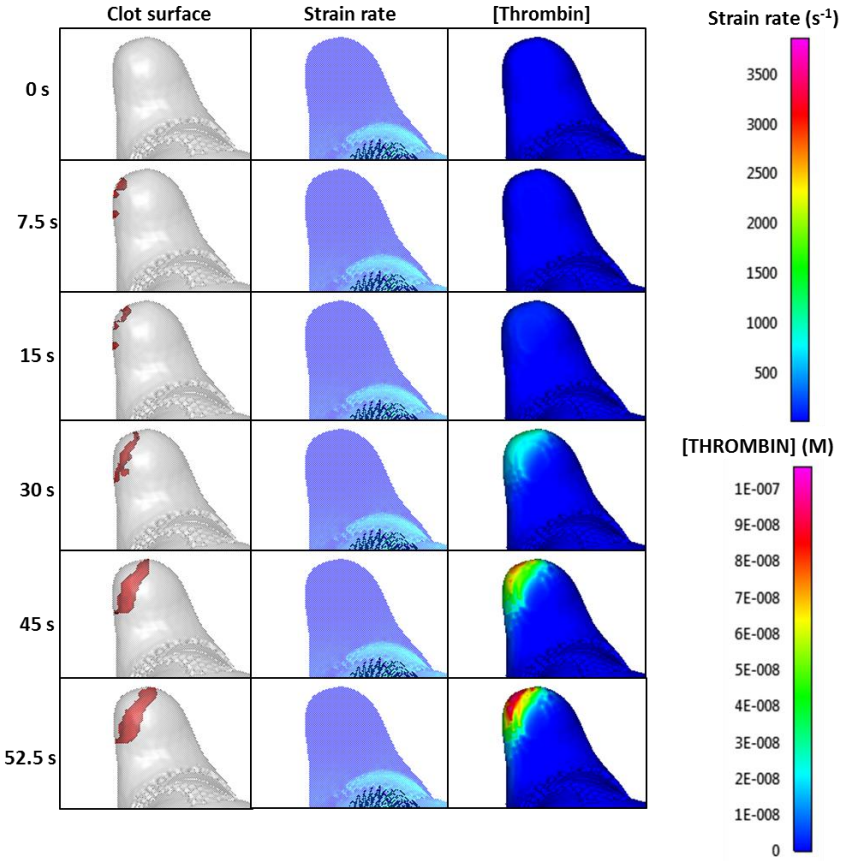


Figure 6.13: Clot growth, strain rate and thrombin concentration for Case 3 with a flow diverter. Strain rate is uniformly low across the aneurysm dome. Clot propagation is initiated at the dome.

6.3.4. Discussion

The results presented in this chapter show the applicability of the tool developed in the previous chapter to endovascular device evaluation. Three different aneurysm cases were presented. For each case, clot development was observed both before and after flow diverter placement. In some cases, flow diverter placement encouraged the development of a clot which occluded the aneurysm sac and stabilised the aneurysm. In other cases, the clot quickly grew into and occluded the parent vessel, a situation which should be avoided. Moiseyev and Bar-Yoseph highlighted the need for a computational model which would be able to examine the efficacy of different vascular implants and this model provides a possible way of achieving this [205].

The results illustrate that by using a strain rate threshold, the subendothelial layers are likely to be exposed in regions where platelets would gather and adhere due to low flow velocities [107], [198]. These regions are then able to express tissue factor and the end result of the coagulation reaction system is the formation of thrombin and subsequently, fibrin. The clot propagation velocity is directly related to thrombin concentration hence propagation of the clot takes place in regions where injury first occurred. The interplay between the growing clot and the fluid field then, in turn, further influences the manner in which the clot grows.

Case 1 illustrated that the placement of a flow diverter resulted in sufficient stabilization of the flow field for significant clot formation. Prior to flow diverter placement, a clot was initiated in the aneurysm sac. This clot, however, did not spread very much across the wall of the aneurysm sac nor did it propagate away from the aneurysm wall. The presence of a thrombus in a giant aneurysm without endovascular intervention is not an altogether absurd prediction. Whittle et al reported that spontaneous clotting was observed in fifty percent of giant, unruptured aneurysms [13]. In their study, the authors observed both partial and total occlusion of the aneurysm sac.

Once a flow diverter had been placed in the aneurysm in Case 1, the clot observed propagated from the aneurysm wall at a much more rapid rate. The clot is initially eccentric but proceeds in a manner which would suggest full occlusion at a later stage. Tähtinen et al found that the placement of a flow diverter resulted in full occlusion of the aneurysm sac in seventy percent of the cases examined [155]. The occlusion persisted for at least nine months in these cases but some of the aneurysms later ruptured. This suggests that even if results seem positive at first, regular monitoring of the clot and aneurysm remains necessary.

Case 2 is an example of an aneurysm where the placement of a flow diverter is likely to

cause further complications. Prior to intervention, no clot was seen to develop in the aneurysm sac. After intervention, a clot which occluded the aneurysm sac was seen to develop. Under most circumstances, this would be a desirable outcome [10], [155] . The problem with this specific aneurysm is that the thrombus then extended into the parent vessel and resulted in occlusion. This observation is reminiscent of a case where two mirror aneurysms were found in a patient [151]. One of the aneurysms remained clot free and was asymptomatic up until the patient's death. The other aneurysm with the thrombus grew, recanalized and eventually ruptured, resulting in the patient's death. Even though this case was one of spontaneous thrombosis, it illustrates the point that thrombus development in aneurysms is not always desirable. The development of a clot is highly patient-specific and its effect can only be known for a single case.

Case 3 presents an interesting scenario where the clot in the case without the flow diverter seems to proceed at a more rapid rate than the case with a flow diverter. At a later stage, the propagation of the clot with flow diverter placement overtakes the case without. While greater normal propagation of the clot is observed in the flow diverter case, the clot is seen to spread much more evenly over the surface of the aneurysm sac. It is difficult to predict whether or not the clot in the flow diverter scenario will be limited to the aneurysm sac. It is also questionable whether or not the clot will fully occlude the sac, resulting in a more

stable aneurysm. Such a case would require further investigation before any decisive measures are taken.

A limitation of the method developed in this chapter is the computational cost incurred from the manner in which the computational code is written. A more efficient code could result in faster computation of results and more accurate prediction of clot development. The assumptions made for clot initiation and propagation could be refined. This would require more accurate *in vivo* and experimental data. The code should also be implemented in many more geometries to determine model sensitivity. Finally, the framework presented here needs to be validated with data taken from clinical cases.

7. Conclusions and future work

This chapter summarizes the development of a computational model of clotting in aneurysms. It examines the objectives of the work and then details the manner in which these were achieved. This is done by summarizing each chapter and the contribution that it makes to the entire body of work. A discussion detailing future work follows.

7.1. Summary

The starting objective of this thesis was to develop a computational model of thrombus development in cerebral aneurysms. The purpose of this model is to assist in interventional planning of cerebral aneurysm treatment by providing a means of endovascular implant evaluation. This is achieved by predicting clot or thrombus growth in a patient specific geometry with and without an endovascular device. The resulting clot indicates whether or not the specific intervention would be suitable. The secondary purpose of the model would be its use as a tool for better elucidating and understanding thrombus development in cerebral aneurysms. The platform developed can easily be adjusted to test out various hypotheses at a relatively low cost.

Chapter 1 motivated the reason for the development of the platform presented in this work. This was supported by a review of cerebral aneurysms which aimed to explain the

condition and the various treatment modes which are employed. The next section explored coagulation in the human body and detailed some of the aspects of a process that is a sustained balance between coagulant and anticoagulant mechanisms. Once those two broad topics had been covered, a survey of coagulation in aneurysms was presented.

Chapter 2 presented a review of existing computational models of coagulation. This covered models which focused on the coagulation cascade and those that emphasised the role of platelets. Reaction-mass transport models and integrated models were also discussed. The section was concluded with a review of computational models of clotting in aneurysms.

Chapter 3 presented a detailed explanation of the methods used to achieve the aims of this thesis. The first section focuses on Computational Fluid Dynamics and the finite volume method which is used to solve the flow equations and accounts for the transport of the biochemical proteins and agents involved in the process of coagulation. The second section focuses on the solution of the equations which describe the reactions between the different coagulation proteins. This section also includes the description of the stiff equation solver used to solve these equations. The final section is a detailed account of Level Set methods which are used to capture the surface of the growing clot in complex three-dimensional

geometries. This section includes an explanation of implicit functions and signed distance functions.

Chapter 4 documents the development of a two-dimensional physiological model of clotting in an idealised artery. The purpose of developing such a model is that it is necessary to first understand clotting under physiological conditions, before attempting to model it under pathological conditions. There is more information available on physiological clotting hence it is important that a model which can be verified under those conditions be developed prior to venturing into less understood territory. The model is then used to study the effect of critical thrombin concentration, tissue factor and underlying biochemical cascade on thrombin production and clot development. The critical thrombin concentration at which coagulation moves from the initiation phase to the propagation phase was found to be [TH] = 1 – 10nM. The effects of surface bound tissue factor and blood borne tissue factor were also examined. The blood-borne tissue factor models illustrated a more realistic thrombin curve than the surface bound tissue factor models. It was found that initial tissue factor concentration had an effect on thrombin production. An increase in tissue factor correlated with a decreased lag time in thrombin production. Blood borne tissue factor diffusivity was examined and values below $1\times10^{-9}m^2s^{-1}$ had similar profiles. A comparison between the Wagenvoord and Mann models revealed that

the models produced similar trends for blood borne tissue factor. Both models accounted for anticoagulant mechanisms and both excluded the effect of protein C.

Chapter 5 extended the model developed in Chapter 4 to three dimensions. The geometry changed from a two-dimensional idealised physiological artery to a three dimensional idealised pathological artery with a cerebral aneurysm. Level Set methods were introduced to enable clot propagation and to capture the surface of the growing clot. Clot propagation and initiation were examined. These details are crucial for a model which would be able to predict clot growth in a realistic geometry. Clot propagation velocity was first linked to mechanical factors. An inverse relationship between strain rate and velocity resulted in reasonable clot growth. The propagation was then linked to the concentration of various coagulation proteins. A direct relationship with thrombin resulted in realistic clot growth. This was thought to be reasonable as thrombin is responsible for platelet activation and is the key player in fibrin production. Clot initiation was then examined by considering the effects of tissue factor, strain rate and location of endothelial damage. The most suitable tissue factor concentration was found to be [TF] = 1×10^{-17}M. Strain rate threshold values below which tissue factor could be expressed were investigated. It was found that below $500s^{-1}$, clot growth was present while above the value, no clotting was observed. The different types of clots classified by Lawton were reproduced by varying the spatial

location of 'damaged endothelial cells' on the aneurysm sac.

Chapter 6 extended the model of Chapter 5 to realistic, three-dimensional, patient-specific geometries. Three geometries were selected and clot growth was initiated according to the strain rate threshold investigated in Chapter 5. Clot propagation velocity was directly linked to thrombin concentration. The same realistic geometries had flow diverters placed in the parent artery across the neck of the aneurysm. Clots were computed for these geometries. Spontaneous clotting was observed prior to flow diverter placement in two out of the three cases. In both of these cases, the clot remained quite close to the aneurysm wall and did not grow to fully occlude the aneurysm sac. Non-spontaneous clotting was observed for all three cases following flow diverter placement. The first case is likely to result in full occlusion of the aneurysm sac without obstructing the parent vessel. In the second case, the clot eventually resulted in occlusion of the parent vessel. The final case produced indeterminate results. In this case, it is difficult to predict whether the clot will fully occlude the aneurysm sac without growing into the parent vessel. This would be an example of a case where flow diverter placement is not necessarily the best treatment method. An examination of the different cases showed that clotting in aneurysm was highly patient specific and that clotting could either improve or worsen the situation. This underpins further the importance and potential value of patient-specific modelling.

Novel techniques and elements have been introduced in this work. The framework developed makes use of computational fluid dynamics, computational biochemistry and Level Set Methods in patient-derived, three-dimensional geometries and is applied to clot prediction in these cerebral aneurysm geometries. The clot region has an effect on the flow field because it assumes different porosity and permeability values. The flow field, in turn, has an impact on the clot region. It has been shown that the tool can be used for interventional planning and for elucidation of disease aetiology. Up until now, existing models of thrombus development have focused on physiological clotting in idealised geometries. Those that have examined clotting in aneurysms have focused on matching flow conditions to regions of thrombus development. The inclusion of the biochemical cascade allows for further investigation of a rather complex process. Level Set methods enable the tracking of the surface of the growing clot. This powerful method also enables the linking of growth and initiation to a number of mechanical and biochemical factors. This is achieved through the clot propagation velocity.

The framework was then used to clarify certain features of the process of physiological clotting. A novel study examining the effect of critical thrombin concentration is presented. In addition, an in-depth study of blood-borne tissue factor and its effect on thrombin production under physiological conditions is conducted. This unique study looks at the

difference in thrombin production between a system which consists of blood-borne tissue factor and one that accounts for surface-bound tissue factor only. Finally, a comparative study of two different biochemical cascades is examined. Existing studies focus on the effect of a single cascade. The three-dimensional studies conducted in this work also present novel work. The presentation of an unsteady, three-dimensional framework which examines the initiation and growth of clots in cerebral aneurysms under the effect of mechanical and biochemical factors is unique. In addition, an original study examining the correlation of clot type with region of damage is presented. Finally, the evaluation of device implantation with a predicted clotting outcome is novel. While more work would be required to verify the results, the tool presents a possible valuable clinical endpoint.

In order to use the two-dimensional model as a basis for the three-dimensional work, it was necessary that aspects of that model be validated. This is important as little is understood about clotting in aneurysms but the process is a derivation of the physiological one. The critical thrombin concentration study was matched with results observed from studies conducted by Butenas and Mann. The former is an experimental study while the latter is a computational study. The blood-borne tissue factor studies and the Wagenvoord model were validated by work presented by Hockin et al. Their work presented a computational study based on previous experimental work conducted by the same team.

Finally, the Mann model was validated by work done by Bodnar and Sequeira and Anand. Both models are computational.

7.2. Contributions

Based on the observations made from some of the studies carried out in this thesis, several contributions can be made.

- It is highly likely that blood-borne tissue factor plays a role in cerebral aneurysm clot development. The role of subendothelium-bound tissue factor in this specific pathology is still not fully understood. The participation of subendothelium-bound tissue factor would require damage to the vessel wall and subsequent exposure of the subendothelial layers. While this is highly likely in cerebral aneurysms, which arise as a result of vessel wall thinning, it cannot be assumed that the damage which occurs results in the removal of endothelial cells.
- The area of endothelial tissue damage (i.e. region where subendothelial tissue factor is expressed) has significant impact on the type of clot formed in aneurysm sac. The simulations which aimed to reproduce the types of clots observed by Lawton supported this hypothesis. Endothelial damage towards the dome of the aneurysm is likely to result in an eccentric clot while damage to the entire aneurysm sac results in a concentric clot.

- Linking propagation to thrombin concentration and initiation to a strain rate threshold provides realistic clot growth
- Clot development is a highly patient specific process in cerebral aneurysms. Both biochemical quantities and geometry play a significant role on clot development therefore patient specificity needs to be taken into account. As stands, the Wagenvoord model is the most appropriate model for determining a patient's thrombin profile in a clinical setting. The equations derived from the thrombin curve (CAT) could be used in conjunction with these protein quantities to specify a patient's biochemical cascade. This would then be used to predict clot growth in that patient's cerebral aneurysm.

7.3.Future work

The greatest lesson learnt is that more specific experimental data is required for better understanding of clot evolution in cerebral aneurysms. At present, a lot of data pertaining to cerebral aneurysm clotting is found while carrying out observations focused on other aspects of cerebral aneurysms. In cases where dedicated data for clot development exists, much of the focus is placed on physiological clotting.

- A database consisting of individual patient profiles is necessary. Such a database would need to keep a record of scans (over a number of months) showing the

progression of both the aneurysm and the clot. A thrombogram should also be produced for each patient and reactions be fitted to the curve. Finally, a blood test which determines the quantities of different coagulation proteins should be conducted. This database would provide data which could be used to validate the different models predicted by the framework presented in this thesis.

- Experiments which examine the origin of tissue factor in clots forming in cerebral aneurysms (surface-bound versus blood-borne) would be of great use. These would elucidate a lot of the issues pertaining to the initiation and propagation of the clots in aneurysms.
- It is necessary to obtain data pertaining to timeframes for clot development in cerebral aneurysms. Timeframes differ quite dramatically between spontaneous clots and device-induced clots. There have been reports of clots occluding the aneurysm fully within minutes following endovascular treatment while clot development in untreated aneurysms may take place over a number of months. In order to model the different processes correctly, coefficients for clot propagation velocity would need to be altered according to the overall timeframe.
- In order to be able to use clotting as a predictive outcome for different treatment modes, it is necessary to verify what type of clotting is desirable. Currently, it is believed that clots that occlude the aneurysm sac without extending into the parent

vessel are good while those that fill the sac partially are dangerous. Repetitive experiments carried out on different clot geometries should be carried out to ascertain whether or not this claim is true.

In order to take this work further, several changes can be made in the short and long term.

- The most important players for clot growth in cerebral aneurysms need to be determined. I would hypothesise that platelet concentration, tissue factor, prothrombin, thrombin and antithrombin would be able to describe the system fairly well without sacrificing the simplicity and efficiency of a code. These components would account for clot location, initiation, propagation and growth cessation. It would also be fairly easy to measure the quantities in a clinical setting.
- Further work would incorporate direct platelet activity into the model. This could be achieved by tracking platelet populations and accounting for the various changes that platelets undergo during the process of clotting. In addition, it would be useful to couple platelet response with the flow field and with changes in biochemical species concentrations.
- Codes need to be adapted to run much more efficiently to ensure that clot growth can be predicted within a clinical timeframe for device-induced cases.
- Simulations should be run with clot propagation velocity dependent on more than

one variable at a time. The simultaneous influence of mechanical and biochemical effects on clot growth could prove extremely interesting. Coupling the model to a wall evolution model would also prove interesting.

- The extension of the current device evaluation framework to other devices would be beneficial. This would assist the decision making process during intervention.
- The code needs to be run in abdominal aortic aneurysms to see how applicable it is to the disease. While the aetiology for the two aneurysm types is different, clotting is a pretty standard procedure throughout the body for an individual.

Much can still be done to improve the work presented here. The model presented here does, however, make a small contribution to framing some of the questions that need to be asked about clot development in cerebral aneurysms. It also presents a preliminary means of investigating endovascular device efficacy and clot development in cerebral aneurysms.

Appendix A

In this appendix, the HJ ENO and HJ WENO schemes are described in greater detail. The schemes are first introduced in Chapter 3. While this Appendix offers a more extended coverage of the topic, the interested reader is encouraged to read Osher and Fedkiw [176]. The description provided in that book goes into great depth on Level Set methods and all the important tools associated with their challenges and solution.

Hamilton-Jacobi ENO

The Hamilton-Jacobi ENO scheme is a variation on the upwind differencing method. It provides a more accurate description of ϕ_x^- and ϕ_x^+. This is achieved by using a polynomial interpolation rather than assuming dominance of the upstream value. A polynomial interpolation is used to determine ϕ and then ϕ_x is obtained by differentiation. It does, however, still use V_n to determine the direction from which information is obtained.

The zeroth divided difference of ϕ defined at grid node *i* (located at x_i) is

$$D_i^0\phi = \phi_i \qquad \textbf{Eq. A.1}$$

The first divided difference of ϕ is defined midway between grid nodes and is

$$D^1_{i+1/2}\phi = \frac{D^0_{i+1}\phi - D^0_i\phi}{\Delta x} \qquad \textbf{Eq. A.2}$$

Assuming that Δx is a constant, the second divided difference defined at the grid node is

$$D^2_i\phi = \frac{D^1_{i+1/2}\phi - D^1_{i-1/2}\phi}{2\Delta x} \qquad \textbf{Eq. A.3}$$

The third divided difference, calculated midway between grid nodes is

$$D^3_{i+1/2}\phi = \frac{D^2_{i+1}\phi - D^2_i\phi}{3\Delta x} \qquad \textbf{Eq. A.4}$$

The differences are then used to construct a polynomial which takes the form

$$\phi(x) = Q_0(x) + Q_1(x) + Q_2(x) + Q_3(x) \qquad \textbf{Eq. A.5}$$

Differentiating this polynomial and evaluating it at x_i gives

$$\phi_x(x_i) = Q_1'(x_i) + Q_2'(x_i) + Q_3'(x_i) \qquad \textbf{Eq. A.6}$$

To find ϕ_x^-, k = i – 1 at the start while k = 1 gives ϕ_x^+. From there, we define

$$Q_1(x) = (D^1_{k+\frac{1}{2}}\phi)(x - x_i) \qquad \textbf{Eq. A.7}$$

and it then follows that

$$Q_1' = D^1_{k+\frac{1}{2}}\phi \qquad \textbf{Eq. A.8}$$

From Eq. A.6, it is clear that the contribution made by Q_1' is the backward difference for ϕ_x^- and the forward difference for ϕ_x^+. This means that for the first order accurate case, the result is the upwind differencing method. In order to obtain better accuracy, the Q_2' and Q_3' cases need to be calculated.

In order to calculate the second order accurate method, Q_2' is required, hence we define

$$Q_2(x) = c(x - x_k)(x - x_{k+1}) \qquad \textbf{Eq. A.9}$$

It then follows that

$$Q_2'(x_i) = c(2(i - k) - 1)\Delta x \qquad \textbf{Eq. A.10}$$

If $|D_k^2\phi| \leq |D_{k+1}^2\phi|$, then c = $D_k^2\phi$. Otherwise, c = $D_{k+1}^2\phi$. The choice of c is informed by a desire to minimise dramatic variation which may lead to overshooting in the interpolation function.

Hamilton-Jacobi WENO

The Hamilton-Jacobi WENO method is a more refined version of the HJ ENO scheme. There are three approximations of $(\phi_x^-)_i$. While the HJ ENO scheme chooses the smoothest interpolation, the HJ WENO scheme assigns a weighting to each contribution.

To find ϕ_x^+ and ϕ_x^-, a set of divided differences is calculated. These are then used to calculate the interpolants. In order to calculate ϕ_x^-, we first find

$$v_1 = \frac{\phi_{i-2}-\phi_{i-3}}{\Delta x} \; v_2 = \frac{\phi_{i-1}-\phi_{i-2}}{\Delta x} \; v_3 = \frac{\phi_i-\phi_{i-1}}{\Delta x} \; v_4 = \frac{\phi_{i+1}-\phi_i}{\Delta x} \; v_5 = \frac{\phi_{i+2}-\phi_{i+1}}{\Delta x} \qquad \textbf{Eq. A.11}$$

To find ϕ_x^+,

$$v_1 = \frac{\phi_{i+3}-\phi_{i+2}}{\Delta x} \; v_2 = \frac{\phi_{i+2}-\phi_{i+1}}{\Delta x} \; v_3 = \frac{\phi_{i+1}-\phi_i}{\Delta x} \; v_4 = \frac{\phi_i-\phi_{i-1}}{\Delta x} \; v_5 = \frac{\phi_{i-1}-\phi_{i-2}}{\Delta x} \qquad \textbf{Eq. A.12}$$

The approximation for the derivative $\phi_x^{-/+}$ is given by

$$\phi_x^{-/+} = w_1\left(\frac{v_1}{3} - \frac{7v_2}{6} + \frac{11v_3}{6}\right) + w_2\left(-\frac{v_2}{6} + \frac{5v_3}{6} + \frac{v_4}{3}\right) + w_3\left(\frac{v_3}{3} + \frac{5v_4}{6} - \frac{v_5}{6}\right) \quad \textbf{Eq. A.13}$$

In order to calculate the weights, S is determined as follows

$$\begin{aligned} S_1 &= \frac{13}{12}(v_1 - 2v_2 + v_3)^2 + \frac{1}{4}(v_1 - 4v_2 + 3v_3)^2 \\ S_2 &= \frac{13}{12}(v_2 - 2v_3 + v_4)^2 + \frac{1}{4}(v_2 - v_4)^2 \\ S_3 &= \frac{13}{12}(v_3 - 2v_4 + v_5)^2 + \frac{1}{4}(3v_3 - 4v_4 + v_5)^2 \end{aligned} \quad \textbf{Eq. A.14}$$

Then α is found

$$\begin{aligned} \alpha_1 &= \frac{0.1}{(S_1 + \epsilon)^2} \\ \alpha_2 &= \frac{0.6}{(S_2 + \epsilon)^2} \\ \alpha_3 &= \frac{0.3}{(S_3 + \epsilon)^2} \end{aligned} \quad \textbf{Eq. A.15}$$

Where $\epsilon = 10^{-6}$.

Finally, the weights are given by

$$\begin{aligned} w_1 &= \frac{\alpha_1}{\alpha_1 + \alpha_2 + \alpha_3} \\ w_2 &= \frac{\alpha_2}{\alpha_1 + \alpha_2 + \alpha_3} \\ w_3 &= \frac{\alpha_3}{\alpha_1 + \alpha_2 + \alpha_3} \end{aligned} \quad \textbf{Eq. A.16}$$

References

[1] C. D. Mathers and D. Loncar, "Projections of global mortality and burden of disease from 2002 to 2030.," *PLoS medicine*, vol. 3, no. 11, p. e442, Nov. 2006.

[2] D. B. Morgagni, *De sedibus et causis morborum*. Venetiis: Remondiniana, 1761.

[3] J. L. Brisman, J. K. Song, and D. W. Newell, "Cerebral aneurysms.," *The New England journal of medicine*, vol. 355, no. 9, pp. 928–39, Aug. 2006.

[4] D. O. Wiebers, J. P. Whisnant, J. Huston, I. Meissner, R. D. Brown, D. G. Piepgras, G. S. Forbes, K. Thielen, D. Nichols, W. M. O'Fallon, J. Peacock, L. Jaeger, N. F. Kassell, G. L. Kongable-Beckman, and J. C. Torner, "Unruptured intracranial aneurysms: natural history, clinical outcome, and risks of surgical and endovascular treatment.," *Lancet*, vol. 362, no. 9378, pp. 103–10, Jul. 2003.

[5] B. Seibert, R. P. Tummala, R. Chow, A. Faridar, S. A. Mousavi, and A. A. Divani, "Intracranial aneurysms: review of current treatment options and outcomes.," *Frontiers in neurology*, vol. 2, no. July, p. 45, Jan. 2011.

[6] "Neuroform Stent," *Stryker*, 2002. [Online]. Available: http://www.stryker.com/en-us/products/NeurovascularIntervention/NeuroformEZ/index.htm#. [Accessed: 15-Mar-2013].

[7] I. Larrabide, M. L. Aguilar, H. G. Morales, A. J. Geers, Z. Kulcsár, D. Rüfenacht, and A. F. Frangi, "Intra-aneurysmal pressure and flow changes induced by flow diverters: relation to aneurysm size and shape.," *AJNR. American journal of neuroradiology*, vol. 34, no. 4, pp. 816–22, Apr. 2013.

[8] G. J. E. Rinkel, M. Djibuti, A. Algra, and J. van Gijn, "Prevalence and Risk of Rupture of Intracranial Aneurysms : A Systematic Review," *Stroke*, vol. 29, no. 1, pp. 251–256, Jan. 1998.

[9] G. Guglielmi, F. Vinuela, I. Sepetka, and V. Macellari, "Electrothrombosis of saccular aneurysms via endovascular approach," *Journal of neurosurgery*, vol. 75, pp. 1–7, 1991.

[10] R. Vanninen, H. Manninen, and A. Ronkainen, "Case Report Broad-Based Intracranial Aneurysms : Thrombosis Induced by Stent Placement," *AJNR. American journal of neuroradiology*, vol. 24, no. February, pp. 263–266, 2003.

[11] L.-D. Jou and M. E. Mawad, "Hemodynamic effect of Neuroform stent on intimal hyperplasia and thrombus formation in a carotid aneurysm.," *Medical engineering & physics*, vol. 33, no. 5, pp. 573–80, Jun. 2011.

[12] L. Calviere, A. Viguier, N. A. Da Silva, C. Cognard, and V. Larrue, "Unruptured intracranial aneurysm as a cause of cerebral ischemia.," *Clinical neurology and neurosurgery*, vol. 113, no. 1, pp. 28–33, Jan. 2011.

[13] I. R. Whittle, N. W. Dorsch, and M. Besser, "Spontaneous thrombosis in giant intracranial aneurysms.," *Journal of neurology, neurosurgery, and psychiatry*, vol. 45, no. 11, pp. 1040–7, Nov. 1982.

[14] Z. Kulcsár, E. Houdart, A. Bonafé, G. Parker, J. Millar, A. J. P. Goddard, S. Renowden, G. Gál, B. Turowski, K. Mitchell, F. Gray, M. Rodriguez, R. van den Berg, A. Gruber, H. Desal, I. Wanke, and D. A. Rüfenacht, "Intra-aneurysmal thrombosis as a possible cause of delayed aneurysm rupture after flow-diversion treatment.," *AJNR. American journal of neuroradiology*, vol. 32, no. 1, pp. 20–5, Jan. 2011.

[15] R. Wagenvoord, P. W. Hemker, and H. C. Hemker, "The limits of simulation of the clotting system.," *Journal of thrombosis and haemostasis : JTH*, vol. 4, no. 6, pp. 1331–8, Jun. 2006.

[16] M. F. Hockin, K. C. Jones, S. J. Everse, and K. G. Mann, "A model for the stoichiometric regulation of blood coagulation.," *The Journal of biological chemistry*, vol. 277, no. 21, pp. 18322–33, May 2002.

[17] M. A. Panteleev, M. V Ovanesov, D. A. Kireev, A. M. Shibeko, E. I. Sinauridze, N. M. Ananyeva, A. A. Butylin, E. L. Saenko, and F. I. Ataullakhanov, "Spatial propagation and localization of blood coagulation are regulated by intrinsic and protein C pathways, respectively.," *Biophysical journal*, vol. 90, no. 5, pp. 1489–500, Mar. 2006.

[18] A. S. Bedekar, K. Pant, Y. Ventikos, and S. Sundaram, "A Computational Model Combining Vascular Biology and Haemodynamics for Thrombosis Prediction in Anatomically Accurate Cerebral Aneurysms," *Food and Bioproducts Processing*, vol. 83, no. 2, pp. 118–126, Jun. 2005.

[19] V. L. Rayz, L. Boussel, L. Ge, J. R. Leach, A. J. Martin, M. T. Lawton, C. McCulloch, and D. Saloner, "Flow residence time and regions of intraluminal thrombus deposition in intracranial aneurysms.," *Annals of biomedical engineering*, vol. 38, no. 10, pp. 3058–69, Oct. 2010.

[20] R. Ouared, B. Chopard, B. Stahl, D. A. Rüfenacht, H. Yilmaz, and G. Courbebaisse, "Thrombosis modeling in intracranial aneurysms: a lattice Boltzmann numerical algorithm," *Computer Physics Communications*, vol. 179, no. 1–3, pp. 128–131, Jul. 2008.

[21] J. Biasetti, P. G. Spazzini, J. Swedenborg, and T. C. Gasser, "An integrated fluid-chemical model toward modeling the formation of intra-luminal thrombus in abdominal aortic aneurysms.," *Frontiers in physiology*, vol. 3, no. July, p. 266, Jan. 2012.

[22] T. J. Bowker, "A computational model for thrombus prediction," University of Oxford, 2010.

[23] C. Vega, J. V Kwoon, and S. D. Lavine, "Intracranial aneurysms: current evidence and clinical practice.," *American family physician*, vol. 66, no. 4, pp. 601–8, Aug. 2002.

[24] J. W. Hop, G. J. Rinkel, A. Algra, and J. van Gijn, "Case-fatality rates and functional outcome after subarachnoid hemorrhage," *Stroke*, vol. 28, pp. 660–664, 1997.

[25] S. Inci and R. F. Spetzler, "Intracranial aneurysms and arterial hypertension: a review and hypothesis.," *Surgical neurology*, vol. 53, no. 6, pp. 530–40; discussion 540–2, Jun. 2000.

[26] B. K. Velthuis, G. J. Rinkel, L. M. Ramos, T. D. Witkamp, J. W. Berkelbach van der Sprenkel, W. P. Vandertop, and M. S. van Leeuwen, "Subarachnoid hemorrhage: aneurysm detection and preoperative evaluation with CT angiography.," *Radiology*, vol. 208, no. 2, pp. 423–30, Aug. 1998.

[27] "Types of Aneurysms," *Johns Hopkins Medicine Health Library*. [Online]. Available: http://www.hopkinsmedicine.org/healthlibrary/conditions/adult/cardiovascular_diseases/cerebral_aneurysm_85,P08772/. [Accessed: 15-Mar-2013].

[28] G. A. Holzapfel, T. C. Gasser, and R. W. Ogden, "A New Constitutive Framework for Arterial Wall Mechanics and a Comparative Study of Material Models," *Journal of elasticity*, vol. 61, pp. 1–48, 2000.

[29] G. Bruno, R. Todor, I. Lewis, and D. Chyatte, "Vascular extracellular matrix remodeling in cerebral aneurysms.," *Journal of neurosurgery*, vol. 89, no. 3, pp. 431–40, Sep. 1998.

[30] T. Krings, D. M. Mandell, T.-R. Kiehl, S. Geibprasert, M. Tymianski, H. Alvarez, K. G. TerBrugge, and F.-J. Hans, "Intracranial aneurysms: from vessel wall pathology to therapeutic approach.," *Nature reviews. Neurology*, vol. 7, no. 10, pp. 547–59, Oct. 2011.

[31] B. J. Rajesh, S. Sandhyamani, and R. N. Bhattacharya, "Clinico-pathological study of cerebral aneurysms," *Neurology India*, vol. 52, pp. 82–86, 2004.

[32] K. Kataoka, M. Taneda, T. Asai, A. Kinoshita, M. Ito, and R. Kuroda, "Structural Fragility and Inflammatory Response of Ruptured Cerebral Aneurysms : A Comparative Study Between Ruptured and Unruptured Cerebral Aneurysms," *Stroke*, vol. 30, no. 7, pp. 1396–1401, Jul. 1999.

[33] J. D. Humphrey and P. B. Canham, "Structure , Mechanical Properties , and Mechanics of Intracranial Saccular Aneurysms," *Journal of Elasticity*, vol. 61, pp. 49–81, 2000.

[34] W. E. Stehbens, "Histopathology of cerebral aneurysms.," *Archives of neurology*, vol. 8, pp. 272–85, Mar. 1963.

[35] J. Frösen, A. Piippo, A. Paetau, M. Kangasniemi, M. Niemelä, J. Hernesniemi, and J. Jääskeläinen, "Remodeling of saccular cerebral artery aneurysm wall is associated with rupture: histological analysis of 24 unruptured and 42 ruptured cases.," *Stroke; a journal of cerebral circulation*, vol. 35, no. 10, pp. 2287–93, Oct. 2004.

[36] M. Scanarini, S. Mingrino, R. Giordano, and A. Baroni, "Histological and ultrastructural study of intracranial saccular aneurysmal wall.," *Acta neurochirurgica*, vol. 43, no. 3–4, pp. 171–82, Jan. 1978.

[37] W. I. Schievink, "Intracranial Aneurysms," *New England Journal of Medicine*, vol. 336, no. January 2, pp. 28–40, 1997.

[38] J. E. Cohen, E. Itshayek, E. Yitshayek, J. M. Gomori, S. Grigoriadis, G. Raphaeli, S. Spektor, and G. Rajz, "Spontaneous thrombosis of cerebral aneurysms presenting with ischemic stroke.," *Journal of the neurological sciences*, vol. 254, no. 1–2, pp. 95–8, Mar. 2007.

[39] A. Ronkainen, J. Hernesniemi, M. Puranen, L. Niemitukia, R. Vanninen, M. Ryynanen, H. Kuivaniemi, and G. Tromp, "Familial intracranial aneurysms," *The Lancet*, vol. 349, no. 9049, pp. 380–384, 1997.

[40] A. B. Chapman, D. Rubinstein, R. L. Hughes, J. C. Stears, M. P. Earnest, A. M. Johnson, P. A. Gabow, and W. D. Kaehny, "Intracranial aneurysms in autosomal dominant polycystic kidney disease," *The New England Journal of Medicine*, vol. 327, no. 13, pp. 916 – 920, 1992.

[41] M. M. Belz, G. M. Fick-Brosnahan, R. L. Hughes, D. Rubinstein, A. B. Chapman, A. M. Johnson, K. K. McFann, W. D. Kaehny, and P. A. Gabow, "Recurrence of intracranial aneurysms in autosomal-dominant polycystic kidney disease.," *Kidney international*, vol. 63, no. 5, pp. 1824–30, May 2003.

[42] "International Study of Unruptured Intracranial Aneurysms (ISUIA) Investigators. Factors related to the development and detection of single versus multiple unruptured intracranial aneurysms [abstract].," *Stroke*, vol. 27, no. 178, 1996.

[43] W. E. Dandy, "INTRACRANIAL ANEURYSM OF THE INTERNAL CAROTID ARTERY," *Annals of surgery*, vol. 107, no. 5, pp. 654–659, 1938.

[44] "Moore's treatment of aneurysm," *The Lancet*, vol. 127, no. 3277, pp. 1175–1176, 1886.

[45] S. C. Werner, A. H. Blakemore, and B. G. King, "Aneurysm of the internal carotid artery within the skull: wiring and electrothermic coagulation," *Journal of the American Medical Association*, vol. 116, no. 7, pp. 578 – 582, 1941.

[46] B. Dahlbäck, "Blood coagulation.," *Lancet*, vol. 355, no. 9215, pp. 1627–32, May 2000.

[47] B. Furie and B. C. Furie, "The molecular basis of blood coagulation.," *Cell*, vol. 53, no. 4, pp. 505–18, May 1988.

[48] B. Furie and B. C. Furie, "Molecular and Cellular Biology of Blood Coagulation," *New England Journal of Medicine*, vol. 326, no. 12, pp. 800–806, 1992.

[49] B. Furie and B. C. Furie, "Mechanisms of thrombus formation.," *The New England Journal of Medicine*, vol. 359, no. 9, pp. 938–49, Aug. 2008.

[50] B. Furie, "Pathogenesis of thrombosis.," *Hematology / the Education Program of the American Society of Hematology. American Society of Hematology. Education Program*, pp. 255–8, Jan. 2009.

[51] M. Hoffman, "Remodeling the blood coagulation cascade.," *Journal of thrombosis and thrombolysis*, vol. 16, no. 1–2, pp. 17–20, 2004.

[52] J. P. Riddel, B. E. Aouizerat, C. Miaskowski, and D. P. Lillicrap, "Theories of blood coagulation.," *Journal of pediatric oncology nursing : official journal of the Association of Pediatric Oncology Nurses*, vol. 24, no. 3, pp. 123–31, 2007.

[53] S. a Smith, "The cell-based model of coagulation.," *Journal of veterinary emergency and critical care (San Antonio, Tex. : 2001)*, vol. 19, no. 1, pp. 3–10, Feb. 2009.

[54] H. M. H. Spronk, J. W. P. Govers-Riemslag, and H. ten Cate, "The blood coagulation system as a molecular machine.," *BioEssays : news and reviews in molecular, cellular and developmental biology*, vol. 25, no. 12, pp. 1220–8, Dec. 2003.

[55] S. Falati, P. Gross, G. Merrill-Skoloff, B. C. Furie, and B. Furie, "Real-time in vivo imaging of platelets, tissue factor and fibrin during arterial thrombus formation in the mouse.," *Nature medicine*, vol. 8, no. 10, pp. 1175–81, Oct. 2002.

[56] R. Virchow, *Gesammelte Abhandlungen zur wissenschaftlichen Medicin*. Meidinger, 1856.

[57] L. A. Aschoff, *Lectures on Pathology*. New York: Paul B. Hoeber, 1924, pp. 253, 254, 263.

[58] E. W. Davie and O. D. Ratnoff, "Waterfall Sequence for Intrinsic Blood Clotting Author (s): Earl W . Davie and Oscar D . Ratnoff Published by : American Association for the Advancement of Science Stable URL : http://www.jstor.org/stable/1713886 .," *Science*, vol. 145, no. 3638, pp. 1310–1312, 1964.

[59] R. G. Macfarlane, "An Enzyme Cascade in the Blood Clotting Mechanism, and its Function as a Biochemical Amplifier," *Nature*, vol. 202, p. 498, 1964.

[60] B. Furie and B. C. Furie, "Review series: Thrombus formation in vivo," *The Journal of Clinical Investigation*, vol. 115, no. 12, pp. 3355–3362, 2005.

[61] B. Furie and B. C. Furie, "In vivo thrombus formation," *Journal of thrombosis and haemostasis : JTH*, vol. 5 (Suppl. , pp. 12–17, 2007.

[62] M. Hoffman, D. M. Monroe, and H. R. Roberts, "Cellular Interactions in Hemostasis," *Haemostasis*, vol. 26(suppl 1, pp. 12 – 16, 1996.

[63] M. Hoffman, "A cell-based model of coagulation and the role of factor Vlla," *Blood Reviews*, vol. 17, pp. S1–S5, 2003.

[64] K. S. Sakariassen, P. A. Bolhuis, and J. J. Sixma, "Human blood platelet adhesion to artery subendothelium is mediated by factor VIII-Von Willebrand factor bound to the subendothelium," *Nature*, vol. 279, pp. 636–638, 1979.

[65] H. V Stel, K. S. Sakariassen, P. G. de Groot, J. A. van Mourik, and J. J. Sixma, "Von Willebrand factor in the vessel wall mediates platelet adherence.," *Blood*, vol. 65, no. 1, pp. 85–90, Jan. 1985.

[66] K. Laki and L. Lorand, "On the Solubility of Fibrin Clots," *Science*, vol. 108, no. 2802, p. 280, 1948.

[67] A. G. Loewy, K. Dunathan, R. Kriel, and H. L. Wolfinger, "Fibrinase: I. Purification of substrate and enzyme," *The Journal of biological chemistry*, vol. 236, no. 10, pp. 2625–2633, 1961.

[68] M. Hoffman, D. M. Monroe, J. A. Oliver, and H. R. Roberts, "Factors IXa and Xa play distinct roles in tissue factor-dependent initiation of coagulation.," *Blood*, vol. 86, no. 5, pp. 1794–801, Sep. 1995.

[69] U. Seligsohn, C. K. Kasper, B. Osterud, and S. I. Rapaport, "Activated factor VII: presence in factor IX concentrates and persistence in the circulation after infusion.," *Blood*, vol. 53, no. 5, pp. 828–37, May 1979.

[70] Y. Nemerson, "Tissue factor and hemostasis [published erratum appears in Blood 1988 Apr;71(4):1178]," *Blood*, vol. 71, no. 1, pp. 1–8, 1988.

[71] M. Zur, R. D. Radcliffe, J. Oberdick, and Y. Nemerson, "The Dual Role of Factor VII in Blood Coagulation," *The Journal of biological chemistry*, vol. 257, no. 10, pp. 5623–5631, 1982.

[72] J. A. Oliver, D. M. Monroe, H. R. Roberts, and M. Hoffman, "Thrombin Activates Factor XI on Activated Platelets in the Absence of Factor XII," *Arteriosclerosis, Thrombosis, and Vascular Biology*, vol. 19, no. 1, pp. 170–177, Jan. 1999.

[73] C. Dubois, L. Panicot-dubois, J. F. Gainor, B. C. Furie, and B. Furie, "Thrombin-initiated platelet activation in vivo is vWF independent during thrombus formation in a laser injury model," *The Journal of Clinical Investigation*, vol. 117, no. 4, pp. 953–960, 2007.

[74] K. Buluk, T. Januszko, and J. Olbromski, "Conversion of Fibrin to Desmofibrin," *Nature*, vol. 191, no. 4793, pp. 1093–1094, 1961.

[75] L. Lorand and K. Konishi, "Papain-induced Polymerization of Fibrinogen," *Biochemistry*, vol. 3, no. 7, pp. 915–919, 1964.

[76] R. A. S. Ariens, "Role of factor XIII in fibrin clot formation and effects of genetic polymorphisms," *Blood*, vol. 100, no. 3, pp. 743–754, Jul. 2002.

[77] F. J. Walker, P. W. Sexton, and C. T. Esmon, "The inhibition of blood coagulation by activated protein c through the selective inactivation of activated factor V," *Biochimica et biophysica acta*, vol. 571, pp. 333–342, 1979.

[78] R. A. Marlar, A. J. Kleiss, and J. H. Griffin, "Mechanism of action of human activated protein C, a thrombin-dependent anticoagulant enzyme," *Blood*, vol. 59, no. 5, pp. 1067–1072, 1982.

[79] P. S. Damus, M. Hicks, and R. D. Rosenberg, "Anticoagulant action of heparin," *Nature*, vol. 246, pp. 355–357, 1973.

[80] K. Kurachi, K. Fujikawa, G. Schmer, and E. W. Davie, "Inhibition of Bovine Factor IXa and Factor Xa by Antithrombin III," *Biochemistry*, vol. 15, no. 2, pp. 373–377, 1976.

[81] R. G. Di Scipio, K. Kurachi, and E. W. Davie, "Activation of human factor IX (Christmas factor).," *The Journal of clinical investigation*, vol. 61, no. 6, pp. 1528–38, Jun. 1978.

[82] E. T. Yin, S. Wessler, and P. J. Stoll, "Identity of Plasma-activated Factor X Inhibitor with Antithrombin III and Heparin Cofactor *," *The Journal of biological chemistry*, vol. 246, no. 11, pp. 3712–3719, 1971.

[83] W. H. Seegers, J. F. Johnson, and C. Fell, "An Antithrombin Reaction Related to Prothrombin Activation," *American Journal of Physiology*, vol. 176, no. 1, pp. 97–103, 1953.

[84] U. Abildgaard, "Inhibition of the thrombin-fibrinogen reaction by heparin and purified cofactor.," *Scandinavian journal of haematology*, vol. 5, no. 6, pp. 440–53, Jan. 1968.

[85] L. V Rao and S. I. Rapaport, "Studies of a mechanism inhibiting the initiation of the extrinsic pathway of coagulation.," *Blood*, vol. 69, no. 2, pp. 645–51, Feb. 1987.

[86] L. Bajzar, R. Manuel, and M. E. Nesheim, "Purification and Characterization of TAFI, a Thrombin-activatable Fibrinolysis Inhibitor," *The Journal of biological chemistry*, vol. 270, no. 24, pp. 14477–14484, 1995.

[87] D. Collen and H. R. Lijnen, "Basic and clinical aspects of fibrinolysis and thrombolysis.," *Blood*, vol. 78, no. 12, pp. 3114–24, Dec. 1991.

[88] J. R. Toomey, K. E. Kratzer, N. M. Lasky, J. J. Stanton, and G. J. Broze, "Targeted Disruption of the Murine Tissue Factor Gene Results Embryonic Lethality," *Blood*, vol. 88, pp. 1583–1587, 1996.

[89] P. Carmaliet, N. Mackman, L. Moons, T. Luther, P. Gressens, I. Van Vlaenderen, H. Demunck, M. Kasper, G. Breier, P. Evrard, M. Muller, W. Risau, T. Edgington, and D. Collen, "Role of tissue factor in embryonic blood vessel development," *Nature*, vol. 383, pp. 73–75, 1996.

[90] T. H. Bugge, Q. Xiao, K. W. Kombrinck, M. J. Flick, K. Holmbäck, M. J. Danton, M. C. Colbert, D. P. Witte, K. Fujikawa, E. W. Davie, and J. L. Degen, "Fatal embryonic bleeding events in mice lacking tissue factor, the cell-associated initiator of blood coagulation.," *Proceedings of the National Academy of Sciences of the United States of America*, vol. 93, no. 13, pp. 6258–63, Jun. 1996.

[91] E. W. Davie, K. Fujikawa, and W. Kisiel, "The coagulation cascade: initiation, maintenance, and regulation.," *Biochemistry*, vol. 30, no. 43, pp. 10363–70, Oct. 1991.

[92] Z. Shariat-Madar, F. Mahdi, and A. H. Schmaier, "Assembly and activation of the plasma kallikrein/kinin system: a new interpretation.," *International immunopharmacology*, vol. 2, no. 13–14, pp. 1841–9, Dec. 2002.

[93] M. Schultze, "Ein heizbarer Objecttisch und seine Verwendung bei Untersuchungen des Bluted," *Archiv für mikroskopische Anatomie*, vol. 1, no. 1, pp. 1–42, 1865.

[94] D. B. Brewer, "Max Schultze (1865), G. Bizzozero (1882) and the discovery of the platelet.," *British journal of haematology*, vol. 133, no. 3, pp. 251–8, May 2006.

[95] G. Bizzozero, "Su di un nuovo elemento morfologico del sangue dei mammiferi e sulla sua importanza nella trombosi e nella coagulazione," *Osservatore Gazetta delle Cliniche*, vol. 17, pp. 785–787, 1881.

[96] G. Bizzozero, "Ueber einen neuen Forrnbestandteil des Blutes und dessen Rolle bei der Thrombose und Blutgerinnung," *Archiv fur pathologische Anatomie und Physiologie und fur klinische Medicin*, vol. 90, pp. 261–332, 1882.

[97] G. Bizzozero, "Sur les petites plaques du sang des mammiferes, deuxieme notes.," *Archives Italiennes de Biologie*, vol. 1, pp. 1–4, 1882.

[98] A. O. Yakimenko, F. Y. Verholomova, Y. N. Kotova, F. I. Ataullakhanov, and M. A. Panteleev, "Identification of different proaggregatory abilities of activated platelet subpopulations.," *Biophysical journal*, vol. 102, no. 10, pp. 2261–9, May 2012.

[99] A. A.Tokarev, A.A. Butylin, and F. I. Ataullakhanov, "Platelet adhesion from shear blood flow is controlled by near-wall rebounding collisions with erythrocytes.," *Biophysical journal*, vol. 100, no. 4, pp. 799–808, Feb. 2011.

[100] H. L. Goldsmith and T. Karino, "Interactions of human blood cells with the vascular endothelium.," *Annals of the New York Academy of Sciences*, vol. 516, pp. 468–83, Jan. 1987.

[101] V. T. Turitto and H. R. Baumgartner, "Platelet deposition on subendothelium exposed to flowing blood: Mathematical analysis of physical parameters," *Transactions - American Society for Artificial Internal Organs*, vol. 21, pp. 593–601, 1975.

[102] H. L. Goldsmith, "Red cell motions and wall interactions in tube flow," *Federation Proceedings*, vol. 30, pp. 1578–1590, 1971.

[103] V. T. Turitto and H. J. Weiss, "Platelet and red cell involvement in mural thrombogenesis.," *Annals of the New York Academy of Sciences*, vol. 416, pp. 363–76, Jan. 1983.

[104] J. W. Constantine, I. M. Purcell, and M. Gotthelf, "Platelets, Coagulation and In Vitro Thrombus Formation," *The Journal of Pharmacology and Experimental Therapeutics*, vol. 176, no. 1, pp. 76–82, 1970.

[105] M. Kuwahara, "Platelet Shape Changes and Adhesion Under High Shear Flow," *Arteriosclerosis, Thrombosis, and Vascular Biology*, vol. 22, no. 2, pp. 329–334, Feb. 2002.

[106] V. T. Turitto, H. J. Weiss, and H. R. Baumgartner, "The effect of shear rate on platelet interaction with subendothelium exposed to citrated human blood.," *Microvascular research*, vol. 19, no. 3, pp. 352–65, May 1980.

[107] B. Savage, E. Saldívar, and Z. M. Ruggeri, "Initiation of platelet adhesion by arrest onto fibrinogen or translocation on von Willebrand factor.," *Cell*, vol. 84, no. 2, pp. 289–97, Jan. 1996.

[108] T. H. Spaet and M. B. Zucker, "Mechanism of platelet plug formation and role of adenosine diphosphate," *American Journal of Physiology*, vol. 206, no. 6, pp. 1267–1274, 1964.

[109] A. Gaarder, J. Jonsen, S. Laland, A. Hellem, and P. A. Owren, "Adenosine Diphosphate in Red Cells as a Factor in the Adhesiveness of Human Blood Platelets," *Nature*, vol. 4802, pp. 531 – 532, 1961.

[110] J. Jin, J. L. Daniel, and S. P. Kunapuli, "Molecular Basis for ADP-induced Platelet Activation," *The Journal of biological chemistry*, vol. 273, no. 4, pp. 2030–2034, 1998.

[111] D. S. Sim, G. Merrill-Skoloff, B. C. Furie, B. Furie, and R. Flaumenhaft, "Initial accumulation of platelets during arterial thrombus formation in vivo is inhibited by elevation of basal cAMP levels.," *Blood*, vol. 103, no. 6, pp. 2127–34, Mar. 2004.

[112] G. A. Adams, S. J. Brown, L. V McIntire, S. G. Eskin, and R. R. Martin, "Kinetics of platelet adhesion and thrombus growth.," *Blood*, vol. 62, no. 1, pp. 69–74, Jul. 1983.

[113] W. S. Nesbitt, S. Giuliano, S. Kulkarni, S. M. Dopheide, I. S. Harper, and S. P. Jackson, "Intercellular calcium communication regulates platelet aggregation and thrombus growth.," *The Journal of cell biology*, vol. 160, no. 7, pp. 1151–61, Mar. 2003.

[114] H. L. Goldsmith, K. Takamura, and D. Bell, "Shear-induced collisions between human blood cells.," *Annals of the New York Academy of Sciences*, vol. 416, pp. 299–318, Jan. 1983.

[115] H. L. Goldsmith, D. N. Bell, S. Braovac, A. Steinberg, and F. McIntosh, "Physical and chemical effects of red cells in the shear-induced aggregation of human platelets.," *Biophysical journal*, vol. 69, no. 4, pp. 1584–95, Oct. 1995.

[116] J. Rosing, J. L. van Rijn, E. M. Bevers, G. van Dieijen, P. Comfurius, and R. F. Zwaal, "The role of activated human platelets in prothrombin and factor X activation," *Blood*, vol. 65, pp. 319–332, 1985.

[117] S.A. Maroney and A. E. Mast, "Platelet tissue factor pathway inhibitor modulates intravascular coagulation.," *Thrombosis research*, vol. 129 Suppl , pp. S21–2, May 2012.

[118] D. Basmadjian, "Embolization: critical thrombus height, shear rates, and pulsatility. Patency of blood vessels.," *Journal of biomedical materials research*, vol. 23, no. 11, pp. 1315–26, Nov. 1989.

[119] Y. Nemerson, "The Reaction between Bovine Brain Tissue Factor and Factors VII and X," *Biochemistry*, vol. 5, no. 2, pp. 601–608, 1966.

[120] B. Osterud and S. I. Rapaport, "Activation of factor IX by the reaction product of tissue factor and factor VII: additional pathway for initiating blood coagulation.," *Proceedings of the National Academy of Sciences of the United States of America*, vol. 74, no. 12, pp. 5260–4, Dec. 1977.

[121] R. Bach, Y. Nemerson, and W. Konigsberg, "Purification and characterization of bovine tissue factor.," *The Journal of biological chemistry*, vol. 256, no. 16, pp. 8324–31, Aug. 1981.

[122] G. J. Broze, J. E. Leykam, B. D. Schwartz, and J. P. Miletich, "Purification of Human Brain Tissue Factor," *The Journal of biological chemistry*, vol. 260, no. 20, pp. 10917–10920, 1985.

[123] J. N. Wilcox, K. M. Smith, S. M. Schwartzt, and D. Gordont, "Localization of tissue factor in the normal vessel wall and in the atherosclerotic plaque," *Proceedings of the National Academy of Sciences of the United States of America*, vol. 86, no. April, pp. 2839–2843, 1989.

[124] R. A. Fleck, L. V. M. Rao, S. I. Rapaport, and N. Varki, "Localization of human tissue factor antigen by immunostaining with monospecific, polyclonal anti-human tissue factor antibody," *Thrombosis research*, vol. 57, pp. 765–781, 1990.

[125] T. A. Drake, J. H. Morrissey, and T. S. Edgington, "Selective cellular expression of tissue factor in human tissues. Implications for disorders of hemostasis and thrombosis.," *The American journal of pathology*, vol. 134, no. 5, pp. 1087–97, May 1989.

[126] P. L. Giesen, U. Rauch, B. Bohrmann, D. Kling, M. Roqué, J. T. Fallon, J. J. Badimon, J. Himber, M. A. Riederer, and Y. Nemerson, "Blood-borne tissue factor: another view of thrombosis.," *Proceedings of the National Academy of Sciences of the United States of America*, vol. 96, no. 5, pp. 2311–5, Mar. 1999.

[127] J. J. Hathcock and Y. Nemerson, "Platelet deposition inhibits tissue factor activity: in vitro clots are impermeable to factor Xa.," *Blood*, vol. 104, no. 1, pp. 123–7, Jul. 2004.

[128] Y. Nemerson, "A different view of thrombosis.," *Blood coagulation & fibrinolysis : an international journal in haemostasis and thrombosis*, vol. 11 Suppl 1, no. suppl 1, pp. S1–2, Apr. 2000.

[129] S. Falati, Q. Liu, P. Gross, G. Merrill-Skoloff, J. Chou, E. Vandendries, A. Celi, K. Croce, B. C. Furie, and B. Furie, "Accumulation of tissue factor into developing thrombi in vivo is dependent upon microparticle P-selectin glycoprotein ligand 1 and platelet P-selectin.," *The Journal of experimental medicine*, vol. 197, no. 11, pp. 1585–98, Jun. 2003.

[130] S. Butenas, B. A. Bouchard, K. E. Brummel-Ziedins, B. Parhami-Seren, and K. G. Mann, "Tissue factor activity in whole blood.," *Blood*, vol. 105, no. 7, pp. 2764–70, Apr. 2005.

[131] M. Hoffman, H. C. Whinna, and D. M. Monroe, "Circulating tissue factor accumulates in thrombi , but not in hemostatic plugs," *Journal of thrombosis and haemostasis : JTH*, vol. 4, pp. 2092–2093, 2006.

[132] D. B. Cines, E. S. Pollak, C. A. Buck, J. Loscalzo, G. a Zimmerman, R. P. McEver, J. S. Pober, T. M. Wick, B. A. Konkle, B. S. Schwartz, E. S. Barnathan, K. R. McCrae, B. A. Hug, A. M. Schmidt, and D. M. Stern, "Endothelial cells in physiology and in the pathophysiology of vascular disorders.," *Blood*, vol. 91, no. 10, pp. 3527–61, May 1998.

[133] A. L. Copley, "the Endoendothelial Fibrin Lining, Fibrinogen Gel Clotting, and the Endothelium-Blood Interface," *Annals of the New York Academy of Sciences*, vol. 416, no. 1 Surface Pheno, pp. 377–396, Dec. 1983.

[134] A. R. Pries, T. W. Secomb, and P. Gaehtgens, "The endothelial surface layer," *Pflugers Archiv European Journal of Physiology*, vol. 440, no. 5, pp. 653–666, Aug. 2000.

[135] L. J. Ignarro, G. M. Buga, K. S. Wood, R. E. Byrns, and G. Chaudhuri, "Endothelium-derived relaxing factor produced and released from artery and vein is nitric oxide," *Proceedings of the National Academy of Sciences of the United States of America*, vol. 84, no. December, pp. 9265–9269, 1987.

[136] S. Bunting, R. Gryglewski, and S. Moncada, "Arterial walls generate from prostaglandin endoperoxides a substance (prostanglandin X) which relaxes strips of mesentric and coeliac arteries and inhibits platelet aggregation," *Prostaglandins*, vol. 12, no. 6, pp. 897–913, 1976.

[137] B. T. Mellion, L. J. Ignarro, E. H. Ohlstein, E. G. Pontecorvo, A. L. Hyman, and P. J. Kadowitz, "Evidence for the inhibitory role of guanosine 3', 5'-monophosphate in ADP-induced human platelet aggregation in the presence of nitric oxide and related vasodilators.," *Blood*, vol. 57, no. 5, pp. 946–55, May 1981.

[138] H. J. Weiss and V. T. Turitto, "Prostacyclin (prostaglandin I2, PGI2) inhibits platelet adhesion and thrombus formation on subendothelium.," *Blood*, vol. 53, no. 2, pp. 244–50, Feb. 1979.

[139] A. J. Marcus, M. J. Broekman, J. H. Drosopoulos, N. Islam, T. N. Alyonycheva, L. B. Safier, K. A. Hajjar, D. N. Posnett, M. A. Schoenborn, K. A. Schooley, R. B. Gayle, and C. R. Maliszewski, "The endothelial cell ecto-ADPase responsible for inhibition of platelet function is CD39.," *The Journal of clinical investigation*, vol. 99, no. 6, pp. 1351–60, Mar. 1997.

[140] J. Ryan, J. Brett, P. Tijburg, R. R. Bach, W. Kisiel, and D. Stern, "Tumor necrosis factor-induced endothelial tissue factor is associated with subendothelial matrix vesicles but is not expressed on the apical surface.," *Blood*, vol. 80, no. 4, pp. 966–74, Aug. 1992.

[141] H. J. Brinkman, K. Mertens, J. Holthuis, L. A. Zwart-Huinink, K. Grijm, and J. A. van Mourik, "The activation of human blood coagulation factor X on the surface of endothelial cells: a comparison with various vascular cells, platelets and monocytes.," *British journal of haematology*, vol. 87, no. 2, pp. 332–42, Jun. 1994.

[142] J. Crawley, F. Lupu, A. D. Westmuckett, N. J. Severs, V. V. Kakkar, and C. Lupu, "Expression, Localization, and Activity of Tissue Factor Pathway Inhibitor in Normal and Atherosclerotic Human Vessels," *Arteriosclerosis, Thrombosis, and Vascular Biology*, vol. 20, no. 5, pp. 1362–1373, May 2000.

[143] J. A. Marcum and R. D. Rosenberg, "Anticoagulantly active heparin-like molecules from vascular tissue.," *Biochemistry*, vol. 23, no. 8, pp. 1730–7, Apr. 1984.

[144] D. S. Fair, R. A. Marlar, and E. G. Levin, "Human Endothelial Cells Synthesize Protein S," *Blood*, vol. 67, no. 4, pp. 1168–1171, 1986.

[145] S. Einav, "Dynamics of Blood Flow and Platelet Transport in Pathological Vessels," *Ann.N.Y.Acad.Sci.*, vol. 1015, pp. 351–366, 2004.

[146] M. J. VanWijk, E. VanBavel, A. Sturk, and R. Nieuwland, "Microparticles in cardiovascular diseases.," *Cardiovascular research*, vol. 59, no. 2, pp. 277–87, Aug. 2003.

[147] D. Lee, I. Yuki, Y. Murayama, A. Chiang, I. Nishimura, H. V Vinters, C. J. Wang, Y.-L. Nien, A. Ishil, B. M. Wu, and F. Viñuela, "Thrombus organization and healing in the swine experimental aneurysm model. Part I. A histological and molecular analysis.," *Journal of neurosurgery*, vol. 107, no. 1, pp. 94–108, Jul. 2007.

[148] M. T. Lawton, A. Quiones-Hinojosa, E. F. Chang, and T. Yu, "Thrombotic Intracranial Aneurysms: Classification Scheme and Management Strategies in 68 Patients," *Neurosurgery*, vol. 56, no. 3, pp. 441–454, Mar. 2005.

[149] T. W. Eller, "MRI demonstration of clot in a small unruptured aneurysm causing stroke. Case report.," *Journal of neurosurgery*, vol. 65, no. 3, pp. 411–2, Sep. 1986.

[150] T. Ishikawa, N. Nakayama, T. Yoshimoto, T. Aoki, S. Terasaka, M. Nomura, A. Takahashi, S. Kuroda, and Y. Iwasaki, "How does spontaneous hemostasis occur in ruptured cerebral aneurysms? Preliminary investigation on 247 clipping surgeries.," *Surgical neurology*, vol. 66, no. 3, pp. 269–75; discussion 275–6, Sep. 2006.

[151] M. B. Pritz, "Thrombosis, growth, recanalization, and rupture of a saccular, non-giant cerebral aneurysm.," *Journal of stroke and cerebrovascular diseases : the official journal of National Stroke Association*, vol. 17, no. 3, pp. 158–60, 2008.

[152] J. V Byrne, J. K. Hope, N. Hubbard, and J. H. Morris, "The nature of thrombosis induced by platinum and tungsten coils in saccular aneurysms.," *AJNR. American journal of neuroradiology*, vol. 18, no. 1, pp. 29–33, Jan. 1997.

[153] S. Ishihara, M. E. Mawad, K. Ogata, C. Suzuki, N. Tsuzuki, and H. Katoh, "Case Report Histopathologic Findings in Human Cerebral Aneurysms Embolized with Platinum Coils : Report of Two Cases and Review of the Literature," *AJNR. American journal of neuroradiology*, vol. 23, no. June/July, pp. 970–974, 2002.

[154] J.-N. Vallée, L. Pierot, A. Bonafé, F. Turjman, P. Flandroy, J. Berge, G. Rodesch, and S. Bracard, "Endovascular treatment of intracranial wide-necked aneurysms using three-dimensional coils: predictors of immediate anatomic and clinical results.," *AJNR. American journal of neuroradiology*, vol. 25, no. 2, pp. 298–306, Feb. 2004.

[155] O. I. Tähtinen, H. I. Manninen, R. L. Vanninen, J. Seppänen, T. Niskakangas, J. Rinne, and L. Keski-Nisula, "The silk flow-diverting stent in the endovascular treatment of complex intracranial aneurysms: technical aspects and midterm results in 24 consecutive patients.," *Neurosurgery*, vol. 70, no. 3, pp. 617–23; discussion 623–4, Mar. 2012.

[156] H. C. Hemker, P. Giesen, R. AlDieri, V. Regnault, E. de Smed, R. Wagenvoord, T. Lecompte, and S. Béguin, "The calibrated automated thrombogram (CAT): a universal routine test for hyper- and hypocoagulability.," *Pathophysiology of haemostasis and thrombosis*, vol. 32, no. 5–6, pp. 249–53, 2002.

[157] S. Butenas, C. van 't Veer, and K. G. Mann, "'Normal' Thrombin Generation: Presented in part at the XVIth Congress of the International Society on Thrombosis and Haemostasis, June 6-12, 1997, Florence, Italy (abstr PS-1653), at the 15th International Congress on Thrombosis, October 16-21, 1998, Anta," *Blood*, vol. 94, pp. 2169–2178, 1999.

[158] N. Filipovic, M. Kojic, and A. Tsuda, "Modelling thrombosis using dissipative particle dynamics method.," *Philosophical transactions. Series A, Mathematical, physical, and engineering sciences*, vol. 366, no. 1879, pp. 3265–79, Sep. 2008.

[159] J. E. Purvis, M. S. Chatterjee, L. F. Brass, and S. L. Diamond, "A molecular signaling model of platelet phosphoinositide and calcium regulation during homeostasis and P2Y1 activation.," *Blood*, vol. 112, no. 10, pp. 4069–79, Nov. 2008.

[160] M. S. Chatterjee, J. E. Purvis, L. F. Brass, and S. L. Diamond, "Pairwise agonist scanning predicts cellular signaling responses to combinatorial stimuli.," *Nature biotechnology*, vol. 28, no. 7, pp. 727–32, Jul. 2010.

[161] D. Basmadjian, "The effect of flow and mass transport in thrombogenesis.," *Annals of biomedical engineering*, vol. 18, no. 6, pp. 685–709, Jan. 1990.

[162] M. Anand, K. Rajagopal, and K. R. Rajagopal, "A model for the formation, growth, and lysis of clots in quiescent plasma. A comparison between the effects of antithrombin III deficiency and protein C deficiency.," *Journal of theoretical biology*, vol. 253, no. 4, pp. 725–38, Aug. 2008.

[163] T. Bodnár and a. Sequeira, "Numerical Simulation of the Coagulation Dynamics of Blood," *Computational and Mathematical Methods in Medicine*, vol. 9, no. 2, pp. 83–104, 2008.

[164] A. L. Fogelson and R. D. Guy, "Platelet-wall interactions in continuum models of platelet thrombosis: formulation and numerical solution.," *Mathematical medicine and biology : a journal of the IMA*, vol. 21, no. 4, pp. 293–334, Dec. 2004.

[165] A. L. Fogelson and N. Tania, "Coagulation under flow: the influence of flow-mediated transport on the initiation and inhibition of coagulation.," *Pathophysiology of haemostasis and thrombosis*, vol. 34, no. 2–3, pp. 91–108, Jan. 2005.

[166] R. D. Guy, A. L. Fogelson, and J. P. Keener, "Fibrin gel formation in a shear flow.," *Mathematical medicine and biology : a journal of the IMA*, vol. 24, no. 1, pp. 111–30, Mar. 2007.

[167] K. Leiderman and A. L. Fogelson, "Grow with the flow: a spatial-temporal model of platelet deposition and blood coagulation under flow.," *Mathematical medicine and biology : a journal of the IMA*, vol. 28, no. 1, pp. 47–84, Mar. 2011.

[168] Z. Xu, N. Chen, M. M. Kamocka, E. D. Rosen, and M. Alber, "A multiscale model of thrombus development.," *Journal of the Royal Society, Interface / the Royal Society*, vol. 5, no. 24, pp. 705–22, Jul. 2008.

[169] Z. Xu, N. Chen, S. C. Shadden, J. E. Marsden, M. M. Kamocka, E. D. Rosen, and M. Alber, "Study of blood flow impact on growth of thrombi using a multiscale model," *Soft Matter*, vol. 5, no. 4, p. 769, 2009.

[170] V. L. Rayz, L. Boussel, M. T. Lawton, G. Acevedo-Bolton, L. Ge, W. L. Young, R. T. Higashida, and D. Saloner, "Numerical modeling of the flow in intracranial aneurysms: prediction of regions prone to thrombus formation.," *Annals of biomedical engineering*, vol. 36, no. 11, pp. 1793–804, Nov. 2008.

[171] H. K. Versteeg and W. Malalasekera, *An Introduction to Computational Fluid Dynamics. The Finite Volume Method*. Harlow: Pearson Education Limited, 2007.

[172] ESI, "CFD-ACE+ User Manual." Paris, 2010.

[173] J. H. Ferziger and M. Peric, *Computational Methods for Fluid Dynamics*, Second. Berlin: Springer, 1999.

[174] S. L. Diamond, "Engineering design of optimal strategies for blood clot dissolution.," *Annual review of biomedical engineering*, vol. 1, pp. 427–62, Jan. 1999.

[175] E. Hairer and G. Wanner, *Solving ordinary differential equations II. Stiff and differential-algebraic problems*. Springer, 1993.

[176] S. Osher and R. Fedkiw, *Level Set Methods and Dynamic Implicit Surfaces*, 1st ed. New York: Springer, 2003.

[177] D. Peng, B. Merriman, S. Osher, H. Zhao, and M. Kang, "A PDE-Based Fast Local Level Set Method," *Journal of Computational Physics*, vol. 155, no. 2, pp. 410–438, Nov. 1999.

[178] M. Sussman, P. Smereka, and S. Osher, "A Level Set Approach for Computing Solutions to Incompressible Two-Phase Flow," *Journal of Computational Physics*, vol. 114, no. 1, pp. 146–159, 1994.

[179] A. Kurenkov and M. Oberlack, "Modelling Turbulent Premixed Combustion Using the Level Set Approach for Reynolds Averaged Models," *Flow, Turbulence and Combustion formerly: Applied Scientific Research*, vol. 74, no. 4, pp. 387–407, Nov. 2005.

[180] A. Harten, B. Engquist, S. Osher, and S. Chakravarthy, "Uniformly High-Order Accurate Essentially Non-Oscillatory Schemes III," *Journal of Computational Physics*, vol. 71, no. 2, pp. 231–303, 1987.

[181] X.-D. Liu, S. Osher, and T. Chan, "Weighted Essentially Non-Oscillatory Schemes," *Journal of Computational Physics*, vol. 115, no. 1, pp. 200–212, 1994.

[182] C. W. Shu and S. Osher, "Efficient Implementation of Essentially Non-Oscillatory Schock Capturing Schemes II," *Journal of Computational Physics*, vol. 77, no. 2, pp. 439–471, 1988.

[183] B. A. Bouchard, S. Butenas, K. G. Mann, and P. B. Tracy, "Interactions Between Platelets and the Coagulation System," in *Platelets*, 2nd ed., A. D. Michelson, Ed. Elsevier Inc., 2007, pp. 377–402.

[184] K. G. Mann, K. Brummel, and S. Butenas, "What is all that thrombin for?," *Journal of thrombosis and haemostasis : JTH*, vol. 1, no. 7, pp. 1504–14, Jul. 2003.

[185] R. Bach, R. Gentry, and Y. Nemerson, "Factor VII binding to tissue factor in reconstituted phospholipid vesicles: induction of cooperativity by phosphatidylserine.," *Biochemistry*, vol. 25, no. 14, pp. 4007–20, Jul. 1986.

[186] J. J. Hathcock and Y. Nemerson, "Platelet deposition inhibits tissue factor activity: in vitro clots are impermeable to factor Xa.," *Blood*, vol. 104, no. 1, pp. 123–7, Jul. 2004.

[187] R. Wagenvoord, P. W. Hemker, and H. C. Hemker, "The limits of simulation of the clotting system.," *Journal of thrombosis and haemostasis : JTH*, vol. 4, no. 6, pp. 1331–8, Jun. 2006.

[188] P. K. Kundu and I. M. Cohen, *Fluid Mechanics*, 4th ed. Elsevier Inc., 2008.

[189] J. R. Levick, *An introduction to Cardiovascular Physiology*. London: Hodder Arnold, 2010.

[190] D. U. Silverthorn, *Human Physiology: An Integrated Approach*, 2nd ed. Upper Saddle River, NJ: Prentice Hall, 2001.

[191] K. C. Jones and K. G. Mann, "A Model for the Tissue Factor Pathway to Thrombin," *The Journal of Biological Chemistry*, vol. 169, no. 37, pp. 23367–23373, 1994.

[192] J. K. W. Chesnutt and H.-C. Han, "Tortuosity triggers platelet activation and thrombus formation in microvessels.," *Journal of biomechanical engineering*, vol. 133, no. 12, p. 121004, Dec. 2011.

[193] S. Butenas, T. Orfeo, and K. G. Mann, "Tissue factor in coagulation: Which? Where? When?," *Arteriosclerosis, thrombosis, and vascular biology*, vol. 29, no. 12, pp. 1989–96, Dec. 2009.

[194] N. Mackman and M. Taubman, "Tissue factor: past, present, and future.," *Arteriosclerosis, thrombosis, and vascular biology*, vol. 29, no. 12, pp. 1986–8, Dec. 2009.

[195] O. Morel, L. Jesel, J.-M. Freyssinet, and F. Toti, "Cellular mechanisms underlying the formation of circulating microparticles.," *Arteriosclerosis, thrombosis, and vascular biology*, vol. 31, no. 1, pp. 15–26, Jan. 2011.

[196] B. Osterud, "Tissue factor/TFPI and blood cells.," *Thrombosis research*, vol. 129, no. 3, pp. 274–8, Mar. 2012.

[197] K. Broos, H. B. Feys, S. F. De Meyer, K. Vanhoorelbeke, and H. Deckmyn, "Platelets at work in primary hemostasis.," *Blood reviews*, vol. 25, no. 4, pp. 155–67, Jul. 2011.

[198] M. J. Maxwell, E. Westein, W. S. Nesbitt, S. Giuliano, S. M. Dopheide, and S. P. Jackson, "Identification of a 2-stage platelet aggregation process mediating shear-dependent thrombus formation.," *Blood*, vol. 109, no. 2, pp. 566–76, Jan. 2007.

[199] D. M. Wootton, C. P. Markou, S. R. Hanson, and D. N. Ku, "A Mechanistic Model of Acute Platelet Accumulation in Thrombogenic Stenoses," *Annals of Biomedical Engineering*, vol. 29, no. 4, pp. 321–329, Apr. 2001.

[200] P. D. Goodman, E. T. Barlow, P. M. Crapo, S. F. Mohammad, and K. A. Solen, "Computational Model of Device-Induced Thrombosis and Thromboembolism," *Annals of Biomedical Engineering*, vol. 33, no. 6, pp. 780–797, Jun. 2005.

[201] M. V Ovanesov, N. M. Ananyeva, M. A. Panteleev, F. I. Ataullakhanov, and E. L. Saenko, "Initiation and propagation of coagulation from tissue factor-bearing cell monolayers to plasma: initiator cells do not regulate spatial growth rate.," *Journal of thrombosis and haemostasis : JTH*, vol. 3, no. 2, pp. 321–31, Feb. 2005.

[202] G. R. Sutherland, M. E. King, S. J. Peerless, W. C. Vezina, G. W. Brown, and M. J. Chamberlain, "Platelet interaction within giant intracranial aneurysms.," *Journal of neurosurgery*, vol. 56, no. 1, pp. 53–61, Jan. 1982.

[203] G. Mulder, A. C. B. Bogaerds, P. Rongen, and F. N. Vosse, "On automated analysis of flow patterns in cerebral aneurysms based on vortex identification," *Journal of Engineering Mathematics*, vol. 64, no. 4, pp. 391–401, Mar. 2009.

[204] S. Butenas, C. van 't Veer, and K. G. Mann, "Evaluation of the initiation phase of blood coagulation using ultrasensitive assays for serine proteases.," *The Journal of biological chemistry*, vol. 272, no. 34, pp. 21527–33, Aug. 1997.

[205] G. Moiseyev and P. Z. Bar-yoseph, "Computational modeling of thrombosis as a tool in the design and optimization of vascular implants," *Journal of Biomechanics*, vol. 46, no. 2, pp. 248–252, 2013.

[206] M. C. Villa-Uriol, G. Berti, D. R. Hose, a Marzo, a Chiarini, J. Penrose, J. Pozo, J. G. Schmidt, P. Singh, R. Lycett, I. Larrabide, and a F. Frangi, "@neurIST complex information processing toolchain for the integrated management of cerebral aneurysms.," *Interface focus*, vol. 1, no. 3, pp. 308–19, Jun. 2011.

[207] P. a Yushkevich, J. Piven, H. C. Hazlett, R. G. Smith, S. Ho, J. C. Gee, and G. Gerig, "User-guided 3D active contour segmentation of anatomical structures: significantly improved efficiency and reliability.," *NeuroImage*, vol. 31, no. 3, pp. 1116–28, Jul. 2006.

[208] L. Grady, "Random walks for image segmentation.," *IEEE transactions on pattern analysis and machine intelligence*, vol. 28, no. 11, pp. 1768–83, Nov. 2006.

[209] M. D. Ford, G. R. Stuhne, H. N. Nikolov, D. F. Habets, S. P. Lownie, D. W. Holdsworth, and D. A. Steinman, "Virtual angiography for visualization and validation of computational models of aneurysm hemodynamics.," *IEEE transactions on medical imaging*, vol. 24, no. 12, pp. 1586–92, Dec. 2005.

[210] R. Sunethareswaran, *Mosby's Crash Course: Cardiovascular System*. Mosby, 1998.

List of conferences and publications

Conferences

1. *A Computational Model of Thrombus Development.* Poster presentation. 2nd Meeting of the EPSRC Patient-Specific Modelling Network, 28 – 29 September 2011, University of Edinburgh, UK.
2. *A Computational Model of Thrombus Development in Aneurysms.* Oral presentation. 6th European Congress on Computational Methods in Applied Sciences and Engineering (ECCOMAS), 10 – 14 September 2012, Vienna, Austria.

Publications

1. T.W. Peach, M. Ngoepe, K. Spranger, Y. Ventikos, and D. Zajarias-Fainsod, "Personalizing Flow Diverter Intervention for Cerebral Aneurysms: from Computational Haemodynamics to Biochemical Modeling," *International Journal for Numerical Methods in Biomedical Engineering* (Under revision)
2. M. Ngoepe, T.J. Bowker, and Y. Ventikos "Computational model of thrombus development in aneurysms," *Annals of Biomedical Engineering* (Submitted)
3. M. Ngoepe and Y. Ventikos "Computational model of thrombus development in cerebral aneurysms: Evaluation of flow diverter treatment in specific patients," *Journal of Biomechanics* (Submitted)